



UNIVERSITAT DE
BARCELONA

Characterization of endothelial cell metabolism under different microenvironmental challenges: exploring therapeutic implications of targeting glycogen degradation

Anusha Jayaraman

ADVERTIMENT. La consulta d'aquesta tesi queda condicionada a l'acceptació de les següents condicions d'ús: La difusió d'aquesta tesi per mitjà del servei TDX (www.tdx.cat) i a través del Dipòsit Digital de la UB (diposit.ub.edu) ha estat autoritzada pels titulars dels drets de propietat intel·lectual únicament per a usos privats emmarcats en activitats d'investigació i docència. No s'autoritza la seva reproducció amb finalitats de lucre ni la seva difusió i posada a disposició des d'un lloc aliè al servei TDX ni al Dipòsit Digital de la UB. No s'autoritza la presentació del seu contingut en una finestra o marc aliè a TDX o al Dipòsit Digital de la UB (framing). Aquesta reserva de drets afecta tant al resum de presentació de la tesi com als seus continguts. En la utilització o cita de parts de la tesi és obligat indicar el nom de la persona autora.

ADVERTENCIA. La consulta de esta tesis queda condicionada a la aceptación de las siguientes condiciones de uso: La difusión de esta tesis por medio del servicio TDR (www.tdx.cat) y a través del Repositorio Digital de la UB (diposit.ub.edu) ha sido autorizada por los titulares de los derechos de propiedad intelectual únicamente para usos privados enmarcados en actividades de investigación y docencia. No se autoriza su reproducción con finalidades de lucro ni su difusión y puesta a disposición desde un sitio ajeno al servicio TDR o al Repositorio Digital de la UB. No se autoriza la presentación de su contenido en una ventana o marco ajeno a TDR o al Repositorio Digital de la UB (framing). Esta reserva de derechos afecta tanto al resumen de presentación de la tesis como a sus contenidos. En la utilización o cita de partes de la tesis es obligado indicar el nombre de la persona autora.

WARNING. On having consulted this thesis you're accepting the following use conditions: Spreading this thesis by the TDX (www.tdx.cat) service and by the UB Digital Repository (diposit.ub.edu) has been authorized by the titular of the intellectual property rights only for private uses placed in investigation and teaching activities. Reproduction with lucrative aims is not authorized nor its spreading and availability from a site foreign to the TDX service or to the UB Digital Repository. Introducing its content in a window or frame foreign to the TDX service or to the UB Digital Repository is not authorized (framing). Those rights affect to the presentation summary of the thesis as well as to its contents. In the using or citation of parts of the thesis it's obliged to indicate the name of the author.

**Characterization of endothelial cell metabolism
under different microenvironmental challenges:
exploring therapeutic implications of targeting
glycogen degradation**

**Anusha Jayaraman
Doctoral Thesis
2016**

The picture on the cover is the 'gopuram' or the tower of Shore Temple, located in the South Indian village of Mamallapuram, near the city of Chennai. It was built during the period of Pallava dynasty in the 8th century AD along with many other historic monuments located in this place and is classified as a UNESCO World Heritage site.

TABLE OF CONTENTS

1. INTRODUCTION.....	1
1.1. Angiogenesis	3
1.1.1. Endothelial cells, the protagonists of blood vessel formation	4
1.1.2. Molecular regulation of angiogenesis and the significance of VEGF.....	5
1.1.3. Angiogenesis and cancer	6
1.1.3.1. Tumour microenvironment	6
1.1.3.2. Tumour angiogenesis.....	7
1.1.3.2.1. Hypoxia, the key regulator of tumour angiogenesis.....	8
1.1.4. Anti-cancer therapies targeting angiogenesis	9
1.2. Endothelial cell metabolism.....	12
1.3. Endothelial cell metabolism vs. cancer cell metabolism	16
1.4. Glycogen metabolism as a key target for cancer therapy?	19
1.5. Glycogen metabolism and its regulation	21
1.5.1. Regulation of glycogen phosphorylase	23
1.5.2. Regulation of glycogen synthase	26
1.5.3. Existing therapies targeting glycogen metabolism.....	27
1.5.4. Exploring glycogen metabolism in endothelial cells as a key target in angiogenesis.....	29
1.6. Omics-based methods for studying cellular metabolism	30
1.6.1. Fluxomics	31
1.6.1.1. ¹³ C tracer-based metabolomics experiments	33
1.6.1.2. Estimation of metabolic fluxes based on ¹³ C labelling patterns.....	35
1.6.1.2.1. Direct interpretation of fluxes or ¹³ C tracer analysis	35

1.6.1.2.2. Computational modelling based flux estimation or ¹³ C metabolic flux analysis	36
1.6.2. Targeted and untargeted metabolomics	37
1.6.2.1. LC-MS-based untargeted metabolomics	39
2. OBJECTIVES	43
3. MATERIALS AND METHODS	47
3.1. Cell culture conditions	49
3.2. Cell viability assay	51
3.3. Cell migration assay	52
3.4. <i>In vitro</i> wound healing assay.....	53
3.5. <i>In vivo</i> matrigel plug assay	53
3.6. <i>In vivo</i> tumour efficacy assay.....	54
3.7. Biochemical measurement of extracellular metabolites.....	55
3.8. Protein extraction and determination.....	56
3.9. Enzyme activities.....	56
3.9.1. Glucose 6-phosphate dehydrogenase (G6PD, EC 1.1.1.49).....	57
3.9.2. Glycogen synthase (GS, EC 2.4.1.11)	57
3.9.3. Glycogen phosphorylase (GP, EC 2.4.1.1).....	58
3.10. Western blot	59
3.11. RNA isolation and quantitative reverse transcription-polymerase chain reaction (qRT-PCR)	59
3.12. ¹³ C tracer-based metabolomics using GC-MS.....	60
3.12.1. Glucose.....	61
3.12.2. Lactate.....	61

3.12.3.	Glutamate.....	62
3.12.4.	Amino acids	63
3.12.5.	Ribose	63
3.12.6.	Fatty acids	64
3.12.7.	Glycogen.....	64
3.13.	GC-MS data reduction.....	65
3.14.	¹³ C tracer-based metabolomics: data interpretation	66
3.14.1.	Direct interpretation of fluxes or ¹³ C tracer analysis	66
3.14.2.	Computational modelling based flux estimation or ¹³ C metabolic flux analysis ..	66
3.15.	Mass spectrometry-based targeted metabolomics.....	67
3.16.	LC-MS-based non-targeted metabolomics	68
3.16.1.	Sample preparation.....	68
3.16.2.	LTQ – Orbitrap elite LC-MS analysis.....	69
3.16.3.	Data analysis for untargeted metabolomics	70
3.17.	Statistics	71
4.	RESULTS AND DISCUSSION	73
4.1.	Flux analysis of endothelial cells induced by VEGF: changes under normoxia and hypoxia.....	75
4.1.1.	Introduction	75
4.1.2.	Results.....	76
4.1.2.1.	Net metabolite consumption and production with VEGF stimulation, under normoxia and hypoxia	76
4.1.2.2.	¹³ C-label enrichment in lactate.....	77
4.1.2.3.	¹³ C-label enrichment in ribose	78

4.1.2.4.	¹³ C-label enrichment in fatty acids	81
4.1.2.5.	¹³ C-label enrichment in glycogen and glycogen accumulation	82
4.1.2.6.	¹³ C metabolic flux analysis for estimation of fluxes.....	84
4.1.3.	Discussion.....	87
4.2.	Untargeted metabolomics in endothelial cells induced by VEGF and metastatically different sub-populations of prostate cancer cells.....	93
4.2.1.	Introduction	93
4.2.2.	Results.....	94
4.2.2.1.	Multivariate data analysis.....	94
4.2.2.2.	Metabolite identifications	95
4.2.2.3.	Metabolite set enrichment analysis of the identified metabolites.....	98
4.2.3.	Discussion.....	103
4.3.	Therapeutic implications of glycogen phosphorylase inhibition in <i>in vitro</i> and <i>in vivo</i> angiogenesis.....	109
4.3.1.	Introduction	109
4.3.2.	Results.....	110
4.3.2.1.	Effect of glycogen phosphorylase inhibitor on HUVEC viability and function <i>in vitro</i>	110
4.3.2.2.	Effect of glycogen phosphorylase inhibitor against <i>in vivo</i> neovascularisation, tumour growth and microvessel density.....	113
4.3.2.3.	Effect of the glycogen phosphorylase inhibitor on HUVEC lipid metabolism.....	116
4.3.3.	Discussion.....	118
4.4.	Characterization of glycogen metabolism and its regulation in endothelial cells.....	123
4.4.1.	Introduction	123
4.4.2.	Results.....	124

4.4.2.1. Glycogen degradation at glucose depleted conditions	124
4.4.2.2. Enzyme expressions of glycogen synthase and glycogen phosphorylase	127
4.4.2.3. Enzyme activities of glycogen synthase and phosphorylase	130
4.4.3. Discussion.....	132
5. GENERAL DISCUSSION.....	139
6. CONCLUSIONS.....	149
7. REFERENCES.....	153
8. APPENDIX 1.....	179
9. APPENDIX 2.....	191
10. APPENDIX 3.....	197
11. APPENDIX 4.....	203
12. APPENDIX 5.....	237

ABBREVIATIONS

ABBREVIATIONS

ALC - acetyl L-carnitine
AMP - adenosine monophosphate
ANG/ANG1/ANG2 - angiopoietins
ATP - adenosine triphosphate
BSA – bovine serum albumin
CAFs - cancer-associated fibroblasts
cAMP - cyclic-Adenosine monophosphate
cAMPK - cAMP-dependent protein kinase
CAT – carnitine acetyltransferase
c-Kit - proto-oncogene for stem cell growth factor receptor
CM - complete medium
c-Met - gene encoding hepatocyte growth factor receptor
CoA - co-enzyme A
cpm – counts per minute
CPT1 - carnitine palmitoyltransferase-1
CSC - cancer stem cell
CXCR4 - gene encoding chemokine receptor type 4
DAB - 1,4-dideoxy-1,4-imino-d-arabinitol
DBE - glycogen debranching enzyme
DCA – dichloroacetate
DMG - dimethylglycine
DMSO -dimethyl sulfoxide
dNTP - deoxy-nucleotide triphosphate
DTT - dithiothreitol
EBM - endothelial basal medium
ECM - extracellular matrix
EDTA - ethylenediamine tetraacetic acid
EGF - endothelial growth factor
EGM - endothelial growth medium
EMT - epithelial-mesenchymal transition
ENO1 - alpha-enolase
eNOS - endothelial nitric oxide synthase
FA Acyl-CoA – fatty acid acyl-CoA
FABP3/FABP7 - fatty acid binding proteins
FBS - fetal bovine serum
FGF – fibroblast growth factor
FIA-MS – flow injection analysis-mass spectrometry
FIH - asparagine-hydroxylase factor inhibiting HIF1 α
FLK1 - VEGFR2 receptor
FLT-1 - fms-related tyrosine kinase 1
G1P - glucose-1-phosphate

G6P - glucose-6-phosphate
G6PD - glucose-6-phosphate dehydrogenase
GAPDH - glyceraldehyde-3-phosphate dehydrogenase
GBE - glycogen branching enzyme
GC-MS - gas chromatography coupled to mass spectrometry
GDH - glutamate dehydrogenase
Glc - glucose
GLS - glutaminase
Gly - glycine
GLUT1/GLUT3 - glucose transporters
GP – glycogen phosphorylase
GP_a – phosphorylated GP (active form)
GP_b – dephosphorylated GP (inactive form)
GS – glycogen synthase
GS_a – dephosphorylated GS (active form)
GS_b - phosphorylated GS (inactive form)
GSK3(β) - glycogen synthase kinase - 3(β)
GYS1 – muscle isoform of glycogen synthase
GYS2 – liver isoform of glycogen synthase
HCl – hydrochloric acid
Hcy - homocysteine
HESI - heated electrospray ionization source II
HIF1 α /HIF2 α /HIF1 β – hypoxia-inducible factor - 1 α /2 α /1 β
HK2 - hexokinase 2
HMDB - human metabolome database
HRMS - high resolution mass spectrometry
HUVECs - human umbilical vein endothelial cells
IP - identification points
KEGG - Kyoto encyclopedia of genes and genomes
KF – potassium fluoride
LC-MS - liquid chromatography coupled to mass spectrometry
LDH/LDH-A/LDH-B - lactate dehydrogenases
LOX - protein-lysine 6-oxidase gene
m/z - mass-to-charge ratio
MAPK - mitogen-activated protein kinases
MCT1 - monocarboxylate transporter 1
MDSCs - myeloid-derived suppressor cells
MMP/MMP2/MMP9 - matrix metalloproteinases
MS - mass spectrometry
MSEA - metabolite set enrichment analysis
MTT - 3-(4,5-dimethylthiazol-2-yl)-2,5-diphenyltetrazolium bromide
NAD/NADH - nicotinamide dinucleotide (oxidized/reduced)

NADPH - nicotinamide adenine dinucleotide phosphate (reduced)
NaOH – sodium hydroxide
NMR - nuclear magnetic resonance
NO - nitric oxide
OPLS-DA - orthogonal projection to partial least squares - discriminant analysis
OT1, OT2, OT3 – other sources (contributing to the central carbon metabolism)
OXPHOS - oxidative phosphorylation
PBS – phosphate buffered saline
PC – pyruvate carboxylase
PCA - principal component analysis
PDGF - platelet-derived growth factor
PDH – pyruvate dehydrogenase
PDK – pyruvate dehydrogenase kinase
PFKFB3 - 6-phosphofructo-2-kinase/fructose-2,6-bisphosphatase 3
PGC-1 α - peroxisome proliferator-activated receptor- γ coactivator-1 α
PGF - placental growth factor
PGM - phosphoglucomutase
pGS – phosphorylated glycogen synthase
PHD1/PHD2/PHD3 - prolyl-hydroxylases
PI3K/AKT/mTOR - phosphoinositide 3-kinase/protein kinase B/mammalian target of rapamycin
PIGF - placental growth factor
PKA - protein kinase A
PKC - protein kinase C
PKM2 - pyruvate kinase isozyme type M2
PMSF - phenylmethylsulfonyl fluoride
PP1 – protein phosphatase 1
PPIA - cyclophilin A gene
PPP - pentose phosphate pathway
PYGB – brain isoform of glycogen phosphorylase
PYGL – liver isoform of glycogen phosphorylase
PYGM – muscle isoform of glycogen phosphorylase
QEA - quantitative enrichment analysis
qRT-PCR - quantitative reverse transcription-polymerase chain reaction
R5P - ribose-5-phosphate
RET - proto-oncogene encoding receptor tyrosine kinase for glial cell line-derived signalling molecules
RIOK3 - Serine/threonine-protein kinase RIO3 gene
RM - restricted medium
RMV - restricted medium with VEGF
ROS - reactive oxygen species
RT – retention time
Ru5P - ribulose-5-phosphate

SIM – single ion monitoring mode of MS detector
SMPDB - specialized metabolic pathway databases
TAMs - tumour-associated macrophages
TCA cycle - tricarboxylic acid cycle
TIE2 - Tie family receptor tyrosine kinases
TKT - transketolase
TOF - Time of Flight mass analyzer
TrkB - tropomyosin receptor kinase B
UDP - uridine diphosphate
UHPLC - ultra high performance liquid chromatography
VEGF/VEGF-A/VEGF-B – vascular endothelial growth factors
VEGFR1/VEGFR2/VEGFR3 - VEGF receptors
VHL – von Hippel-Lindau tumour suppressor gene
VIP - variable importance in projection
X5P - xylulose-5-phosphate

1. INTRODUCTION

INTRODUCTION

1.1. Angiogenesis

A continuous supply of oxygen and nutrients is imperative for every cell, tissue and organ in the body for their survival and development, in addition to disposing waste products. Hence a meticulously organized system of blood circulation ensures these vital processes. The process of formation of blood vessels from pre-existing ones is called angiogenesis. Over the course of adulthood the endothelial cells remain quiescent except in situations like wound healing, menstruation, pregnancy and in many pathological conditions when these cells are activated to form blood vessels [1,2]. Several pathologies have been identified due to the excessive blood vessel formation such as cancer [3,4], psoriasis [5,6], arthritis [7-9] and diabetic retinopathy [10]. At the same time, pathological conditions due to insufficient blood vessel growth have also been identified, such as, heart ischemia [11], stroke [12,13], osteoporosis [14,15] and hair loss [16,17]. Thus when a tissue has insufficient blood vessels its oxygen content lessens, leading to ischemia and degradation of its function, whereas when the vessels are over-grown it might encourage the malignant tissue growth or inflammatory disorders [18]. Hence angiogenesis is a powerful process in which the delicate balance of the factors responsible for its induction and regression should be maintained.

Over years, understanding the mechanism of angiogenesis has led us to explain the defective blood vessel development in pathological conditions and it has given new hopes of utilizing this knowledge for therapeutic purposes. Pro-angiogenic factors responsible for the induction of angiogenesis have been tested for promoting revascularization of ischemic tissues and their inhibitors were tested for reducing vascular growth in diseases such as cancer [19]. Inducing angiogenesis is considered one of the hallmarks of cancer and is a key player in sustaining tumour tissues from dying and also aiding in their growth and metastasis [4]. Anti-angiogenic strategies for treating cancer have gained a huge importance in the recent years. Tumour cells are genetically unstable and develop resistance to anti-cancer therapies, in contrast to endothelial cells that are genetically stable and make them an ideal target for treatments

against cancer [20]. Today we have much more information on the molecular basis of angiogenesis and the angiogenic factors involved, upon which current anti-angiogenic therapies have been designed, although the metabolic studies are still nascent. Thus a deeper understanding of the endothelial cell metabolism can reveal new therapeutic targets for tumour angiogenesis that can be combined with conventional therapies for obtaining promising results. This thesis aims to throw some light on the metabolic adaptations of endothelial cells in the presence of angiogenic factors and cancer cells, highlighting the importance and regulation of certain pathways in endothelial cells, which has not been explored before.

1.1.1. Endothelial cells, the protagonists of blood vessel formation

Blood vessels are lined by a layer of endothelial cells that are supported by a protein-rich extracellular matrix (ECM) [21]. Endothelial cells are thin, plastic (can elongate) and are fragile but form strong and efficient channels to transport blood and withstand pressure due to blood flow differences in arteries and veins [22]. The vessels can remain robust for many years and when induced they can begin sprouting to form new vessels in an organized manner, thanks to the efficient cellular communication between themselves and other supporting cells [23]. Endothelial cells have been described to be heterogeneous and have been identified according to their function and location in the blood vessels during the process of angiogenesis [19]. During the vessel sprouting phase of blood vessel formation, certain endothelial cells are 'chosen' as tip and stalk cells that differ both in morphology and function. Tip cells have been found to be enriched with filopodia and show a high rate of motility for migration. These tip cells guide the stalk cells which mainly proliferate and form the length of the new sprouts, show lower motility, connects the parent vessel with the migrating tip cells and maintain cellular junctions [22,24]. Another type of endothelial cells has also been identified, that forms a part of the mature and well-formed blood vessels. These endothelial cells, also called as phalanx cells, exist in a quiescent state and have shown to appear as streamlined and monolayered within the blood vessels, connected by junction proteins [25]. In addition to maintaining vessel barrier, these cells are important for blood vessel dynamicity, expressing oxygen sensing proteins like

the prolyl hydroxylase 2 (PHD2) that regulates the palanx cell phenotype in turn allowing for dynamic reorganization of blood vessels for oxygen delivery [25].

1.1.2. Molecular regulation of angiogenesis and the significance of VEGF

Several factors and signalling molecules have been identified to be involved in the different steps of angiogenesis, from inducing 'angiogenic switch' to the formation of new blood vessels. Pro-angiogenic factors such as vascular endothelial growth factor (VEGF), fibroblast growth factor (FGF), angiopoietins (ANG), matrix metalloproteinases (MMPs), and VE-cadherin aid in the process of angiogenesis [26]. Regulation of each step of the blood vessel formation such as pericyte detachment, ECM degradation, tip cell selection and migration, stalk cell division, vessel elongation, vessel lumen establishment and vessel maturation are carried out with the help of the combined efforts of these different signalling molecules and growth factors along the respective signalling pathways, as reviewed in Stapor *et. al.* and Welti *et. al.* [19,26]. In addition to several proteins, immune cell types, like the macrophages, are also found to help in the process of blood vessel formation by releasing VEGF and other pro-angiogenic factors to bridge the tip cells of the adjacent sprouting vessels and seal the new vessel formed [27,28].

Among all the other pro-angiogenic growth factors and signalling molecules involved in the process of angiogenesis, VEGF has been identified as a predominant regulator of angiogenesis and lymphangiogenesis [29-31]. The family of VEGF consists of VEGF-A, placental growth factor (PGF), VEGF-B, VEGF-C, VEGF-D and two VEGF-like proteins encoded by two strains of parapoxvirus [32,33]. VEGF-A possesses further isoforms: VEGF₁₂₁, VEGF₁₄₅, VEGF₁₆₅, VEGF₁₈₉, VEGF₂₀₆, derived by the alternative splicing of a single gene [34]. VEGF was originally thought as a mitogen only for vascular endothelial cells from arteries, veins and lymphatics, as suggested by its name [35]. But it was also found to influence other cell types such as retinal pigment epithelial cells [36], pancreatic duct cells [37] and Schwann cells [38,39]. Three types of VEGF receptor tyrosine kinases identified are VEGFR1, VEGFR2 and VEGFR3 with distinct signalling pathways mediating different functions, as reviewed in Koch *et. al.*, [34]. VEGF has been found to be the key survival factor for many types of cells including retinal endothelial cells [40],

retinal neurons [41] and tumour cells [42,43] and coherently it was found to be protective against apoptosis in endothelial cells and cancer cells [44-46]. In addition VEGF has been identified to induce progression of tumours, for example, in oral cancer [47], gastric cancer [48] and prostate cancer, in which it is also found to aid metastasis [49,50]. VEGF-A, often referred to as VEGF, is the main stimulating factor for angiogenesis in health and disease and binds to and activates the receptors VEGFR1 and VEGFR2 [34]. While VEGFR2 has been identified as the mainstream receptor for active angiogenesis in both normal and pathological conditions like cancer [51-53], VEGFR1 with a weak tyrosine kinase activity is suspected to act as a decoy for VEGF, 'playing' with its availability to bind VEGFR2 [34,54]. Also VEGFR1 signalling in endothelial, stromal and myeloid cells stimulates pathological angiogenesis [55] and growth of tumour cells [56]. VEGF is found to be regulated by the hypoxia-inducible factor 1 (HIF1) which upregulates its expression in both cancer and non-cancer cells [57-60]. VEGF alone, as a pro-angiogenic factor, is strongly shown to promote abnormal vessel branching, fluid leakage, high interstitial pressures and gaps within vessels [31]. Due to its predominant part as a key player in angiogenesis VEGF is still under study, even after decades of its discovery.

1.1.3. Angiogenesis and cancer

1.1.3.1. Tumour microenvironment

Tumour microenvironment is a milieu of tumours interacting with stromal cell population, aiding for tumour survival and progression [61]. This specialized environment, which is like an organ by itself with respect to the coordinated activities of several other cell types, also has supporting environmental factors set up like the oxygen tension and blood pressure [62] within its milieu that assists tumours in their growth and metastasis. Tumour cells have been speculated to survive by simple diffusion of oxygen and nutrients up to 2 mm diameter [63]. Once they start growing, their needs to survive and propagate increases and hence recruits other stromal cells for the construction of blood vessels and form their own microenvironment. Stromal cells are non-transformed, genetically stable cells and targeting them will not make them resistant to treatments like in the case of tumour cells [20]. The first mark of interaction

between stromal and tumour cells was found in 1863 by Rudolf Virchow when the leukocytes were found infiltrated in tumour tissue (reviewed in [64]). Tumour microenvironment is dynamic, continuously keeps changing and evolving to support the progression of tumours by stromal cell signalling between themselves and the tumours.

Endothelial cells, associated with tumours are one of the main stromal cell populations in the tumour microenvironment and are essential for tumour angiogenesis, as Judah Folkman first proposed in 1971 [65]. Two types of angiogenesis occur in tumour microenvironment – the blood vessel formation and lymphangiogenesis [66]. Tumour vasculature is formed from the endothelial cells, but also with the support of other stromal cells like pericytes, mesenchymal cells, myeloids, macrophages and CAFs, while some of them even release pro-angiogenic factors. Formation of vasculature system is imperative not only for the growth and survival of tumours in the primary tumour environment, but also serves for cancer cell dissemination during metastasis and seeding at secondary sites, with the help of other stromal cells and pro-angiogenic factors, controlled by the tumours themselves [67]. Thus it is important to understand the mechanism and cellular regulations underlying the induction of angiogenesis in order to look for therapeutic strategies targeting both stromal and tumour cells.

1.1.3.2. Tumour angiogenesis

During the process of tumour angiogenesis the delicate balance of pro- and anti-angiogenic factors, which maintains a mature blood vessel network, is disturbed, enabling over-production of pro-angiogenic factors. Moreover the tumour blood vessels formed appear tortuous, leaky and are unorganized [68,69]. Pericytes, that maintain vessel integrity, are not well attached to the tumour vessels, resulting in irregular and even reverse blood flow. Furthermore the changes have been noted even in the cellular phenotype, where unlike normal endothelial cells, tumour endothelial cells are irregular in size and shape, with ruffled margins, long and fragile cytoplasm that projects across vessel lumen leaving intercellular gaps where erythrocytes pool up making 'blood lakes' [70]. Tumours expressing VE-cadherin are found to be capable of filling these cellular gaps and mimicking as endothelium [71]. Metastasis incidence is found higher in

leaky vessels and anti-VEGF treatment has shown to normalize the tumour vessels, improving oxygen flow and reducing metastasis [25], in addition to aiding proper delivery of chemotherapeutic drugs [72]. The formation of blood vessels is induced by the angiogenic factors like VEGF, FGF, ANG1 and ANG2 released by the tumour and stromal cells, mediated by the hypoxic microenvironment [73] which is also a key regulator of angiogenesis.

1.1.3.2.1. Hypoxia, the key regulator of tumour angiogenesis

Hypoxia is an environment of low oxygen tension prevalent within the milieu of tumour microenvironment [62]. The oxygen partial pressure (pO_2) levels across the body ranges from 21% in the upper airway to 1% in the retina [74]. Though it is widely believed that endothelial cells are always in close contact with oxygen during blood flow, it must be noted that they can also become hypoxic during events, like the vessel formation through hypoxic regions of tumours, tissue ischemia and in veins that predominantly carry non-oxygenated blood [25,75]. The hypoxia regulating proteins, the hypoxia inducible factors – HIF1 α and HIF2 α are DNA-binding factors that heterodimerise with HIF1 β and bind to the hypoxia response element in the promoter of certain genes under hypoxia [76,77]. While these HIF proteins are expressed under hypoxia, they are degraded in the presence of oxygen by the process of hydroxylation by PHD's (PHD1, PHD2 and PHD3 – the three isoforms expressed in endothelial cells) and asparagine-hydroxylase factor inhibiting HIF1 α (FIH) which then interacts with the Von-Hippel Lindau (VHL) tumour suppressor protein that mediates HIF ubiquitination and degradation [78]. The HIF proteins are also regulated by the signalling cascades such as the PI3K/AKT/mTOR cell cycle regulating pathway and the MAPK cell surface receptor to DNA signalling pathway [79]. The HIF-regulated genes related to tumour growth are involved in metabolism, angiogenesis and metastasis. These include the genes expressed by tumours under hypoxia such as the glycolytic genes, GLUT1, GLUT3, PDK1, PKM2, PFKFB3, GYS1, ENO1, LDHA, HK2 and GAPDH [80], angiogenic genes, VEGF, FLT-1, ANG1, ANG2, TIE2, PDGF, MMP2, MMP9 and FLK1 [80,81] and tumour invasion and metastasis related genes such as c-Met, CXCR4, RIOK3 and LOX [82]. In the tumour microenvironment, hypoxia not only attracts endothelial cells but also other stromal

cells by the over-expression of monocytic chemotactic proteins, VEGF, semaphoring 3A and interleukin 1 [83].

Under hypoxia HIF1 α is stabilized and is essential for angiogenesis and tumour re-oxygenation [84], while HIF2 α can activate transcription at normoxia also and is important for vessel maturation [85]. Hypoxia induces the VEGF production by tumours and other stromal cells, which in turn activates the VEGF receptor VEGFR2 in endothelial cells following the activation of tip and stalk cells and related signalling pathways, for angiogenesis. As the tip cells migrate towards the hypoxic regions HIF1 α remains stabilized while the PHDs and FIH are inactivated, necessary for inducing VEGF and VEGFR2 [84]. As slowly the oxygen tension rises, HIF2 α mediates the transcription of VE-cadherin and VEGFR1 for vessel stability [86]. These PHDs, FIH1 and HIF hypoxia regulatory proteins are also regulated by other factors like FGF and EGF that stabilize HIF2 [87]. It was shown that targeting the gene PHD2, stabilized HIF2 protein and inhibited cancer cell intravasation, reduced vessel permeability and hypoxia while increasing perfusion and improved the delivery of chemotherapeutic drugs through the blood flow [88]. Thus hypoxia, being a promoter of tumour angiogenesis, can be an efficient therapeutic target for inducing HIF-stabilized vessel maturity, reducing the hypoxic areas in tumours and in turn reducing acidic environment, as well as reducing metastasis of cancer cells.

1.1.4. Anti-cancer therapies targeting angiogenesis

Until date, anti-cancer therapies based on anti-angiogenic strategies, that have been clinically approved and in use, are focussed on targeting angiogenic receptor ligands and inhibiting the signalling pathways that are involved in inducing angiogenesis [89-92]. One of the first anti-angiogenic treatments developed was bevacizumab, which is a monoclonal antibody targeting VEGF-A against binding with receptors VEGFR1 and VEGFR2, that was clinically approved for metastatic colorectal cancer in combination with chemotherapy, [93-95]. Bevacizumab was approved further for the treatments of non-squamous non-small cell lung cancer, metastatic renal cell carcinoma, glioblastoma multiforme and advanced cervical cancer [95]. Although it showed an improvement in progression free survival, it had not elevated the overall survival

rate and in addition caused many adverse effects such as hypertension, nosebleed and rectal haemorrhage [96]. Similarly, other angiogenic inhibitors under light are aflibercept that targets VEGF-A, -B and PlGF ligands, and showed improvement in overall survival rate in phase III clinical trials of metastatic colorectal cancer patients [97], and ramucirumab targeting VEGFR2 and approved as monotherapy or in combination with paclitaxel for advanced gastric cancer or gastro-oesophageal junction adenocarcinoma [98,99]. Treatments targeting multiple signalling pathways and angiogenic receptor ligands were also developed and clinically approved because of the resistance developed for treatments targeting single angiogenic factors or receptors, in addition to the resulting adverse effects [100-102]. Some of the multi-targeting drugs approved are sorafenib, sunitinib, axitinib, pazopanib, cabozantinib, vandetanib, regorafenib and nintedanib, focussed on simultaneously targeting multiple signalling pathways belonging to VEGF family, FGF and other proteins, receptors and oncogenes such as c-Met, RET, c-Kit, TrkB, etc [92,103,104]. This multiple target strategy has shown effective anti-angiogenic and anti-tumour effects by mechanisms such as endothelial apoptosis, reduction of vessel density, vessel permeability and integrity and delaying tumour growth and preventing metastasis. The multi-target strategy has shown positive effects for improving progression-free survival of cancer patients, but they have not shown effective improvements in overall survival rates and are not completely free from adverse side effects. Moreover, these treatments vary according to the types of cancers being tested and have shown effective response only for those types like the renal cell carcinoma, hepatocellular carcinoma, non-small cell lung cancer and ovarian cancer which were used for developing these drugs [103]. Whereas some other types of cancers like the breast, pancreatic and prostate cancers have either shown resistance or much more adverse effects to the anti-angiogenic treatments targeting molecular signalling pathways [103,105]. Anti-angiogenic therapy based on vascular disrupting agents such as combretastatin A-4 phosphate (zibrestat), which work by reducing revascularization by targeting highly proliferating endothelial cells and reducing tumour perfusion, was tested alone and in combination with bevacizumab in pre-clinical and clinical studies, but also had considerable side-effects [106,107].

One of the anti-angiogenic therapeutic responses identified was the induction of hypoxia within

the tumours due to the blood vessel decrease [108-110], which in turn induces an adaptive resistance of upregulating pro-angiogenic molecules and increasing blood vessel formation [111]. Hypoxia increases acidity in the tumour microenvironment by upregulating lactate production, forcing a metabolic shift towards glycolysis [112]. In addition significant metabolic changes have been associated as responses to anti-angiogenic treatments [113]. In a xenograft glioblastoma tumour model with bevacizumab treatment, an upregulation of glycolytic and pentose phosphate pathway (PPP) genes and downregulation of those that regulate oxidative phosphorylation (OXPHOS) were observed [114]. In a similar study, an increase in the expression of fatty acid binding proteins, FABP3 and FABP7, that are responsible to accumulate lipids during hypoxia, were observed in the *in vivo* model of human U87 glioblastoma cells [115]. Increase in lipid metabolism and tricarboxylic acid cycle (TCA cycle) in the tumour models were attributed to the post-treatment response of anti-angiogenic therapy [114,116]. These studies show that the metabolic responses to the existing anti-angiogenic or anti-cancer treatments can be explored as alternative therapeutic strategies to use in combination for targeting tumour angiogenesis. In fact, some studies have proven the effectiveness of metabolic targets in reducing angiogenesis and tumour growth. The use of dichloroacetate (DCA), an inhibitor of pyruvate dehydrogenase kinase (PDK), along with bevacizumab in glioblastoma increased OXPHOS [114]. In addition DCA with sorafenib treatment of hepatocellular carcinoma reduced lactate, increasing reactive oxygen species (ROS) and ATP levels while overcoming the resistance to sorafenib [117]. Successful therapeutic studies based on metabolic targets against tumour angiogenesis has been shown by metformin, which is a metabolic drug used for treating type 2 diabetes and is under phase II clinical trials in combination with bevacizumab for metastatic pulmonary adenocarcinoma and other types of cancers [111]. These studies show that anti-angiogenic treatments are still a long way from reducing tumour growth without much adverse effects or reaching treatment resistances. Exploring alternative strategies like the direct metabolic adaptations of tumours and associated blood vessels and metabolic adaptations in response to anti-angiogenic or anti-cancer treatments can further help in developing stronger combination therapies. To achieve that it is imperative to understand the endothelial cell and tumour cell metabolisms and explore their similarities and differences.

1.2. Endothelial cell metabolism

Many studies have shown sufficient understanding about the molecular mechanisms and the cell signalling pathways during the induction and process of angiogenesis, while metabolic pathway responses in endothelial cells to angiogenic signals and tumour microenvironmental cues are yet to be completely understood. In this section recent studies on endothelial cell metabolism has been covered (as illustrated in Figure 1.1), relating the metabolic pathways as driving factors or responses to angiogenic processes.

Endothelial cells are reported to be highly glycolytic, especially when activated for proliferation and migration [118,119]. The importance of glycolytic pathway for endothelial cell survival and function is highlighted by reducing this flux with 2-deoxy-D-glucose by 80% which in turn reduced endothelial cell viability [119]. In addition VEGF activation has shown to increase the expressions of glucose transporter GLUT-1 under hypoxia [120] and of glycolytic enzymes like lactate dehydrogenase-A (LDH-A) and 6-phosphofructo-2-kinase/fructose-2,6-bisphosphatase-3 (PFKFB3) [119,121]. It is also shown that silencing PFKFB3 impairs *in vitro* proliferation, migration and sprouting of endothelial cells and causes impaired angiogenesis *in vivo* in mice [119]. The preference to glycolysis for the ATP production is shown to be relevant especially in endothelial cells with filopodia as they need quicker form of energy needs for migration [119].

Although it is shown that the mitochondria in endothelial cells take up only 4% of the intracellular space, while this amounts to 28% in hepatocytes [122] and endothelial cells have been reported to be glycolytic for ATP production, there are evidences that suggest mitochondrial oxidation could be valuable for these cells in a number of ways. First of all, during conditions of laminar sheer stress due to the frictional force created by the blood flow in blood brain barrier, or when glycolysis is impaired [123,124]. In addition the mitochondrial ROS in endothelial cells, at non-toxic levels have shown to stimulate angiogenesis by upregulating VEGF and VEGFR2 signalling [125,126]. Mitochondrial release of cytochrome c for inducing apoptosis during vessel regression has also been reported in endothelial cells [127,128]. VEGF has also shown activation of peroxisome proliferator-activated receptor- γ coactivator-1 α (PGC-

1α), a master regulator of mitochondrial biogenesis and OXPHOS, in endothelial and other cell types [129], while PGC-1α expression stimulates vascularisation in heart and muscle cells [130].

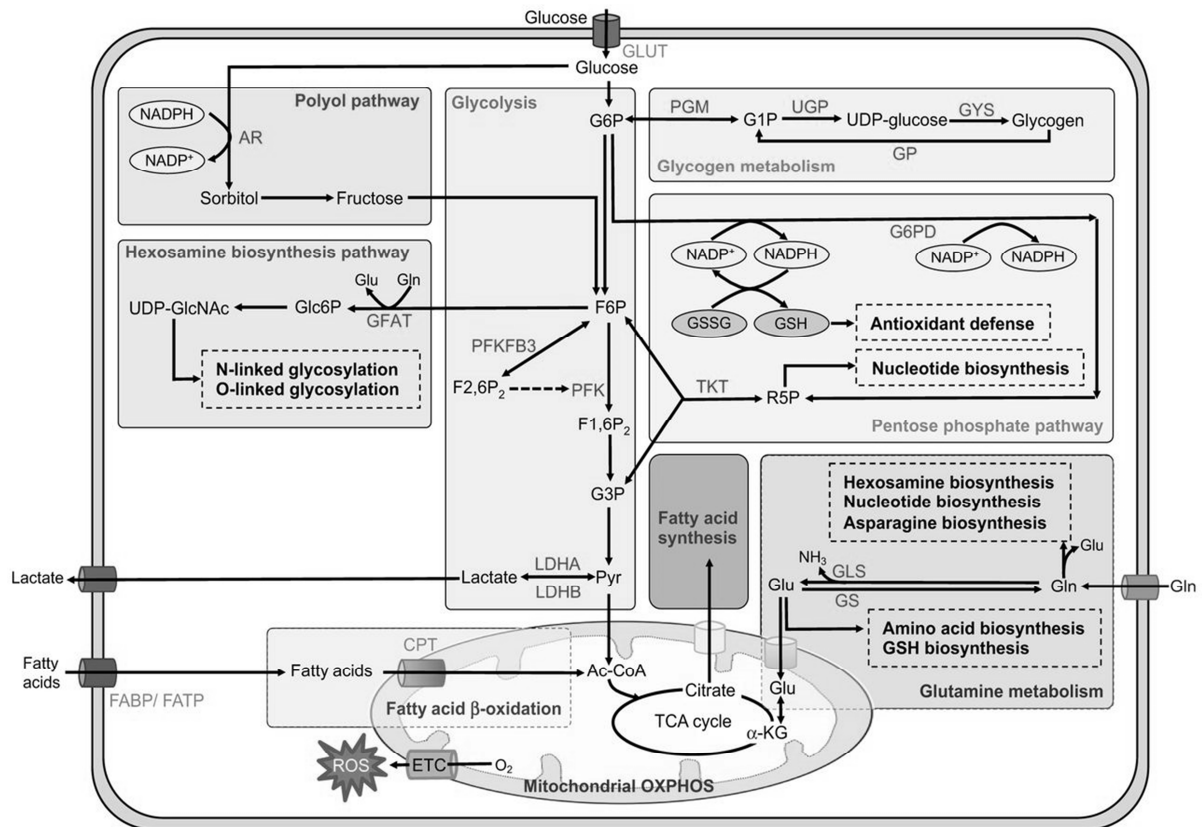


Figure 1.1: Metabolic pathways of endothelial cell. An illustration of the metabolic pathways studied so far in endothelial cells, with influx and efflux of metabolites and cellular responses. The metabolic changes studied in endothelial cells mainly covers pathways such as glycolysis, mitochondrial oxidation and ROS production, fatty acid uptake and oxidation, PPP covering the oxidative and non-oxidative branches, glycogen metabolism, amino acid metabolism, hexosamine biosynthesis and polyol pathway. α -KG - α -ketoglutarate; Ac-CoA - acetyl coenzyme A; AR - aldolase reductase; CPT - carnitine palmitoyltransferase; ETC - electron transport chain; F1,6P₂ - fructose-1,6-bisphosphate; F2,6P₂ - fructose-2,6-bisphosphate; F6P - fructose-6-phosphate; FABP - fatty acid binding protein; FATP - fatty acid transport protein; G1P - glucose-1-phosphate; G3P - glyceraldehyde-3-phosphate; G6P - glucose-6-phosphate; G6PD - glucose-6-phosphate dehydrogenase; GFAT - glutamine fructose-6-phosphate amino-transferase; Glc6P - glucosamine-6-phosphate; Gln - glutamine; GLS - glutaminase; Glu - glutamate; GP - glycogen phosphorylase; GLUT - glucose transporter; GS - glutamine synthetase; GSH - glutathione; GSSG - glutathione disulfide; GYS - glycogen synthase; LDH - lactate dehydrogenase; OXPHOS - oxidative phosphorylation; PFK - phosphofructokinase; PFKFB3 - phosphofructokinase-2/fructose-2,6-bisphosphatase isoform 3; PGM - phosphoglucomutase; Pyr - pyruvate; R5P - ribose-5-phosphate; ROS - reactive oxygen species; TKT - transketolase; TCA - tricarboxylic acid; UDP-GlcNAc - uridine diphosphate-N-acetylglucosamine; UDP-glucose - uridine diphosphate glucose; UGP - UDP-glucose phosphorylase. Copyrights: Stapor *et. al.*, 2014, licensee: Company of Biologists Ltd.

The PPP has two main branches, the oxidative branch for generating NADPH to maintain redox homeostasis and non-oxidative branch to generate macromolecules for supporting cellular proliferation. The PPP in endothelial cells have mostly been reported to play a protective role against oxidative stress. They have shown to upregulate the enzyme glucose-6-phosphate dehydrogenase (G6PD) that catalyzes the oxidative branch of PPP and in turn increasing NADPH and nitric oxide (NO) that protect the cells from ROS damage [131]. In diabetes-related vascular endothelial cells the high glucose-mediated impediment of G6PD activity and the resulting cell death due to increased ROS levels has shown to be reversed by restoring G6PD activity [132,133]. While G6PD increase has shown to promote VEGF-induced angiogenesis, contrarily VEGF stimulation has been reported to increase G6PD activity in endothelial cells [134]. Interfering either the oxidative or non-oxidative pathways, by inhibiting G6PD or transketolase (TKT) has shown reduced in vitro endothelial cell proliferation and migration [135].

Fatty acids can be efficient energy storage compounds and endothelial cells have been reportedly taking up free fatty acids circulating in the blood [136]. In addition VEGF-A has shown to induce fatty acid uptake [137] and VEGF-B upregulates fatty acid transport proteins 3 and 4 in endothelial cells [138,139]. On the other hand, fatty acid oxidation is shown to be favoured by endothelial cells in the absence of glucose [140], in contrast high glucose levels have also shown to increase fatty acid oxidation [141]. While the purpose of fatty acid oxidation in endothelial cells was not known for a long time, a recent study showed that this metabolism is used for DNA synthesis and cellular proliferation during angiogenesis and not preferably for redox homeostasis or energy production [142]. When the enzyme carnitine palmitoyltransferase-1 (CPT1), that transports fatty acids to mitochondria for oxidation, was silenced in endothelial cells it showed reduction in cell proliferation in vitro and higher permeability of endothelial cell monolayers causing leaky blood vessels in vivo [143]. Also studies using ¹³C tracer-based experiments in endothelial cells showed that fatty acids were used for generating nucleotides through salvage pathways [142].

Amino acid metabolism is still not very well studied and remains unclear in its role in angiogenesis. Endothelial cells have shown to take up glutamine through the amino acid

transporter SLC1A5 and system N family of amino acid transporters [144] and have shown to produce glutamine from glutamate during nutrient starvation [145]. Knocking down of glutaminase activity, that converts glutamine to glutamate in endothelial cells, has shown to inhibit endothelial cell proliferation and induction of senescence-like cellular state [146]. On the other hand, smaller changes in additional metabolic pathways of endothelial cells have been recognized. In the hexosamine biosynthesis pathway, another branch of glycolysis, the conversion of fructose 6-phosphate into glucosamine 6-phosphate which is then metabolized to uridine diphosphate N-acetylglucosamine, a substrate for glycosylation reactions, has been found to be important for cell signaling aspects in endothelial cells [147]. In the polyol pathway aldose reductase produces sorbitol from glucose utilizing NADPH. Deficiency of aldose reductase has shown to reduce the excess angiogenesis in vascular retinopathy [148] and decrease VEGF-induced angiogenesis [149].

Metabolism of glycogen in endothelial cells is yet to be explored and the presence of glycogen have been reported in very few studies [150-152]. Some evidences have been observed from preliminary studies with human umbilical vein endothelial cells (HUVECs) in our laboratory, showing that glycogen reserve and metabolism may be important for angiogenic processes of the endothelial cells. Glycogen is found completely utilized when glucose is depleted under normoxia but is found to be conserved under hypoxia. In addition, flux analysis of the ¹³C labelling patterns in glucose-derived glycogen in endothelial cells have shown that there could be an active turnover of glycogen and could be related to endothelial cell survival observed from the *in vitro* experiments with glycogen phosphorylase (GP) enzyme inhibitor [135].

While it is important to understand the metabolic pathways in endothelial cells and changes caused during angiogenesis, comparing them with the metabolic pathways in tumours can provide us with common pathways that could be explored as therapeutic strategies against cancer and tumour angiogenesis.

1.3. Endothelial cell metabolism vs. cancer cell metabolism

Our understanding of the signalling pathways in blood vessel formation have shown some powerful targets, based on targeting pro-angiogenic factors like VEGF, to reduce tumour angiogenesis and cause cancer regression. But eventually these therapies have proven inefficient in completely stopping the tumour growth due to development of therapeutic resistance and causing cancer relapse [20], probably switching to alternative mechanisms for blood vessel formation. Even if pro-angiogenic pathways other than those related to VEGF may be upregulated by cancer cells with anti-VEGF therapy, all angiogenic regulations end up in metabolic changes which are the downstream responses to such signalling pathways. Thus in the recent years endothelial cell metabolism has been explored in finding alternative targets for reducing endothelial proliferation and angiogenesis [153]. Figure 1.2 shows the general metabolic pathways of cancer cells and endothelial cells, illustrating the similarities between the metabolic characteristics in both the cells, in order to explore therapeutic clues for targeting both types of cells as an anti-cancer strategy.

Cancer cells are known to be highly glycolytic, displaying Warburg effect even in the presence of oxygen and producing high lactate in its environment [154]. They show elevated expression of PFKFB3, inducing PFKFB3-driven glycolysis for proliferation [155,156]. As discussed in the previous section, endothelial cells are also reported to be highly glycolytic, especially in the migratory tip cells [157] and VEGF stimulation has shown to upregulate the expression of PFKFB3 whose inhibition causes decreased vessel sprouting and branching [119,158]. In the highly glycolytic tumour microenvironment cancer cells competitively utilize glucose, producing a huge amount of exogenous lactate and leaving the stromal cells to exploit the lactate or other sources of energy. Endothelial cells reportedly showed higher expression of monocarboxylate transporter 1 (MCT1) which enables lactate influx into the cells [159] and an upregulation of LDH-B, that enables exogenous lactate to enter into cellular metabolism, by tumour endothelial cells [160]. In some cases lactate is shown to be pro-angiogenic, where lactate-induced angiogenesis through endothelial MCT1 was observed in tumours [161].

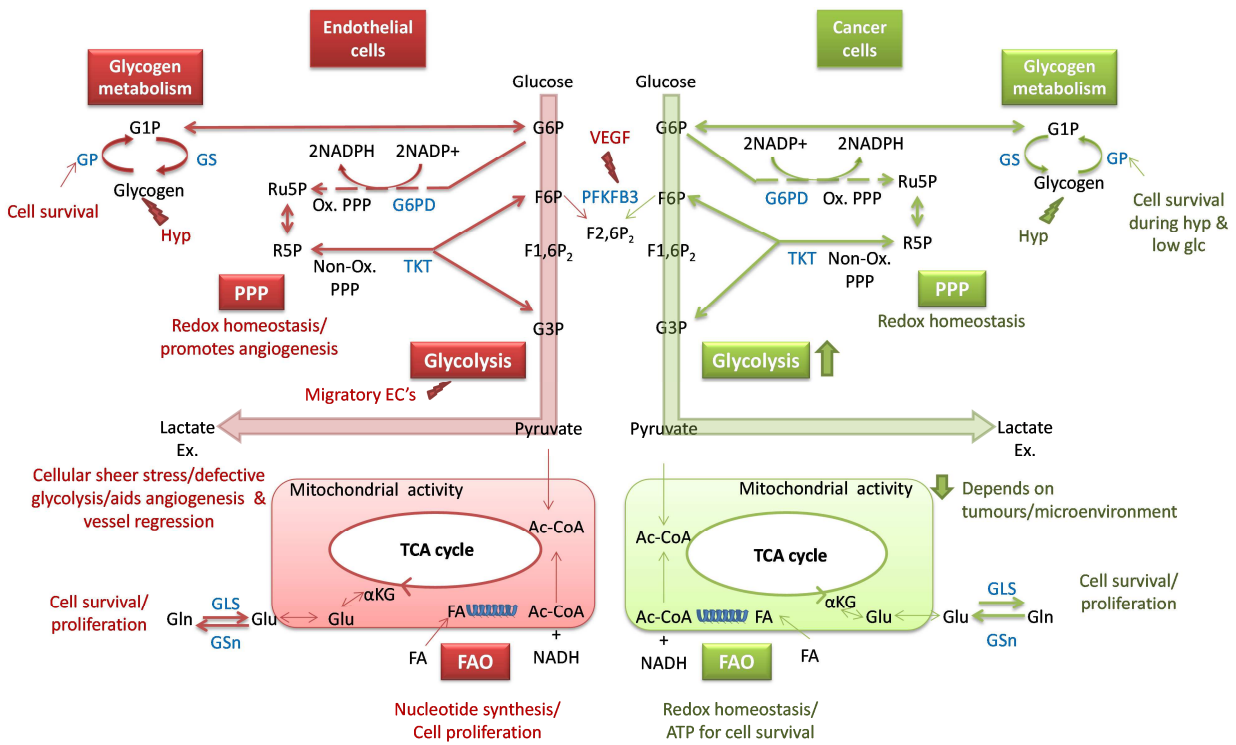


Figure 1.2: Endothelial and cancer cell metabolism. The metabolic pathways that show similarities between endothelial and cancer cells are illustrated, in addition to the known cellular functions linking each of these pathways. Glycolysis is upregulated both in endothelial and cancer cells, especially in the migratory endothelial cells. Glycogen degradation is important for both endothelial and cancer cell survival, especially during hypoxia and low glucose conditions in cancer cells. PPP aids in redox homeostasis in both endothelial and cancer cells, while also promoting angiogenesis. Mitochondrial activity is upregulated in endothelial cells during cellular mechanical stress and defective glycolysis and helps in endothelial apoptosis during vessel regression, while low levels of mitochondrial ROS induces angiogenic signalling. In the case of cancer cells though mitochondrial activity is found to be generally lower, it is found to change depending on the type of tumour and environmental conditions. The conversion of glutamine to glutamate is important for both endothelial and cancer cell survival and proliferation. Fatty acid oxidation was found to contribute to nucleotide synthesis and cell proliferation in the case of endothelial cells, while it aids in redox homeostasis and ATP generation for cancer cell survival. For clarity purposes only the main reactions and metabolites that have shown commonalities between the cell types are shown in this figure and enzymes are highlighted in blue. α KG – α -ketoglutarate, Ac-CoA – acetyl-CoA, F1,6P₂ - fructose 1,6 bisphosphate, F2,6P₂ - fructose 2,6 bisphosphate, F6P - fructose 6-phosphate, FA - fatty acid, FAO – fatty acid oxidation, G1P – glucose-1-phosphate, G3P – glyceraldehydes-3-phosphate, G6P – glucose-6-phosphate, G6PD - glucose-6-phosphate dehydrogenase, glc – glucose, GLS - glutaminase, GP – glycogen phosphorylase, GS – glycogen synthase, GS_n - glutamine synthetase, hyp – hypoxia, Lactate Ex. – extracellular lactate, NADH – nicotinamide adenine dinucleotide (reduced), NADP⁺/NADPH – nicotinamide adenine dinucleotide phosphate (oxidised/reduced), Non-Ox. PPP – non-oxidative branch of PPP, Ox. PPP – oxidative branch of PPP, PFKFB3 - 6-phosphofructo-2-kinase/fructose-2,6-bisphosphatase-3, PPP - pentose phosphate pathway, R5P - ribose 5-phosphate, Ru5P - ribulose 5-phosphate, TCA - tricarboxylic acid, TKT - transketolase.

On the other hand, mitochondrial respiration and its preference for ATP production is, in general, less active in cancer cells [81], though in some cases the mitochondrial activity is found

upregulated [162], while in endothelial cells mitochondrial respiration has shown to be favoured during sheer cellular stress and when glycolysis is compromised [123,124], as discussed in the previous section. Oxidative PPP is found important for both cancer cells and endothelial cells for redox control during stressful conditions in both the cell types while in endothelial cells PPP is also used to promote angiogenesis [135,163]. Fatty acid metabolism is also found important in both the cell types where cancer cells have shown to use fatty acid oxidation for redox homeostasis under stressful conditions and for generating ATP for survival [164], while in contrast the endothelial cells have shown to use fatty acids for nucleotide synthesis, for cell proliferation, and not significantly for redox homeostasis [142] and they have not been reported to rely on fatty acid oxidation for ATP production [119]. On the other hand, glutamine is necessary for cancer cell survival and proliferation [165], while in endothelial cells glutaminase inhibition and thus inhibiting the conversion of glutamine to glutamate inhibits its proliferation and induces senescence [146].

In the case of glycogen metabolism, cancers related to breast, kidney, uterus, bladder, ovary, skin and brain were found to accumulate varying and high amounts of glycogen [166]. A type of clear cell carcinoma (neoplasms having clear cytoplasm) of the breast cancer was found to be rich in glycogen granules and have shown high lymphangiogenesis and extremely aggressive behaviour [167]. In addition it was reported in many studies that hypoxia induces glycogen accumulation in cancer cells. Upregulation of glycogen synthesis was found to be regulated by HIF1 α /HIF2 α activation and stabilisation in cancer cells [168,169] and upregulates muscle isoform of glycogen synthase (GS) enzyme [169-171]. In the case of endothelial cells, glycogen was found to be conserved during hypoxia more than under normoxia and it was speculated that glycogen metabolism could be important for cellular survival [135]. The similarity of the higher glycogen content under hypoxia by both cancer and endothelial cells show that glycogen synthesis under hypoxia could be an important therapeutic target to be explored for tumour angiogenesis.

These studies show that many metabolic pathways and responses in endothelial cells are common to those of cancer cells and some pathways such as the glycogen metabolism that has

shown significant changes in angiogenic functions and cancer cell survival remain uncharacterized. In order to study further on the unexplored area of glycogen metabolism, we intend to understand general characteristics and regulations existing in this pathway.

1.4. Glycogen metabolism as a key target for cancer therapy?

In the cancer cells glycogen content and proliferation rates are found inversely correlated to each other and glycogen breakdown is used for sustaining cancer cell growth [166,172]. In addition glycogen metabolism in cancer cells has been reported to play an important role to overcome stressful conditions like hypoxia and glucose deprivation and to maintain cellular proliferation [170]. Cancer cells have also been found to respond to hypoxic condition by increasing their glycogen levels and inducing a glycogen turnover [171,173,174]. Moreover, glucose deprivation in cancer cells have shown to deplete rapidly the glycogen accumulated by hypoxic-induction, while normoxic cells were found to lose viability upon glucose removal [174]. Glycogen metabolism has also been implicated to play a protective role during nutrient starvation in cancer cells and the importance of targeting GP, the key enzyme catalyzing the glycogen degradation pathway has also been reported in many studies. When pancreatic cell lines, with GP brain isoform gene knocked down, were treated with 2-deoxy glucose, an inhibitor of glycolysis and glucose utilization, it resulted in cell death, reiterating the importance of glycogen utilization and also the brain isoform of GP during glucose starvation [175]. In addition, depletion of GP enzyme in cancer cells is found to reduce cell proliferation with concomitant reduction in PPP flux and increase in ROS production [170,176]. In gastric cancer cell line increased activity of brain isoform of GP and glycogen breakdown was observed to reduce cancer cell apoptosis upon serum starvation [177].

Multiple uses of glycogen metabolism in cancer cells have been proposed, in account of previous studies, in Zois *et. al.*, where it can be used for generating ATP, biosynthesis of macromolecules for cell proliferation or ROS scavenging through PPP. On the other hand, while acute hypoxia can increase glycogen accumulation, prolonged hypoxia and/or starvation can

induce glycogen degradation through increased GP expression which provides energy to the cells and protects from ROS [170,178,179]. Thus under hypoxia, glycogen reserves in cancer cells seem to play an important role for cellular protection. Furthermore it was shown that while hypoxia markedly increased glycogen levels of cancer cells *in vitro*, treatment with the anti-angiogenic drug bevacizumab [180], in an *in vivo* glioblastoma xenograft model upregulated the glycogen regulating genes and the hypoxia marker CA9 [170]. It has to be noted that anti-angiogenesis treatment indeed would create a hypoxic microenvironment within the tumour by disrupting the blood vessels and oxygen delivery to cancer tissues, and when this event is correlated with the upregulation of glycogen levels it opens a therapeutic window of targeting glycogen metabolism in combination with anti-angiogenic therapy in treating cancer. Thus the reported studies also show that glycogen accumulation and metabolism in cancer could be related to the hostile environment it is exposed to. The tumour microenvironment is mostly deprived of oxygen and nutrients and the cancer cells are subjected to constant stressful conditions. Rapid ATP production by glycolysis and a readily-available source like glycogen could be an immediate resolution for cellular survival [178], which could be an important anti-cancer strategy to exploit in the future.

Interestingly some anti-cancer therapies that are under clinical trials have either shown apparent changes in glycogen metabolism within the tumour or have had a history of glycogen metabolic changes reported in other cell types. For example, lithium which has shown changes in glycogen metabolism in several cell types like astrocytes, rat liver and salivary glands [181-183], is under clinical trials for testing against prostate cancer (NCT02198859). In addition to its effects on glycogen metabolism in normal cells, lithium has shown to inhibit glycogen synthase kinase - 3β (GSK- 3β) and affect growth in tumours such as ovarian cancer [184,185], endometrial cancer [186], gliomas [187], neuroendocrine tumours [188], leukemia cells [189], colorectal cancer cells [190] and prostate cancer [191,192]. Another drug valproate is under clinical trials in combination with bevacizumab for advanced cancers (NCT01552434) and it was implicated for the upregulation of PYGB, the brain isoform of GP, and decrease in glycogen accumulation in the skeletal muscles in McArdle's disease, a glycogen storage disorder [193]. In addition, the type 2 diabetes drug metformin, as discussed in the section 1.1.4, is under clinical

trials for cancer therapy in combination with other anti-cancer and anti-angiogenic drugs and it has been observed that this drug stimulates the glycogen utilization in myeloid leukaemia cells and in lung, prostate and breast cancer cell lines [194,195]. These studies prove that anti-cancer therapies influence the glycogen metabolism, and in turn targeting glycogen metabolism can affect the cancer cell viability especially when combined with other strategies like inducing hypoxia and depleting nutrient sources. Thus glycogen metabolism can be a novel therapeutic target for treating cancers and can prove to be an effective strategy when combined with anti-angiogenic or other conventional anti-cancer treatments.

1.5. Glycogen metabolism and its regulation

Glycogen is a glucose storage form in animals, which is made of polymers of glucose attached to the protein glycogenin and is primarily cytosolic. An equivalent form of glucose polymer is stored in plants in the form of starch [196]. Liver and muscle are the major glycogen storage tissues in the body and their metabolisms have been studied extensively, while research has also revealed the importance of glycogen metabolism in brain function and survival during stressful conditions [197-199]. Other cells that are known to metabolize glycogen are kidney, heart and fat tissues [200-203]. It is reported that the first discovery of glycogen, in liver tissues, was around 160 years ago in 1857 by Claude Bernard [204]. Liver uses its glycogen to maintain blood glucose homeostasis, that is, it mainly stores glucose to release it to the neighbouring tissues when glucose is deprived, while skeletal muscle uses glycogen for its own energy requirements during extreme activities or 'fight or flight' response. In the brain tissues both astrocytes and neurons have been found to store little glycogen but possess an active metabolism, the former has been speculated to use the metabolism as an altruistic purpose to provide substrates for neurons, while the latter uses it to protect brain function from hypoxic damage [197,205,206].

The structure of glycogen consists of a central glycogenin protein to which glucose units are attached linearly by $\alpha(1-4)$ -glycosidic bonds and the branches are attached by $\alpha(1-6)$ -glycosidic

bonds, as shown in Figure 1.3a. An accepted model of glycogen molecule consists of inner B-chains with two branch points each and outer A-chains with no branches (Figure 1.3b). Mathematical modelling suggested that the observed average length of about 13 glucose residues per branch in mammalian glycogen is optimal for glucose storage and mobilization [207-209]. The molecule is not just composed of glucose moieties but also associated with various proteins like glycogenin, the enzymes GS, GP and the debranching enzyme (DBE), regulatory proteins such as phosphorylase kinase, protein phosphatase IG family and the β -subunit of AMP-activated protein kinase (AMPK) [210,211].

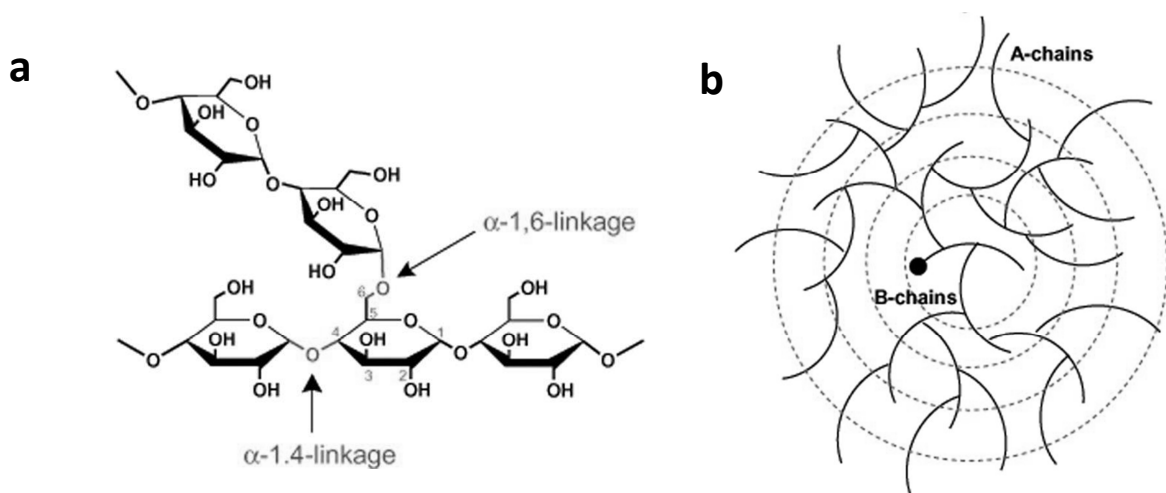


Figure 1.3: Structure of glycogen. (a) Glucose moieties are linked by α -1,4-glycosidic bonds linearly and by α -1,6-glycosidic bonds at the branching points. (b) The glycogen structure showing a tiered model of inner B-chain, connected to glycogenin (black circle) and outer A-chains, with B-chain proposed to carry two branches on an average and the outer A-chains remain unbranched. Copyrights: Roach *et al.*, 2012, licensee: Portland press Ltd.

The metabolism of glycogen, illustrated in Figure 1.4, is mainly regulated by the rate-limiting enzymes – glycogen synthase and glycogen phosphorylase. GS catalyzes the formation of glycogen by the addition of UDP-glucose molecules to the glucose polymer and GP induces the breakdown of glycogen to glucose-1-phosphate (G1P). These enzymes are controlled by mechanisms such as covalent modification (phosphorylation/dephosphorylation) and allosteric regulation. The addition or removal of phosphate group can activate/deactivate the key enzymes, while the allosteric regulators regulate the phosphorylated/dephosphorylated forms of the enzymes [212-214]. Glycogen degradation is mediated by two other enzymes in addition to GP, where glycogen DBE removes the branches of the glucose moieties and makes way for

GP to act on the main chains and phosphoglucomutase (PGM) converts G1P generated by breaking down of glycogen to glucose-6-phosphate (G6P) [215] to enable it to enter glycolysis, PPP or gluconeogenesis. Also along the glycogen synthesis there are other enzymes involved in addition to GS, where UDP-glucose pyrophosphorylase converts UTP to UDP-glucose for use in glycogen synthesis and glycogen branching enzyme (GBE) mediates the formation of $\alpha(1-6)$ -glycosidic bonds at the branches [216]. Co-ordinated action of GS and GBE generates spherical forms of granular glycogen called β -particles that are $\sim 20-50$ nm in diameter and can have up to 55000 glucose units. β -particles can aggregate to form larger α -rosettes that are ~ 200 nm in diameter as seen in liver cells. This highly branched structure facilitates solubility in cytosol, providing many docking sites for the glycogen-binding proteins [178]. The rates of glycogen formation and breakdown depends on the rates of phosphorylation/dephosphorylation of the key enzymes and in turn are controlled by hormones like glucagon, insulin and epinephrin in liver and muscle tissues [217].

1.5.1. Regulation of glycogen phosphorylase

In mammals three isoforms of GP enzyme have been discovered – the liver isoform (molecular weight, 97 kDa) which mediates glycogen degradation for the glycaemic needs of the other neighboring cells, muscle isoform (97 kDa) and brain isoform (96.6 kDa) mediating glycogen utilization by the respective tissues for their own energy requirements. Many types of cells have been reported to express a variation of these isoforms of GP [218-220]. On the other hand, the function of GP enzyme depends on its activation state and as mentioned in the section 1.5, the GP enzyme is activated or inactivated by the mechanism of reversible phosphorylation, at a single site of phosphorylation at the N-terminus serine residue 14, and regulated allosterically at several GP sites [221]. The active or phosphorylated form of GP is represented as GP_a and the inactive or dephosphorylated form as GP_b. This reversible phosphorylation process involves a bicycle enzyme cascade system in which GP is phosphorylated to active GP_a form by the enzyme phosphorylase kinase, which is phosphorylated and activated by protein kinase A (PKA), also with Ca^{2+} , where PKA is activated

in the presence of the intracellular signalling molecule cyclic-AMP (cAMP). While the dephosphorylation and inactivation to GPb form occurs by protein phosphatase 1 (PP1) [212].

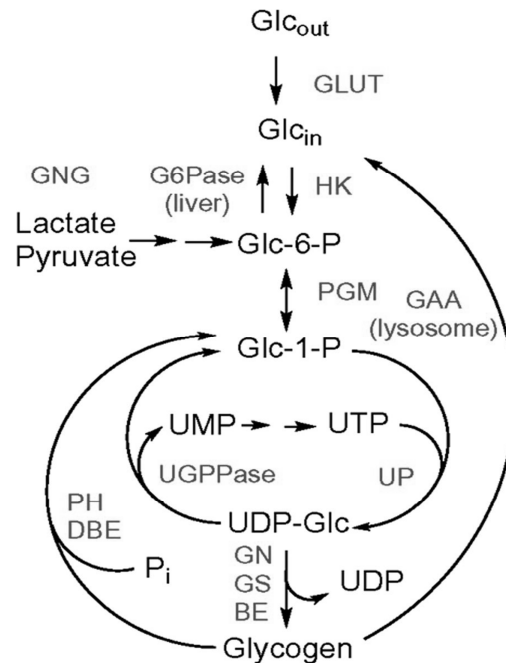


Figure 1.4: Glycogen metabolism. An illustration of the general metabolic pathways related to glycogen shows, the uptake of extracellular Glc_{out} by the cells by GLUT receptors, which in turn is converted to Glc-6-P and is subjected to a reversible conversion to Glc-1-P and then synthesis of glycogen is achieved by forming the intermediary UDP-Glc . Glycogen is degraded to Glc-1-P , which is converted to Glc-6-P either for generating ATP by further glycolysis or mitochondrial oxidation, or could be converted to Glc in the case of liver cells, which can also generate Glc from lactate or pyruvate by gluconeogenesis. Glycogen can also be degraded by lysosomal activity. BE - branching enzyme, DBE - debranching enzyme, GAA - lysosomal α -glucosidase, GNG - gluconeogenesis, Glc_{out} - extracellular glucose, Glc_{in} - intracellular glucose, GN - glycogenin, GS - glycogen synthase, G6Pase - glucose-6-phosphatase, HK - hexokinase, PH - glycogen phosphorylase, PGM - phosphoglucomutase, UGPPase - UDP-glucose pyrophosphatase, UP - UDP-glucose pyrophosphorylase. Copyrights: Roach *et al.*, 2012, licensee: Portland press Ltd.

Apart from the covalent modification, the GP enzyme is subjected to allosteric regulation by the effectors like ATP, AMP and G6P which are the intracellular sensors of the cellular metabolic state and cause conformational changes to GP_a or GP_b, thus converting them into more or less active states. The allosteric effectors can bind to several regulatory sites in GP such as the catalytic site, purine nucleotide inhibitor site, AMP site, glycogen storage site and the indole inhibitor site [221]. Both GP_a and GP_b exist in T (tense) and R (relaxed) states and switch from one form to another by the binding of the allosteric ligands. Normally the

equilibrium of GP_a favours the R-state and so it is usually active, and that of GP_b favours the T-state and is inactive. T-state is the less active form of GP having low affinity for the substrate, on the other hand, R-state is the active form of GP having greater substrate affinity [212].

Figure 1.5 illustrates the activation/inactivation of GP and GS, affected by phosphorylation/dephosphorylation mechanisms and allosteric effector binding regulating GP enzyme activity. The allosteric effectors induce the shift to T- or R-states of the GP depending on the enzyme isoform and the metabolic state of the tissues concerned. In the case of muscle isoform of GP, the GP_b is the most responsive form for inter-conversion between T- and R-states. Since the glycogen utilization in muscles is mainly for its own energy production, the transition between T- and R-states of the GP_b form depends on the levels of the energy substrates - AMP and ATP. AMP is found to be a potent activator of muscle and brain isoforms of GP, by favouring the R-state of GP_b and hence inducing the conversion of GP_b to GP_a form, increasing the activity of GP [221,222]. On the other hand, the GP_b form is shifted to a less active T-state in the presence of ATP which makes it completely inactive, while G6P also shows a feedback inhibition of GP_b by shifting it to the T-state. Glucose and caffeine are also found to stabilize the T-state of the enzyme [212,222,223]. While in the liver, since the glycogen metabolism is important for producing glucose for the neighbouring cells when blood glucose levels are low, and does not depend on its own energy requirements, the GP activation is not effective in the presence of AMP but reacts to the levels of glucose [223,224]. Glucose can shift the GP_a form of the liver isoform towards the T-state thus making it less active and conserving the glycogen content to utilize during starvation. Also caffeine has shown to act synergistic with glucose, and stabilize the T-state of the liver isoform of the enzyme [223]. In the case of brain GP, AMP has shown to be a potent activator like in the muscle isoform, while G6P has shown to be a weak inhibitor of GP_b, suggesting that brain isoform favours activators than inhibitors at the AMP catalytic site which normally binds both AMP and G6P [222,225]. In addition, while astrocytes co-express muscle and brain isoforms of GP [220], a recent study showed that the muscle isoform of GP responded to hormonal stimulation such as norepinephrine, whereas the brain isoform responded to an increase in AMP levels during glucose starvation, reporting the importance of GP regulation in astrocytes in brain [226].

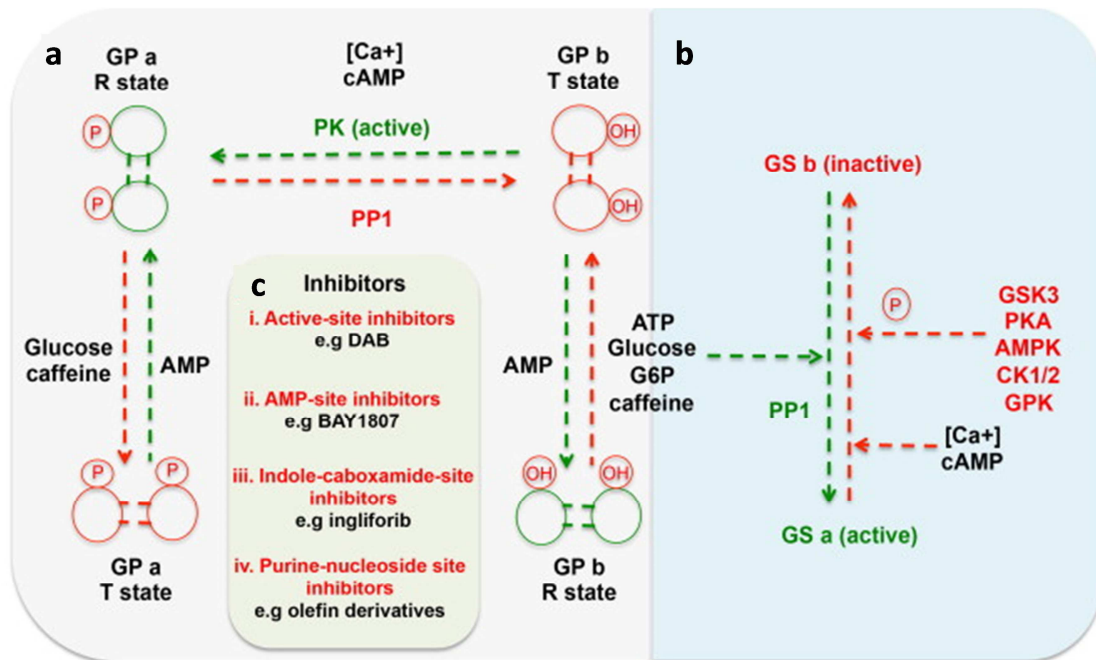


Figure 1.5: Glycogen phosphorylase and glycogen synthase enzyme regulation. The regulation of glycogen metabolism by GP and GS enzymes and by phosphorylation/dephosphorylation and allosteric regulators is shown. (a) The GP enzyme is converted to the active GP_a form by active PK phosphorylation and is converted back to GP_b inactive form by PP1 mediated dephosphorylation of the enzyme. GP_a and GP_b forms exist in equilibrium between the more active R-state and less active T-state. Allosteric effectors like AMP converts the T-state GP_a and GP_b to R-state GP_a and GP_b, respectively, thus activating them. Other effectors like glucose, caffeine, ATP and G6P convert the GP_a and GP_b forms to the less active T-state. (b) The GS enzyme activated to GS_a form by dephosphorylation with PP1, favoured by the allosteric effectors like ATP, glucose, G6P and caffeine. The conversion to inactive GS_b form is achieved by phosphorylation of GS involving GSK3, PKA, AMPK, CK1 and CK2 and GPK, while cAMP and Ca²⁺ favour the inactive GS_b form. (c) Major classes of GP inhibitors developed based on the binding sites in GP. AMP – adenosine monophosphate, AMPK – AMP-activated protein kinase, ATP – adenosine triphosphate, cAMP – cyclic-AMP, CK1 and CK2 – protein kinases, DAB - 1,4-dideoxy-1,4-imino-d-arabinitol, G6P – glucose-6-phosphate, GSK3 – glycogen synthase kinase 3, GP – glycogen phosphorylase, GPK – phosphorylase kinase, GS – glycogen synthase, PK – phosphorylase kinase, PP1 – protein phosphatase 1, PKA – protein kinase A, R-state – relaxed state, T-state – tense state. Copyrights: Zois *et. al.*, 2014, licensee: Elsevier.

1.5.2. Regulation of glycogen synthase

Two kinds of isoforms of GS have been identified – the liver isoform (molecular weight, 81 kDa) expressed predominantly in liver and the muscle isoform (84 kDa) expressed in many other cell types in addition to skeletal muscle. In contrast to GP, the enzyme GS has multiple phosphorylation sites, in which 9 different sites have been identified in muscle isoform near

N- and C-terminus out of which Ser⁷ (site 2), Ser⁶⁴¹ (site 3a) and Ser⁶⁴⁵ (site 3b) are confirmed as key regulators of the GS activity [227,228]. The liver isoform of GS has been reported to possess seven phosphorylation sites, homologous to that of the muscle isoform [229]. The phosphorylation takes place in a hierarchical manner [230] by kinases such as PKA, protein kinase C (PKC), protein kinases CK1 and CK2, phosphorylase kinase, GSK-3 and cAMP-dependent protein kinase (cAMPK) [231].

In the case of GS the cAMP cascade phosphorylates and inactivates the enzyme (GSb form), where either PKA or phosphorylase kinase can phosphorylate GS, whereas PP1 dephosphorylates, in turn activating the GS enzyme (GSa form) [217]. The phosphorylated/inactive GSb loses the affinity for the substrate UDP-glucose, while the allosteric activator G6P can make conformational changes to GS to make it a better substrate for PP1 to covalently dephosphorylate and convert the inactive GPb to the active GSa form (Figure 1.5) [232]. Insulin plays a role in inducing the activation of GS by activating the insulin receptor tyrosine kinase, which in turn activates PI3K and Akt pathway inhibiting GSK3 and activating PP1 that causes the dephosphorylation of GS [214].

1.5.3. Existing therapies targeting glycogen metabolism

Glycogen metabolism has been traditionally targeted for the metabolic disorder type 2 diabetes [233] using inhibitors developed for the enzymes regulating this metabolism such as GP or GSK3 β [233,234]. Many studies have indicated that targeting the enzymes regulating glycogen metabolism can also have beneficial effects in diseases other than diabetes, such as cancer [235,236], Alzheimer's disease [237] and stroke [238].

The two key enzymes modulating glycogen synthesis and degradation, GS and GP, respectively, can be efficient therapeutic targets that can directly affect the abnormal glycogen accumulation or utilization. No specific inhibitors for GS have been identified, speculated due to the complicated regulatory mechanism involved [178]. On the other hand, the enzymes GSK3 β and

AMPK, that indirectly affect the glycogen synthesis pathway by phosphorylating and inactivating GS, are studied extensively as therapeutic targets in diseases such as diabetes, obesity, cancer and neurological disorders, where GSK3 β plays an important role in many cellular functions like proliferation, differentiation, motility and survival [239] and AMPK has been shown to regulate cellular energy homeostasis [240]. Lithium, like valproate, is a drug which is already in use for bipolar disorders [241], has been found to inhibit other types of enzymes in the glycogen metabolism, such as PGM, that catalyzes the reversible conversion of G1P to G6P, in rat brain and increases the phosphorylation of GS in astrocytes inhibiting glycogen synthesis [181-183]. Additionally this compound has been found to inhibit GSK3 β in cancer cells thus compromising cancer cell survival [189,190] and have led to the clinical trials for different types of cancers, as discussed in the section 1.4.

The enzyme GP has been extensively studied as a target for inhibiting glycogen degradation and control of hyperglycaemic condition, as it is responsible for the excessive glucose production by glycogenolysis in type 2 diabetes [242,243]. In addition it is speculated that GP could make a good target for anti-cancer therapy, as a significant glycogen metabolism reprogramming was observed in cancer cells under hypoxia and serum starvation conditions that was associated with cancer cell survival [170,175,177]. A wide array of GP inhibitors have been developed, targeting the effector binding sites such as the allosteric site that binds AMP [244], the inhibitor site that binds purines, nucleosides, nucleotides and other heterocyclic compounds [245], catalytic site that binds glucose, G1P and inorganic phosphate [246] and a novel inhibitor site binding to the indole inhibitors [247], as illustrated in Figure 1.5. AMP-site inhibitors like BAY3401 that is metabolized to BAY1807 works by converting GP_a to GP_b in liver and skeletal muscle [248]. The inhibitor site compounds are those that include purines like caffeine and adenine, nucleosides and nucleotides like adenosine, AMP, ATP and flavopiridinol which is an anti-tumour drug, and these inhibitors block the catalytic site favouring the T-state (reviewed in [221,233]). The glucose analogue 4-dideoxy-1,4-amino-D-arabinitol (DAB) is an active-site potent liver GP_a inhibitor showing greater than 80% inhibition of GP at 5-20 μ M [249] and it concomitantly inactivates the GS enzyme [250]. The indole carboxamide inhibitors bind to the special indole site, thus stabilizing the T-state of GP_a [251], which then releases the GP_a from

inhibition of PP1-G_L (the complex of PP1 and glycogen targeting protein G_L), in turn activating GS and promoting glycogenesis [221,252]. Several indole carboxamides for GP inhibition in type 2 diabetes have been developed by Pfizer and Astrazeneca (as reviewed in [233,253]). These indole inhibitors, such as the commercially available CP-91149 and CP-316819 have been found to inhibit GP synergistically with high glucose or caffeine [242,254,255] and have been studied not only in liver but also extensively in brain glycogen metabolism to observe the effects of hypoglycaemia and hypoxic ischemia [255-257]. Thus these GP inhibitors targeting the different binding sites of GP have proven to be effective in the direct inhibition of glycogen degradation and can be useful for studying the effect of blocking glycogen metabolism in various disease models.

1.5.4. Exploring glycogen metabolism in endothelial cells as a key target in angiogenesis

Glycogen metabolism in endothelial cells has not been studied in detail and limited information is available on the regulation of enzymes modulating the GS and GP enzymes, as reported in the section 1.2. Hence the therapeutic importance of targeting glycogen metabolism in endothelial cells as an anti-angiogenic strategy is still yet to be uncovered. Some *in vitro* studies on diabetic endothelial progenitor cells, where the inhibition of GSK-3 β , have shown to reduce their apoptosis, improving the cell yield, attributing to the therapeutic improvement of the progenitor cell therapy in diabetes mellitus [258]. A preliminary study from our laboratory has shown a significant accumulation of glycogen in HUVECs under normoxia and a higher accumulation under hypoxia, similar to the case of cancer cells [135,169]. The process of angiogenesis begins with angiogenic signalling by factors such as VEGF, FGF, etc., as discussed in the section 1.1.2, and hypoxia further induces the expression of these factors (section 1.1.3.2.1). Thus the accumulation of glycogen or its active metabolism by endothelial cells under hypoxia might be related to a protective role, as in the case of cancer cells and neurons [174,256]. Also, as discussed in the section 1.4, the anti-angiogenesis treatment in an *in vivo* tumour model showed that targeting blood vessel formation accompanies reprogramming of

glycogen metabolism, upregulating hypoxia in the tumour microenvironment [170]. Hence a combined therapy targeting glycogen metabolism and inducing hypoxia could have an effective response against endothelial cell survival and angiogenesis. In addition the utilization of glycogen under glucose depletion in endothelial cells [135] shows that glycogen could be an important alternative fuel in needs of emergency, which can also be explored as a target accompanying hypoglycaemic condition.

Furthermore, the preliminary *in vitro* study conducted in our laboratory on the inhibition of the endothelial GP enzyme showed that it compromised the cell viability [135], which indicates that glycogen metabolism could be important to sustain endothelial cell survival. Thus from these studies it is clear that glycogen metabolism is important for endothelial cells and eventually for angiogenesis, but we do not have sufficient information as to how it influences the endothelial cell activities. Thus a complete characterization of the endothelial glycogen metabolism is the need of the hour to understand the key regulatory pathways and further studies on targeting the key enzymes of glycogen metabolism could help in recognizing the key roles of glycogen reserves in endothelial cell survival and angiogenic activities.

1.6. Omics-based methods for studying cellular metabolism

For many years biological research has been focused on reductionist approach, where studies on single gene, protein and its function or a pathway are explored. Yet this approach cannot aid in comprehending the complexity of biological systems, in which individual biological components are connected together in a network [259]. This prompted to develop methods based on holistic approach where studies of biological components using different methods are integrated together and a holistic response to certain perturbations are studied, which is termed as Systems Biology [260]. Since the beginning of mapping of the genomes a number of omics-based research has been developed, such as proteomics, transcriptomics, genomics, metabolomics, lipidomics and epigenomics, that involve the global analysis of proteins, RNA, genes, metabolites, lipids and modified histone proteins in chromosomes, respectively [261].

The data sets generated from these studies are so huge and they encompass high-throughput techniques and strong methodologies to support the global biological study [262] that the omics can be rightly termed as a scientific field, rather than a method.

Metabolome is the complete set of metabolites in a cellular system and metabolomics is the study of the metabolome and its interactions via metabolic pathways and enzymes involved [263]. Biological systems have been studied using genomics, proteomics and transcriptomics approaches for a number of years, and according to Medline statistics the studies published up to the year 2013 are about 120036 for genomics and 50810 for proteomics alone and only 7613 studies have been published on metabolomics (Statistics retrieved on 9 Jan 2016, <http://dan.corlan.net/medline-trend.html>). Metabolomics is emerging as a powerful approach and gives much deeper information of a biological system as the metabolites and their variations directly reflect the underlying biochemical state of the cells and hence best represents a molecular phenotype [263]. Different strategies have been used to perform metabolomics studies, such as the non-targeted metabolomics involving global metabolic profiling and the targeted metabolomics approach where concentrations of known metabolites are measured [263]. Fluxomics is a different approach of metabolomics in which a dynamic picture of the phenotype is generated using labelled metabolites as tracers and this can complement the metabolomics study that provides a static view of a cellular metabolic profile [264]. Nuclear magnetic resonance (NMR) and mass spectrometry (MS) based analytical techniques are most widely used for metabolomics measurements. While NMR is advantageous over MS in the context of simple sample preparation techniques and has a high analytical reproducibility, it lacks the sensitivity that the MS-based techniques can provide [263].

1.6.1. Fluxomics

A quantitative metabolomics study of the upregulation or downregulation of metabolite contents can provide information about the metabolic footprint, which is only a snapshot of the biological system. However, a ^{13}C tracer-based metabolomics study can provide a descriptive

map of the changes in the metabolic network, showing pathways that are most affected by a treatment and the contribution of nutrients for the production of other metabolites. The rates of transformation of metabolites by the enzymes can be associated with the genetic control of the enzymes and these can aid in identifying therapeutic targets in diseased cells [265]. Isotopic tracers are powerful in following the metabolic reactions to determine the origin and fate of a metabolite within cells, together with the magnitude of the reaction fluxes [266]. Although the consumption and production of extracellular metabolites can be assessed by measuring the concentrations in the spent medium in time-dependent manner, intracellular metabolites are maintained under dynamic balance between production and consumption and the reaction fluxes can be assessed by using metabolites labelled with isotopes such as ^{13}C or ^2H [267,268]. The fate of the heavy isotopes through the metabolic network can be experimentally assessed, which provides information on the use of alternative pathways and the relative magnitudes of the associated fluxes [269].

Flux analysis can imply stationary and non-stationary experiments according to the kind of final result anticipated. On the one hand, stationary experiments involve measuring the labelling patterns at the end-points when they become invariant with respect to time, that is when isotopic equilibrium is reached [270]. In this case, the measurement of these labelling patterns are completely independent of metabolite levels and can be useful to compare the relative contributions of different pathways for the change of an intermediate. On the other hand, in the non-stationary experiments kinetics of tracer flow through the pathways are measured before the isotopic equilibrium is reached [271,272] and needs more than one experimental time point and metabolite levels.

The estimation of fluxes based on ^{13}C tracer-based metabolomics experiments can use a combination of different methods, such as the direct interpretation of the labeling patterns and computational model-based approaches [273,274], that are described in the section 1.6.1.2. In our study, described in Chapter 4.1, we have applied a combination of both the approaches mentioned above, in order to estimate the fluxes in the central carbon metabolic network and

to observe the relative contributions of the metabolic pathways, induced by different cellular treatments.

1.6.1.1. ^{13}C tracer-based metabolomics experiments

Tracking the flow of changes along a metabolic pathway is made possible by using stable isotopes such as ^{13}C , incorporated in the substrate that can enter into the pathway of interest. The ^{13}C tracer-based metabolomics experiments involve the incubation of a cell culture with labelled substrates like ^{13}C -glucose or ^{13}C -glutamine and measuring the percentage of the labelled carbons in the downstream products. The measured metabolites are chosen from the pathways of interest and the labelled carbons are incorporated in unique numbers and positions in the metabolites depending on the cellular condition [275]. In the context of ^{13}C labeling for a specific metabolite, there is a possibility of 2^n number of *isotopomers*, which are the isotopic isomers depending on the position of labelled carbons. In addition, there can be $n+1$ possible number of *isotopologues* (or *mass isotopomers*) which are the isotopic isomers of different masses depending on the different number of ^{13}C substitutions and are irrelevant of the position of the labeled carbons [275]. For example, in the case of a three carbon metabolite such as lactate, the possible numbers of isotopomers are 2^n , i.e., $2^3 = 8$, where the ^{13}C labels can be incorporated in the positions C_1 , C_2 and C_3 , while the labeled lactate isotopologues can be of $n+1$, i.e., $3+1=4$ numbers, depending on the number of carbons labeled ($m0$: $^{12}\text{C}_1\text{-}^{12}\text{C}_2\text{-}^{12}\text{C}_3$; $m1$: $^{13}\text{C}_1\text{-}^{12}\text{C}_2\text{-}^{12}\text{C}_3$, $^{12}\text{C}_1\text{-}^{13}\text{C}_2\text{-}^{12}\text{C}_3$, $^{12}\text{C}_1\text{-}^{12}\text{C}_2\text{-}^{13}\text{C}_3$; $m2$: $^{13}\text{C}_1\text{-}^{13}\text{C}_2\text{-}^{12}\text{C}_3$, $^{12}\text{C}_1\text{-}^{13}\text{C}_2\text{-}^{13}\text{C}_3$, $^{13}\text{C}_1\text{-}^{12}\text{C}_2\text{-}^{13}\text{C}_3$; $m3$: $^{13}\text{C}_1\text{-}^{13}\text{C}_2\text{-}^{13}\text{C}_3$).

While MS based techniques can distinguish between isotopologues [276-278], NMR can deduce positional information or the isotopomers [279,280]. Different label choices are present for performing ^{13}C tracer-based metabolomics and they can be chosen according to the outcome that is needed, in case if a global picture of all reaction fluxes involved in central carbon metabolism is necessary or just those fluxes of some chosen pathways are sufficient. It is also taken into account that a single tracer might not give all the necessary flux distributions in all

the interested pathways. In these cases parallel experiments can be performed with different tracers and the flux analysis can later be combined and incorporated into the flux model [281]. The most widely used tracers are based on ^{13}C -glucose and ^{13}C -glutamine as they are the main substrates for most of the cell types. The tracer $[1,2-^{13}\text{C}_2]$ -glucose is considered one of the most useful ones and allows for studying the overall central carbon metabolism including glycolysis, PPP, glycogen metabolism, fatty acid synthesis and TCA cycle, at the expense of glucose metabolism (Figure 1.6 shows part of the analysis that can be done using $[1,2-^{13}\text{C}_2]$ -glucose tracer) [282].

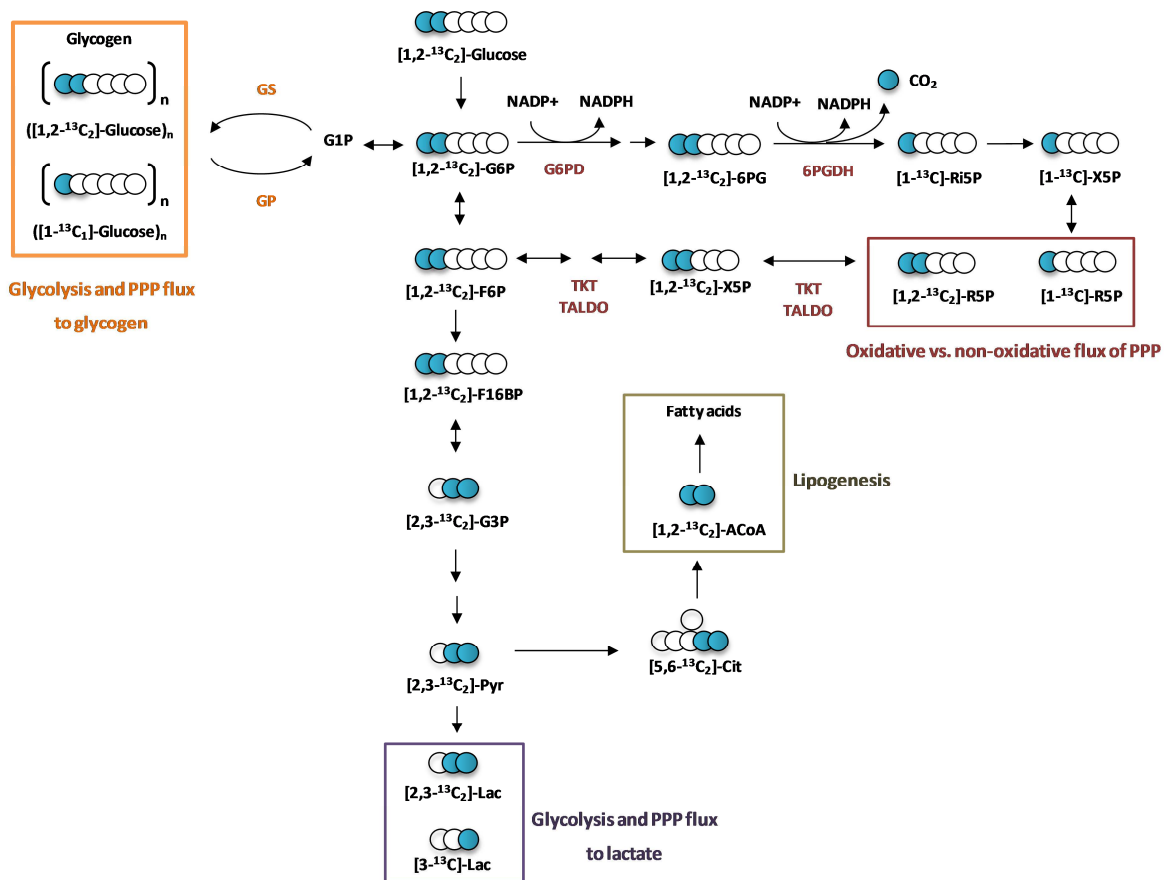


Figure 1.6: ^{13}C -mediated metabolomics experiment using $[1,2-^{13}\text{C}_2]$ -glucose. Illustration of ^{13}C label flow through possible metabolic pathways in the central carbon metabolism [275]. Use of $[1,2-^{13}\text{C}_2]$ -glucose as a tracer allows us to estimate the fluxes through majority of the pathways such as glycolysis, PPP, glycogen synthesis and degradation and fatty acid synthesis. The measurement of isotopologue distribution of RNA ribose in R5P molecules can help in quantifying the percentage of m1-ribose ($[1-^{13}\text{C}_1]$ -R5P) with respect to that of m2-ribose ($[1,2-^{13}\text{C}_2]$ -R5P) which helps in identifying the relative contribution of oxidative to non-oxidative branches of PPP, respectively, for the production of R5P, needed for nucleotide synthesis. On the other hand, the measurement of

1.6.1.2. Estimation of metabolic fluxes based on ^{13}C labelling patterns

Intracellular fluxes in central carbon metabolism are not directly measurable, but they can be deduced by using ^{13}C labelled nutrients as cellular substrates. When these labelled nutrients metabolize, the unique rearrangement pattern of the ^{13}C tracers through the metabolic pathways can give us an idea of the flux pattern through the central carbon metabolism [283]. The estimation of metabolic fluxes and the relative contributions of certain metabolic pathways based on ^{13}C labelling patterns can be performed using a variety of methods, from direct interpretation to computational modelling methods, which are described below.

1.6.1.2.1. Direct interpretation of fluxes or ^{13}C tracer analysis

Direct interpretation of ^{13}C labelling patterns, termed as “ ^{13}C tracer analysis”, is a simple approach that allows the understanding of the relative pathway activities, pathway

isotopologue distribution in glucose derived from the cellular glycogen gives the contribution of glycolysis (direct from glucose) and the combination of glycolysis and PPP pathways to the synthesis of glycogen from the percentages of m2-glucose ($[1,2-^{13}\text{C}_2]$ -glucose) and m1-glucose ($[1-^{13}\text{C}_1]$ -glucose/ $[3-^{13}\text{C}_1]$ -glucose), respectively. In the case of m1-glucose ($[1-^{13}\text{C}_1]$ -glucose/ $[3-^{13}\text{C}_1]$ -glucose) for glycogen, this labelled molecule is re-introduced into glycolysis to F6P from the non-oxidative branch of PPP and which in turn by the reversible conversion of F6P into G6P, enters into the glycogen synthesis. The relative contributions of glycolysis and the combination of glycolysis and PPP pathways to the production of lactate is estimated by quantifying m2-lactate ($[2,3-^{13}\text{C}_2]$ -lactate) and m1-lactate ($[3-^{13}\text{C}_1]$ -lactate), where $[3-^{13}\text{C}_1]$ -lactate is produced when m1-ribose ($[1-^{13}\text{C}_1]$ -ribose) produced from oxidative PPP is re-introduced into glycolysis through the non-oxidative PPP. The tracer incorporation in fatty acids palmitate and stearate are measured by quantifying ^{13}C in even-numbered masses m2, m4, m6..., of these metabolites which are synthesized either by the addition of $[1,2-^{13}\text{C}_2]$ -ACoA from m2-glucose ($[1,2-^{13}\text{C}_2]$ -glucose) through glycolysis. Only the isotopologue distributions of main metabolites are shown for clarity purpose. The procedures used for the measurements and analysis of the isotopologue distributions are detailed in the Methods sections 3.12 and 3.14. 6PG – 6-phosphogluconate, 6PGDH – 6-phosphogluconate dehydrogenase, ACoA – acetyl-CoA, Cit – citrate, F16BP – fructose-1,6-bisphosphate, F6P – fructose-6-phosphate, G1P – glucose-1-phosphate, G3P – glyceraldehydes-3-phosphate, G6P – glucose-6-phosphate, G6PD – glucose-6-phosphate dehydrogenase, GS – glycogen synthase, GP – glycogen phosphorylase, PPP – pentose phosphate pathway, Pyr – pyruvate, R5P – ribose-5-phosphate, Ri5P – ribulose-5-phosphate, TALDO – transaldolase, TKT – transketolase, X5P – xylulose-5-phosphate.

contributions via alternative metabolic routes and the contributions of nutrients for the production of different metabolites [269]. For this purpose we apply simple analytical formulas based on the previous knowledge of the metabolic pathways to perform this direct interpretation of ^{13}C labelling patterns [275]. Flux ratios within the main biochemical pathways, as shown in Figure 1.6, can be estimated using simple calculations. For example in PPP, the relative contribution of fluxes in oxidative to non-oxidative pathways can be estimated from the measurement of labels in ribose, where oxidative branch yields m_1 ribose and non-oxidative branch yields m_2 ribose. In the case of glycogen, the measurement of labelled glucose from glycogen yields the percentage of m_2 -glucose that is produced directly from glucose (glycolysis) and m_1 -glucose is produced via PPP and glycogenesis combined together, as detailed in Figure 1.6. The percentage of glucose metabolism for the contribution of fatty acid synthesis can be estimated by measuring the even-numbered masses, m_2 , m_4 , m_6 ... of the fatty acids palmitate and stearate. In addition, the measurement of isotopologue distribution in lactate combined with lactate concentrations can estimate the flux ratio of ^{13}C from glucose through glycolysis and PPP.

1.6.1.2.2. Computational modelling based flux estimation or ^{13}C metabolic flux analysis

In contrast to the direct interpretation of fluxes or ^{13}C tracer analysis, mentioned above, in the ^{13}C metabolic flux analysis approach the metabolic fluxes are computationally estimated using more descriptive methods, by combining the labelling patterns in intracellular metabolites, the rate of consumption and production of metabolites by the cells and a prior knowledge of the biochemical reaction network [269]. Together with the direct interpretation of fluxes through simple formulas, we apply a ^{13}C metabolic flux analysis strategy that intends to reduce the solution space for fluxes by using the data from the cellular uptake and secretion rates of metabolites and biochemical reactions from prior knowledge as constraints that impose system boundaries [269]. In addition, by an iterative procedure, the propagation of labels measured as the isotopologue distributions in metabolites representative of the pathways under study, are

used to additionally reduce the solution space. Although the ^{13}C metabolic flux analysis approach has the disadvantage of the necessity of computational tools to be developed, it is highly advantageous over direct interpretation method. The computational method helps to get a holistic information by constructing metabolic networks and validating the ^{13}C tracer analysis conclusions with a more detailed model, which can take into account the fundamental metabolic constraints such as the conservations affecting NAD/NADH or acetyl-CoA/CoA. This can provide a simple biochemical model with fewer number of measured rates of metabolites sufficient to estimate the fluxes in the model [284].

1.6.2. Targeted and untargeted metabolomics

The tracer-based metabolomics, or in other words fluxomics discussed in the previous section, is a targeted analysis using labelled nutrient sources in which the relative contributions of metabolic pathways for the production of certain metabolites are studied. Whereas, metabolomics is the study of a set of metabolites and their concentration changes in a biological system [263,285]. Relative quantitative changes of metabolites (their upregulations or downregulations), without requiring an in-depth knowledge of pathway contributions, is sufficient to discover biomarkers [286,287] and are widely used in clinical studies and also have been adopted in other fields such as food safety and environmental contaminant analysis [288-290]. The metabolomics study can typically be classified into two categories: targeted metabolomics and untargeted metabolomics based on the outcome expected and the methodology used [263,291,292], as shown in Figure 1.7. Targeted metabolomics is used to study the changes of already known metabolites that are associated with a specific pathway, chemical or biological activity [263]. Untargeted metabolomics is a relatively more comprehensive analysis of metabolites which aims to analyze all the detectable metabolites in a biological sample [263,285]. The experiments involving untargeted analysis are mostly hypothesis generating rather than hypothesis driven as in the case of targeted analysis [293]. The untargeted analysis typically involves a generic extraction, chromatographic separation and detection of analyte ions, data pre-processing and analysis, followed by identification of

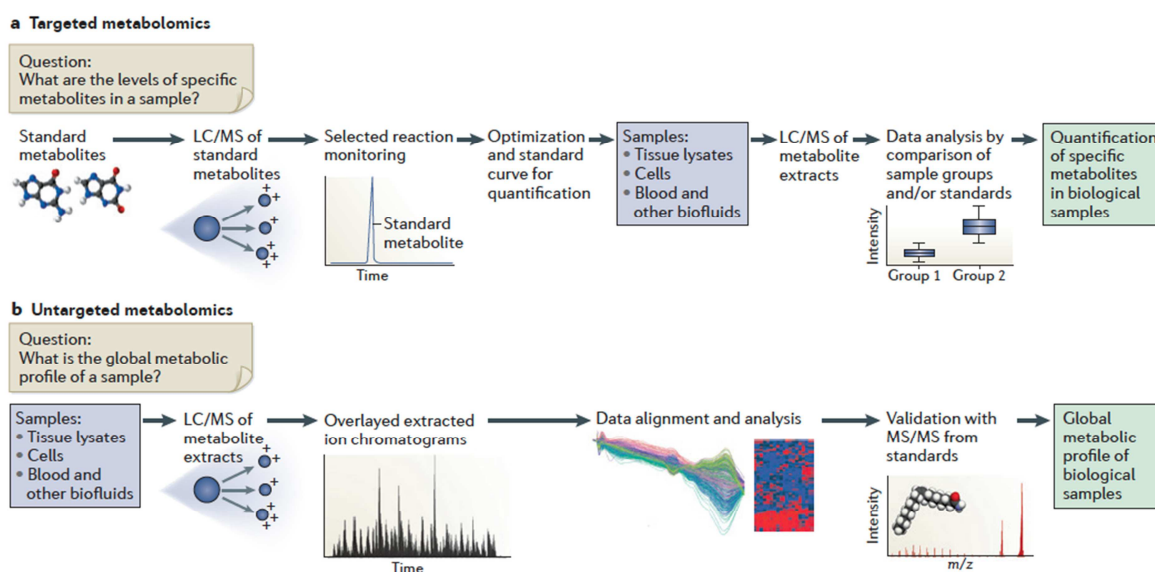


Figure 1.7: Two types of quantitative metabolomics. The changing metabolome in a biological system can be quantified using two types of approaches, (a) targeted and (b) untargeted metabolomics. Both kinds of approaches differ in the aim of the study and the methodologies used. In the case of targeted analysis levels of known metabolites are analyzed and it needs the use of analytical standards for method development and setting the retention time and m/z parameters and to set up calibration curve for quantification. The experimental samples are then analyzed using this prior information, to find the concentrations and changes among the control and treated samples. In the case of untargeted analysis the aim is to explore the global metabolic profile of the samples and if possible also validate the metabolites that could be identified from the untargeted data. The sample extracts are simply passed through the LC-MS with a generic method for LC separation, MS ionization and detection and the full scan data are subjected to basic data analysis tools for peak alignment and filtering. Then selected ion may be subjected to MS/MS fragmentation and fragment match could be found using several online tools and databases available in recent times for the untargeted data analysis for metabolite identification. Figure acquired with permission from NPG (Patti *et. al.*, 2012).

interested metabolites without *a priori* information [294]. A targeted metabolomics analysis is carried out according to a specific scientific problem and needs a thorough design of the methodology including the knowledge of all the metabolites analyzed. In addition it has the disadvantage of the need for the use of analytical standards for all the metabolites under study for quantification purpose, which can sometimes increase the expenses of the study, and a prior knowledge of the properties of the metabolites analyzed is required [263]. On the other hand, untargeted metabolomics can be very useful to characterize an unknown biological system. Hence, a global methodology for sample extraction and sample analysis can be carried out and the outcome can provide a preliminary view of metabolite changes in the system [295]. The suspected metabolites can further be validated using fragmentation of selected masses and

comparing with the fragmentation information in online databases [263,296] and if needed, standards can be used for comparing the fragmentation information of the expected metabolites [295]. Typically, sample analysis for untargeted metabolomics experiments are carried out with high resolution mass spectrometers (HRMS) like the Time of Flight (TOF) or Orbitrap-based instruments. These provide high resolution and mass accuracy with full scan capability, which will aid in resolving metabolites having close range molecular masses [263,297-299]. This type of study does not require extensive planning like in the case of targeted analysis, and can be a good starting point to continue the study for further targeted analyses, if required [296]. Typically, liquid chromatography coupled to mass spectrometry (LC-MS) has been widely used for untargeted analysis due to its wide coverage of metabolites studied, according to their physical properties such as volatility, thermal stability and polarity [292], while in some cases gas chromatography coupled to MS (GC-MS) and NMR have also been under use [295,296].

1.6.2.1. LC-MS-based untargeted metabolomics

Mass spectrometry based untargeted analysis is one of the techniques, more powerful when used with a high resolution detector like an Orbitrap-based mass spectrometer, that is widely used for metabolite identifications in recent times [300,301]. In short, MS based untargeted analysis can be described as a holistic study of the entire metabolome of the system that consists of combining the accurate mass measurements and MS/MS fragmentation patterns to search for similar structures in databases for identifying the metabolites [285,300]. It is a large-scale analysis and encompasses step-by-step procedures, as described in the Figure 1.8, for sample preparation, sample analysis through the chromatography-mass spectrometer, comprehensive data analysis to filter the unwanted features and select those that are relevant, fragmentation of the selected ions and comparison with database [302]. These steps can be customized according to the goals and outcomes of the study and several tools have been developed for data analysis purpose [286], which is one of the main steps of this procedure.

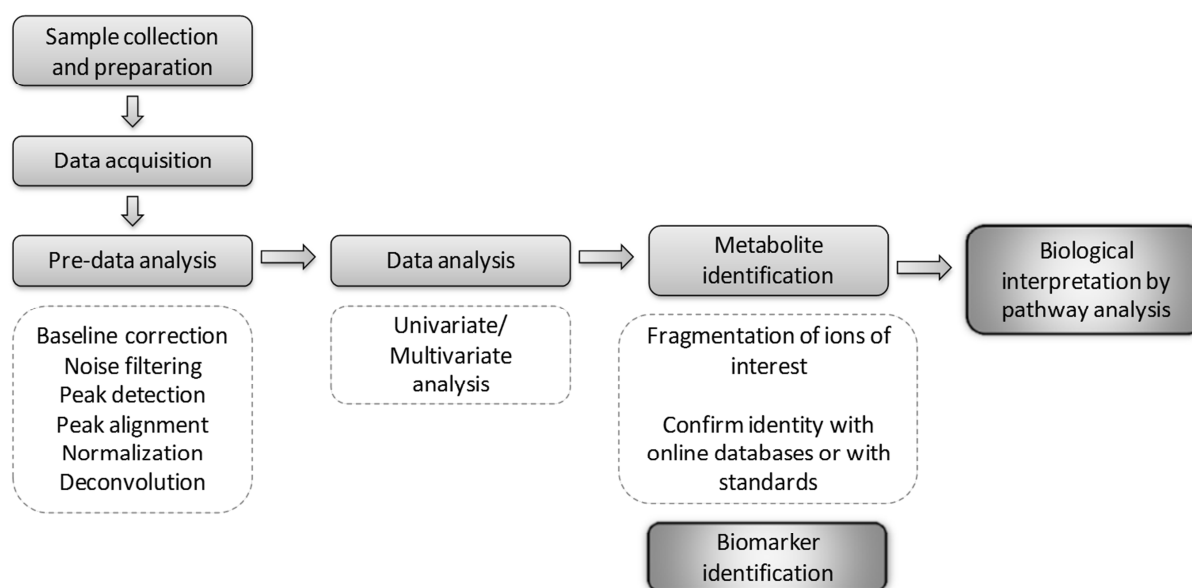


Figure 1.8: A general methodology for untargeted analysis. This figure illustrates a step-by-step procedure for carrying out the untargeted analysis and can be customized according to the types of samples studied and the outcome of the results expected. The general methodology involves biological sample collection, sample preparation according to the type of metabolites to be extracted and the instruments used, then sample run and data acquisition using LC-MS or GC-MS based instruments. Then spectral data collection and pre-data analysis which involves preparation of the raw data for further analysis and once the raw data is corrected for baseline, peak aligned and noise filtered, the main data analysis is carried out for detecting metabolites from the features of the raw data. The data analysis part can encompass some chemometric tools for performing univariate or multivariate analyses, in which classification of the experimental groups can be done and the most changing features can be extracted. Then for the metabolite identification part, the masses of the interesting features can be fragmented and the fragmentation pattern can either be confirmed using online database tools or using fragmentation patterns of reference standards, at which point biomarkers can be identified. Then according to the outcome of the results required, biological interpretation can be done by pathway analysis or metabolite set enrichment analysis.

A typical untargeted analysis involves generic extraction of metabolites from the biological specimen, followed by data acquisition in full scan HRMS instrument, data pre-processing and data analysis. In order to aid identification, HRMS with faster scan times, high mass resolution and accuracy combined with a full scan capability and fragmentation in a dedicated cell is preferred [303]. Reverse phase or hydrophilic interaction chromatography coupled with HRMS provides a robust platform to analyze diverse group of metabolites and therefore is widely used for metabolomics [263,304]. In LC-MS based untargeted metabolomics, thousands of peaks can be detected from biological specimens and they correspond to unique mass-to-charge ratios (m/z) and retention times (RT), which are termed as features [263].

However, it has to be noted that the number of metabolites that can be analyzed is dictated by the number of metabolites that can be extracted and ionized in the ion source. Data pre-processing include baseline correction, noise filtering, peak detection, RT alignment and deconvolution procedures. Untargeted data analysis typically involves chemometric tools like the univariate or multivariate statistics to observe if there is really a difference between the control and treated groups, from the global metabolic features extracted [286,295]. A major bottleneck in untargeted metabolomics is the identification of unknown features and relating it to the suspected metabolites. Orthogonal data from HRMS like accurate mass of precursor ion match, fragmentation pattern match and isotopic pattern match are normally used for aiding the identification of the metabolites [300,302]. A common way for metabolite identification is to query the high resolution spectral libraries with m/z values of precursor ions and matching them with the fragmentation patterns. However, the number of metabolites available in high resolution spectral libraries is low [305].

Metabolite identification is a key step to get any biological meaning from the acquired data. There are some useful online tools developed for the purpose of analyzing targeted and untargeted metabolomics data which have embedded database search tools and can also provide a list of the possible metabolite identifications of the aligned features [300]. For example XCMS Online is one such web-based untargeted metabolomics data analysis tool which detects and aligns features, performs statistical analysis of the raw data and provides cloud plots, heat maps and principal component analysis (PCA) plots of the control vs. treatments groups in the system and in addition provides tentative metabolite identifications and pathway interpretations [306].

The identified metabolites could further be associated with corresponding metabolic pathways and pathway analysis is a method that has been adopted in recent years to achieve this, which provides an additional insight into the metabolism of the biological system [307]. MetaboAnalyst 3.0 is a web server that was developed for metabolomic data processing, statistical analysis and find biologically meaningful patterns using metabolite set enrichment analysis (MSEA) [308]. Their pathway analysis and enrichment analysis tools are based on

databases such as the specialized metabolic pathway databases (SMPDB) and richly annotated metabolite databases like the human metabolome database (HMDB) [308,309]. They were developed especially for metabolomics studies and they use the high-quality Kyoto Encyclopedia of Genes and Genomes (KEGG) metabolic pathways as a background knowledge base [309]. Overall these tools aid in a reliable identification of the most changing metabolites using the untargeted method and even without further validations this analysis can be powerful in identifying the overall metabolome changes. Although further targeted analysis could be performed to validate the identified metabolites, untargeted analysis is the first step necessary to understand the unknown metabolome in a biological system using the holistic approach which will give huge insights for narrowing down the study further to achieve the expected and unexpected outcomes [296].

2. OBJECTIVES

OBJECTIVES

The main objective of this thesis is to explore the metabolic plasticity of endothelial cells, using HUVECs as a model cell line, and probe into alternative strategies targeting tumour angiogenesis. Accordingly, we have studied the metabolic adaptation of endothelial cells in the presence of different microenvironmental stimulants, exploring therapeutic targets based on the altered metabolic pathways and have characterized the endothelial glycogen metabolism which has not been explored before. The main objective of the thesis is sub-divided into the following specific objectives:

1. Characterization of HUVEC metabolism using fluxomics and untargeted metabolomics to reveal its metabolic reprogramming in the presence of VEGF, hypoxia and the metastatically different sub-populations of prostate cancer cells.
2. Investigation of the inhibition of glycogen phosphorylase as a therapeutic target against tumour angiogenesis.
3. Characterization of the glycogen metabolism in HUVECs under normoxia and hypoxia and exploring the enzyme isoforms expressed in HUVECs.

The successful outcome of these studies will help in understanding metabolic pathway changes that have not been explored before in endothelial cells and enable us to find therapeutic relevance of key metabolic pathways as targets against pathological angiogenesis.

3. MATERIALS AND METHODS

MATERIALS AND METHODS

3.1. Cell culture conditions

Human Umbilical Vein Endothelial Cells (HUVECs-pooled, Lonza) were maintained on 1% gelatine-coated flasks at 37°C in a humidified atmosphere of 5 % CO₂ and 95 % air in MCDB131 (Gibco, Life Technologies) medium, supplemented with recommended quantity of endothelial growth medium SingleQuots (EGM, Lonza), 10 % fetal bovine serum (FBS) (Gibco, Life Technologies) and 2 mM glutamine (Gibco, Life Technologies). The normoxia experiments were carried out at humidified atmosphere with 5 % CO₂ at 37°C for the indicated time periods and hypoxia experiments were carried out in the same conditions but with 1 % O₂. For all the experiments, unless otherwise specified, the cells were seeded in 1% gelatine-coated cell culture plates and kept for attachment to plate surface for 6h and then the medium was replaced to the MCDB131 basal medium, supplemented with 2 % FBS, 2 mM glutamine and 0.1 % Streptomycin (100 µg/mL)/Penicillin (100 units/mL) (Gibco, Life Technologies), incubating overnight for nutrient deprivation, before starting the experiment with a specifically-modified medium. The nomenclatures used for the experimental substrate conditions for growing cells or for reporting the cells themselves in these conditions, throughout this thesis, are given as, CM – complete medium, which contains a basal medium supplemented with 10 % FBS, Lonza EGM SingleQuots, 2 mM or 4 mM glutamine, with or without glucose and 0.1 % streptomycin/penicillin mixture; RM – restricted medium containing a basal medium supplemented with 2 % FBS, 2 mM or 4 mM glutamine, with or without glucose and 0.1 % streptomycin/penicillin mixture; RMV – restricted medium with VEGF containing a basal medium supplemented with 30 ng/mL human recombinant VEGF165 (Miltenyi Biotec), 2 % FBS, 2 mM or 4 mM glutamine, with or without glucose and 0.1 % streptomycin/penicillin mixture.

For the ¹³C metabolomics and fluxomics experiments (Chapter 4.1), 2×10^5 cells were seeded for normoxia and 1×10^6 cells for hypoxia. After nutrient deprivation (represented as time 0h), the medium in the cells were replaced with fresh MCDB131 RM (control condition) and

MCDB131 RMV, both media supplemented with 10 mM of 50 % [1,2-¹³C₂]-glucose (Sigma-Aldrich) and were incubated for 40h. For the glycogen time course experiment the cells were processed at time periods of 3h, 7h, 24h, 40h and 72h. The media and cells at initial (t = 0h) and final time points were collected. Cells generated for RNA-ribose and fatty acids assays were trypsinized and counted using a Scepter™ Handheld Automated Cell Counter (Merck Millipore, Billerica, MA, USA), and both cell pellets and media were kept frozen (at -80°C and -20°C, respectively) for further processing. Cells generated for glycogen content and label estimation were processed as mentioned in glycogen processing for ¹³C tracer experiments in the section 3.12.7.

For the untargeted metabolomics experiments (Chapter 4.2), the PC-3/M and PC-3/S cell sub-populations, derived clonally from the human prostate cancer cell line PC-3 as described in Celia-Terrassa *et. al.* [310], were co-cultured with HUVECs. Both PC-3 sub-populations were maintained at 37°C in a 5 % CO₂ atmosphere in RPMI 1640 (Sigma-Aldrich or Biowest) medium supplemented with 10 mM glucose, 2 mM glutamine, 10% FBS (PAA Laboratories), 1% pyruvate (1 mM) (Biological Industries), 1% streptomycin (100 µg/mL)/penicillin (100 units/mL) and 1% nonessential amino acids (Biological Industries). HUVECs were seeded in 6-well plates (Falcon) coated with gelatin and after 6h they were deprived of nutrients/hormones with DMEM (Sigma) RM overnight. Simultaneously, PC-3/M and PC-3/S cells were seeded in cell culture inserts supported in separate 6-well plates (Falcon) in RPMI complete medium. After 24h all the cells were washed with PBS and DMEM RM was added to all the cells, specifically 1.5 mL to the lower wells containing HUVECs and 1 mL to the upper inserts containing PC-3/M or PC-3/S cells. The inserts were placed over the wells, ensuring that the insert membranes with PC-3/M and PC-3/S cells were in contact with the medium in the wells with HUVECs. For the control cells, 2.5 mL of only DMEM RM was added to the wells containing HUVECs without inserts. For VEGF treatment the negative control medium was supplemented with 30 ng/mL of VEGF and added to HUVECs in wells without inserts. Following a 24h incubation under normoxia, the inserts with PC-3/M and PC-3/S cells were discarded, HUVECs trypsinized, and cells from 3 wells were combined for each sample replicate and counted. Then the pellets were frozen with liquid nitrogen, to be stored at -80°C until extraction.

For the glycogen characterization experiments (Chapter 4.4), DMEM-based media (no glucose, Gibco) was used and 3 set of samples – corresponding to cells incubated in RM, RMV and CM, were generated. HUVECs for all sample sets were seeded (4×10^5 cells for RM/RMV and 2×10^5 for CM conditions) initially in complete medium with 15 mM glucose. The HUVECs under CM condition were maintained with complete medium and 15 mM glucose for 24h and then complete medium without glucose was replaced to the cells. HUVECs under RM condition were deprived with restricted medium and 15 mM glucose, overnight, and then restricted medium without glucose was replaced to the cells. HUVECs under RMV were first deprived off nutrients overnight, like in the case of HUVECs in RM, and then restricted medium with VEGF and 15 mM glucose was added and incubated for 3h for the cells to adapt to the VEGF condition. Then the medium was changed to restricted medium with VEGF, without glucose. From all the three substrate conditions, HUVEC samples were extracted before (0h) and after 1h, 5h and 24h of replacing the media without glucose. The above experimental design was carried out for normoxia experiment. In the case of hypoxia experiment, HUVECs with CM, and those with RM and RMV after nutrient deprivation and 30 ng/mL VEGF added to the RMV cells, were pre-conditioned in hypoxia for 3h with glucose for the cells to adapt to the low oxygen environment and then kept incubated for 5h without glucose in hypoxia. The cells at initial time point with glucose ($t = 0h$) and at final time points without glucose (1h, 5h, 24h for normoxia and 5h for hypoxia) were collected and processed for glycogen extraction, as described in the section 3.12.7.

3.2. Cell viability assay

Cell viability assay was performed using a modified method described by Mosmann [311]. 5×10^3 HUVECs per well were seeded in triplicate cultures in CM, in 96-well flat-bottom plates. After 24h the medium was replaced with fresh media containing increasing concentrations of each of the tested compounds - CP316819 (Sigma), CP-320626 (kindly provided by Dr. Loranne Agius, Newcastle, UK), CP-91149 (Sigma), Isofagomine (Santa Cruz Biotechnology), BAYU6751 (Sigma), 1,4-dideoxy-1,4-imino-d-arabinitol (DAB, Sigma) and Ketoconazole (Sigma). After 72h of incubation, the cell culture medium was removed and 100 μ L of a mixture of fresh cell

culture medium and 1 mg/mL of 3-(4,5-dimethylthiazol-2-yl)-2,5-diphenyltetrazolium bromide (MTT) in PBS was added to each well. After 1h incubation the MTT solution was removed and 100 μ L of dimethyl sulfoxide (DMSO) was added to each well in order to dissolve the formazan product. Absorbance of the formazan solution in each well, which is proportional to initial cell number, was measured at 550 nm using an ELISA plate reader (Tecan Sunrise MR20-301, TECAN, Austria). From the results, the concentrations of each compound, needed to inhibit 50% of cell viability with regards to the control condition, were estimated.

3.3. Cell migration assay

For this cell migration assay, transwell HTS FluoroBlokTM Multiwell Insert System with 8 μ m pores (Becton Dickinson) was used with 24-well cell culture plates (Falcon). The upper and lower surfaces of the insert membranes were coated with 15 μ g/mL of Type I Collagen for a minimum of 30 min at 37°C and then 5×10^4 HUVECs were seeded on the upper surface of the inserts in 100 μ L of non-supplemented endothelial basal medium (EBM, Lonza) without serum and incubated for 4h at 37°C. Then 500 μ L of EGM with 10% FBS and SingleQuots supplements (Lonza) containing the inhibitors at varying concentrations (10, 40 and 100 μ M of CP-316819, BAYU6751, Isofagomine and 40 and 100 μ M of DAB) was added to the lower wells of the 24-well plates. For the negative control 500 μ L of only EBM and for positive control 500 μ L of only EGM were added to the lower wells. After 24h of incubation at 37°C the cells that had migrated to the lower surface of the inserts were stained with Calcein-AM (Calciochem, Merck) at a concentration of 5 μ M in EBM with 0.1% FBS for 30 min at 37°C under dark conditions and then the migrated cells were counted under a light microscope at a magnification of X10. All samples were normalized with respect to the positive control, which shows the maximum possible migration and is assumed to be 100%.

3.4. *In vitro* wound healing assay

The *in vitro* wound healing assay (or scratch assay) was performed based on a modification of previously described protocols [312,313]. Before beginning the experiment the outer bottoms of the wells of 12-well plates were cross-marked with a razor blade or an ultra-fine marker as reference for the scratch to be created. 2×10^4 HUVECs were then seeded in gelatin-coated wells with CM and incubated for 24h at 37°C until a confluent monolayer is formed. Then scratches were created on the cellular monolayer using a p200 pipette tip and the debris were removed by washing the wells with cell culture medium without FBS or supplements. Cell culture media was then replaced with 1 mL of fresh media (CM for positive control, only MCDB131 medium without any factors for negative control, and 40 and 100 μ M of CP-316819 in CM) and incubated for 14h and 21h at 37°C. Images before scratching and after scratching at 0h and at 14h and 21h of incubation were captured using phase-contrast microscope, and the capacity of the compounds to alter wound healing capacity was assessed visually in the treated samples with respect to the positive control which is assumed to have the maximum wound healing capacity.

3.5. *In vivo* matrigel plug assay

This procedure involving animal experimentation was carried out in collaboration with the Leitat Technological Center (Barcelona). Five groups of male C57BL6 10-week-old mice were supplied by Harlan Iberica (Barcelona). Each group containing 10 animals were used for this experiment. A matrigel mix was prepared for each group of animals: for the negative controls, 5.5 mL of growth factor reduced matrigel without phenol red (Becton Dickinson) was mixed with 64 U/mL of heparin (Sigma); for positive controls, 250 ng/mL VEGF (Isokine) was mixed with the matrigel-heparin mix; for the treatment groups, either 10 μ M or 50 μ M of CP-316819, or 50 μ M of Ketoconazole was mixed with the matrigel-heparin-VEGF mix. 500 μ L of each of the matrigel mix was injected subcutaneously in the abdominal part of each of the mice in their respective groups. After 7 days the mice were sacrificed, then the matrigel was removed and

the haemoglobin content from the blood vessels formed in the matrigel was measured using Drabkin reagent (Sigma), according to supplier recommendations. The haemoglobin quantified was normalized with the respective mg matrigel.

3.6. *In vivo* tumour efficacy assay

This *in vivo* assay was carried out in collaboration with the Leitat Technological Center, Barcelona. Two groups of 6-weeks old female nude mice (Hsd:ATHymic Nude-Foxn1^{nu} nu/nu strain), supplied by Harlan Iberica (Barcelona), were used in this study. A volume of 100 μ L of PBS/Matrigel (1/1) containing about 5×10^6 human myelomonocytic leukemia MV(4;11) cells (DSMZ) was injected subcutaneously in each mice. After cell injection, the tumour growth was monitored by measuring the weight of the animals and the volume of tumours with a caliper three times a week, until it reached an inferred mean tumour volume of approximately 150 mm³. Then the animals were sorted to select those with the most homogenous tumour values and divided into two groups with 7 animals each. The mice in one group were treated with 25 mg/Kg of the compound CP-316819 orally, while the mice in the control group were treated with only the vehicle (DMSO 10%/(2-Hydroxypropyl)- β -cyclodextrin 20 %), every alternate day for 2 weeks. The tumour volume and weight of the mice were monitored simultaneously. Tumour growth was calculated using the formula, $V = (D \times d^2)/2$, where V = volume, D and d are the longest and shortest axes of the tumour, respectively. The relative tumour volume (RTV) was calculated based on the formula:

$$\text{RTV (\%)} = 100 \times \frac{\text{median of tumour volume at the end of treatment}}{\text{median of tumour volume before treatment}}$$

The results were analyzed using GraphPad Prism 3.02 software. After two weeks of treatment the mice were sacrificed, their blood was extracted by cardiac puncture, and the tumours were excised and weighed. The tumours were embedded in optimum cutting temperature (O.C.T) compound (Tissue-Tek[®], Sakura) and paraffin for immunostaining analysis. For assessing the tumour microvessel density, the cryosections of the central part of each tumour were fixed with acetone/chloroform (1:1), treated with H₂O₂ and after blocking with 2% PBS-BSA / 5%

rabbit serum (Vector) and Avidin-biotin blocking solution (Dako) they were incubated with a rat anti-mouse monoclonal antibody against CD31 (dilution 1;200, BD PharMingen). After incubation with a biotinylated polyclonal anti-rat secondary antibody (dilution 1:500, Vector) and avidin-biotin complex (ABC) reagent (Pierce), the sections were then incubated with NovaRed (Vector) and stained with hematoxin Harris (Sigma) and mounted using DPX non-aqueous mounting system (Sigma). The quantification of angiogenesis was done based on the following two calculations:

M. V. D (Microvessel density)

$$= 10^6 \times \frac{\text{Sum of vessels of each tumour (image A + image B + \dots + image N)}}{\text{Area of one tumour in } \mu\text{m}^2 \text{ (area A + area B + \dots + area N)}}$$

A. A (fractional area of vessels)

$$= \frac{\text{Area of vessels of each tumour (image A + image B + \dots + image N)}}{\text{Area of one tumour in } \mu\text{m}^2 \text{ (area A + area B + \dots + area N)}}$$

The surface areas of the images were expressed in μm^2 and the unit of the M.V.D formula was expressed in mm^2 . The image analysis was done using NIH ImageJ software.

3.7. Biochemical measurement of extracellular metabolites

Extracellular metabolites such as glucose, lactate, glutamine and glutamate were quantified from cell culture media using COBAS MIRA plus spectral analyzer (Horiba ABX, Japan), by monitoring at 340 nm wavelength the production of NADPH in specific reactions involving the respective metabolites. The concentration of glucose was measured using hexokinase (HK) and G6PD coupled enzymatic reactions (ABX Pentra Glucose HK CP, HORIBA ABX, France). The concentration of lactate was measured by LDH reaction carried out at 37°C by mixing the media samples with 1.55 mg/mL NAD^+ and 87.7 U/mL LDH (Roche) in 0.2 M hydrazine, 12 mM EDTA buffer (final buffer pH 9.0). The glutamate concentration is determined by the conversion of glutamate in the media samples to α -ketoglutarate by glutamate dehydrogenase (GDH) in the presence of ADP. For this purpose, 2.41 mM ADP, 3.9 mM NAD^+ and 39 U/mL of GDH (Roche) in 0.5 M glycine/0.5 M hydrazine buffer (pH 9) were added to the media samples and the reaction

was carried out at 37°C. Glutamine concentration was determined by first converting it to glutamate through glutaminase (GLS) reaction, incubating the media with 125 mU/mL GLS in 125 mM acetate buffer (pH 5) for 30 min at 37°C in agitation and then the glutamate obtained was quantified by the method described above. The actual glutamate measured was subtracted from the total glutamate concentration (obtained by converting glutamine to glutamate) to obtain the concentration equivalent to the actual glutamine concentration in the cell culture media.

The consumption/production rates of the metabolites were calculated by measuring the metabolite concentrations in cell culture media, at initial and final time points, and were normalized with respect to both cell numbers and incubation time (h). Results were expressed in micromols of metabolite consumed or produced per hour per million cells.

3.8. Protein extraction and determination

The total protein was extracted from the cell cultures at the end of the experiment by washing the cells twice with ice-cold PBS and scrapping them from the plates with a lysis buffer containing 20 mM Tris HCl (pH 7.5), 1 mM dithiothreitol (DTT), 1 mM EDTA, 0.2 g/L Triton X-100, 0.2 g/L sodium deoxycholate, 0.4 mM phenylmethylsulfonyl fluoride (PMSF), 1% protease inhibitor cocktail and 1% phosphatase inhibitor cocktail (Thermo Fisher Scientific Inc.). Then the scrapped extract was incubated in ice for 20 min before the cell lysates were disrupted by sonication using a titanium probe (VibraCell, Sonics & Materials Inc, USA) and centrifuged at 4°C for 20 min at 12000 g. The resulting supernatant was recovered for protein content estimation, which was determined according to BCA kit (Pierce Biotechnology) instructions.

3.9. Enzyme activities

Fresh cell cultures were washed with ice-cold PBS and the cells were lysed using the method mentioned in the previous section 3.8. Enzyme activities were performed using COBAS MIRA

spectrophotometer, monitoring the increment or decrement of NADPH at 340 nm wavelength. The enzyme activity results were normalized using proteins estimated from the supernatant of the cell lysates.

3.9.1. Glucose 6-phosphate dehydrogenase (G6PD, EC 1.1.1.49)

G6PD specific activity was measured by incubating the protein extracts with 0.5 mM NADP⁺ in 50 mM Tris-HCl (pH 7.6) at 37°C and the reaction initiated by adding glucose 6-phosphate at a final concentration of 2 mM.

3.9.2. Glycogen synthase (GS, EC 2.4.1.11)

For this enzyme activity 1.2×10^6 HUVECs were seeded in p60 plates and after the glucose deprivation experiment explained in section 3.1 for glycogen characterization, the fresh cell cultures were used for measuring GS activity. The GS enzyme activity was measured by determining the incorporation of radioactive UDP-[¹⁴C]-glucose in glycogen (Thomas, Schlender, 1968). The cells were homogenized by adding ice-cold buffer containing 10 mM Tris-HCl (pH 7), 150 mM KF, 15 mM EDTA, 15 mM 2-mercaptoethanol, 0.6 M sucrose, 1 mM benzamidine, 1 mM PMSF, 1% protease inhibitor cocktail and 1% phosphatase inhibitor cocktail. The scrapped cell lysates were incubated in ice for 20 min and then sonicated and centrifuged as described in section 3.8. The supernatants were collected for GS enzyme activity measurement.

In this method the enzyme activity was measured in the presence and absence of the allosteric activator G6P. The GS activity measured in the presence of G6P (+ G6P) corresponds to the total amount of enzyme and that measured in its absence (– G6P) corresponds to the active (unphosphorylated) GS form. The ratio of the activities (– G6P / + G6P) gives the estimation of the active states of the enzyme and is independent of the total enzyme levels and thus can be compared among different cellular conditions and their corresponding GS expressions. To measure the GS activity in absence of G6P, 4000 cpm/μL of UDP-[¹⁴C]-glucose (PerkinElmer)

was used in a solution containing 6.7 mM UDP-glucose, 10 mg/mL glycogen, 50 mM Tris-HCl (pH 7.8), 20 mM EDTA and 25 mM KF. Enzyme activity was measured in the presence of G6P using 2000 cpm/ μ L of UDP- 14 C-glucose and 10.8 mM G6P with the rest of the above mentioned solution mix. The ratio of the activities – G6P / + G6P gave the normalized value of the proportion of active GS in the samples.

The assay was carried out by mixing 20 μ L of the samples with 40 μ L of the reaction mix, prepared as mentioned above, and kept incubated in a 30°C hot bath for 30 min. After 30 min 50 μ L of the sample-reaction mix, for each sample, was deposited on a small piece of 31-ET paper (Whatmann) and quickly dropped into 66% ice-cold ethanol, to stop the reaction by glycogen precipitation. The pieces of papers were washed for 10 min with 66% ice-cold ethanol and then replaced with fresh 66% ethanol and washed twice at room temperature for 20 min each. Then the papers were immediately washed with acetone to remove the residual ethanol and dried. After the papers were completely dry they were kept in separate vials containing scintillation liquid Ecolite (MP Biomedicals). The radioactivity was measured using a scintillation counter, Rack BETA 1217 (LKB). The GS activity was expressed in mU/mg protein.

3.9.3. Glycogen phosphorylase (GP, EC 2.4.1.1)

For the GP enzyme activity the samples were prepared in the same way as mentioned in the previous section 3.9.2. This enzyme activity was based on the incubation of GP in conditions that force the synthesis of glycogen than its degradation. The activity was carried out by measuring the incorporation of 14 C-glucose-1-phosphate (14 C-G1P), based on a previously described technique [314].

This assay was carried out in the presence of 2000 cpm/ μ L of 14 C-G1P with a reaction mix containing 100 mM G1P, 200 mM KF, 1% glycogen and caffeine to a final concentration of 1mM. In the presence of caffeine, which is an inhibitor of the inactive GP_b form, we measure the active form of GP (GP_a). Same procedure as GS (in section 3.9.2) was carried out for processing the samples, beginning with the incubation of samples with GP reaction mix for 30

min at 30°C. The GP enzyme activity measured in the presence of caffeine was assumed as a representative measurement of active GP in the samples.

3.10. Western blot

Proteins were extracted from the cells contained in fresh or frozen plates using homogenization buffer (10 mM Tris-HCl (pH 7), 150 mM KF, 15 mM EDTA, 15 mM 2-mercaptoethanol, 0.6 M sucrose, 1 mM benzamidine, 1 mM PMSF, 1% protease inhibitor cocktail and 1% phosphatase inhibitor cocktail), following the same method described in section 3.8. Then 50 µg of protein for each condition were loaded onto SDS-polyacrylamide gels, separated according to their molecular weights using electrophoresis and transferred to polyvinylidene difluoride (PVDF) membranes (Bio-Rad). The membranes were then blocked with 3% BSA in 0.1% PBS-Tween solution for 1h and subsequently incubated with the different specific primary antibodies overnight at 4°C. The membranes were then washed with 0.1% PBS-Tween and incubated with appropriate secondary antibodies for 1h in room temperature. The membranes were then washed again, treated with Immobilon ECL Western Blotting Detection Kit Reagent (EMD Millipore) and exposed to autoradiography films (VWR International), which were then developed. The primary antibodies used were: anti-muscle/liver glycogen synthase (MGS/LGS, #3886, Cell Signalling Technology), anti-brain glycogen phosphorylase (GPB1, produced by Eurogentec, Köln, Germany), anti-liver glycogen phosphorylase (GP2, kindly provided by Dr. J.J.Guinovart, IRB, Barcelona) and anti-phospho glycogen synthase, P^{Ser}-641/645 (#44-1092G, BioSource). The secondary antibodies used were: anti-rabbit (NA934V, Amersham Biosciences) and anti-chicken (Jackson ImmunoResearch).

3.11. RNA isolation and quantitative reverse transcription-polymerase chain reaction (qRT-PCR)

Fresh or frozen plates of HUVECs grown in the CM condition under normoxia were processed for RNA isolation using Trizol reagent (Invitrogen) following manufacturer's instructions. The

Trizol lysates were mixed with chloroform and centrifuged in RNAase-free eppendorfs so that they would separate into organic and aqueous phases. The aqueous phase was carefully collected into another RNAase-free eppendorf containing cold isopropanol and then centrifuged at 12000 g for 15 min at 4°C in order to precipitate RNA. The supernatant was removed and the pellet was washed with 75% cold ethanol several times, before being dried and resuspended in RNAase-free water. Total RNA was quantified using Nanodrop spectrophotometer (ND 1000 V3.1.0, ThermoFisher Scientific Inc.). Reverse transcription to cDNA was carried out at 37°C for 1h by mixing 1µg of RNA with the kit reagents: 5X Buffer (Invitrogen), 0.1 M DTT (Invitrogen), Random Hexamers (Roche), 40 U/mL RNAsin (Promega, Fitchburg, USA), 40 mM dNTPs (Bioline, UK) and 200 U/mL and M-MLV-RT (Invitrogen). Then gene expression analysis was performed through Applied Biosystems 7500 Real-Time PCR System according to manufacturer's protocol, using the following Taqman gene specific sequences: GYS1 (Hs00157863_m1), GYS2 (Hs00608677_m1), PYGL (Hs00958087_m1), PYGB (Hs00765686_m1) and PYGM (Hs00989942_m1) (Applied Biosystems, ThermoFisher Scientific Inc.). The reaction mixture was prepared with 9 µL of cDNA mixture and 11 µL of the corresponding Taqman in Master Mix (Applied Biosystems). The parameters used for carrying out the Real-Time PCR were: initial incubation for 2 min at 50°C, denaturing at 95°C for 10 min and then 40 cycles at 95°C and 60°C for 15s and 1 min, respectively. The reference gene used was Cyclophilin A (PPIA, Hs99999904_m1, Applied Biosystems). Assuming an amplification efficiency of 2 the relative abundance of the GS and GP genes with respect to the PPIA gene was calculated as $2^{-\Delta C_T}$, where ΔC_T is the difference between the cycle thresholds of the gene of interest and the PPIA reference gene.

3.12. ¹³C tracer-based metabolomics using GC-MS

For the ¹³C tracer-based metabolomics analysis, the experiments were carried out with 50% [1,2-¹³C₂]-glucose and the samples were collected and stored as described in the section 3.1 for fluxomics experiments. Media samples were used for measuring concentrations of the extracellular metabolites such as glucose, lactate, glutamine and glutamate, as described in the section 3.7, and for analysing the isotopologue enrichment in glucose, lactate, glutamate,

alanine, glycine, methionine, aspartate/asparagine, proline and serine. Cell culture plates were used for analysing isotopologue distribution pattern in RNA ribose, fatty acids and glycogen.

This isotopologue distribution analysis is carried out using GC-MS from Agilent 7890A GC equipped with a HP-5 capillary column and connected to an Agilent 5975C MS (Agilent Technologies, USA). Isotopologue distribution pattern in fatty acids were measured using GCMS-QP 2012 Shimadzu (Shimadzu Corporation, Japan) equipped with a BPX70 column (SGE Analytical Science, Australia). In both cases 1 μ L of sample injection at 250°C was carried out, with helium as the carrier gas at a flow rate of 1 mL/min. The procedures for metabolite isolation, derivatization and GC/MS detection for each of the metabolites are described below.

3.12.1. Glucose

Glucose from cell culture media was isolated using a tandem Dowex column containing Dowex-1X8/Dowex-50WX8 ion-exchange columns by eluting the metabolite with water. The liquid collected from elution was evaporated to dryness with air flow, overnight. Then the isolated metabolite was derivatized by first heating it to 100°C with 2% (v/v) hydroxylamine hydrochloride in pyridine for 30 min and then with acetic anhydride for 60 min. Then the mixture was evaporated with N₂ gas flow and the final derivative was dissolved with ethyl acetate and injected into GC/MS for analysis under chemical ionisation mode. Sample injection was done at 250°C and the oven temperature parameters were programmed to be: 230°C for 2 min, then increased to 260°C at the rate of 10°C/min, followed by an increase to 270°C at the rate of 25°C/min and held for 2 min. The retention time (RT) of the chromatographic peak was 3.7 min. The detector monitoring was carried out using single ion monitoring (SIM) where the ions were monitored in the range of 327-334 m/z for the C1-C6 molecule.

3.12.2. Lactate

For this metabolite, first HCl was added to the cell culture media and the lactic acid formed was

extracted with ethyl acetate and the mixture evaporated to dryness under N₂ gas flow. The lactic acid isolated was derivatized to its lactic acid n-propylamide-heptafluorobutyric ester by incubating with 2,2-dimethoxypropane and 0.5N methanolic HCl 75°C for 1h. Then n-propylamine was added to the mixture and heated for 1h at 100°C and then the samples dried under N₂ gas flow. The precipitate was then resuspended in ethyl acetate and then filtered through a glass wool packed Pasteur pipette. The filtered solution was then dried under a stream of N₂ gas and then the precipitate resuspended with dichloromethane and heptafluorobutyric anhydride and incubated at room temperature for 10 min. The samples were again dried with N₂ gas flow and resuspended with dichloromethane for GC/MS analysis under chemical ionisation mode. Samples were injected at 200°C and the oven temperature was programmed as: 100°C for 3 min, increase to 160°C at the rate of 20°C/min and held for 2 min. The RT of the chromatographic peak was 5.4 min. Ions were monitored by SIM recording the ion abundance of C1-C3 molecule in the range of 327-332 m/z.

3.12.3. Glutamate

In this case the cell culture medium was first passed through a Dowex-50WX8 column and then the amino acids in the Dowex mesh were eluted with 2N ammonium hydroxide and collected in glass tubes and were then dried under airflow overnight. For glutamate derivatization the dried precipitate was incubated with butanolic HCl at 100°C for 1h and then was dried under N₂ gas flow. Then the dried precipitate was dissolved with dichloromethane and trifluoroacetic anhydride and incubated at room temperature for 20 min. Then the mixture was dried under N₂ flow and the derivative dissolved with dichloromethane for GC/MS analysis under electron impact ionization mode that yields C2-C4 and C2-C5 glutamate fragments. Samples were injected at 250°C and the oven temperature was programmed as: 215°C for 2 min, increase to 224°C at the rate of 9°C/min, then to 233°C at the rate of 3°C/min and held for 2 min. The RT of the chromatographic peak was 3.9 min. Ions were monitored by SIM recording the ion abundance of C2-C4 fragment in the range of 151-157 m/z and C2-C5 fragment in 197-203 m/z.

3.12.4. Amino acids

For amino acids the cell culture medium was treated as in glutamate in the previous section 3.12.3, by passing through Dowex-50WX8 column and eluting with 2N ammonium hydroxide. After drying the solution under airflow overnight the derivatization process was carried out with butanolic HCl, dichloromethane and trifluoroacetic anhydride in the same manner as described in section 3.12.3. Then the derivative dissolved in dichloromethane was analysed by GC/MS under chemical ionisation mode. Samples were injected at 250°C and the oven temperature was programmed as: 110°C for 1 min, increase to 125°C at the rate of 10°C/min, then to 153°C at the rate of 5°C/min, then to 200°C at the rate of 50°C/min, to 216°C at the rate of 5°C/min and held for 1 min and finally to 250°C at the rate of 25°C/min and held for 2 min. Ions were monitored by SIM recording the ion abundance for C1-C3 alanine in the range of 241-246 m/z (RT: 5.3 min), C1-C4 aspartate/asparagines within 341-348 m/z (RT: 11.5 min), C1-C5 glutamate/glutamine within 383-390 m/z (RT: 12.8 min), C1-C2 glycine within 227-231 m/z (RT: 5.7 min), C1-C4SC5 methionine within 329-336 m/z (RT: 10.8 min), C1-C4 methionine within 253-259 m/z (RT: 10.8 min), C1-C5 proline within 295-302 m/z (RT: 9.6 min) and C1-C3 serine within 353-358 m/z (RT: 6.6 min).

3.12.5. Ribose

RNA ribose was isolated by treating the cell cultures with Trizol reagent, as described in the section 3.11. The purified RNA was then hydrolysed in 2 mL of 2N HCl at 100°C for 2h and the solution was evaporated to dryness under airflow overnight. Ribose was then derivatized using the same procedure as described for glucose in the section 3.12.1. The GC/MS analysis was carried out under chemical ionisation mode. Samples were injected at 250°C and the oven temperature was programmed as: 150°C for 1 min, increase to 275°C at the rate of 15°C/min and then to 300°C at the rate of 40°C/min. The RT of the chromatographic peak was 5.3 min. Ions were monitored by SIM recording the ion abundance of C1-C5 molecule in the range of 256-262 m/z.

3.12.6. Fatty acids

Fatty acids palmitate and stearate were analysed from the interphase and lower organic phase obtained from the cell cultures by the addition of Trizol and chloroform (as described in the section 3.11). 100% ethanol and 30% potassium hydroxide were added to these two phases to hydrolyse the fatty acids. Samples were incubated overnight at 70°C and the free fatty acids were extracted twice with petroleum ether and then the mixture evaporated with N₂ flow. Then the fatty acids derivatives were dissolved in hexane to be analysed using GC/MS under chemical ionisation mode. Samples were injected at 250°C and the oven temperature was programmed as: 120°C for 1 min and increase to 220°C at the rate of 5°C/min and held for 1 min. The RT's of the chromatographic peaks were 9.2 min for palmitate and 11.9 min for stearate. Ions were monitored by SIM recording the ion abundance for palmitate in the range of 269-279 m/z and stearate in the range of 297-307 m/z.

3.12.7. Glycogen

For quantifying the glycogen content and analyse its isotopologue distribution, the plates of cell cultures, after the experiment, were washed twice with ice-cold PBS, scrapped with 0.1 M NaOH and heated to 100°C for 15 min for protein denaturation. The samples were then sonicated for 5 min 2-3X using an ultrasonic bath (Branson 200 Ultrasonic Cleaner, Emerson Industrial Automation, St Louis, MO, USA). The pH of the samples was adjusted to pH 6-7 and then a fixed quantity of [U-¹³C-D₇]-glucose was added as an internal standard for all them. Then 200 µL of 1.25 mg/mL α-amylglucosidase in 0.4 M acetate buffer was added to digest the glycogen and the mixture was incubated overnight at 37°C under agitation. Then both the glucose released from glycogen and the glucose internal standard were isolated using Dowex-1X8/Dowex-50WX8 ion-exchange columns, eluting with water. The eluted samples were then dried overnight under airflow. After drying completely the glucose was derivatized in the similar procedure described in section 3.12.1. The GC/MS analysis was carried out under chemical ionisation. Sample injection, oven temperature and RT parameters were similar to that of

glucose in section 3.12.1. Ions were monitored by SIM recording the ion abundance for C1-C6 glucose in the range of 327-334 m/z and of [U-¹³C-D₇]-glucose in the range of 339-345 m/z. In order to build a calibration curve for the glycogen quantification the same quantity of the internal standard [U-¹³C-D₇]-glucose used for the samples above was added to varying quantities of ¹²C-glucose. The calibration solutions were derivatized in the similar manner as the samples to be measured in GC-MS. The glycogen content estimated using the calibration curve was normalized with protein content measured as described in section 3.8.

3.13. GC-MS data reduction

The MS spectral data shows the distribution of ions of a compound or a fragment with a specific m/z value. Monitoring such specific m/z values for the ion distributions in each metabolite will give us the fractional distribution of the artificially introduced ¹³C. The peak areas for all the ions in the cluster were integrated and extracted from the raw data using MSD5975C Data Analysis (Agilent technologies) or GCMS Postrun Analysis (Shimadzu Corporation) softwares. Each peak area corresponds to the fraction of ions within the ion cluster under analysis. These observed m/z values may be contaminated with natural abundance of the ¹³C isotopes and during derivatization process other isotopes, such as that of silicon from the reagents, can be added to the actual derivatization product of the metabolite under analysis. In order to distinguish the known, artificially introduced labels, isotopes contaminating from other modes described above must be subtracted. This kind of label correction is carried out using an in-house developed algorithm based on R programming. The resulting data corrects for the unwanted isotope enrichments mentioned above and gives only the enrichment due to the ¹³C atoms from the precursor tracer introduced in our experiment. The final data is represented as fractional isotopologue distribution designated as m₀, m₁, m₂,.. etc. where the number indicates the corrected labelled carbons (¹³C). The sum of all the isotopologues of the ion clusters is equal to 1 (or 100%) and the total ¹³C enrichment is calculated as 1 (or 100%) minus m₀.

3.14. ¹³C tracer-based metabolomics: data interpretation

The data from the metabolite consumption and production and the label distribution measurements, obtained as described in the above sections, can be used to predict intracellular fluxes in the central carbon metabolic pathway. In order to achieve this, two kinds of data analysis are combined, ¹³C tracer analysis based on simple formulas and a computational model-based ¹³C metabolic flux analysis, that are described in the following sections.

3.14.1. Direct interpretation of fluxes or ¹³C tracer analysis

In this type of analysis, a direct interpretation of the ¹³C labelling patterns measured using GC-MS is performed with the help of simple analytical formulas [275]. Also we have used the metabolite consumption and production data, measured using the method described in section 3.7 for glucose, lactate, glutamine and glutamate, and glycogen content measured as described in section 3.12.7, in addition to the ¹³C label distribution data measured in lactate, glutamate, ribose, glycogen and fatty acids as described in the section 3.12. Since [1,2-¹³C₂]-glucose is the tracer and source of the ¹³C labels in other metabolites measured in our experiments and we have not observed a change in the label distribution of glucose which remains 50% since the beginning until the final time point of 40 hours, we have not considered it for the flux estimations. The label distributions shown in the results section of the Chapter 4.1 used simple calculations described as follows: 1) In the case of ¹³C enrichment in lactate the total ¹³C lactate, Σm is obtained by the sum of m1, m2 and m3 isotopologue distributions measured in lactate; 2) In the case of ribose the ratio m1/m2 isotopologue distributions in ribose is done to calculate the contribution of oxidative to non-oxidative branch of PPP.

3.14.2. Computational modelling based flux estimation or ¹³C metabolic flux analysis

This part of flux estimation was done by Dr. Pedro Atauri of our laboratory and the method

employs the use of a computational tool (Mathematica[®]) to develop steady state model-based ¹³C flux estimations. To predict this network of reactions, the data from the metabolite consumption and production (section 3.7 for glucose, glutamine, lactate and glutamate, and 3.12.7 for glycogen) and the ¹³C label enrichments (section 3.12) were combined along with a prior knowledge of the biochemical reaction pathways computationally. In the first step of the analysis intracellular reaction fluxes were estimated from the metabolite consumption and production data and a range of values possible for the fluxes of the respective reactions were estimated, as detailed in Table A1.1 of the Appendix 1. In the second step of the analysis, the isotopologue distributions of each of the metabolite were predicted by using a set of balance equations of all possible isotopomers for that metabolite. By iteratively changing the ratios of flux estimations from the first step and applying them for predicting the label distributions in the second step, the difference among the predicted and the measured ¹³C label distributions as per section 3.12 are reduced to a minimum level. The set of flux estimations (from the first step) at this level is assumed to be the result of this computational analysis and are included in constructing the network of reactions in the model of the central carbon metabolism. A detailed description of the methodology used for this study, flux ranges estimated and flux ratios used in iteratively predicting the label enrichments are described in Appendix 1.

3.15. Mass spectrometry-based targeted metabolomics

The frozen tumour tissues and plasma samples prepared from the tumour efficacy assay, as described in section 3.6, were sent to the Biocrates Life Sciences AG, Austria, to perform a targeted metabolomics analysis of the samples using their p180 Absolute IDQ kit. Using this kit absolute and semi-quantifications of a large number of metabolites were carried out using API 4000 triple quadrupole mass spectrometer (Applied Biosystems/MDS Sciex), where amino acids and biogenic amines were quantified by LC-MS and lipids, acylcarnitines and hexoses were semi-quantified by flow injection analysis (FIA) coupled to MS. The protocol for tissue extraction of metabolites involved the use of ethanol-phosphate buffer (85/15 v/v), based on the methods tested by Romisch-Margl *et. al.* [315]. The supernatants from the homogenized

tissues containing the extracted metabolites were loaded on to the 96-well plate kit at a volume of 10 μL per sample and the metabolite derivatization, extraction and filtration were carried out as described in the user manual instructions. The plasma samples were directly added to the 96-well kit and processed in the same manner as in tissue extracts. For the FIA-MS analysis $2 \times 20 \mu\text{L}$ of sample injections, with a flow rate of 30 $\mu\text{L}/\text{min}$ was carried out, and both positive and negative ionisation methods were used. In the LC/MS method 10 μL of sample was injected, with a flow rate of 500 $\mu\text{L}/\text{min}$ and positive ionisation method was used. The results were then exported to the MetIDQ database, to a project already registered for the samples, for further data analysis, as described in the user manual. The metabolite concentrations in the results exported were represented in μM and was normalized by tissue weight in g for the tissue metabolites.

3.16. LC-MS-based non-targeted metabolomics

The samples generated from co-culture experiments, explained in section 3.1, were used for non-targeted metabolomics analysis using LC-MS technique, performed in collaboration with Beaumont Research Institute, MI, USA. The sample preparation and analysis are described in the following sections.

3.16.1. Sample preparation

500 μl of 50% ice-cold MeOH/water was added to frozen cell pellets and 25 μl of 0.001 mg/mL tryptophan D3 (internal standard) was spiked to all the samples before extraction. Samples were mixed using a microplate shaker for 10 min, followed by ultrasonication at 4°C for 20 min, vortexed vigorously to make sure pellets are completely dissolved and mixed using a microplate shaker for 10 min. Subsequently, the samples were centrifuged at 13,000 g at 4°C for 20 min and the supernatant collected. The supernatant was evaporated to dryness under vacuum at room temperature and reconstituted in 150 μl of ultra-pure water. The sample extract was filtered using Whatmann syringeless filters (0.2 μm). 5 μl was injected onto the LC/MS (n=3

technical replicates). A pool sample was made from all samples together as a quality control and to be used for fragmentation later [316,317].

3.16.2. LTQ – Orbitrap elite LC-MS analysis

Dionex Ultra High Performance Liquid Chromatography (UHPLC) coupled with an Orbitrap Elite was used for acquiring the data. The chromatographic system was coupled to the mass spectrometer with a heated electrospray ionization source II (HESI). The optimized HESI conditions for both ESI+ and ESI- were: spray voltage of 3.5 kV; sheath gas flow rate (N₂), 60 units; auxiliary gas flow rate, 45; sweep gas flow rate, 1; capillary temperature, 320°C; S lens RF level, 35; heater temperature, 400°C. Nitrogen produced by a nitrogen generator (Peak Scientific) was employed as both the collision and damping gas. The mass calibration of the Orbitrap was performed once a week to ensure a working mass accuracy of < 5 ppm. Pierce LTQ Velos ESI Positive ion and Pierce LTQ Velos ESI Negative ion calibration solutions from Thermo Fisher Scientific (Rockford, IL, USA) were used to calibrate the mass spectrometer. A mass range of 50–1200 m/z and resolving power of 60,000 FWHM at 400 m/z were used for full scan acquisitions. Data dependent acquisitions with MS/MS list having precursor ion accurate mass and RT were used for identification experiments. The precursor ions were isolated in the LTQ at an isolation width of 1 m/z, fragmented in the HCD cell and analyzed in the Orbitrap at a mass range of 100–750 m/z and resolving power of 60,000 FWHM at 400 m/z. The fragmentation was completed at 4 different collision energies, NCE–10, 30, 50 and 70 %. The chromatographic column used was an Acquity BEH C18, 1.7 μm 2.1 x 100 mm (Waters, Wexford Ireland) and the mobile phases used were 0.1% formic acid in water (A) and 0.1 % formic acid in methanol (B). The ESI+ gradient was as follows, (time in minutes, %B): (0, 1), (2.5, 1), (16, 99), (18, 99), (18.11, 1), (20, 1) with a flow rate of 0.4 ml/min. In ESI-, the same gradient with a flow rate of 0.36 ml/min was used.

3.16.3. Data analysis for untargeted metabolomics

Xcalibur 2.2 from Thermo Fisher Scientific (MA, USA) was used for instrument control and acquisition of the high resolution LC-MS data. The acquired .raw files were converted to .mzML format using the Proteowizard msconvert tool [318]. The data were uploaded to XCMS online for data pre-processing and analysis. The pre-processing parameters used are as follows: feature detection with centWave (m/z tolerance of 5 ppm, minimum and maximum peak widths of 5 and 20 respectively), RT correction with obiwarp method (profStep1), chromatographic alignment with mzwid - 0.05, minfrac 0.5 and bw 5. The multi-group data analysis was carried out using the Kruskal-Wallis non-parametric test with post hoc analysis. Peak intensities/area were normalized against cell counts. Multivariate analysis (orthogonal projection to partial least squares discriminant analysis; OPLS-DA) was completed in SIMCA v14.1 (Umetrics, Umea, Sweden) to visualize differences between sample groups and produced prediction models. For the metabolite identification by fragmentation the masses were chosen based on the variable importance in projection plots (VIP plots) generated by the SIMCA tool for the multi-group analysis. From this list significant features with p-value ≤ 0.05 , q-value ≤ 0.05 and peak intensity $\geq 10^5$ were chosen for identification. The high resolution mass spectral library, mzcloud was used for identification of unknown metabolites. The identified metabolites under different experimental conditions (HUVECs in RM, RMV, co-cultured with PC-3/S and PC-3/M cells) were represented by column plots. The identified features and their peak areas were analyzed using the MSEA tool in MetaboAnalyst [319] to identify the pattern of metabolite changes within the pre-defined metabolite set libraries. Peak area data was uploaded pairwise, as conditions of control (RM) vs RMV, PC-3/S and PC-3/M co-cultured HUVECs. In this case a quantitative enrichment analysis (QEA) was carried out with the peak area data, associated with the identified metabolites, uploaded into the web-based software and a Q-statistic was estimated for each metabolite set that describes the correlation between the peak area profiles, X, of the matched metabolite set and the phenotype labels, Y, which in our case are the different conditions of HUVECs with RM, RMV, PC-3/S and PC-3/M cells. Fold enrichment obtained from the MetaboAnalyst application of MSEA is calculated as the ratio of calculated statistic/expected statistic [309,320].

3.17. Statistics

Statistical analysis was carried out using Student's t-test, two-tailed for independent samples. For the *in vivo* efficacy assay, non-parametric Kruskal-Wallis test was employed followed by multiple comparisons using Dunn's test. Bar graphs represent the values of mean \pm standard deviation. Statistical significance was estimated by calculating the p-value and was indicated by asterisk (*) for differences among conditions and by hash (#) for differences among normoxia/hypoxia (Chapter 4.1) or time points (Chapter 4.3) (* $p \leq 0.05$, ** $p \leq 0.01$, *** $p \leq 0.001$, **** $p \leq 0.0001$). In some cases, to project the importance of no difference among conditions, non-significant differences were indicated as 'ns'.

4. RESULTS AND DISCUSSION

Chapter 4.1

4.1. Flux analysis of endothelial cells induced by VEGF: changes under normoxia and hypoxia

4.1.1. Introduction

As discussed in the introduction, VEGF is one of the most important factors driving angiogenesis and various changes induced by VEGF associated to signalling pathways have been identified recently [29,30]. In addition, it has been identified that hypoxia plays a main role in inducing angiogenesis to re-oxygenate the ischemic tissues and also induces an over-expression of VEGF by tumour and other stromal cells in order to activate endothelial cells for blood vessel formation [73,321-323]. Although molecular signalling pathways in endothelial cells linking VEGF and hypoxia inductions have been extensively studied, the metabolic changes that occur downstream of these activations are poorly understood. Hence we have applied the fluxomics approach in which we have combined the experimental measurements of ^{13}C labelling patterns, together with the data of consumption and production of selected metabolites for the estimation of metabolic fluxes [324]. Using this approach we have intended to characterize the metabolic pathways in the central carbon metabolic network of HUVECs, used as a model for endothelial cells, that are altered by VEGF and hypoxic conditions.

For this purpose, HUVECs were initially deprived of excess nutrients and hormones by maintaining them overnight in a restricted medium with only 2% fetal bovine serum, VEGF was then added (condition RMV) and incubated for 40 hours in the presence of the tracer [1,2- $^{13}\text{C}_2$]-glucose until sample collection, as described in the Methods section 3.1. In parallel, the control cells were incubated only with restricted medium (condition RM) containing the same tracer indicated above and for the same 40 hours. In the following sections we describe the results on the characterization of central carbon metabolism, obtained by the measurements of consumption and production of metabolites such as glucose, glutamine, lactate and glutamate

and the GC-MS analysis of ^{13}C isotopologue distribution in selected metabolites related to the main central carbon metabolic pathways. Our tracer based metabolomics approach combined a direct interpretation of ^{13}C labelling patterns with a computational model-based ^{13}C metabolic flux analysis approach [269,325], using the above-mentioned metabolite concentrations and label distribution measurements. Our combined approach consistently revealed the more subtle metabolic adaptations of HUVECs due to VEGF, within the expected larger remodelling associated to hypoxia.

4.1.2. Results

4.1.2.1. Net metabolite consumption and production with VEGF stimulation, under normoxia and hypoxia

Glucose and glutamine are the two main sources of cellular energy and are important for the formation of major macromolecules for cell proliferation, survival and function. Hence we first wanted to compare the utilization of these energy sources and production/consumption of lactate and glutamate by HUVECs in the presence of VEGF, under normoxia and hypoxia. These cells were incubated with 10 mM of glucose and 2 mM of glutamine during the experiment, as discussed in the Methods section 3.1. Figures 4.1.1a and 4.1.1b show the extracellular fluxes measured at 40 hours from the cell culture spent medium.

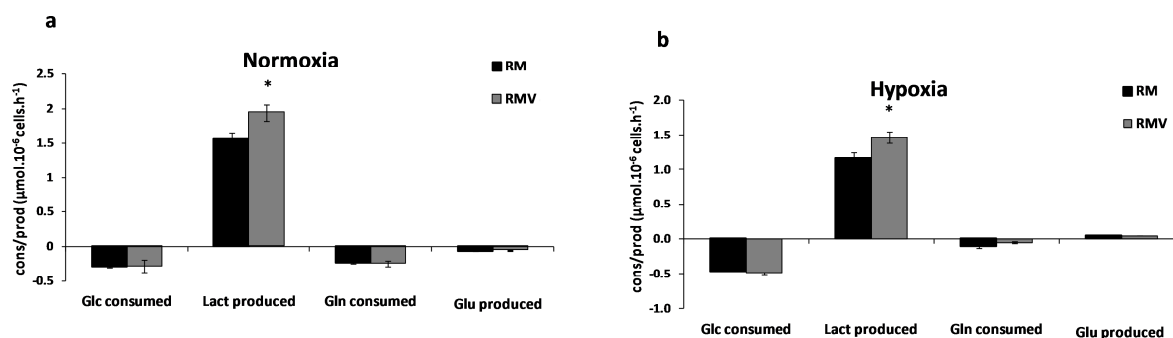


Figure 4.1.1: Net consumption and production of metabolites. The rates of the metabolite uptake (negative values) and secretion (positive values) in the spent cell culture medium are measured in the absence and presence of VEGF, under (a) normoxia, 21% O₂ and (b) hypoxia, 1% O₂. HUVECs were incubated with 10 mM of glucose and

From the Figure 4.1.1, we see that the presence of VEGF induces a significantly higher production of lactate under both normoxia and hypoxia, while there is no change in the glucose, glutamine or glutamate consumed with VEGF under both conditions. Moreover, HUVECs showed relatively higher glucose and lower glutamine consumption under hypoxia with respect to normoxia, showing that HUVECs under hypoxia are more glucose-dependent than the HUVECs under normoxia.

4.1.2.2. ¹³C-label enrichment in lactate

To gain more insights in the intracellular metabolic flux changes we incubated the HUVECs with 10 mM of 50% [1,2-¹³C]-glucose, as mentioned in the Methods section 3.1, to measure the ¹³C enrichment in lactate. Isotopologue distribution data for lactate and other metabolites analysed are shown as supplementary information in Appendix 2. It has to be reminded that m1, m2 and m3 are the fractional isotopologue distribution, where the number indicates the number of labelled carbons in the metabolite measured, as described in the Introduction section 1.6.1.1. The fraction m2 lactate, i.e., the lactate with two carbons labelled, is obtained by glycolytic pathway from the m2 labelled glucose, added at the beginning of the experiment. The results show that under normoxia VEGF induces a higher percentage of ¹³C-lactate enriched in m2, shown in Figure 4.1.2a while it does not seem to affect HUVECs under hypoxia (Figure 4.1.2b). Moreover, the total ¹³C-lactate calculated as the sum of m1, m2 and m3 lactate isotopologues, shown in Figure 4.1.2c, is significantly higher under hypoxia than normoxia, which clearly reflects that under hypoxia glucose is the main substrate for lactate production.

2 mM of glutamine for 40 hours, in the presence and absence of VEGF and the metabolite concentrations measured at the initial and final time points of incubation with VEGF were used for calculating consumption and production rates. Data are normalized using cell number and time (h). Lact – lactate, Glc – glucose, Gln – glutamine, Glu – glutamate, RM – HUVECs in restricted medium (control); RMV – HUVECs with RM+VEGF. Statistically significant difference among RM and RMV: * $p \leq 0.05$.

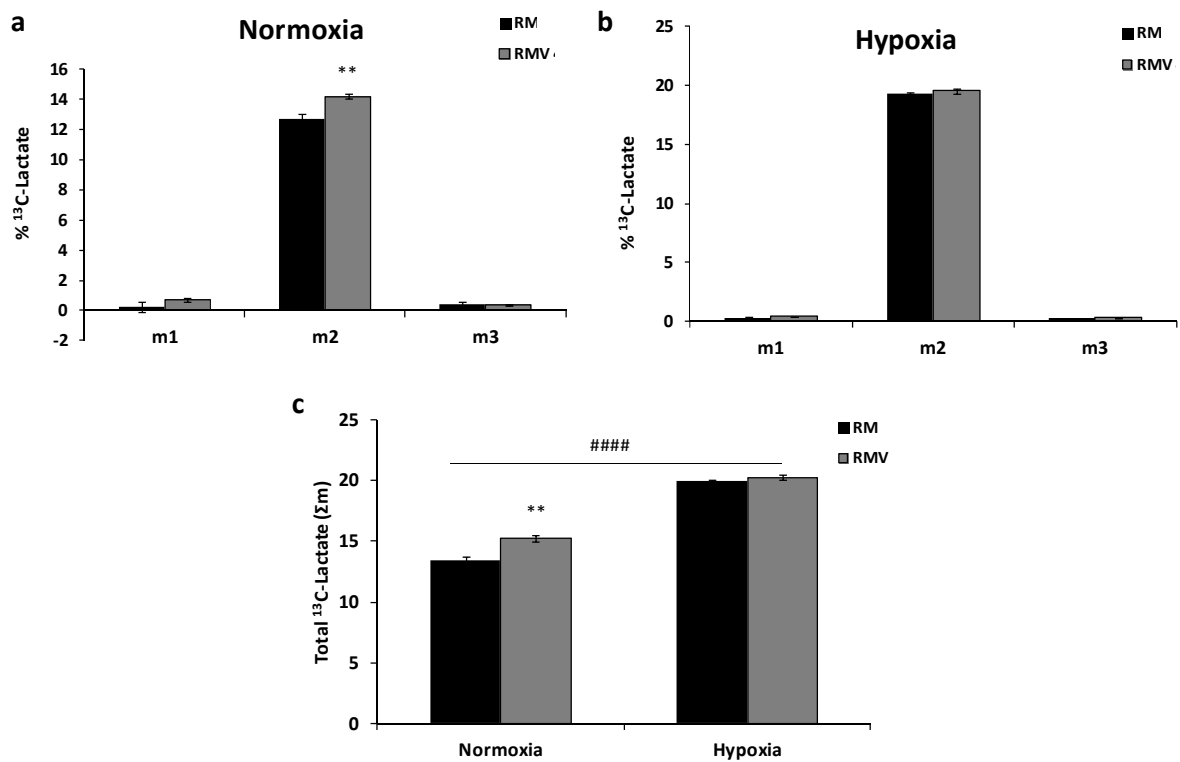


Figure 4.1.2: Comparison of the enrichment of ¹³C enrichment in HUVECs under normoxia and hypoxia, in the presence of VEGF. The % ¹³C-lactate enrichment in HUVECs under, (a) normoxia, (b) hypoxia and (c) the total ¹³C-enriched lactate, Σm calculated as the sum of m1+m2+m3, under both normoxia and hypoxia. HUVECs were incubated with or without VEGF and 50% of 10 mM [1,2-¹³C₂]-glucose as tracer, under normoxia and hypoxia for 40 hours and the ¹³C enrichment in lactate was measured from the spent cell culture medium after the incubation. RM – HUVECs in restricted medium (control); RMV – HUVECs with RM+VEGF. Statistically significant difference among RM and RMV: ** p ≤ 0.01, among RM/RMV of normoxia and hypoxia, respectively: #### p ≤ 0.0001.

4.1.2.3. ¹³C-label enrichment in ribose

Pentose phosphate pathway is important for cells to adapt themselves to two main kinds of situations, for producing macromolecules for cell proliferation or to produce NADPH to maintain redox homeostasis. These are carried out under different branches of PPP, the reversible non-oxidative and the irreversible oxidative branches controlled by the rate-limiting enzymes TKT and G6PD, respectively. Upon analyzing the ¹³C-label enrichment in lactate in HUVECs induced by VEGF under normoxia and hypoxia, we wanted to study the fluxes through PPP by measuring ¹³C enrichment in ribose. The isotopologue m1 ribose depicts the

contribution of the oxidative branch of PPP for the formation of ribose while m2 ribose gives the fractional contribution of non-oxidative branch of PPP for its formation, as explained in the general isotopologue distribution model with [1,2-¹³C]-glucose (which includes the label position information) in the Figure 1.6 of the Introduction part 1.6.1.1 of fluxomics. Figure 4.1.3 shows the ¹³C label enrichments and distribution in ribose and relative contributions of oxidative to non-oxidative PPP in producing ribose in HUVECs with VEGF under normoxia and hypoxia.

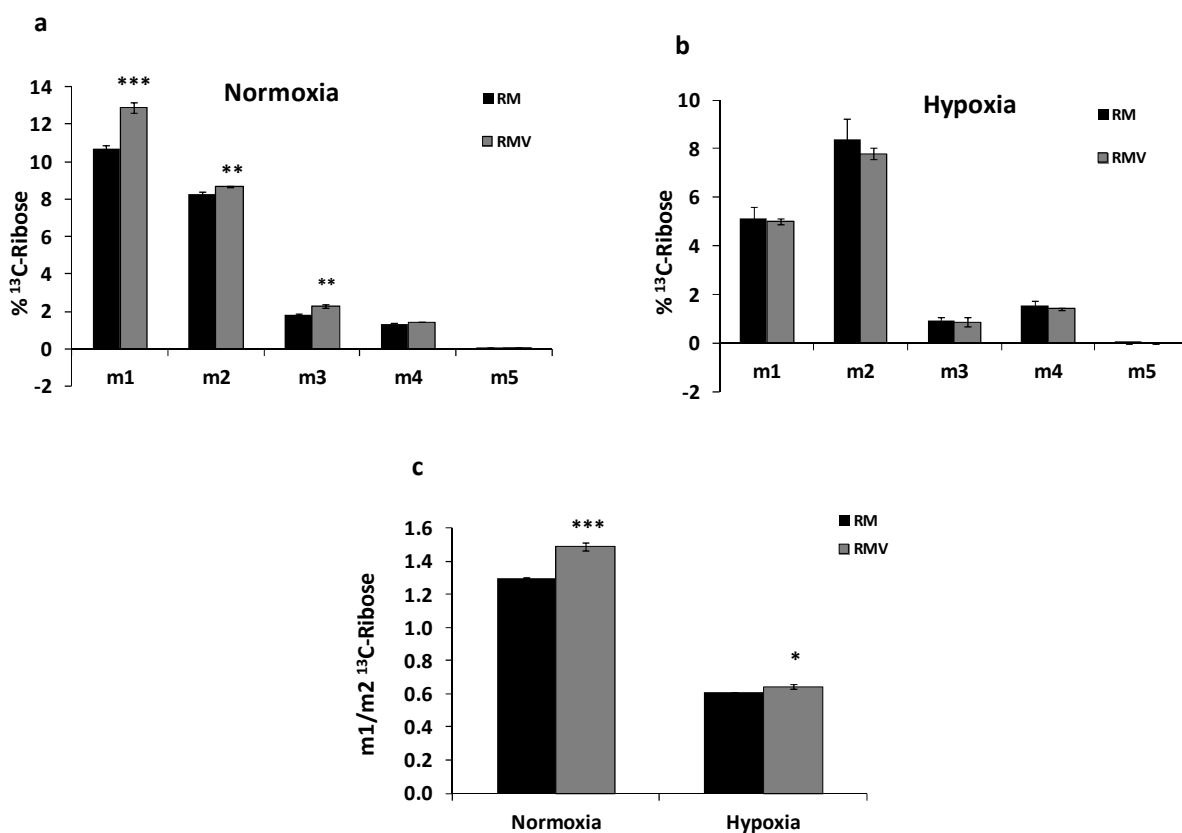


Figure 4.1.3: Glucose-derived carbon for the production of ribose through PPP is studied with ¹³C-enriched ribose. Isotopologue distribution in ribose under (a) normoxia, (b) hypoxia, (c) Ratio of the isotopologues m1/m2 indicative of oxidative to non-oxidative contributions to PPP, under normoxia and hypoxia. The label enrichment in ribose is calculated from the cell extracts after incubating HUVECs with and without VEGF and 50% of 10 mM [1,2-¹³C₂]-glucose, under normoxia and hypoxia for 40 hours. RM – HUVECs in restricted medium (control); RMV – HUVECs with RM+VEGF. Statistically significant difference among: RM and RMV - *p ≤ 0.05, **p ≤ 0.01, ***p ≤ 0.001.

Upon comparing the % ^{13}C ribose under normoxia and hypoxia in Figures 4.1.3a and 4.1.3b, we observe that the m2 and m4 ^{13}C ribose are similar under both conditions, while the m1 and m3 ^{13}C ribose under hypoxia are lower than that of normoxia. This shows that hypoxia reduces the flux of oxidative branch of PPP (depicted by the lower m1 fraction compared to normoxia) for the production of ribose in HUVECs. This is further supported by the ratio of the isotopologues m1/m2 ribose depicting the ratio of oxidative to non-oxidative branch of PPP, in Figure 4.1.3c, which is significantly reduced under hypoxia compared to normoxia. In addition VEGF induces a significant increase in ^{13}C -ribose under normoxia (Figure 4.1.3a) and a shift towards the synthesis of ribose through oxidative branch of PPP evident from the significantly higher m1/m2 ratio of ribose (Figure 4.1.3c).

In addition to the ^{13}C isotopologue analysis that shows VEGF increases the oxidative PPP under normoxia, the enzyme activity study of the rate-limiting enzyme of the oxidative PPP branch G6PD, measured under normoxia as shown in Figure 4.1.4, also depicts an increase of the activity with VEGF, supporting that VEGF induces an increase in the oxidative branch of PPP in HUVECs under normoxia.

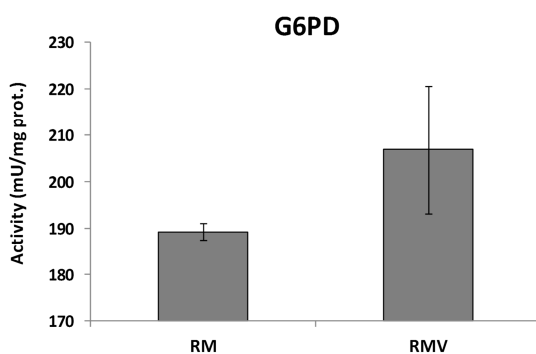


Figure 4.1.4: G6PD enzyme activity under normoxia, with and without VEGF. Enzyme activity assay of G6PD in cell extracts prepared after 40 hours of incubation of HUVECs with and without VEGF. G6PD – glucose-6-phosphate dehydrogenase; RM – HUVECs in restricted medium (control); RMV – HUVECs with RM+VEGF.

4.1.2.4. ¹³C-label enrichment in fatty acids

Fatty acids are an important part of cellular environment and are not only significant for energy storage, but also for maintaining cell membrane structure or as signalling molecules. Hence studying fatty acids metabolism is important for understanding its role in the central carbon metabolism of endothelial cells. In our study, we measured the ¹³C enrichment in the fatty acids palmitate and stearate, from labelled glucose, under both normoxia and hypoxia. The results are shown in Figure 4.1.5.

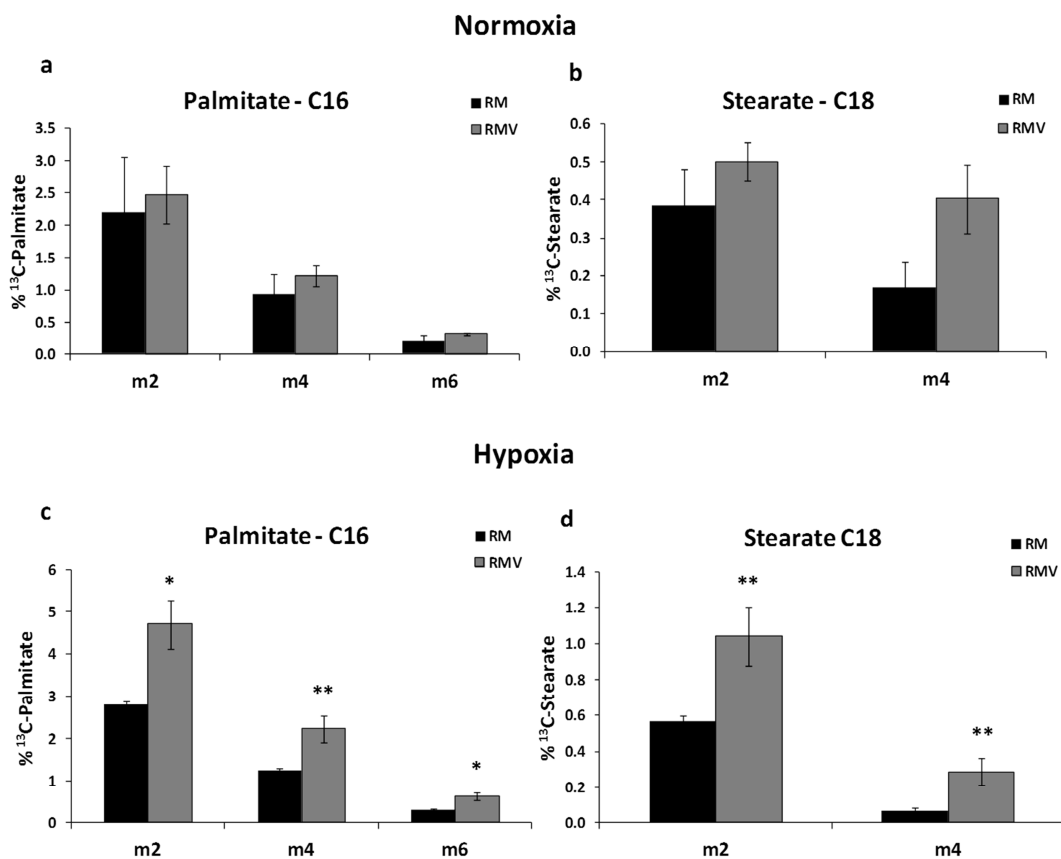


Figure 4.1.5: Isotopologue distribution in fatty acids, induced by VEGF. The ¹³C enrichments from glucose source in palmitate and stearate are shown under, (a) and (b) normoxia and (c) and (d) hypoxia, respectively. The ¹³C enrichments in fatty acids of HUVECs incubated with and without VEGF and 50% of 10 mM [1,2-¹³C₂]-glucose, under normoxia and hypoxia for 40 hours, were estimated from the cell extracts. RM – HUVECs in restricted medium (control); RMV – HUVECs with RM+VEGF. Statistically significant difference among RM and RMV - *p ≤ 0.05, **p ≤ 0.01.

The m2, m4 and m6, shown in the results, represent the ^{13}C enrichment from [1,2- ^{13}C]-glucose. Moreover, VEGF shows a tendency of increasing label enrichments in palmitate and stearate under both normoxia and hypoxia, although under hypoxia it is more significantly observed than under normoxia (Figures 4.1.5c and 4.1.5d). This label enrichment suggests that VEGF clearly induces higher fatty acid synthesis from the glucose-derived carbons and more significantly under hypoxia.

4.1.2.5. ^{13}C -label enrichment in glycogen and glycogen accumulation

Glycogen is a readily available energy store for cells and has varied significance for different cell types. Since the glucose carbons have a direct turnover (entrance and exit) to glycogen, we decided to measure the influence of VEGF and hypoxia on the glycogen content and glycogen ^{13}C enrichment from the labelled glucose in HUVEC, incubating the cells with 10 mM of 50% [1,2- ^{13}C]-glucose for 40 hours. Upon measuring the glycogen content in the presence and absence of VEGF we observe that VEGF induced a significant reduction of glycogen with respect to the control under both normoxia and hypoxia, as shown in the Figure 4.1.6. Moreover, under hypoxia the glycogen content was increased in HUVECs irrespective of the presence of VEGF, compared to normoxia.

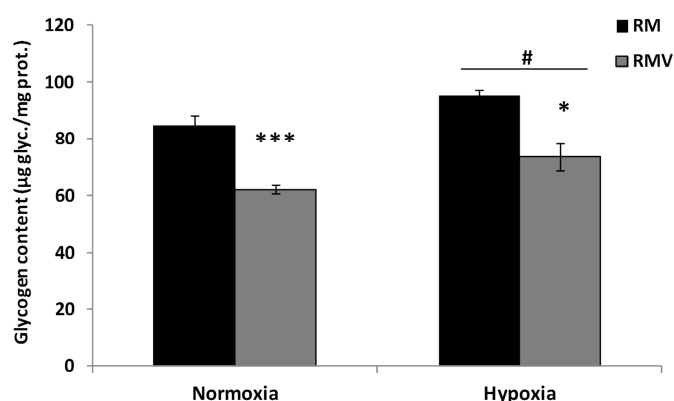


Figure 4.1.6: Glycogen content in HUVECs. Glycogen content (μg glycogen/mg protein) measured in HUVECs, both with and without VEGF incubation, under normoxia and hypoxia. The measurements were performed using the cell extracts of HUVECs after 40 hours of incubation with and without VEGF, under normoxia and hypoxia, and with

Although the results obtained (in Figure 4.1.6) were for 40 hours of incubation with labelled glucose and VEGF, the glycogen ^{13}C enrichment measured at this time point was at similar level to that measured at 72 hours incubation period (shown in Figure 4.1.7b), under normoxia. This showed that the label enrichment in glycogen was saturated at these time points and that only the glucose molecules that form the external structure of the glycogen molecule participate in glycogen turnover. Hence it is difficult to explain if there is an active glycogen turnover in HUVECs from these results and so in order to explore the glycogen metabolism better we performed a short time course experiment for 3, 7 and 24 hours under normoxia and measured the glycogen content and ^{13}C enrichment from glucose, as displayed in Figure 4.1.7. As shown in Figure 4.1.7a, VEGF decreased glycogen content in HUVECs from 7 hours. Moreover, we see a constant increase in ^{13}C enrichment of glycogen in Figure 4.1.7b, which also reveals that VEGF significantly lowers the ^{13}C enrichment at the time points of 3, 7 and 24 hours. These results indicate that glycogen turnover works slower in VEGF-treated cells than in control cells.

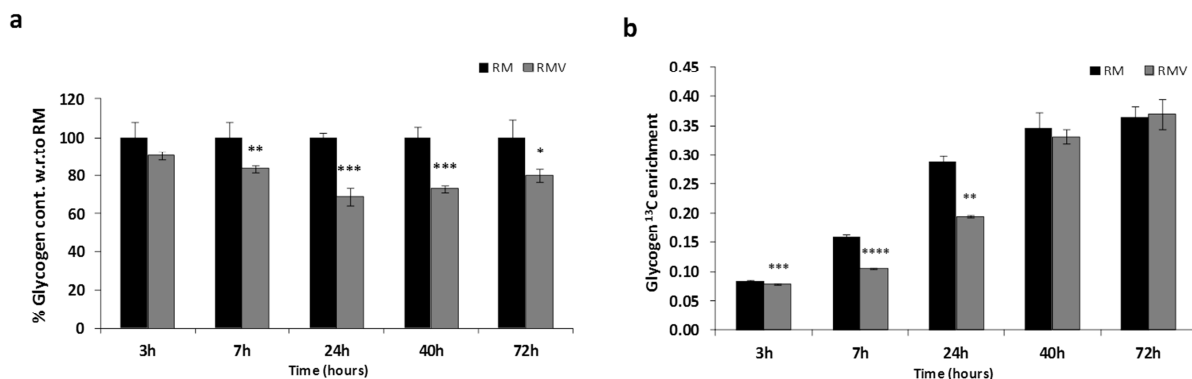


Figure 4.1.7: Glycogen accumulation and ^{13}C enrichment of HUVECs incubation with and without VEGF. The time-course experimental results show glycogen content and ^{13}C -enrichment in glucose-derived from glycogen in HUVECs under normoxia. (a) Percentage of glycogen content in RMV condition with respect to the control RM, (b) Glycogen ^{13}C enrichment. RM – HUVECs in restricted medium (control); RMV – HUVECs with RM+VEGF. Statistically significant difference among: RM and RMV - * $p \leq 0.05$, ** $p \leq 0.01$, *** $p \leq 0.001$, **** $p \leq 0.0001$.

10 mM of glucose. RM – HUVECs in restricted medium (control); RMV – HUVECs with RM+VEGF. Statistically significant difference among: RM and RMV - * $p \leq 0.05$, *** $p \leq 0.001$; among normoxia and hypoxia - # $p \leq 0.05$.

4.1.2.6. ¹³C metabolic flux analysis for estimation of fluxes

In order to estimate the flux distribution in the central carbon metabolic network, the results obtained from the measurements of metabolite consumption and production and the ¹³C labelling patterns of the different metabolites (shown in Appendix 2) were used in computational modelling. This method was used to develop a model of the central carbon metabolism, comparing the measured and predicted ¹³C isotopologue distributions, as described in the Methods section 3.14.2 of ¹³C flux analysis and Appendix 1. Importantly, the metabolic network included the conservation of cytoplasmic and mitochondrial NADH/NAD⁺ and mitochondrial acetyl-CoA/CoA, which are the fundamental constraints for central carbon metabolism. The ¹³C tracer analysis results of the metabolites glucose, lactate, glutamate, ribose and glycogen, described in the previous sections, were used for constructing the model that assumes an experimental steady state, while the data from the fatty acid ¹³C enrichment could not be used as the label enrichments have not reached a steady state even after 40 and 72 hours of incubation with the tracer (72 hours data for fatty acids not shown). Although the ¹³C label distributions in amino acids such as proline, serine, aspartate+asparagine and glutamate+glutamine have not shown changes in both the control and VEGF-incubated HUVECs (data not shown), the data were used for the ¹³C flux analysis using computational modelling. The network of reactions considered as well as the flux distributions predicted by the model for the four conditions studied (control and VEGF-treated HUVECs under normoxia and those under hypoxia) are shown in Figure 4.1.8. This network of reactions in the model compares the changes in the absolute values of fluxes through key reactions of the control and VEGF conditions under normoxia and hypoxia. The absolute flux values covering the transformation and oxidation of glucose, amino acids and fatty acids, including the synthesis of pentose-phosphates and release of lactate and glutamate were used to perform the quantitative analysis of metabolic flux distribution.

The model reveals that there is an important metabolic reorganization induced by hypoxia that is affecting in parallel both the control HUVECs (RM) and VEGF-treated cells (RMV). Clearly, cells under normoxia have a metabolism with a more relevant role for mitochondria and the use of

carbon sources other than glucose, while hypoxia leads to a more clearly dominant glycolytic pattern, in agreement with previous observations [326]. This prediction is consistent with the analysis in the section 4.1.2.1 where, irrespective of the slightly higher lactate production under normoxia, compared to hypoxia, higher glucose utilization was observed under hypoxia (Figure 4.1.1) and the model prediction gives additional information that under normoxia pathways other than glycolysis are also active. Accordingly, in order to predict the measured ^{13}C labelling patterns, the computational process of flux estimation considered the ratios among fluxes associated with mitochondrial activity versus the flux of lactate release. Also, changes in the ratios among fluxes were performed to emphasize a relevant reorganization of PPP, suggesting a clear decrease of the activity of the oxidative branch of PPP under hypoxia, as shown by the reduction of flux distribution by hypoxia in the reaction R_{G6PD} in the computational model in Figure 4.1.8. This supports the calculation of PPP in the results section 4.1.2.3 where hypoxia showed a decrease in the oxidative branch of PPP with respect to the non-oxidative branch. Also, the model is consistent with a slightly higher oxidative PPP activity for VEGF treated cells suggested by our previous analysis.

In addition, though at a lesser extent, the model also shows that under normoxia VEGF increases mitochondrial reactions by using carbon sources other than glucose. However, in contrast to this observation, under hypoxia these smaller changes are not observed at the level of the ratios among fluxes that are required to predict the measured ^{13}C labelling patterns. The use of alternative pathways in addition to glycolysis (for lactate production) predicted under normoxia can be explained by the fact that the reduced NADH produced by glycolysis is not enough to support the observed LDH's NADH-dependent release of lactate, then requiring additional NADH from other sources. On the other hand, this higher ratio also implies alternative sources other than glucose that are providing the carbons for lactate. Altogether the results suggest that a strong homeostatic regulation is associated with all the processes induced in our experiments. Homeostatic adaptations have the potential to lead to stressing equilibria and then to emphasize metabolic fragilities that could be exploited following a biomedical objective.

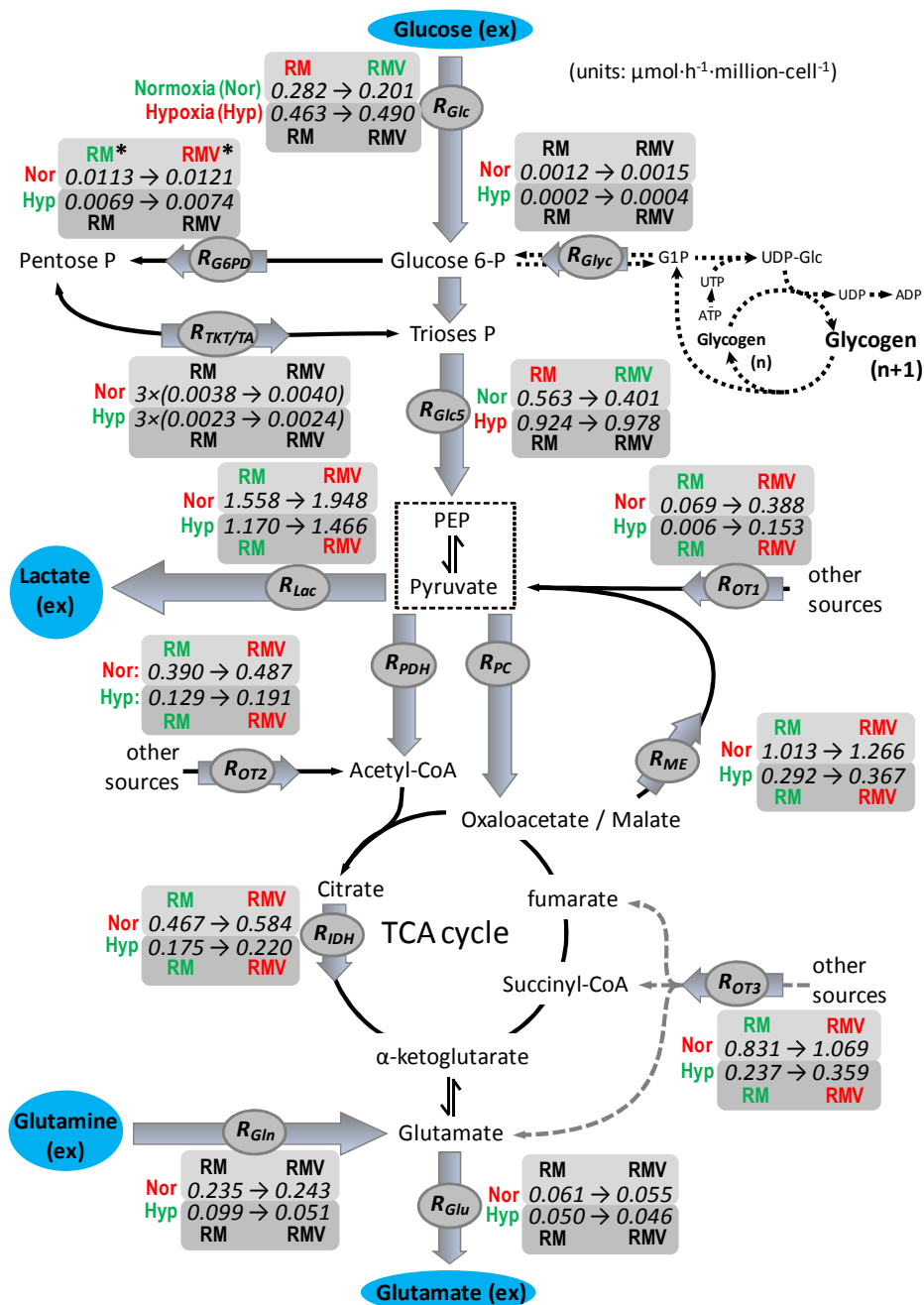


Figure 4.1.8: Computational network model of flux distributions. The ^{13}C flux analysis shows the flux distributions in the central carbon metabolism of HUVECs in the presence of VEGF, under normoxia and hypoxia. Fluxes are predicted with the ^{13}C tracer analysis encompassing ^{13}C label enrichment analysis and the concentrations of the consumption/production of metabolites measured. The flux distributions are represented as the reactions (R_i) covering the central carbon metabolism. Nor – Normoxia, Hyp – Hypoxia, RM – HUVECs in restricted medium (control); RMV – HUVECs with RM+VEGF, IDH – isocitrate dehydrogenase, Lac – lactate, G6PD – glucose-6-phosphate dehydrogenase, Glc – glucose, Gln – glutamine, Glu – glutamate, Glyc – glycogen, ME – mitochondrial reaction flux, OT1, OT2, OT3 – group of reactions with alternative sources of carbons, PC – pyruvate carboxylase,

4.1.3. Discussion

Endothelial cells are imperative for the formation of blood vessels which is important for the blood supply for entire human body and are affected in many pathological angiogenic processes like diabetes and cancer [327]. In addition, endothelial cells are in constant contact with blood and its constituents and have to adapt to local environmental changes like differing oxygen tensions, growth factors and angiogenic factors, according to the changes in organs in which they form the blood vessels. All these constant environmental changes can ultimately cause a metabolic reprogramming of the endothelial cells to adapt to the signals to survive, proliferate and form blood vessels. The most important factors that can affect the endothelial cells are the changing oxygen tensions and secretion of angiogenic factors by neighbouring cells that are in need of blood vessel formation. An overall study of the metabolic adaptations due to these changes is vital to find key pathways in the endothelial cells that can be used as therapeutic targets against the pathologies that require blood vessel formation, such as diabetic retinopathy and tumour angiogenesis. Few important methods can be implied for this holistic approach such as fluxomics and metabolomics. Fluxomics is a targeted study and uses ^{13}C -labelled isotopic tracers in studying the cellular metabolism by determining the relative pathway contributions in the metabolic pathways under study. Mass spectrometry is a powerful technique used widely to quantify the ^{13}C labelling patterns accurately with smaller confidence intervals [328]. The measured label distributions along with the metabolite consumption/production data can then be subjected to a direct interpretation of fluxes using simple analytical formulas based on the previous knowledge of the metabolic pathways [275]. In addition to this ^{13}C tracer analysis approach, model-based predictions known as ^{13}C flux analysis are helpful in constructing a holistic metabolic network of reactions with the information from ^{13}C tracer analysis and also by predicting flux distributions, increasing the confidence of the biological conclusions. This modelling-based flux analysis can be used to

PDH – pyruvate dehydrogenase, TKT/TA – transketolase/transaldolase. Red colour denotes increase and green colour denotes decrease in fluxes in the respective conditions.

validate the ^{13}C tracer analysis interpretations and also provide additional information on flux estimations [269].

In our study we have characterized the metabolic reprogramming of HUVECs, as a model of endothelial cells, under normoxia (with 21% oxygen) and hypoxia (with 1% oxygen) and in the presence of the pro-angiogenic factor VEGF. Our results have revealed key changes in the metabolic pathways along the central carbon metabolism. Thus, our results show that hypoxia induces a major metabolic adaptation by HUVECs revealing a more glucose-dependent phenotype, compared to normoxia. In addition, HUVECs under hypoxia show a lower flux of the irreversible oxidative PPP branch compared to normoxia. Under hypoxia VEGF induced an increase of fatty acid synthesis from glucose. Moreover, VEGF reduced glycogen turnover in HUVECs under normoxia. Also hypoxia induced an increase of glycogen content, compared to normoxia, and VEGF reduced the glycogen content under both normoxia and hypoxia. Other smaller but significant changes of HUVECs with VEGF include a slight but significantly higher production of lactate, under both normoxia and hypoxia and the increase of the oxidative branch of PPP under normoxia.

Endothelial cells in general are observed to be highly glycolytic, in the presence or absence of oxygen, unless under stress when they shift to mitochondrial oxidation [118,119]. Hypoxia is known to induce glycolysis further [326] and upregulate hypoxia-associated stress proteins such as the glycolytic enzymes glyceraldehyde-3-phosphate dehydrogenase (GAPDH) and non-neuronal enolase in endothelial cells [75,329]. Moreover VEGF promotes increased expression of GLUT1 transporter [120] and glycolytic enzymes like LDH-A and PFKFB3 [119,121] in endothelial cells. Hence the preference of glycolysis by endothelial cells could be due to reasons such as varying oxygen tension in the blood flow and their exposure to tissues with low oxygen levels to perfuse them with blood vessels. Moreover our computational ^{13}C flux analysis shows that normoxic HUVECs depend on other pathways to produce lactate in addition to glycolysis which could be possible as the endothelial cells have been shown to utilize glucose oxidation by OXPHOS during conditions of high metabolic demand or stress [124]. In addition, the ^{13}C flux analysis predicts a preference of VEGF-induced mitochondrial activity under normoxia from our

study. It has been shown that VEGF increases mitochondria biogenesis and ROS production *in vitro* in endothelial cells [129,330] and mitochondria-derived ROS has been implicated as pro-angiogenic signalling molecules at non-toxic levels [331,332].

The oxidative branch of PPP is governed by the rate-limiting enzyme G6PD and this pathway is required for the conversion of G6P into ribulose-5-phosphate (Ru5P) to produce NADPH for maintaining cellular redox balance and R5P to synthesize nucleotides. Under normoxia the mitochondrial activity is higher in general compared to hypoxia and there is higher production of ROS for the same. The need for maintaining cellular homeostasis induces a shift to produce ROS-reducing molecules such as NADPH by increasing G6PD activity. It is shown that the vascular endothelial cells overexpress G6PD producing NADPH that functions as a cofactor for endothelial nitric oxide synthase (eNOS) for the production of the endothelial pro-angiogenic signal NO and the reduction of ROS [131]. It was also shown that VEGF increases G6PD activity in endothelial cells [134] and inhibiting or silencing G6PD enzyme decreased the endothelial cell proliferation, viability, migration and tube formation *in vitro* [135,333] under normoxia. These observations show that the oxidative branch of PPP has a protective role against oxidative stress in endothelial cells. We have observed from our results of VEGF induction in HUVECs at normoxia, an increase of the oxidative branch of PPP thus depending on the stress-reducing pathway. From our results we have also observed that hypoxia induced a shift of glucose carbons to the non-oxidative branch relative to the oxidative branch of PPP. In a similar case, in drug resistant leukemia cells the HIF1 α has shown to promote non-oxidative branch compared to the oxidative branch of PPP, by activating the enzyme TKT [334]. Endothelial cells forming blood vessels sense and respond to different forms of pathological stresses in particular due to deficient oxygen such as those prevailing in hypoxic regions of tumours. Formation of blood vessels in these regions re-oxygenates the tumour regions and helps them in survival and spread to other tissues through metastasis.

Endothelial cells have shown to express enzymes that are essential for fatty acid synthesis such as, ATP citrate lyase that produces acetyl-CoA from citrate, acetyl-CoA carboxylase that converts acetyl-CoA into malonyl-CoA, and fatty acid synthase that is involved in the synthesis

of long-chain fatty acids like palmitate from malonyl-CoA and acetyl-CoA (reviewed in Harjes, 2015 [335]). And it has been reported that inhibiting fatty acid synthase in endothelial cells reduces the endothelial cell fatty acid synthesis, cell proliferation and the exposure of VEGFR2 on cell surface that can disrupt the binding of VEGF, in addition inducing anti-angiogenic effects [336,337]. In turn we observe from our results that VEGF induces an increase in fatty acid synthesis from glucose which, taking into account the previous studies mentioned above, could be important for the endothelial cell survival or angiogenesis.

Finally, we have noticed a metabolic change in HUVECs in this study related to glycogen metabolism. Glycogen is an important energy reserve for many cell types. In liver tissues glycogen breakdown is important for the production of glucose to feed other tissues, while in muscles glycogen is the main fuel for generating its own ATP during strenuous exercise. They have also shown to play key roles in other cell types such as astrocytes and neurons, where astrocytes have been reported to use glycogen for producing lactate to fuel its neighbouring cells, while neurons depend on glycogen during acute hypoxic stress for its survival [256,338,339]. Glycogen utilization has also been shown essential for cancer cell survival, whose inhibition has shown to induce cellular apoptosis [176]. Endothelial cells have shown to divert a fraction of glucose to glycogen reserves [150,152]. In a previous study in our lab we showed that the glycogen reserves in HUVECs are utilized during glucose deprivation [135], indicating that they are essential for sustaining endothelial cell glycolysis. In our present study we have observed the presence of a futile cycle in glycogen metabolism in HUVECs and the presence of VEGF reduces this turnover. A preliminary study by inhibiting glycogen degradation showed a reduction in HUVEC viability and migration [135]. However the role of glycogen metabolism and its functional relevance is still underestimated in endothelial cells due to the lack of sufficient studies. It is clear that though the glycogen reserve is simply observed as an energy store, its metabolism is involved in distinct cellular functions and in most of the cases for the fundamental cellular protection and survival. The significant flux changes and the active glycogen metabolism observed in HUVECs in our study in addition strengthens this observation and tempts us to consider that the glycogen reserve and metabolism could possess far more significance in endothelial cell metabolism.

Chapter 4.2

4.2. Untargeted metabolomics in endothelial cells induced by VEGF and metastatically different sub-populations of prostate cancer cells

4.2.1. Introduction

Tumour angiogenesis is an important hallmark of cancer and the study of its metabolic adaptations can reveal attractive targets for inhibiting cancer growth. In the tumour microenvironment, endothelial cells interact with heterogeneous tumour cell types that drive angiogenesis and metastasis [340]. In Chapter 4.1 we saw the differences in HUVEC metabolism induced by VEGF in normoxic and hypoxic conditions, although following the flux changes only along a limited part of the central carbon metabolic pathways targeting glycolysis, PPP, fatty acid metabolism, amino acid metabolism and glycogen metabolism. In the present chapter we have intended to characterize globally the metabolic alterations in HUVEC with VEGF and in the presence of tumour cells with extremely different metastatic abilities, using untargeted analysis.

In order to understand the metabolic changes that affect the angiogenesis associated with tumours it is important to choose a method that can focus only on the affected endothelial cells, which is not quite possible *in vivo* as it could be complex to extract different types of stromal cells from the tumour tissues. The *in vitro* co-culture method employed in this study is both simple and also intends to closely imitate the tumour-endothelial cell association *in vivo*. When combined with the HRMS-based metabolomics, the method can give us a global picture of the early metabolic events induced by tumour cells on endothelial cells. In this study HUVECs were incubated under normoxia for 24 hours with VEGF and also co-cultured under same conditions with prostate cancer sub-populations that exhibit extreme metastatic abilities: the PC-3/M cell line that is rich in cancer stem cell (CSC) properties and is highly metastatic and the PC-3/S cell line displaying epithelial-mesenchymal transition (EMT) program and is highly

invasive but poorly metastatic. HUVECs under restricted medium were included as control in the study. The pellets harvested after incubation were subjected to metabolite extraction and analyzed using UHPLC coupled with Orbitrap Elite mass spectrometer, as described in the Methods section 3.16. Sample analysis was done under both positive and negative ionization modes. The untargeted MS data extracted was subjected to feature detection using the XCMS Online software, preliminary multivariate data analysis using SIMCA tool and metabolite identifications were done based on selected ion fragmentation and were confirmed with the online mass spectral fragmentation database, as described in the Methods section 3.16.3. Following this the MSEA was used to explore the metabolites highly enriched and associated with possible metabolic pathways and the results of metabolite changes and pathway enrichments obtained with each condition are discussed in the following section. These results provide an overall preview of the metabolic plasticity of endothelial cells in the heterogeneous tumour microenvironment, which could be exploited in combined therapies targeting not only the tumour cell reprogramming, but also the metabolic changes of endothelial cells induced by this microenvironment.

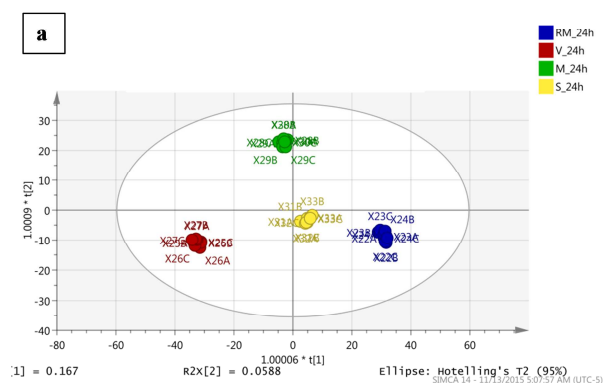
4.2.2. Results

4.2.2.1. Multivariate data analysis

After 24 hours incubation of HUVECs with VEGF and the PC-3/S and PC-3/M cell lines, the cell samples were collected and metabolite extraction was done to inject into the LC-MS to carry out the untargeted analysis, as described in the Methods section 3.16.1. After the sample runs the raw spectral data extracted from mass spectrometer was analysed through XCMS Online, a web-based software for processing LC-MS data for metabolomics [306,341]. Using this online platform we could identify 5285 features in ESI+ and 1366 features in ESI- by multi-group analysis, based on retention time and m/z value matches. Within XCMS Online each feature is putatively matched with its structural identity through METLIN database. Multivariate data analysis for all the conditions was done using OPLS-DA and the scores plot is represented in

Figure 4.2.1. The ESI+ data showed cumulative values of $R^2(Y) = 99.7\%$ and $Q^2 = 86.2\%$ and ESI- showed $R^2(Y) = 97.9\%$ and $Q^2 = 86.3\%$, where R^2 indicates the variation shown by all the components in the model and Q^2 is the accuracy of the model prediction of the class membership. These high values show a clear distinction between the control and the different treatment conditions (VEGF, PC-3/S cells and PC-3/M cells).

ESI+:



ESI-:

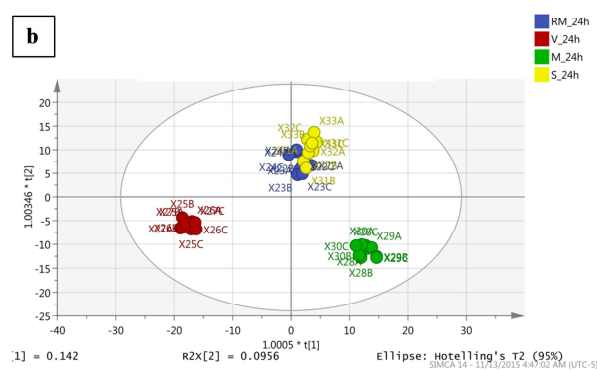


Figure 4.2.1: Multivariate data analysis of the experimental groups. Orthogonal projection to partial least squares discriminant analysis (OPLS-DA) plots of the experimental groups of data from: (a) ESI+ ionization mode, (b) ESI- ionization mode. R^2 indicates the variation shown by all the components in the model and Q^2 is the accuracy of the model prediction of the class membership. The peak area data extracted from the XCMS Online analysis of the untargeted raw data was analyzed through the SIMCA tool for performing this OPLS-DA multivariate statistics. RM_24h – Control HUVECs incubated in restricted medium for 24h, V_24h - HUVECs incubated in restricted medium with VEGF for 24h, M_24h – HUVECs co-cultured with PC-3/M cells for 24h, S_24h – HUVECs co-cultured with PC-3/S cells for 24h.

4.2.2.2. Metabolite identifications

Following the multivariate statistical analysis we selected top 200 features from the VIP plots based on their higher variance among the experimental groups of HUVECs mentioned above. We then short-listed them by cross checking their chromatographic peak shapes, peak intensities and p-values in their corresponding spectral profiles in XCMS and removing the ions of peak intensity < 100000 and p-value > 0.05 . The short-listed ions were subjected to MS/MS fragmentation, as described in the Methods section 3.16.2, and the identification of the metabolites were confirmed by comparing with the metabolite fragmentation pattern in the

high resolution mass spectral library mzCloud (<https://www.mzcloud.org>). Untargeted mass spectral metabolomics profiling is currently bottlenecked due to the lack of available spectral libraries. However identification confidence increases with the use of one or more of following data: accurate mass, isotopic pattern match, retention time match with reference standards and fragmentation spectral match. The metabolomics community is increasingly consensus of the need for reporting the confidence and means of identification and, as a result, different scoring systems have been suggested [300,342-344] . In this work, we adapted a quantitative metabolite identification metric as proposed by Sumer *et.al.* [342]. Briefly, the authors have proposed an identification scoring system, which sums the identification points gained from each type of data used for identification of the feature. The identification points system is shown in Table A3.1 of Appendix 3. A minimum score of the identification points (IP) is suggested to be 5 [342]. In this work, accurate mass match with a tolerance of 5 ppm (1.0 IP), accurate mass tandem mass spectrum (2.0 IP), molecular formula from accurate mass and isotopic pattern (1.0 IP), followed by match with a high resolution spectral library were used for all the identified metabolites. The total score for each metabolite is calculated as, (1+2+1)*1.5=6 (the score is multiplied by 1.5 for spectral library or 2 for the use of standards). The list of the putatively identified metabolites is given in Table 4.2.1.

Table 4.2.1. Putative metabolite identifications with ESI+ and ESI- modes.

ESI+

Identified metabolites	Accurate mass from XCMS Online [M+H]	Retention time (min)	p-value
L-Glutamate	148.0600	0.7	0.00509
L-Arginine	175.1182	0.65	0.00007
L-Glutathione reduced	308.0900	1.15	0.00067
L-Tryptophan	205.0965	5.3	0.00001
L-Tyrosine	182.0805	1.49	0.00002
L-Methionine	150.0579	1.13	6.07226e-6
Nicotinamide dinucleotide (NAD+)	664.1141	1.30	7.25358e-6
Pantothenic acid (CID match)	220.1173	5.09	0.00004
Oleamide	282.2781	16.32	0.00342
γ -L-Glutamyl-L-Glutamic acid	277.1021	0.93	0.00125

Identified metabolites ESI+ cont...	Accurate mass from XCMS Online [M+H]	Retention time (min)	p-value
Spermine	203.2223	0.51	ns
<i>trans</i> 3-Indole acrylic acid/Indole 3- acrylic acid	188.0700	5.3	0.00001
Cysteinylglycine	179.0479	1.15	0.00046
Guanine	152.0561	0.91	0.00017
Creatine	132.0763	0.73	0.0005
Hypoxanthine*	137.0453	1.19/ 2.71	0.00007/ 0.00401
Acetyl L-Carnitine	204.1222	1.01	1.66321e-6

*Hypoxanthine shows two isotopic peaks at the same accurate mass.

ESI-

Identified metabolites	Accurate mass from XCMS Online [M-H]	Retention time (min)	p-value
L-Aspartate	132.0298	0.74	0.01284
L-Glutamate [#]	146.0454	0.75	ns
Glycerol 3-phosphate	171.0058	0.82	ns
Pantothenic acid [#]	218.1026	5.26	0.00013
Uridine	243.0613	1.72	0.00445
L-Glutathione reduced [#]	306.0752	1.24	0.00052
Uridine monophosphate	323.0273	1.10	0.04184
Adenosine monophosphate	346.0544	1.11	ns
Galactonic acid	195.0503	0.76	ns
Guanosine	282.0834	2.82	0.01496

[#]Metabolites present both in ESI+ and ESI- modes. p-values extracted from the XCMS Online data analysis are for the entire group (Kruskal-Wallis non-parametric statistical test [306]). ns – not significant.

The chromatographic peak, accurate mass of the precursor ion, fragmentation spectral match of the identified metabolites and the isotopic pattern match are shown in the Figure A4.1 of Appendix 4. It is clear that while ESI+ mode is better in extracting higher number of features and metabolites, both ESI+ and ESI- negative modes provide complementary information and different sets of metabolites, except for the redundancy observed in L-glutamate, pantothenic acid and L-glutathione. The normalized peak areas of the metabolites identified, for each of the condition are shown in the Table A3.2 of Appendix 3.

4.2.2.3. Metabolite set enrichment analysis of the identified metabolites

The putatively identified compounds were then subjected to MSEA, which is similar to the gene set enrichment analysis (GSEA), through the MetaboAnalyst 3.0 software [308,319], where a biologically meaningful pattern was estimated for our identified metabolites using a pre-defined set of metabolites, associated to the metabolic pathways. In this case the peak area profiles of the identified metabolites, given in Table A3.2 in Appendix 3, were uploaded to the web-based MSEA software and a pair-wise analysis using QEA [320], which correlates the peak area profiles of the matched metabolite sets and the phenotype labels (in our case the different conditions of the experiment), was performed for each pairs of conditions: control (RM) vs VEGF, PC-3/S and PC-3/M co-cultured HUVECs. Figure 4.2.2 summarizes the pathways that are altered at higher fold enrichments for each of the pairs of conditions (the complete result of the MSEA analysis is shown in Figure A3.1 of Appendix 3).

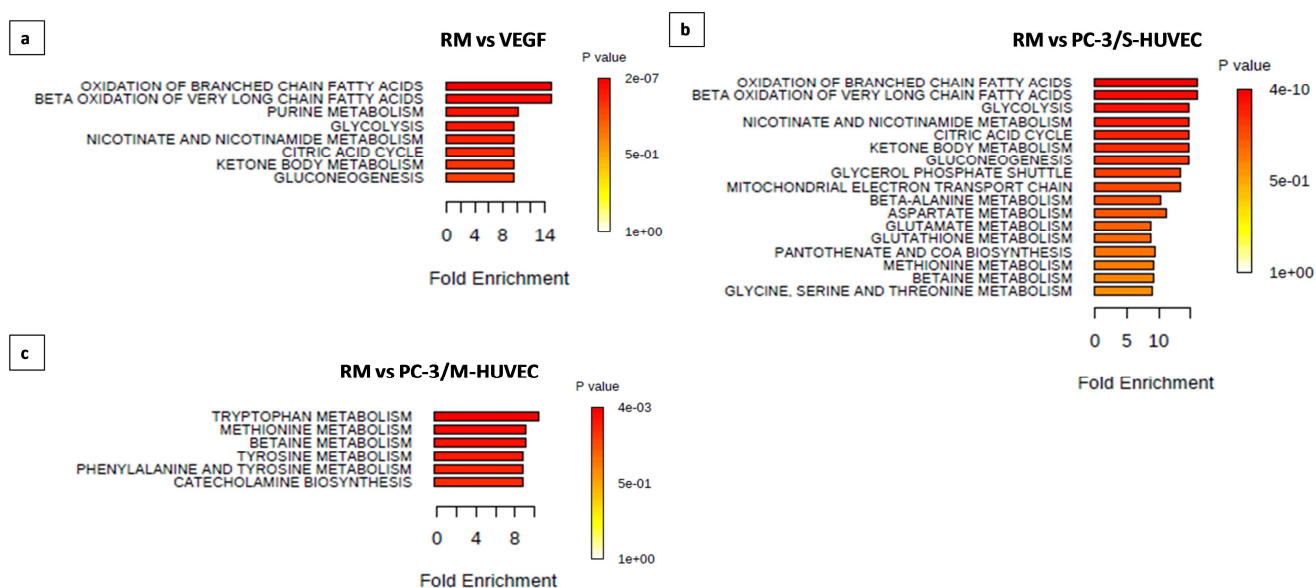


Figure 4.2.2: Metabolite Set Enrichment Analysis for pathway analysis. Pathways associated with MSEA on HUVECs in the presence of (a) VEGF, (b) PC-3/S and (c) PC-3/M cells compared to the control (RM). This representation shows the pathways enriched by the identified metabolites and their quantitative values, irrespective of the upregulation or downregulation of the individual metabolites within the pathways identified.

The analysis reveals that most of the metabolic pathways that are altered in HUVEC are in common for both the conditions of VEGF and PC-3/S cell co-culture. The common metabolic pathways altered in HUVECs in the presence of VEGF and PC-3/S cells are those related to fatty acid β -oxidation (associated with acetyl L-carnitine (ALC)) and glycolysis, nicotinate and nicotinamide metabolism, citric acid cycle, ketone body metabolism and gluconeogenesis (all of these related to NAD⁺). Apart from these VEGF also induces a change in purine metabolism (hypoxanthine, guanine and AMP), while PC-3/S cells alter metabolites related to the pathways of glutathione, pantothenate and amino acid metabolism. In the case of PC-3/M (Figure 4.2.2c), pathways related to methionine and betaine are shown to be enriched, also included in the condition of HUVECs with PC-3/S, while in addition it alters other pathways related to tryptophan and tyrosine (tyrosine and phenylalanine metabolism and catecholamine biosynthesis). Although this metabolite enrichment data shows the arrangement of the identified metabolites into meaningful metabolic pathways, it does not give us the information of the upregulation or downregulation of the respective metabolites, with respect to the control. Thus in order to deeply understand the results we constructed bar graph models for the peak areas of the identified metabolites and incorporated them into the ad hoc pathways, generated with the help of the MSEA, as shown in Figures 4.2.3 - 4.2.5.

In Figure 4.2.3, the bar graphs show the changes in peak areas of the metabolites among the conditions of HUVECs in RM, VEGF and PC-3/S co-culture. Figure 4.2.3a shows that ALC is upregulated in HUVECs both under VEGF and PC-3/S co-culture, where the fold change is $\geq 1.5X$ in both the cases, and is associated with fatty acid oxidation according to the MSEA (Figures 4.2.2a and 4.2.2b). In Figure 4.2.3b, we observe an upregulation of metabolites such as NAD⁺,

This MSEA was carried out using QEA by estimating the correlation between the peak area profiles, X, of the matched metabolite set and the phenotype labels, Y. P-value expresses that none of the matched compounds in the metabolite set is associated to the clinical outcome, Y. Fold enrichment is estimated from the ratio of calculated statistic/expected statistic [309]. RM – HUVECs incubated in restricted medium (control), VEGF – HUVECs incubated with VEGF, PC-3/S-HUVEC – HUVECs co-cultured with PC-3/S cells, PC-3/M-HUVEC – HUVECs co-cultured with PC-3/M cells.

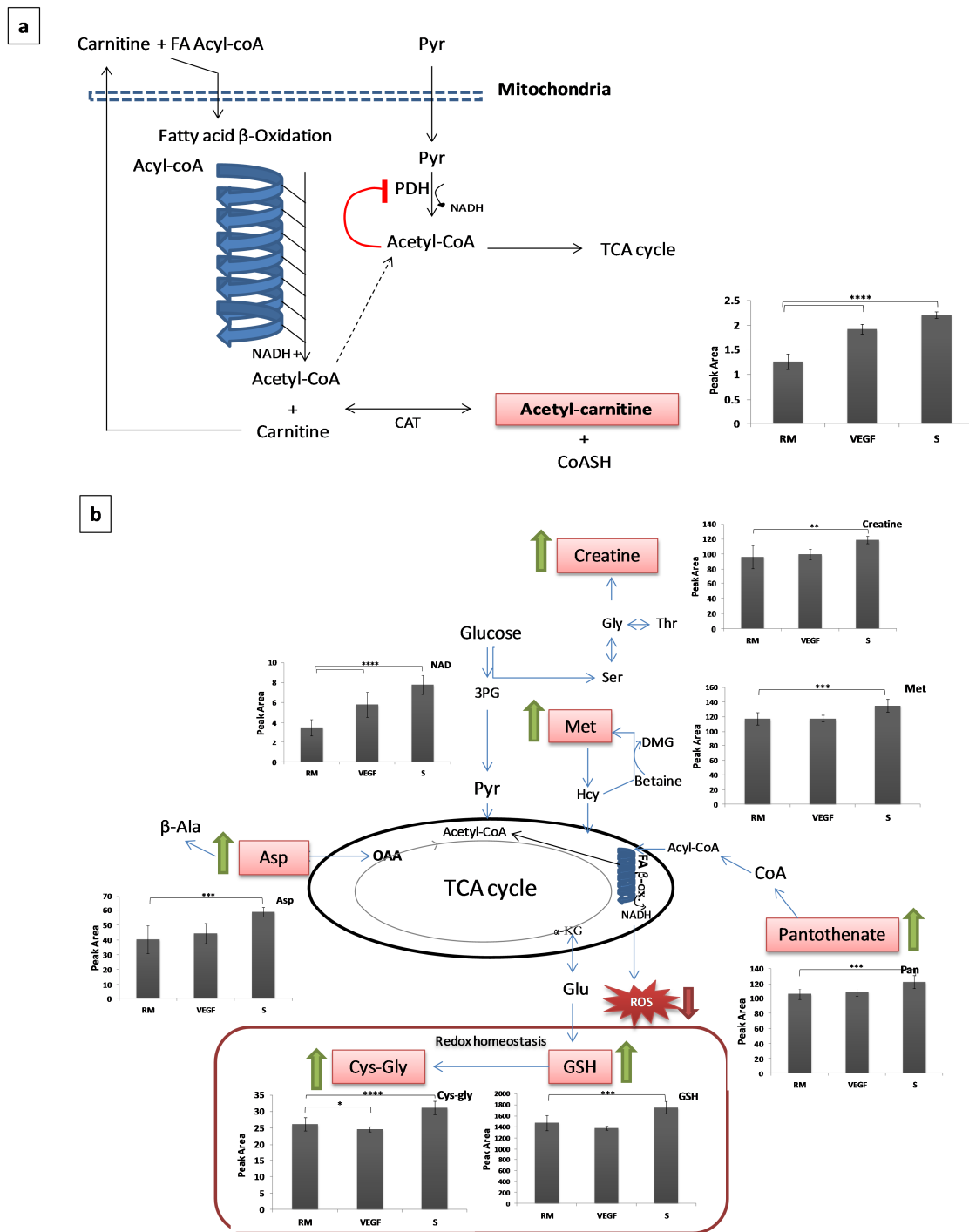


Figure 4.2.3: Metabolite changes induced by VEGF and PC-3/S cells on HUVECs. The pathways identified by MSEA analysis are illustrated, incorporated with the metabolite changes that correspond to these pathways, showing (a) ALC, associated to β -oxidation of fatty acids as shown by MSEA, (b) NAD-induced pathway alterations and other changes only induced by PC-3/S cells, such as in creatine, methionine, pantothenate, glutathione reduced, cysteinylglycine and aspartate. 3PG – 3-phosphogluconate, α KG – α -ketoglutarate, β -Ala – β -Alanine, ALC – acetyl L-carnitine, Asp – aspartate, CAT – Carnitine acetyltransferase, CoASH – reduced co-enzyme A,

creatine, methionine, pantothenate, glutathione reduced, cysteinylglycine and aspartate, incorporated along the pathways identified by the MSEA (Figures 4.2.2a and 4.2.2b). It has to be noted that only NAD⁺ is upregulated in both VEGF and PC-3/S conditions (1.6X and 2.2X, respectively), while all other metabolites are upregulated only in PC-3/S condition, although fold changes are lower.

Figure 4.2.4 (in the following page) shows the peak area changes of HUVECs among RM, VEGF and PC-3/S conditions, in the metabolites inosine, hypoxanthine, guanosine, guanine and AMP, which are associated under purine metabolism by the MSEA (Figure 4.2.2a). From this data we observe that there are significant changes in these metabolites in HUVECs under VEGF induction, while PC-3/S cells did not show such changes. Especially, the metabolites guanine and hypoxanthine are upregulated by a fold change > 3X by VEGF and AMP is downregulated by a fold change of ~5X.

Figure 4.2.5a (in the following page) shows the oleamide identified in all the experimental conditions and Figure 4.2.5b shows other metabolite changes significantly induced by PC-3/M in HUVECs which are associated with tyrosine, methionine and tryptophan related pathways by the pair-wise MSEA (Figure 4.2.2c). Oleamide identified was not associated with any metabolic pathways by the MSEA and strikingly it shows a 4X upregulation by PC-3/M cells, while other conditions do not show changes in this metabolite. On the other hand, the enriched pathways identified by MSEA (Figure 4.2.2c) show a significant downregulation of the respective metabolites induced in HUVECs by PC-3/M, as shown in Figure 4.2.5b.

Cys-Gly – cysteinylglycine, DMG – Dimethylglycine, FA Acyl-Coa – fatty acid acyl-CoA, Hcy – homocysteine, Gly – glycine, GSH – glutathione reduced, Glu – glutamate, Met – methionine, OAA – oxaloacetate, PDH – pyruvate dehydrogenase, Pyr – pyruvate, ROS – reactive oxygen species, Ser – serine, Thr – threonine, RM – control HUVECs, VEGF – HUVECs treated with VEGF, S – HUVECs co-cultured with PC-3/S. Peak area = Peak area $\times 10^5$ (A.U. per 10^6 cells). Statistical significance shown by p-values: * p \leq 0.05, ** p \leq 0.01, *** p \leq 0.001, **** p \leq 0.0001.

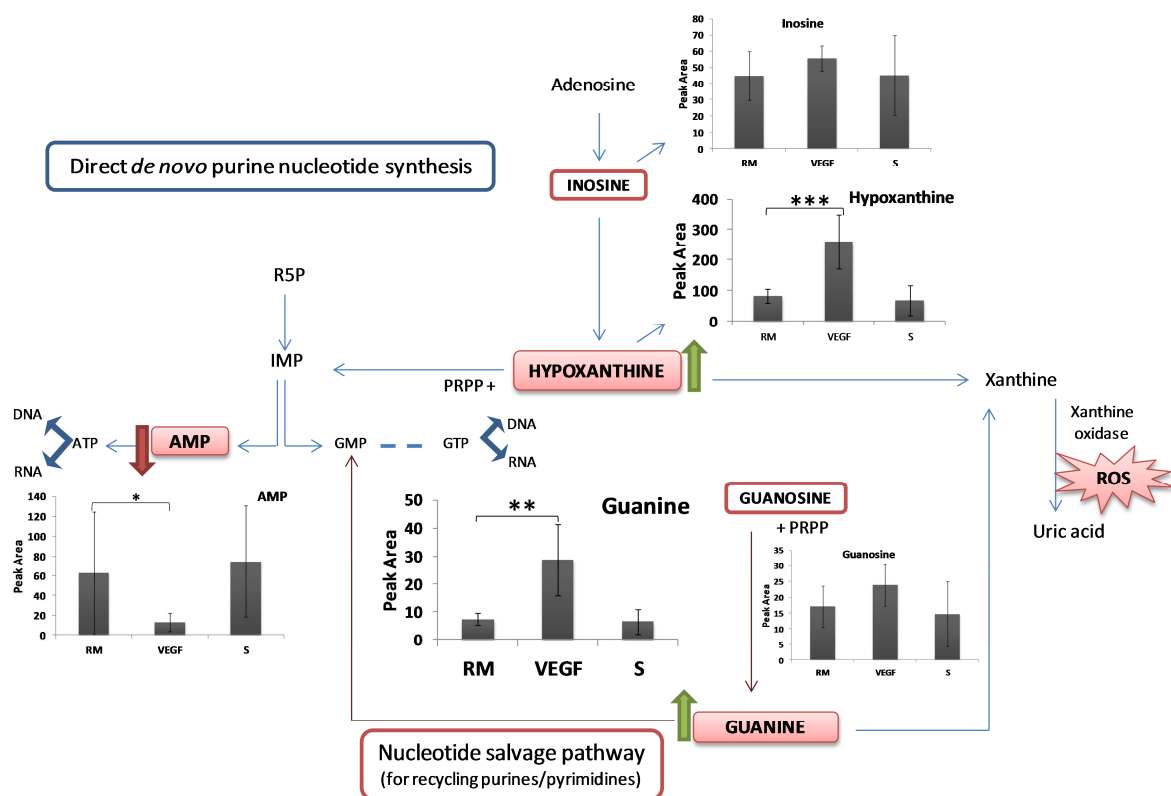


Figure 4.2.4: Metabolite changes induced by VEGF and PC-3/S cells on HUVECs related to purine metabolism. AMP – adenine monophosphate, ATP – adenine triphosphate, GMP – guanine monophosphate, GTP – guanine triphosphate, IMP – inosine monophosphate, PRPP – Phosphoribosyl pyrophosphate, R5P – ribose-5-phosphate, ROS – reactive oxygen species, RM – control HUVECs, VEGF – HUVECs treated with VEGF, S – HUVECs co-cultured with PC-3/S. Peak area = Peak area $\times 10^5$ (A.U. per 10^6 cells). Statistical significance shown by p-values: * $p \leq 0.05$, ** $p \leq 0.01$, *** $p \leq 0.001$.

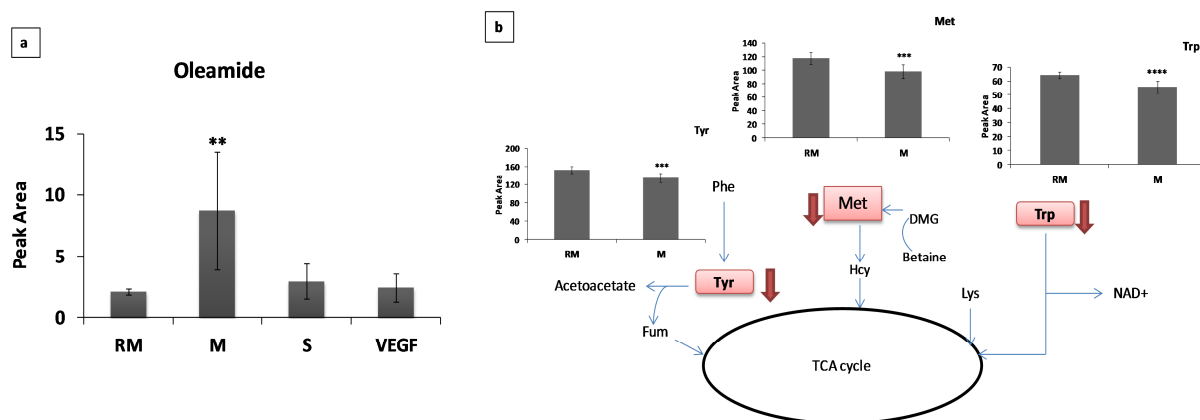


Figure 4.2.5: Metabolite changes and pathway enrichments induced by PC-3/M cells in HUVECs. The MSEA analysis of pathway enrichments in HUVECs under different experimental conditions show, (a) changes in oleamide by PC-3/M and PC-3/S co-cultures, and VEGF incubation, compared to the RM control; (b) Changes in tyrosine, methionine and tryptophan metabolism by PC-3/M condition. DMG – Dimethylglycine, Fum – fumarate,

4.2.3. Discussion

In order to grow and spread to other organs cancer cells recruit endothelial cells for tumour angiogenesis [65] and to achieve this they induce several changes in endothelial cells that can alter their molecular signalling and metabolic pathways. Studies on molecular angiogenesis have led to the development of anti-angiogenic therapies in the past decades, although the success rate has been low [345]. Since metabolism is the ultimate description of the changes in a cellular phenotype targeting metabolic pathways could be an attractive strategy against tumour angiogenesis. Although endothelial cell metabolism has been under study in the past few years they have not been particularly focused on the effect of cancer cells on endothelial cells. In our co-culture study with the help of the HRMS technique we were able to provide a global metabolic fingerprint of the endothelial cells in which changes related to the direct effect of cancer cells were observed. In addition we also have been able to distinguish clearly the distinctive metabolic changes caused by cancer cell sub-populations displaying different metastatic capacities (PC-3/S – low metastatic and highly invasive; PC-3/M – highly metastatic). We found that the metabolic alterations induced by PC-3/S cells are similar to that of VEGF, at the least for the highest fold changing metabolites such as ALC and NAD⁺. In line with this similarity, the PC-3/S cells have been found to upregulate the expression of VEGF-A mRNA, compared to the expression in PC-3/M cells (T.M. Thomson, personal communication, Feb 3, 2016) and it has been found *in vivo* that another low metastatic DU145 cell line secretes 3 times higher VEGF than the PC-3/M cell lines [346]. Supported by the above reports, our results suggest that the metabolic alterations induced by PC-3/S cells in HUVEC are partially due to PC-3/S-secreted VEGF, shown by the common metabolite upregulations of ALC and NAD⁺ by VEGF and PC-3/S cells in HUVECs (Figures 4.2.2a, 4.2.2b and 4.2.3). However PC-3/S cells also upregulate other metabolites shown in Figures 4.2.2b and 4.2.3b, not upregulated by VEGF.

Hcy – homocysteine, Lys – lysine, Met – Methionine, Phe – phenylalanine, Trp – Tryptophan, Tyr – Tyrosine, RM – control HUVECs, VEGF – HUVECs treated with VEGF, S – HUVECs co-cultured with PC-3/S cells, M – HUVECs co-cultured with PC-3/M cells. Peak area = Peak area $\times 10^5$ (A.U. per 10^6 cells). Statistical significance shown by p-values: ** p \leq 0.01, *** p \leq 0.001, **** p \leq 0.0001.

This difference may be attributed to the additional factors involved in the PC-3/S condition, which is not uncovered yet. While only VEGF has induced a high alteration in purine metabolism (Figure 4.2.4), PC-3/S cells have not shown significant changes in purines. Cells under the influence of a single factor or a combination of factors can induce different types of phenotypic or functional changes. It has also been reported that different angiogenic effects are induced by the combination of pro-angiogenic factors with respect to that induced by a single factor alone in endothelial cells [347,348], reiterating the fact that the differences observed in the metabolome between HUVECs cultured either in the presence of VEGF or in the presence of PC-3/S cells in our study could be due to the combination of additional factors secreted by the PC-3/S cells.

ALC is produced from carnitine and acetyl-CoA by carnitine acetyltransferase (CAT) and we observe an upregulation in HUVEC with VEGF and PC-3/S to almost a fold change of 2, as seen in the peak area plot in Figure 4.2.3a. ALC is closely related to fatty acid oxidation in which the acetyl-CoA generated from fatty acid breakdown can combine with carnitine to produce ALC, illustrated in Figure 4.2.3a. This reaction is reversible and carnitine that can be produced from the breakdown of ALC can be recycled back to cytoplasm for transporting more fatty acid acyl-CoA's for β -oxidation [349], which in turn produces more acetyl-CoA. Fatty acid oxidation has been found important in endothelial cells for its contribution to dNTP synthesis and driving endothelial cell proliferation for vessel sprouting [142]. In addition, it has been observed that the conversion of carnitine and acetyl-CoA to ALC can contribute to glucose metabolism homeostasis by eliminating the excess acetyl-CoA which is an allosteric inhibitor of the enzyme pyruvate dehydrogenase that enables the entry of pyruvate into TCA cycle [350,351]. Also, ALC supplementation has been reported to possess therapeutic implications in protecting vascular function against oxidative stress [352] and in protecting endothelial structure in blood-brain barrier [353]. On the other hand in the case of NAD⁺, it is implicated in various pathways (glycolysis, nicotinamide metabolism, citric acid cycle, ketone body metabolism and gluconeogenesis) as shown in the pathway enrichment analysis (Figures 4.2.2a and 4.2.2b) and pathway illustrations (Figure 4.2.3b), however it has to be taken into account that the related reactions involve the inter-conversions between the oxidized and the reduced forms where the

reduced NADH form is unstable and hence it is probable that the NAD⁺ measured could be a mixture of both forms. Hence NAD⁺ cannot be completely relied as a stable biomarker.

The altered purine metabolism in HUVEC has been unique to the VEGF condition in our study (Figure 4.2.4). VEGF is a potent regulator of endothelial cell proliferation and angiogenesis [354] and in order to proliferate, cells have to generate excess of nucleotide components. Purine metabolism is important for the production of DNA and RNA components, in addition, they can also generate xanthine oxidase-derived ROS, as illustrated in Figure 4.2.4. The implications of the changes in hypoxanthine, guanine and AMP by VEGF in endothelial cells have not been reported before. On the other hand it has been shown that VEGF can induce the production of mitochondrial ROS which in turn can function as a signalling factor for mediating endothelial cell migration [355]. ROS-mediated angiogenesis is also observed by NADPH-generated ROS [356].

While VEGF and PC-3/S cells are observed to be affecting similar metabolic pathways in HUVEC, PC-3/M cells show distinct alterations from the other two conditions, as discussed in the Results section. Figure 4.2.5 illustrates the pathways altered by PC-3/M cells in HUVEC which shows a clear and high upregulation in oleamide and significant downregulation of pathways related to tryptophan, methionine and tyrosine. It has been shown that some of the proteins over-represented in the conditioned medium obtained from PC-3/M cells are related to cell adhesion and cell organization [357], which are typical for a metastatic cell line. The oleamide, observed in our study, has also been implicated to anti-metastatic roles when used as a therapeutic supplement, by inhibiting the protein connexin 26 that enables the gap junction-mediated intercellular communications during metastasis [358]. In addition oleamides are suspected to play a role in preventing the spread of apoptotic proteins from a damaged cell to the neighbouring cell through cellular junctions [359]. During metastasis tumour cells have shown to induce endothelial cell damage and apoptosis in order to extravasate from the blood vessel to invade secondary metastatic sites [360,361]. Although oleamide has been found in some types of cells including human breast cancer cells [362] and mouse neuroblastoma cells [363] and in biological samples like the human serum [364] and rat cerebral spinal fluid [365], it

has not been reported in HUVECs before and from our study it seems like this metabolite is expressed as a defence mechanism against the cellular damage from the metastatic PC-3/M cancer cell line.

Overall, our untargeted metabolomics approach combined the co-culture technique with the high throughput Orbitrap mass spectrometry to deduce for the first time, the metabolic fingerprints of tumour-affected endothelial cells. The co-culture experimental technique closely mimics the *in vivo* tumour-endothelial cross-talk and indicates changes in endothelial cells, which would otherwise be difficult to assess *in vivo* for only these cell types. Our method intended to capture the early events of metabolic adaptations and identified 25 metabolites enriched in several pathways including fatty acid oxidation, central carbon metabolic pathways related to NAD⁺, pathways related to amino acids and redox homeostasis. Our results showed a distinct similarity in the metabolic profiles of endothelial cells affected by VEGF and low metastatic cancer cells and contrasting metabolic profile induced by the high metastatic cancer subtype. These observations provide a preliminary view of the tumour-affected endothelial cells which can contribute to the future biomarker discoveries distinct for tumour subtype related angiogenesis.

Chapter 4.3

4.3. Therapeutic implications of glycogen phosphorylase inhibition in *in vitro* and *in vivo* angiogenesis

4.3.1. Introduction

In the Chapters 4.1 and 4.2 we characterized the metabolic reprogramming in HUVECs in the presence of different microenvironmental challenges using fluxomics and untargeted metabolomics approaches, respectively. Among the general metabolic changes, the ¹³C-based metabolomics and fluxomics study revealed that there is a considerable glycogen reserve in HUVECs and the presence of a high glycogen turnover, the purpose for which is not known yet in this cellular type. Glycogen reserve and its metabolism have been proven to be highly significant for the survival and function of certain cell types, to overcome cellular stress due to hypoxia or nutrient starvation conditions, like in cancer cells [170,176], neurons [256], astrocytes [338] and functions as an energy sensor in adipocytes [203]. We hypothesize that the glycogen turnover observed in our endothelial cells must be linked to a functional significance distinct for these cell types that could be related to the functions of angiogenesis, comprising endothelial cell proliferation, migration and blood vessel formation.

Previous studies in our laboratory on glycogen metabolism of HUVECs have shown that inhibiting VEGF-induced proliferation of cells decreased the utilization of glycogen and some preliminary *in vitro* experiments have shown a decrease in HUVEC viability upon inhibiting glycogen degradation [135]. Following this previous observation in our laboratory and the significant findings from our fluxomics study, we wanted to test further the importance of glycogen metabolism in endothelial cell survival and function. The futile cycle of glycogen metabolism could be due to the continually opposing activities of both GS and GP enzymes, which drive for synthesizing and degrading glycogen, respectively. While both enzymes could be significant for HUVEC survival and/or function, we target glycogen degradation pathway by

choosing inhibitors for GP, as there is no direct inhibitor for the GS enzyme and its regulation is complex [178]. In addition there are many direct inhibitors of GP that are patented [253,366] and commercially available, under clinical trials for therapeutic uses of Type 2 diabetes and related diabetic complications [367]. Hence in this chapter we show the observations of GP inhibitors on distinct endothelial cell functions and survival such as the cell viability, migration and wound healing *in vitro* and the effect *in vivo* on angiogenesis and tumour growth.

4.3.2. Results

4.3.2.1. Effect of glycogen phosphorylase inhibitor on HUVEC viability and function *in vitro*

In order to choose a GP inhibitor that is effective against the HUVEC viability, we tested several of these compounds in the *in vitro* viability and migration assays. For this purpose HUVECs were treated under normoxic condition with the indole carboxamide inhibitors such as CP-316819, CP-320626 and CP-91149 and other inhibitors such as isofagomine, BAYU6751 and DAB, as described in detail in the Methods sections 3.2 for *in vitro* viability assay and 3.3 for *in vitro* migration assay. Figure 4.3.1 shows the results of HUVEC *in vitro* viability assay.

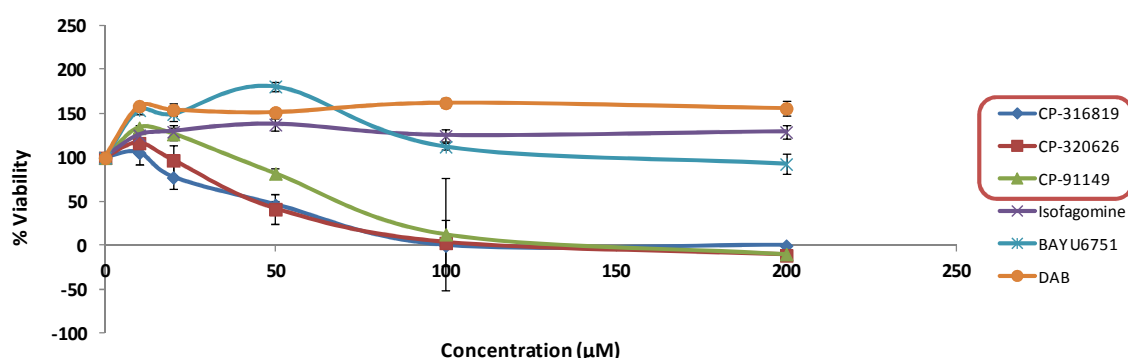


Figure 4.3.1: *in vitro* viability assay of HUVECs with GP inhibitors. The HUVEC viability test was performed by MTT assay with GP inhibitors: CP-316819, CP-320626, CP-91149, Isofagomine, BAYU6751 and DAB. For this assay .../...

In the *in vitro* viability assay we observed that the indole carboxamide-based inhibitors CP-316819, CP-320626 and CP-91149 affected the HUVEC viability effectively showing a half maximal inhibitory concentration (IC₅₀) in the range of 45 to 70 μ M, while the other GP inhibitors Isofagomine, BAYU6751 and DAB did not show a reduction in cell viability until the 200 μ M concentration tested. From the three indole carboxamide inhibitors tested in the *in vitro* viability assay we chose CP-316819 for further experiments as it showed comparatively lower IC₅₀ than CP-91149 and in addition was commercially available, unlike CP-320626 which was not commercially available but showed similar IC₅₀ to CP-316819. Also the other inhibitors: BAYU6751, Isofagomine and DAB, which did not show reduction in viability, were included in the migration assay to check if they show effect on HUVEC migration (Figure 4.3.2).

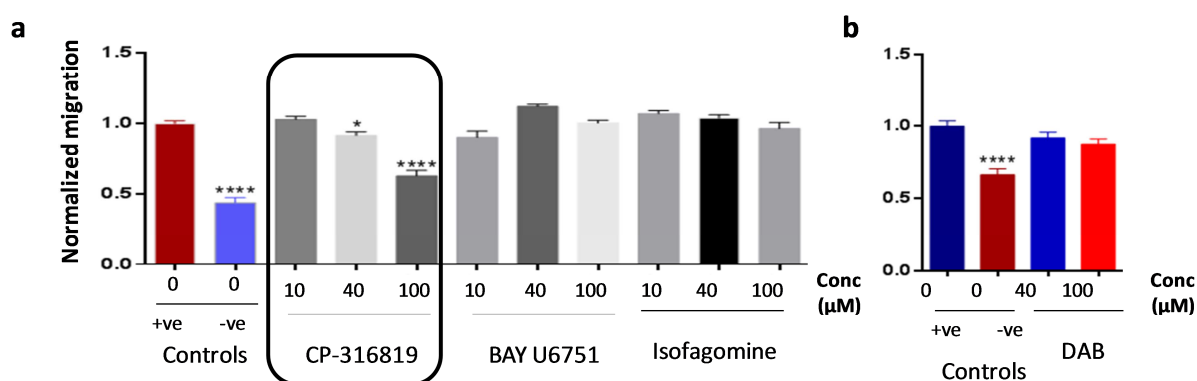


Figure 4.3.2: *in vitro* migration assay of HUVECs with GP inhibitors. HUVECs treated with the different inhibitor types were tested for their effects against cell migration. (a) Migration assay result with CP-316819, BAYU6751 and Isfagomine, (b) Migration assay with DAB showing. The controls are without the GP inhibitors: +ve control, representing maximum migration induction, has HUVECs in the presence of the complete medium with 10% FBS and Lonza SingleQuots supplements that shows effective migration and –ve control, representing least induction of migration, has HUVECs in the presence of endothelial basal medium without serum and additional factors. Cells in the endothelial basal medium were incubated at the upper well, while the complete medium with or without inhibitors were placed in the lower wells of the transwell plates and incubated for 24 hours before measuring the migration of cells to the lower part of the upper well, as described in the Methods section 3.3. DAB - 1,4-dideoxy-1,4-imino-d-arabinitol. *p \leq 0.05, ****p \leq 0.0001.

.../...

HUVECs were incubated with the GP inhibitors under varying concentrations, up to 200 μ M, under normoxic condition for 72 hours in 96-well plates and at the end of the assay the cell viability was estimated using MTT assay, as described in the Methods section 3.2. DAB - 1,4-dideoxy-1,4-imino-d-arabinitol.

The migration assay was performed with varying concentrations of the inhibitors (10, 40 and 100 μM). For this assay, HUVECs deprived of nutrients and hormones were kept in endothelial basal medium without serum or supplements in the upper chamber of the transwell plates and the inhibitors mixed with complete medium with 10% FBS and Lonza SingleQuots supplements were placed in the lower wells. After incubation the migration of cells through the pores from the upper well to the surface facing the lower side, which is in contact with the complete medium (with or without inhibitors), was assessed through quantitative fluorescence absorption measurement (see Methods section 3.3 for more details). The results, in Figure 4.3.2, show that the GP inhibitor CP-316819 significantly reduced HUVEC migration at 40 μM and 100 μM of concentrations while the other inhibitors have not shown an effect against the migration.

In order to test the effect of GP inhibitors further on angiogenic properties of HUVECs, *in vitro* wound healing assay or scratch assay was performed in which a physical scratch was created on the cellular monolayer to study the migration of cells to heal the 'wound', mimicking the *in vivo* situation [312]. In this case, we did the wound healing assay with HUVECs to check the effectiveness of the inhibition of both cellular proliferation and migration by the GP inhibitor CP-316819, that showed effective reduction against HUVEC viability and migration in the assays described in the previous paragraphs. For this assay HUVECs were maintained in complete medium with 10% FBS and Lonza SingleQuots supplements and the GP inhibitor CP-316819 was added at either the concentration of 40 μM or 100 μM . In the positive control the cells were maintained in the complete medium and in the negative control the cells were incubated with the restricted medium containing 2% FBS and no supplements, both the controls without the GP inhibitor. At the end of the incubation times of 14 and 21 hours the cells under all the conditions were analyzed for 'wound healing' capacity, as described in the Methods section 3.4. Figure 4.3.3 shows the pictures taken before and after treatment of the cells for the time points mentioned above. We observe that as the positive control partially closes the wound at 14 hours and completely closes it at 21 hours, the negative control does not show a closure at both time points. At 40 μM and 100 μM , the CP-316819 treated cells have inhibited the wound closure both at 14 and 21 hours.

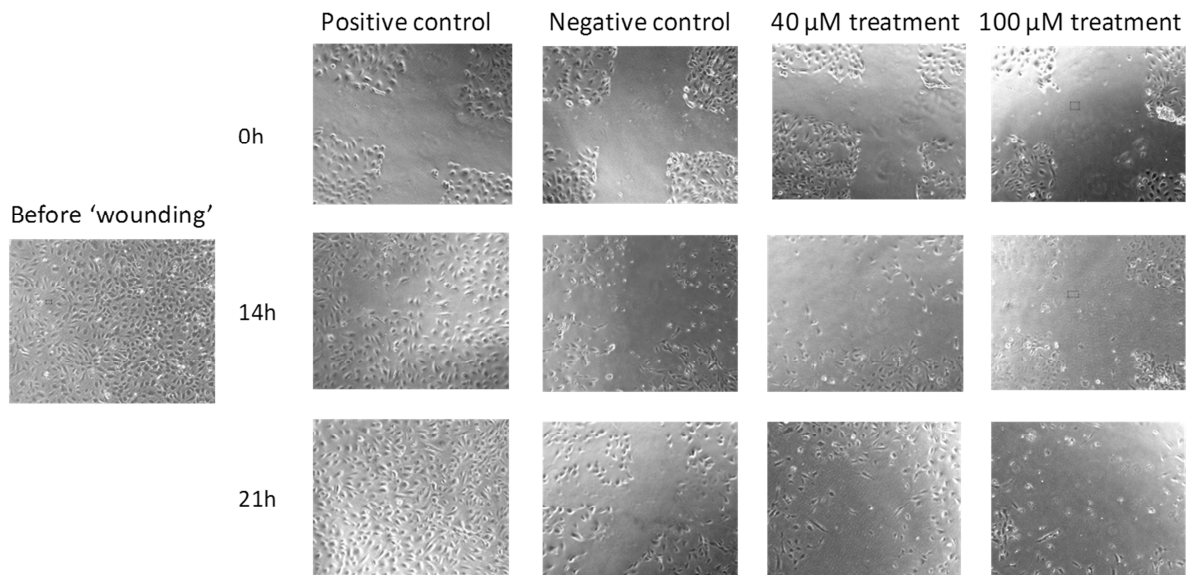


Figure 4.3.3: Wound healing assay of HUVECs with GP inhibitor CP-316819. For this assay HUVECs in positive control and the treated cells were in the presence of complete medium with 10% FBS and Lonza SingleQuots supplement, either in the absence or presence of the GP inhibitor, respectively. The cells in the negative control were in the presence of restricted medium with 2% FBS without supplements. For this assay a physical scratch was created on the cellular monolayer and the HUVECs were incubated with the compound CP-316819 at concentrations 40 and 100 μM and for 14 and 21 hours. The cellular monolayers under the different conditions before and after treatment were recorded under the phase contrast microscope and the photographs analyzed for the effectiveness of the compound CP-316819 in inhibiting the 'wound' closure.

4.3.2.2. Effect of glycogen phosphorylase inhibitor against *in vivo* neovascularisation, tumour growth and microvessel density

The results described in the previous section showed that the GP inhibitors were effective in reducing HUVEC viability and function *in vitro*. In order to further test its effect on *in vivo* angiogenesis we performed a matrigel plug assay [368]. In this assay we test the anti-neovascularization effect of the GP inhibitor CP-316819 in the mice model C57BL6, by injecting the matrigel with or without the GP inhibitor (see Methods section 3.5 for more details). The positive control contains matrigel along with the pro-angiogenic factor VEGF and the negative control contains only matrigel. The treatment group contains both VEGF and the GP inhibitor CP-316819 with varying concentrations (10 and 50 μM). In this assay we assessed the effectiveness of the GP inhibitor in reducing the blood vessel formation by quantifying the

haemoglobin quantity in the matrigels of the treated animals. As shown in Figure 4.3.4, the negative control showed a very low haemoglobin quantity while the positive control showed elevated haemoglobin. We observed that at the given dosages of the GP inhibitor the haemoglobin quantity was not significantly lower as compared to the positive control.

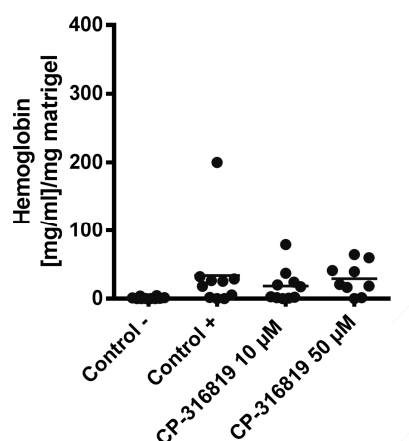


Figure 4.3.4: *In vivo* matrigel plug assay to test the anti-neovascularization effect of the GP inhibitor. The GP inhibitor CP-316819 at the doses 10 μ M and 50 μ M were injected with the matrigels and VEGF into a mice model and incubated for 7 days. After treatment the extracted matrigels were processed for assessing the haemoglobin quantity, as described in the Methods section 3.5. The graph shows the haemoglobin quantity in the matrigels extracted from controls and CP-316819-treated mice. The negative control is only matrigel injected subcutaneously into mice abdominal area and the positive control contains matrigel injected along with VEGF. The treated groups contain both the GP inhibitor CP-316819 and VEGF.

We next wanted to check if the GP inhibition had an impact on the tumour growth and the tumour angiogenesis. For this *in vivo* efficacy assay we used an experimental animal model of nude mice injected subcutaneously with a human myelomonocytic leukemia cell line (see Methods section 3.6 for more details). One group of mice was kept as control without treatment, with only vehicle and the second group of mice were treated with 25 mg/kg CP-316819 injected on alternate days for two weeks. Figure 4.3.5a shows the relative tumour volume (with respect to the volume at day 0 of the treatment) of the control and treated mice recorded during the treatment regimen. We see that though the injection of the compound CP-316819 does not cause a visible variation in the tumour size during the initial days of the treatment the tumour size seems to reduce during the second week, while reaching about 15% of reduction at the end of the treatment when compared with the controls, though the

reduction was not statistically significant. Figures 4.3.5b and 4.3.5c show the measurements of the percentage CD31 tumour microvessel density and vessel area of the treatment group with respect to the control group. From these results we observe that the area occupied by the tumour microvessels does not change, but an estimated reduction of about 30% of the tumour microvessels can be observed.

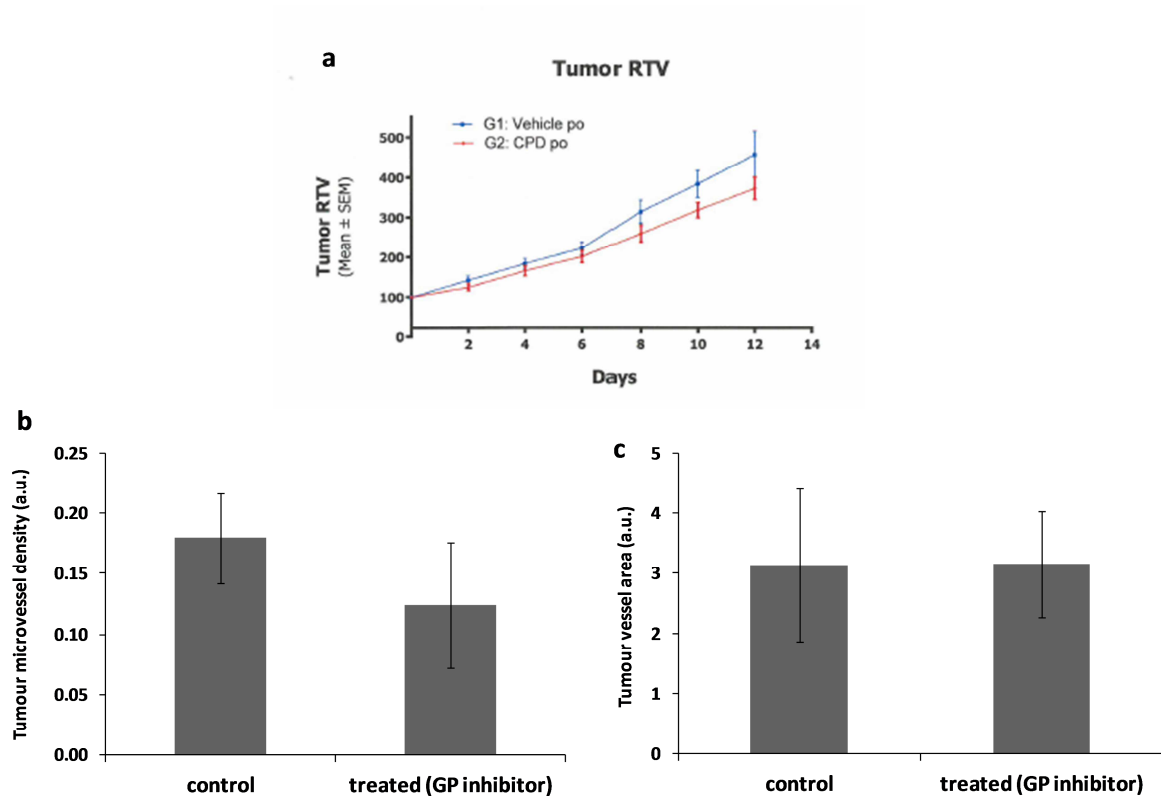


Figure 4.3.5: The effect of GP inhibitor CP-316819 on *in vivo* tumour efficacy assay. In this assay, results of the (a) measurements of relative tumour volumes of the tumours measured in the control mice (Vehicle, blue) and treated mice (CPD, red) during the treatment regimen, (b) estimation of tumour microvessel density and (c) estimation of tumour vessel area, are shown, with and without treatment of the tumour models with the GP inhibitor CP-316819. In this assay the mice model injected subcutaneously with tumours were subjected to a treatment with CP-316819 GP inhibitor every alternate day for 12 days, at a dosage of 25 mg/Kg. The tumour size was measured during the treatments and at the end of the dosage regimen the tumours were extracted and analyzed for tumour vessel density and area, as described in the Methods section 3.6. a.u. – arbitrary units.

4.3.2.3. Effect of the glycogen phosphorylase inhibitor on HUVEC lipid metabolism

The indole inhibitors were claimed to have additional therapeutic relevance to hypercholesterolaemia and hyperlipidemia [366]. Hence in order to check if the effect of the GP inhibitor CP-316819 on *in vitro* and *in vivo* angiogenesis can be attributed to any additional side-effects on other metabolic pathways like the lipid metabolism, we used ketoconazole, an anti-fungal agent which also inhibits the synthesis of cholesterol and phospholipids [369,370] in the *in vitro* and *in vivo* angiogenesis assays. For the *in vitro* viability assay, HUVECs were incubated with ketoconazole under normoxia for 72 hours similar to the viability assay with GP inhibitors described in the section 4.3.2.1. The results in Figure 4.3.6a show that the HUVEC viability was affected with a slightly higher IC₅₀ of about 70 μ M with ketoconazole, than that obtained with HUVECs when treated with the GP inhibitors (Figure 4.3.1). Then the effect of ketoconazole on *in vivo* angiogenesis was tested by matrigel plug assay, carried out in the similar manner as described with the GP inhibitor CP-316819 in the section 4.3.2.2. Upon measuring the haemoglobin content from the extracted matrigels the results in Figure 4.3.6b indicate that the haemoglobin content with ketoconazole treatment has not shown a decrease with respect to the untreated positive control that shows a higher haemoglobin content, similar to the results with GP inhibitor CP-316819 (Figure 4.3.4), reiterating that the compound ketoconazole has not affected the *in vivo* neovascularisation in the matrigels.

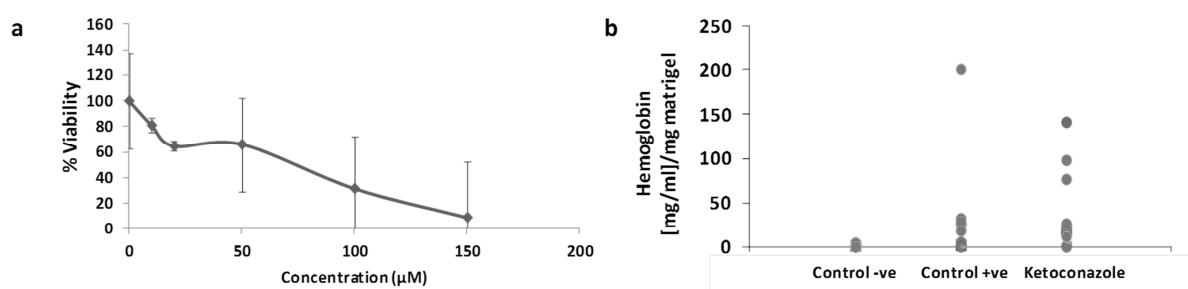


Figure 4.3.6: Effect of the lipid metabolism inhibitor ketoconazole on HUVEC viability and function. The compound ketoconazole possessing anti-lipid metabolic properties was used to check if blocking lipid metabolism has any effect against *in vitro* and *in vivo* angiogenesis. The results show, (a) the *in vitro* viability assay with

From the above *in vitro* viability and *in vivo* matrigel experiments we observed a slight to no effect of the lipid metabolism inhibitor on the activities of angiogenesis, to validate that the indole carboxamide GP inhibitor used was not affecting endothelial cell viability and function based on other metabolic pathways such as those of lipids, than the glycogen metabolism. In order to further validate this hypothesis we intended to check if there was a change in the levels of lipids from the *in vivo* CP-316819-treated samples. For this purpose the same samples of controls and CP-316819-treated tumour tissues and the plasma extracted from the respective mice models from the *in vivo* tumour efficacy assay, performed and discussed in section 4.3.2.2, were subjected to an LC-MS-based targeted metabolomics analysis, using Biocrates AbsoluteIDQ kit where the metabolites extracted from the tumour tissues and plasma were measured for lipids using LC-MS, as described in the Methods section 3.15. Figure 4.3.7, in the following page, shows the concentrations of the metabolites, glycerophospholipids and sphingolipids in the plasma and tumour tissues with and without CP-316819 treatment. From these results we observe no significant change in lipid contents with the GP inhibitor treatment with respect to the control samples and hence we have not observed any compelling evidence that the changes observed in the experiments with CP-316819 were due to changes in lipids.

HUVECs, (b) the *in vivo* matrigel assay in which the haemoglobin content was measured in the presence and absence of ketoconazole. The *in vitro* viability assay was performed in the similar manner as with the GP inhibitors, described in section 4.3.2.1 where HUVECs were incubated for 72 hours under normoxic condition with ketoconazole and its effect on cell viability was estimated after treatment. The *in vivo* matrigel assay was also performed under similar conditions as with the GP inhibitor CP-316819 described in the section 4.3.2.2, where the matrigels with VEGF and ketoconazole were injected into the mice and after 7 days the matrigels extracted were subjected to a measurement of haemoglobin content obtained from the neovascularized areas of the matrigels. The control matrigels contain only VEGF for positive control and only matrigel for negative control. The haemoglobin content was normalized with mg matrigel.

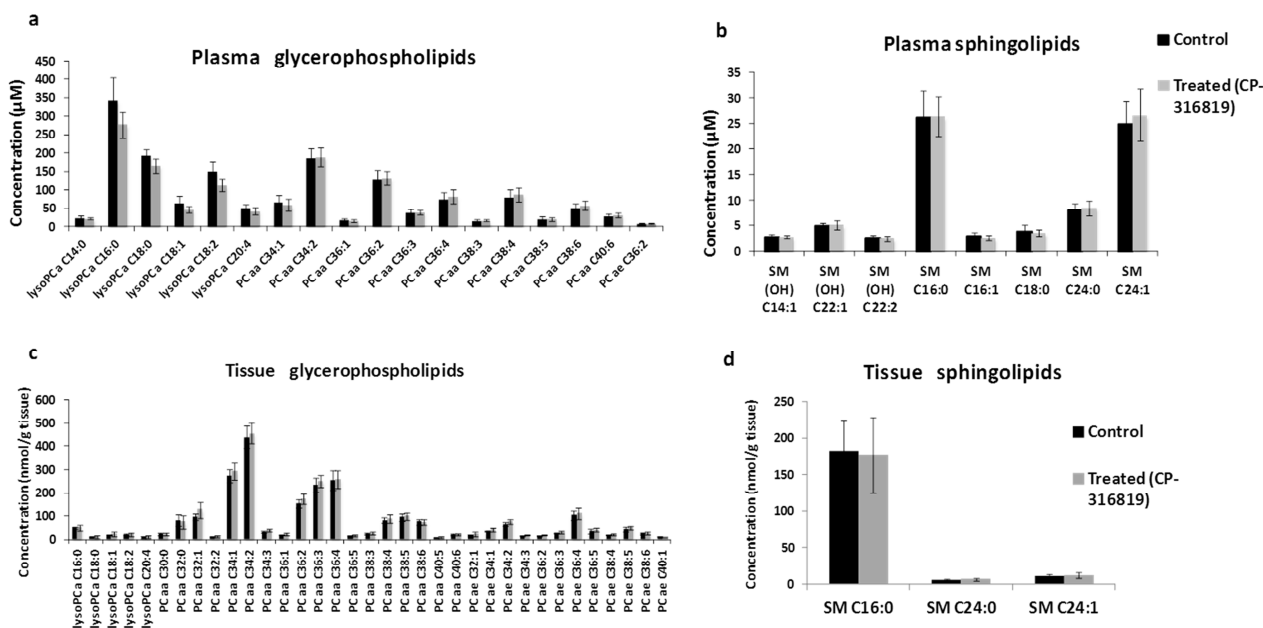


Figure 4.3.7: LC-MS- based targeted metabolomics analysis of lipids on CP-316819-treated *in vivo* samples. The levels of glycerophospholipids and sphingolipids in the tumour tissues and plasma samples from the tumour mice models treated with CP-316819 were measured to check if the GP inhibitor showed changes in lipid metabolism. The results show the levels of, (a) Plasma glycerophospholipids, (b) Plasma sphingolipids, (c) Tissue glycerophospholipids and (d) Tissue sphingolipids. For this *in vivo* efficacy, the tumour incorporated mice were treated with 25 mg/Kg of CP-316819 on alternate days and after 12 days of treatment the mice were sacrificed and blood and tumour tissues were extracted. The plasma extracted from the blood samples and the tumour tissues were subjected to metabolite extraction procedure for LC-MS analysis and the extracted metabolites were measured for lipids content. LysoPCa – lyso-phosphotidylcholines with acyl side chains, PC – phosphotidylcholines, SM – sphingomyelins, PCaa – phosphotidylcholines with acyl residues in the side chains, PCae – phosphotidylcholines with alkyl and alkenyl residues in the side chains, SM (OH) – sphingomyelins with substituted OH groups in the side-chains,. Cx:y indicates the lipids with total number of x carbons with y double bonds.

4.3.3. Discussion

In our study we attempted to verify the efficacies of GP inhibition in HUVECs in the reduction of *in vitro* cell proliferation, migration and *in vivo* angiogenesis and tumour growth. In the *in vitro* assays we found that the GP inhibitor CP-316819 lowered the HUVECs cell viability, cellular migration and wound healing capability. Although it was efficient *in vitro*, it showed very little effect *in vivo* in reducing the angiogenesis and tumour growth. The haemoglobin quantity measured in the matrigel assay did not show a significant reduction with the GP inhibitor

compared to the positive control, while in the tumour efficacy assay there was an observable reduction in the microvessel density.

The haemoglobin content measurement is an indirect estimation of the quantity of blood in the vessels formed. In turn the blood content measured in the newly formed blood vessels can be affected by the size of the vessels and by the extent of stagnant pools of blood at certain areas [371]. In our results of the matrigel assay the uneven and higher blood content from the haemoglobin measurement observed with the GP inhibitor treated samples could be attributed to these vessel morphology discrepancies such as the uneven sizes of blood vessels and blood stagnation as mentioned above. Hence, including a direct visualization of vessel morphology in the matrigels extracted, in addition to the indirect haemoglobin content analysis, could have supported the study for a better understanding of the effect of CP-316819 on blood vessels. In the case of the *in vivo* tumour efficacy assay, although the reduction in tumour growth was not significant, the decrease in tumour microvessel density could be attributed to some significant anti-angiogenic activity by GP inhibition. It is already reported in some studies that anti-angiogenesis treatments induce reduction in tumour microvessel density, with or without reducing tumour size, which is attributed to the morphological changes of tumour vessels causing vessel normalization [372-374]. These studies show that even if the treatments focussed on inhibiting angiogenesis do not show a direct effect on reducing tumour growth, some important effects are observed which indirectly can aid in anti-cancer treatments. It is shown that normalized vessels can improve the blood flow and aids in effective response to chemotherapy, immunotherapy and radiation therapy to treat cancer [372]. Thus our results seem to show that inhibiting glycogen degradation has an indirect effect on angiogenesis and tumour vessels which could possess a therapeutic importance that has to be explored further.

In addition, the choice of tumour models can affect the treatment results as some types of tumours may require more or less quantity of blood vessels for their survival and propagation. Studies using inhibitors of angiogenic factors have shown that certain types of tumours such as rhabdomyosarcoma, glioblastoma and melanoma [93,375] vary in their responses to the anti-angiogenic treatments reducing tumour vessel density and tumour growth, as some types of

tumours may be more angiogenesis-dependent than others. Thus a better choice of *in vivo* tumour models that provide effective tumour microenvironment for angiogenesis can improve the efficiency of compounds tested for angiogenesis [376]. In addition to that, it is important to understand the process of angiogenesis at the metabolic level for designing better therapies, as discussed in the previous chapters. Thus a better understanding of the metabolic regulations in glycogen metabolism of endothelial cells will throw a light on targeting this pathway for pathological angiogenesis. Regulation of glycogen metabolism has not been studied before in endothelial cells and we have intended to characterize it in the following chapter using HUVECs as the endothelial cellular model.

Chapter 4.4

4.4. Characterization of glycogen metabolism and its regulation in endothelial cells

4.4.1. Introduction

Studies on endothelial cell metabolism have been under focus in recent years in search for a strong therapeutic target against pathological angiogenesis, among which the glycogen metabolism is still unexplored. In a preliminary study in our laboratory it was shown that endothelial cells accumulate significant amount of glycogen both under normoxia and hypoxia [135]. In the Chapter 4.1 we have observed a similar pattern, of glycogen accumulation by HUVECs and the presence of glycogen turnover revealed by the ¹³C-based metabolomics and fluxomics studies. The purpose of this glycogen metabolic pattern in endothelial cells was not clear, but from our *in vitro* and *in vivo* studies described in Chapter 4.3 we have observed that inhibiting GP enzyme actually affected HUVEC viability and function and have even caused changes to tumour angiogenesis by affecting the tumour microvessel density. These observations are revealing a protective role of glycogen degradation in endothelial cells similar to that observed in other cell types, like in cancer cells and neurons [176,256]. Although the importance of glycogen metabolism is beginning to reveal itself with these preliminary studies in endothelial cells, and direct inhibitors to GP may be a good therapeutic target to explore anti-angiogenic strategies, there are not sufficient information about the glycogen metabolism and regulation in these cells which could assist in a better therapeutic design. The GP inhibitor was effective *in vitro* in endothelial cells but did not show an expected tumour inhibition or a strong anti-angiogenic pattern *in vivo*, as seen in Chapter 4.3. It is known that glycogen metabolism and its key enzymes, GP and GS have complex regulatory mechanisms [212,217] and inhibition of one of the enzymes could involve changes in factors affecting its regulatory pathways. Hence we decided to extend this study further, to characterize the glycogen

metabolism of HUVECs by assessing their glycogen reserves, expressions of GP and GS enzyme isoforms, and measuring the GP and GS enzyme activities under different substrate conditions.

For this purpose our experiments with HUVECs involved growing the cells under three different substrate conditions: (i) in a medium with VEGF (represented as RMV) containing 2% FBS and 30 ng/mL VEGF, (ii) in a complete medium (represented as CM) containing 10% FBS and with growth hormones such as hydrocortisone and human epidermal growth factor and, (iii) in a restricted medium (represented as RM) containing only 2% FBS, which is used as the control condition (see Methods section 3.1 for more details on these cell culture conditions). The experimental condition with VEGF (RMV) was included because it was found that VEGF receptor inhibition reprogrammed the glycogen metabolism in HUVECs [135] and in addition our studies in Chapter 4.1 have shown that VEGF reduces the glycogen content in HUVECs and thus we wanted to check if this angiogenic factor causes a change in GP and GS enzyme expressions or activities in HUVECs. Additionally we wanted to check if glycogen stores or enzyme expressions and activities were different when HUVECs were under highly proliferating and growth hormone-rich condition as in CM as opposed to the low proliferating conditions of RM and RMV. Additionally we have studied the effect of normoxia and hypoxia and the presence and absence of glucose in glycogen accumulation/degradation in all the conditions mentioned above and characterized the enzyme expressions and activities under normoxia, the results of which are discussed in the following sections.

4.4.2. Results

4.4.2.1. Glycogen degradation at glucose depleted conditions

Previous results have demonstrated that glycogen is mobilized in the absence of glucose under normoxia [135], as well in Chapter 4.1 we have observed the effect of VEGF in reducing the glycogen reserves in HUVECs. Hence to investigate it further, we have measured the glycogen content in HUVECs cultivated under normoxia, in different substrate conditions of RM, RMV

and CM, initially with 15 mM of glucose and then deprived of glucose for different time points. Figure 4.4.1 shows the results of the glycogen content measurement in HUVECs incubated in the conditions mentioned above, with (0h) and without glucose (1h, 5h and 24h of glucose deprivation).

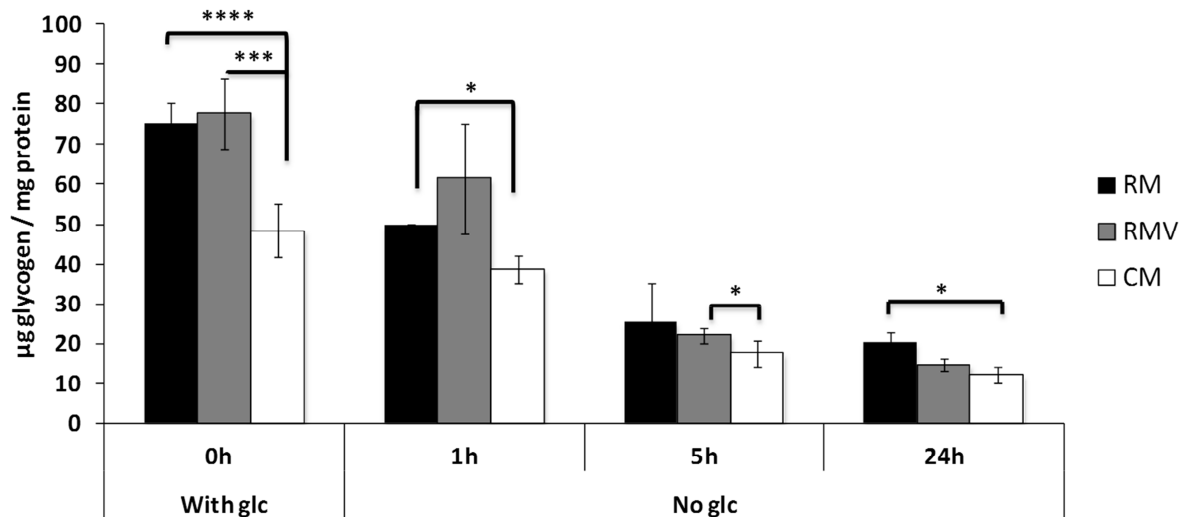


Figure 4.4.1: Glycogen content measured in the presence and absence of glucose under normoxia. Measurement of glycogen levels in HUVECs incubated with glucose (0h) and without glucose (after 1h, 5h and 24h), with different substrate conditions of RM, RMV and CM under normoxia. The glucose, derived from the degradation of glycogen extracted using α -amylglucosidase, was measured using GC-MS, as described in the Methods section 3.12.7. glc – glucose, RM – restricted medium with 2% of FBS, RMV – restricted medium with 2% FBS and VEGF, CM – complete medium with 10% FBS and Lonza EGM SingleQuots. Statistically significant difference among RM and CM or RMV and CM - **** $p \leq 0.0001$, *** $p \leq 0.001$, * $p \leq 0.05$.

From the Figure 4.4.1, we see that in the presence of glucose in the cell culture media the glycogen accumulation is high in all the three conditions. Upon depriving glucose completely the glycogen content is degraded to a minimum level at 5h, to almost 70% of the content at 0h, and remains almost at the same level until 24h of glucose deprivation. It can be observed that glycogen is not degraded completely and there is always a minimum amount left even at 24h without glucose. Though VEGF does not induce significant change in glycogen content with respect to RM, the cells incubated in CM show significantly reduced glycogen accumulation. Although VEGF (RMV condition) showed a significant reduction of glycogen content in

Chapter 4.1, which was not observed for the experiments in the present chapter, we assume this difference could be due to the lower incubation period of 3h with VEGF in the present experiments where sufficient metabolic adaptation of HUVECs to VEGF could not have been achieved, compared to those in Chapter 4.1 where the incubation periods were longer.

For the experiment under hypoxia, HUVECs in RM, RMV and CM conditions were pre-conditioned under hypoxia for 3h in the presence of glucose and then the respective media without glucose were replaced and the cells were maintained for 5h more under hypoxia (refer to Methods section 3.1 for cell culture conditions for more details). The result of the glycogen content measurement under hypoxia in HUVECs with (0h) and without glucose (5h) is shown in Figure 4.4.2, where we see that the glycogen is almost depleted in the absence of glucose, to about 90% compared to those at 0h, in the cells maintained in all the substrate conditions. As seen under normoxia (Figure 4.4.1), under hypoxia also the HUVECs in CM condition accumulate lesser glycogen (seen at 0h with glucose in Figure 4.4.2), while the cells in RMV condition does not show significant difference with respect to those in RM.

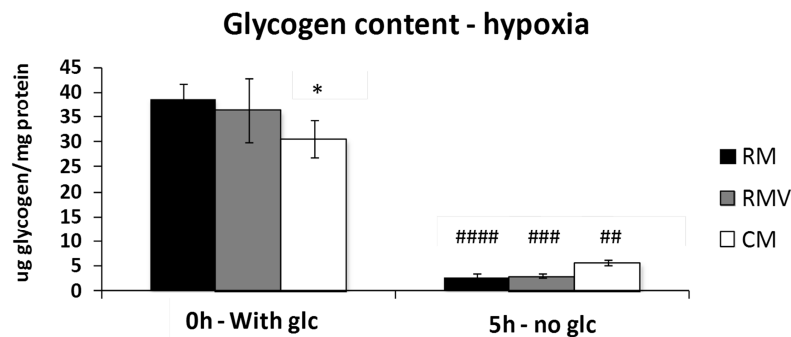


Figure 4.4.2: Glycogen content measured in the presence and absence of glucose under hypoxia. The measurement of glycogen content of HUVECs is shown under hypoxia with glucose and after 5h without glucose, under the substrate conditions RM, RMV and CM. HUVECs in RM, RMV and CM were initially pre-incubated under hypoxia for 3h and then the cells were maintained under hypoxia for 5h more without glucose, before finishing the experiment. The glucose, derived from the degradation of glycogen extracted using α -amylglucosidase, was measured using GC-MS, as described in the Methods section 3.12.7. glc – glucose, RM – restricted medium with 2% of FBS, RMV – restricted medium with 2% FBS and VEGF, CM – complete medium with 10% FBS and Lonza EGM SingleQuotes. Statistically significant difference among: RM and CM - * $p \leq 0.05$; among time-points (with and without glucose), between respective incubation conditions - ## $p \leq 0.01$, ### $p \leq 0.001$, #### $p \leq 0.0001$.

4.4.2.2. Enzyme expressions of glycogen synthase and glycogen phosphorylase

The observations, in the previous section, of the glycogen utilization when glucose was deprived in HUVECs suggest that there is an active participation of the enzymes of glycogen metabolism. In order to better understand the role of glycogen in HUVECs, it is important to uncover the characteristics, enzyme activities and regulations of GS and GP enzymes in these cells. As an initial step of characterizing the key enzymes of glycogen metabolism in HUVECs we aimed to find out which isoforms of GS and GP are expressed in HUVECs. Moreover it is of our interest to check if there is a relevant difference in the expression of these isoforms when the cells are incubated under different substrate conditions of RM, RMV and CM. Hence, HUVECs were grown in the presence (0h) and absence of glucose (1h and 5h), under normoxia in RM, RMV and CM conditions and were processed for analyzing the protein expressions of the different isoforms of the enzymes GS (liver and muscle) and GP (liver, muscle and brain). Also, RNA was extracted for qRT-PCR analysis, for estimating their expressions corresponding to GS and GP isoforms.

Figure 4.4.3a.i shows the results of the protein expressions of the GS enzyme in HUVECs under different substrate conditions, with and without glucose. It is shown that HUVECs express muscle isoform of GS and liver isoform expression was not observed (data not shown for liver GS). In addition, we observed that the bands of the muscle GS protein, after 5h of incubation in the absence of glucose, run faster than those at other time points, attributing to the possible differences in phosphorylated states of the enzyme. On the other hand, the expression of these isoforms did not change due to different incubation conditions. In order to further validate the differences in phosphorylated states of the muscle GS at different time points of incubation, we checked the protein expression of phosphorylated GS. It has to be noted that phosphorylated GS form corresponds to inactive GS enzyme, while the unphosphorylated GS corresponds to the active form of the enzyme. Figure 4.4.3b.i shows the results of the protein expressions of muscle GS in HUVECs phosphorylated at serine residues 641/645, in which we clearly see relatively low intense bands of the phosphorylated GS enzyme at 5h compared to the other time points. Figure 4.4.3a.ii shows the protein quantification of the total muscle GS,

Figure 4.4.3b.ii shows the quantification of the phosphorylated muscle GS bands and Figure 4.4.3c shows the ratio of phosphorylated to total muscle GS. It is evident that at 0 and 1h, in the presence of plenty of glycogen (as shown in the results in Figure 4.4.1), GS enzyme is highly phosphorylated which shows that it is inactive, while at 5h at minimum glycogen levels the phosphorylated GS is too low showing that the enzyme is highly active.

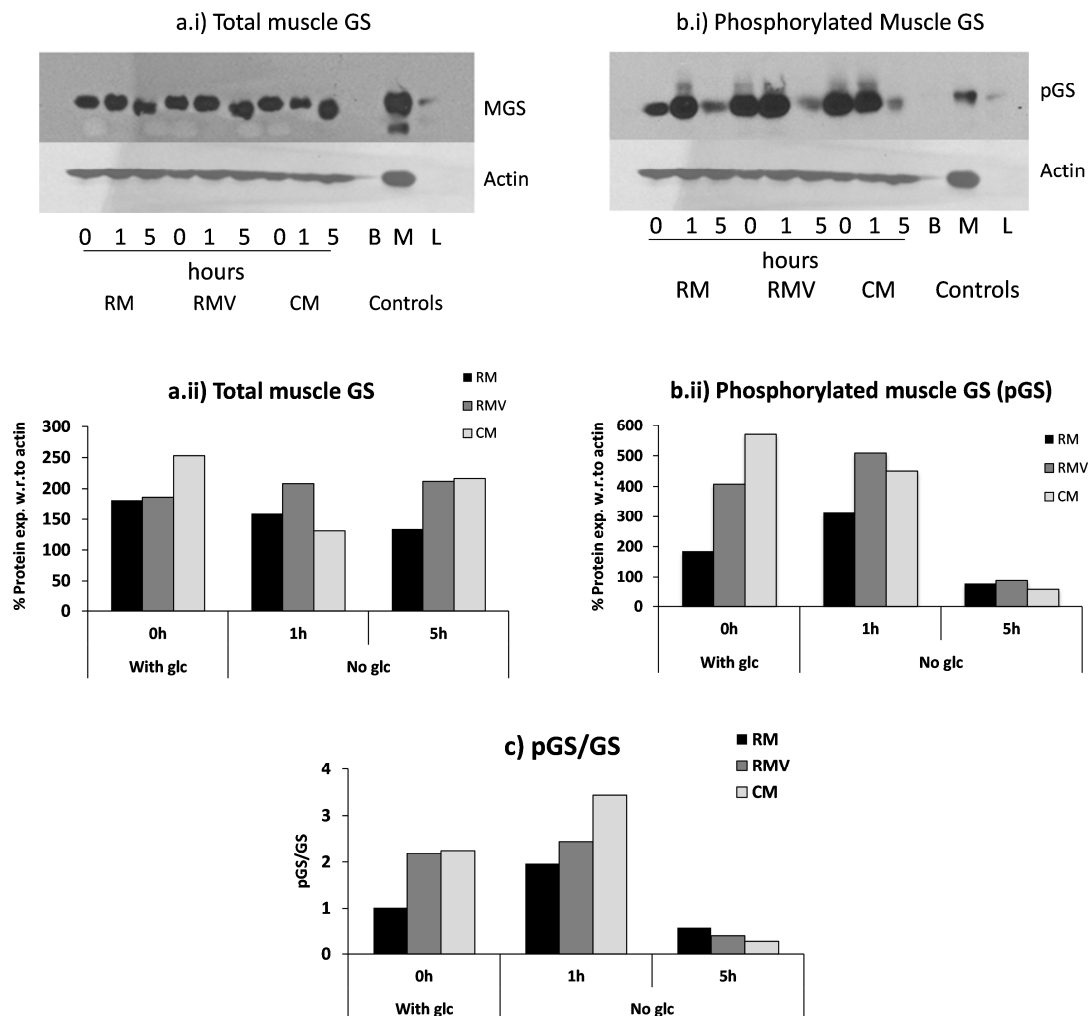


Figure 4.4.3: GS enzyme expression in HUVECs. (a.i) Protein expression of total muscle GS (83.7 kDa), (a.ii) quantification of total muscle GS protein (b.i) protein expression of GS enzyme phosphorylated at serine 641/645, (b.ii) quantification of the phosphorylated muscle GS protein, (c) ratio of the phosphorylated GS to the total GS (pGS/GS), in HUVECs grown in the substrate conditions of RM, RMV and CM and also with (0h) and without glucose (glucose deprivation for 1h and 5h). B, M and L are the protein expressions of the mice brain, muscle and liver tissues, respectively, as controls for the enzyme isoforms. GS – glycogen synthase, MGS – muscle GS isoform, pGS – phosphorylated GS, RM – restricted medium with 2% of FBS, RMV – restricted medium with 2% FBS and VEGF, CM – complete medium with 10% FBS and Lonza EGM SingleQuots.

In the case of GP enzyme, HUVECs co-expressed brain and liver isoforms of GP, as shown in Figure 4.4.4, while muscle GP was not expressed (data not shown). Additionally, no apparent difference was observed in expression of these isoforms in HUVECs incubated neither under different substrate conditions nor in the presence or absence of glucose.

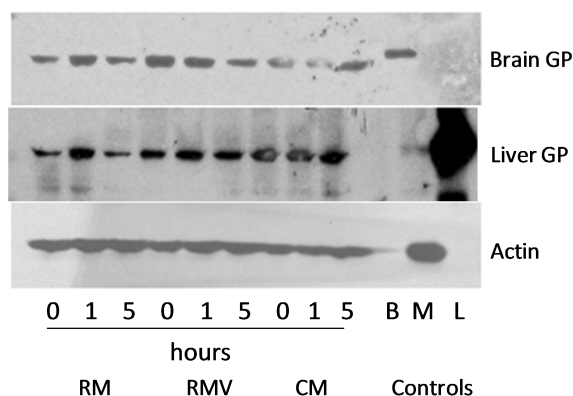


Figure 4.4.4: GP enzyme isoform expression in HUVECs. Protein expressions of brain GP (96.6 kDa) and liver GP (97.1 kDa) enzyme isoforms are shown in HUVECs grown in the substrate conditions of RM, RMV and CM and also with (0h) and without glucose (glucose deprivation for 1h and 5h). B, M and L are the protein expressions of the mice brain, muscle and liver tissues, respectively. as controls for the enzyme isoforms. BGP – brain GP isoform, LGP – liver GP isoform, RM – restricted medium with 2% of FBS, RMV – restricted medium with 2% FBS and VEGF, CM – complete medium with 10% FBS and Lonza EGM SingleQuots.

The expressions of muscle GS, and brain and liver GP isoforms in HUVECs were also validated by the mRNA expression levels from the quantitative RT-PCR analysis. As shown in Table 4.4.1 the relative abundances of mRNA expressions of muscle GP (GYS1), brain GP (PYGB) and liver GP (PYGL), with respect to the reference gene PPIA, were much higher than the other isoforms - the liver GS (GYS2) and the muscle GP (PYGM) which were almost undetectable.

Table 4.4.1: Quantitative RT-PCR. Relative abundances of the genes of muscle GS, brain GP and liver GP enzymes with respect to PPIA reference gene in the measured RNA expression levels in HUVECs: The mRNA levels were calculated on the assumption of theoretical amplification efficiency of 2.

	Genes	% Relative abundance
GS	GYS1 (Muscle)	12.8 ± 2.5
	GYS2 (Liver)	0.003 ± 0.002
GP	PYGB (Brain)	22.9 ± 4
	PYGL (Liver)	10.7 ± 1.4
	PYGM (Muscle)	0.009 ± 0.002

4.4.2.3. Enzyme activities of glycogen synthase and glycogen phosphorylase

The mobilization of glycogen in the absence of glucose and the differences in phosphorylation states of the muscle GS enzyme with respect to the glucose content in the incubation media, as observed in the above results, show that the GP and GS enzymes are actively involved in the glycogen metabolism in HUVECs. Hence we wanted to observe the enzyme activities of GP and GS enzymes in HUVECs in the same incubation conditions. The results of the GS enzyme activity assay are shown in Figure 4.4.5.

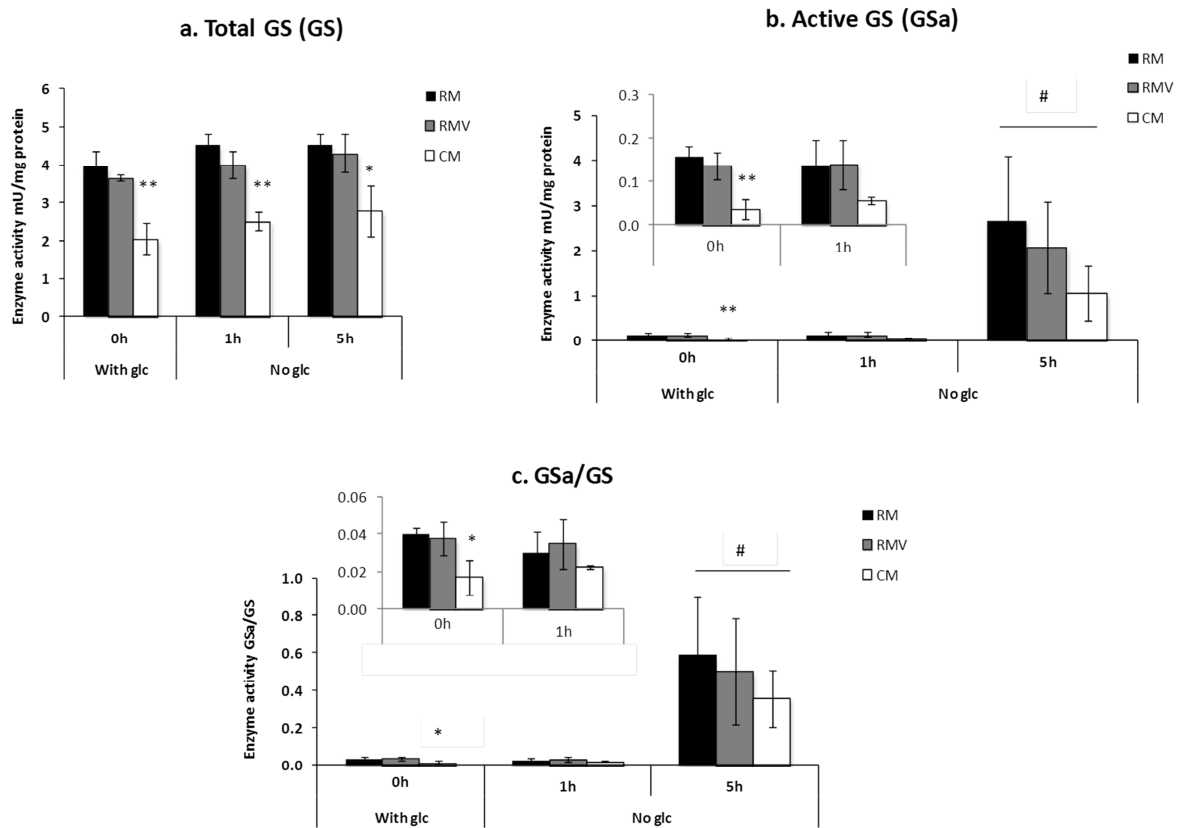


Figure 4.4.5: Enzyme activity assay of GS in RM, RMV and CM, in the presence and absence of glucose. (a) Total GS activity, (b) active GS form, with an expanded plot of 0h and 1h embedded into the main plot and, (c) the ratio of active to total GS, with the plots of 0h and 1h expanded and embedded within the main graph. The total GS activity was measured in the presence of the allosteric activator G6P and the active GS was measured in the absence of it. GS – glycogen synthase, GSa – active GS form, glc – glucose, RM – restricted medium with 2% of FBS, RMV – restricted medium with 2% FBS and VEGF, CM – complete medium with 10% FBS and Lonza EGM SingleQuots.

In the case of the GS enzyme, the total enzyme activity (that correlates with all GS protein present in these cells) (Figure 4.4.5a), the actual GS activity (corresponding to the active GS proteins) (Figure 4.4.5b) and the ratio of the active GS to total GS, that gives the estimation of the active state of GS, (Figure 4.4.5c) are displayed. From the results we observe that the total GS activity remains the same in the presence or absence of glucose (Figure 4.4.5a) irrespective of the substrate conditions of RM, RMV and CM. Moreover, we see that the real GS activity at 5h is more than 15 times compared to that at time points 0h and 1h (Figure 4.4.5b). Accordingly, the ratio of active to total GS in Figure 4.4.5c is much higher at 5h, compared to 0h and 1h. This result is consistent with the result from protein expression of phosphorylated GS shown in Figure 4.4.3b, where the phosphorylation of GS, that inactivates GS, was much lower at 5h compared to 0h and 1h. In addition HUVECs in CM condition show significantly lower total GS and active GS levels (Figures 4.4.5) compared to the cells in RM and RMV. VEGF did not seem to induce significant changes in the enzyme activity and remained similar to the control cells in RM.

The enzyme GP is described to be regulated by covalent phosphorylation, where phosphorylation activates GP enzyme, in contrary to GS where it inactivates the enzyme. This active GP form is represented as GP_a, while the dephosphorylated or the inactive GP form is represented as GP_b. Both these forms of GP can be regulated by some allosteric regulators that can favour either the GP_a or the GP_b forms of the enzyme, and in addition, can be selective to the GP isoforms (see Introduction section 1.5.1). In Figure 4.4.6, we show the enzyme activity measurement of the GP_a in HUVECs, in the presence of caffeine which allosterically inhibits the GP_b forms of the liver and brain isoforms of GP. The GP_a enzyme activity decreases significantly at 5h when glycogen is depleted, uniformly for all medium conditions. Although the activity range for GP and GS enzymes are not of the same order (almost 3 mU/mg in the graph of Figure 4.4.5b for GS and 30 mU/mg in Figure 4.4.6 for GP), clearly at 5h the reduction of GP activity is lower and is of the order of 3x than that of the increase in GS activity which is more than 15x, with respect to their 0 and 1h activities. The insufficient knowledge of other allosteric activators for the liver isoform of GP (where AMP is described to activate brain isoform of GP, but not

effective for the liver isoform), did not allow to measure the total GP enzyme activity which is based on AMP activation of GPb to GPa form.

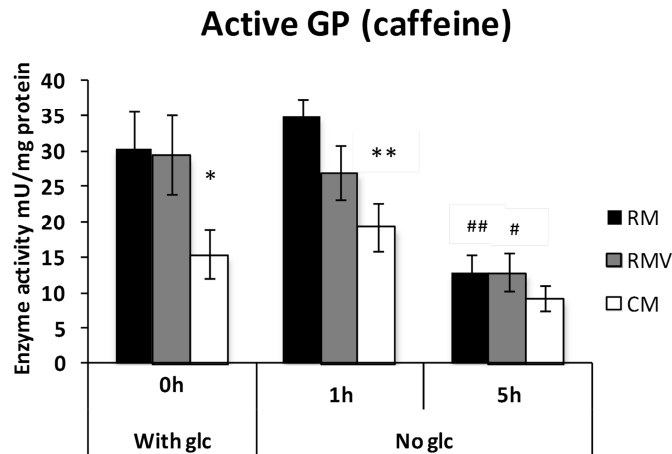


Figure 4.4.6: GP activity measured in the conditions RM, RMV and CM, in the presence and absence of glucose.

The GP activity was measured for its active GP_a form in the presence of caffeine in HUVECs that were incubated under normoxia in RM, RMV and CM conditions, with (0h) and without glucose (1h and 5h). glc – glucose, GP – glycogen phosphorylase, RM – restricted medium with 2% of FBS, RMV – restricted medium with 2% FBS and VEGF, CM – complete medium with 10% FBS and Lonza EGM SingleQuots.

4.4.3. Discussion

Very few studies have reported the presence of glycogen in endothelial cells [150-152] and so far glycogen metabolism has not been characterized in this type of cells. The glycogen accumulation in HUVECs, as observed from our results, and the role of its utilization for cellular functions poses a significant question, why do endothelial cells need glycogen? In the *in vivo* situation, endothelial cells are engaged in the process of angiogenesis and even though when they are in constant contact with blood carrying nutrients in the blood vessels, during angiogenesis the endothelial cells have to proliferate and migrate towards tissues that might be depleted in nutrients and oxygen. Unless the blood vessels are formed with proper lumen and the blood flow is established, the endothelial cells forming new vessels might have to be shortly under nutrient or oxygen-deficient environment and in such situations a readily-available form

of energy store will be highly useful or even protective against cellular damage. In addition, endothelial cells are considered highly glycolytic, also shown and prefer glycolysis over mitochondrial oxidation [118], and if a glycolytic substrate is available this might be preferred the most during glucose-deficient conditions. Glycogen is an emergency fuel store and can be an immediate source of energy when the cells are in demand [377]. Endothelial cells meet acute demands of fuel during their physiological functions of angiogenesis and it would be easier for them to seek a readily-available form of energy in such strenuous situations. These speculations make it worthy to characterize and understand the glycogen metabolism in endothelial cells that is essential to identify the roles of glycogen synthesis and degradation in the functions of these cells.

In this study we intended to study the glycogen degradation pattern under glucose-depleted conditions, reveal the isoforms of the key enzymes of glycogen metabolism, GS and GP expressed by HUVECs, and show the associated enzyme activity patterns. In addition these studies were carried out in different substrate conditions in order to deduce the additional effects of VEGF and growth factors and hormones on glycogen metabolism of HUVECs. The glycogen degradation pattern obtained when HUVECs were depleted of glucose shows that VEGF did not induce significant differences in glycogen levels or degradation pattern in HUVECs, probably because they were incubated for a shorter time of 3h with VEGF before removing glucose, compared to the longer incubation periods in the experiments of Chapter 4.1 which showed significant reduction of glycogen. On the other hand, HUVECs in the presence of high serum and mitogens showed lower glycogen levels both under normoxia and hypoxia. It has been shown that elevated glycogen levels are regularly associated with slow growing cells [378] and are enhanced during non-proliferative state of cells when they are at G1-G0 arrest, as seen in cancer cells *in vitro* and *in vivo* [166,379]. The growth factor and serum deprivation can drive the cells into quiescence or non-proliferative G0 phase [380]. Also HUVECs did not grow in the presence of RM and those cells incubated in CM showed a high proliferation rate (unshown data), suggesting that the high glycogen accumulation from our studies could be related to the low proliferation rate of HUVECs and vice versa.

Moreover, in our present study we observed a higher utilization of glycogen in the absence of glucose under hypoxia, compared to that under normoxia, as seen at 5h of glucose depletion in both conditions. In cancer cells hypoxia has shown to induce rapid glycogen depletion when glucose was deprived [170,174]. This utilization of glycogen was shown to protect cancer cells from cell death by harsh conditions like anoxia or glucose depletion [170,174], similar to the conditions encountered in tumour microenvironment. In fact under low oxygen conditions and in the absence of glucose the readily available substrate for ATP production by cells could be from glycogen degradation.

The types of isoforms of enzymes within the metabolic pathways are important for deciding the functional relevance of these enzymes or the metabolism depending on the cell type. In our study it was important to identify the enzyme isoforms of GS and GP in order to understand the rationale behind the glycogen accumulation and utilization and relate to the functional roles of endothelial cells. We found that HUVECs express muscle isoform of GS which is commonly expressed by many cell lines while liver isoform of GS is specific only to the liver tissue [381,382]. In addition, the GS enzyme activity (Figure 4.4.5) has shown an inversely proportional relationship with the glycogen content, concomitant with the observation in muscle tissue by W. H. Danforth [383]. This reiterates a product inhibition phenomenon where the presence of high glycogen levels inhibits GS enzyme activity by converting it to a less active form.

On the other hand HUVECs co-expressed brain and liver isoforms of GP enzyme. Although individually, the brain isoform of GP is expressed in cell types other than brain, such as heart, skeletal muscle [219] and developing fetus [384,385], the liver isoform of GP is believed to be related only to liver tissues [212]. In addition, the expression of chimeric GP isoforms in certain types of cells is not new. Astrocytes and cardiomyocytes have been reported to co-express brain and muscle isoforms of GP and their isoform-specific enzyme regulations and its relation to cellular functions have been under study [219,220,226]. Co-expression of the GP isoforms has also been speculated for mutual functional roles of each isoform in pathological cases. For example in the case of astrocytes which express both muscle and brain isoforms of GP, a

deficiency in muscle GP isoform encountered in patients with McArdle's glycogen storage disease, does not affect brain functions and it is believed that this is due to the alternative brain isoform expressed by astrocytes that protects the brain tissues from damage in the absence of muscle GP [226].

The GP enzyme isoforms, like those of GS, can be regulated by covalent phosphorylation and also by a variety of allosteric regulators. The brain isoform of GP is said to be strongly activated by the allosteric regulator AMP [386], in contrary to the liver GP isoform which is poorly activated by AMP [222]. These differential regulations of the isoforms help to meet different metabolic demands of the cell. In this study the experimental set up of analyzing GP activity under glucose depletion is ideal for observing the isoform-selective activity as glucose deprivation lowers ATP and increases cytosolic AMP by adenylate kinase [226]. This AMP could activate the brain GP, than the liver isoform and we speculate that most of the glycogen degradation observed in the absence of glucose could be due to the active brain GP isoform. In addition, the active GP measured in the presence of caffeine shows a mild but significant reduction of GP activity at the minimum glycogen condition (at 5h) concomitant to the sharp increase of GS activity with much higher fold change.

A research into the chimeric GP isoform expression in HUVECs would help us to understand their possible functional relevance. Liver isoforms of GS and GP have unique functions of glucose and glycogen regulation in liver cells. Thus liver GP isoform expression by HUVECs arises a question of its functional relevance correlating to the liver type and there are no evidences yet to show the similarity of endothelial cells with liver cells. Liver cells are capable of both taking up and releasing glucose moieties due to their expression of the bi-directional glucose transporter GLUT2, while the endothelial cells have been found to express only the mono-directional GLUT1 glucose transporter that is involved in the uptake of glucose [144,387]. Although liver GP is unique to its cellular type and function, we have to note that PYGL (the gene encoding the liver isoform of GP enzyme) was shown to be one of the hypoxia-regulated genes expressed in head and neck squamous cell carcinoma *in vivo* [388]. Studies on brain, breast and colon cancer cell lines showed an increased expression of the PYGL gene under

HIF1 α activation, that sustains cancer cell proliferation and the PYGL knockdown showed increased cellular senescence *in vitro* by increasing ROS levels and impaired tumor growth *in vivo* [170]. At this point it would be interesting to note that both tumour cells and endothelial cells might encounter similar physiological conditions during the process of tumour angiogenesis. Both types of cells need to survive such hostile tumour microenvironment that has unstable or low oxygen tensions, low glucose and high acidosis. The liver isoform of GP seems to be functionally related to cancer cell survival which makes us wonder if similar possibility could exist for endothelial cells that share the tumour microenvironment. Further studies are required to reveal the functional significance of liver isoform of GP in HUVECs.

To understand the functional relevance of brain isoform of GP expressed by HUVECs, we intended to understand the glycogen utilization by brain cells. Neurons that express the brain isoform of GP enzyme have found to accumulate very little glycogen, but its metabolism has been found to protect these cells from damage during ischemic conditions [256]. Hence neurons seem to possess active glycogen metabolism, expressing brain GP isoform, for utilizing glycogen for its own purpose, to protect itself from adverse conditions. In the case of astrocytes, expressing both brain and muscle forms of GP, they are found to be more altruistic during nutrient-depleted conditions by letting the neighbouring neurons to use the blood-borne glucose, while the astrocytes themselves obtain energy from glycogen-derived pyruvate oxidation [205]. Also astrocytes are reported to use glycogen to produce lactate that could be shuttled to neurons for oxidation during nutrient-depleted conditions [338,339]. There is no clear correlation of glycogen metabolism of astrocytes and HUVECs, but from the results of the angiogenesis assays with GP inhibitors in Chapter 4.3, where we showed that inhibiting glycogen degradation compromised HUVEC viability, migration and wound healing capacity. Hence we could deduce that glycogen reserves in HUVECs could be relevant for their own use like in neurons and glycogen metabolism could be related to the cellular protection and function. In addition our observation of the increased utilization of glycogen under hypoxia seems to show that this metabolism could also play an important role during hypoxic stress of HUVECs.

5. GENERAL DISCUSSION

GENERAL DISCUSSION

In this thesis we have studied the metabolic reprogramming of endothelial cells contributed by different microenvironmental factors and have focussed upon the study of glycogen metabolism and its target for therapeutic angiogenesis. Endothelial cells are the main components of blood vessels and they play an important role in blood vessel formation or angiogenesis in normal and pathological situations. Although various studies on molecular mechanisms of angiogenesis, based on endothelial cell signalling pathways, have been carried out, the metabolic control of angiogenesis is yet to be understood completely. Anti-angiogenic therapies based on targeting pro- and anti-angiogenic factors are under clinical trials, and yet they have not been proven completely successful. Hence, alternative strategies that target pathological angiogenesis need to be developed. The study of the metabolic reprogramming in endothelial cells when activated for angiogenesis can reveal the adaptations of the cells for the pathological condition or the treatment strategies, which can be efficient targets to interfere such cellular adaptations and inhibit their survival or growth. In our study we present a holistic view on the metabolic reprogramming in endothelial cells in the presence of conditions that are encountered during angiogenesis, with HUVE cells using different techniques. The ^{13}C -assisted metabolomics and fluxomics study in Chapter 4.1 has revealed some major metabolic adaptations of HUVECs under hypoxia in general, and those changes induced by the pro-angiogenic factor VEGF under both normoxia and hypoxia. The untargeted metabolomics study in Chapter 4.2 has also provided complementary information on the effect of VEGF on HUVEC metabolism under normoxia, in addition to the differentially metastatic prostate cancer cell lines on HUVEC metabolism, a condition representing tumour-endothelium interaction *in vivo*.

Endothelial cells, lining the blood vessels, encounter varying oxygen levels during the blood flow and the perfusion of hypoxic tissues. One of the main cellular adaptations during such environmental changes and hypoxic condition is metabolic reprogramming, which we aim to characterize in Chapter 4.1. The results from our study reveal a strong metabolic adaptation of HUVECs under hypoxic condition, showing a higher shift towards glycolytic flux and non-

oxidative PPP branch, compared to HUVECs under normoxia. This shift of metabolism was observed both in the presence and absence of VEGF under hypoxia, when compared to those under normoxia. Hypoxia can cause a major disturbance in endothelial cells [389,390] and are in fact one of the major factors regulating angiogenesis [391,392]. Previous studies have shown that hypoxia can induce an upregulation of glycolytic activity in bovine artery endothelial cells [326] and an upregulation of glycolytic proteins [329,393,394] in brain capillary endothelial cells, supporting our results of glycolytic metabolic shift in HUVECs.

In addition to the major metabolic adaptation under hypoxia, VEGF induction under both normoxia and hypoxia showed varying effects of metabolic reprogramming in HUVECs. Our results showed that under normoxia, HUVECs induced with VEGF upregulated alternative pathways in addition to glycolysis for lactate production, compared to those without VEGF induction. In addition, oxidative PPP was increased and G6PD activity was upregulated under normoxia in the presence of VEGF. Studies have reported an upregulation of the enzyme G6PD in endothelial cells in the presence of VEGF, under normoxia [134,333,395], which could be important for counteracting the ROS production due to mitochondrial oxidation. The presence of VEGF also showed an increasing flux from glucose to the synthesis of fatty acids in HUVECs, compared to the cells in the absence of VEGF, which is more significantly observed under hypoxia. Another metabolic pathway found to be affected by VEGF and hypoxia in HUVECs was identified to be glycogen metabolism. VEGF reduced the glycogen content under both normoxia and hypoxia and decreased the glycogen turnover under normoxia. In addition, HUVECs under hypoxic condition were found to accumulate higher glycogen content, produced from glucose as the main substrate. It is worth noting that in some of the cell types, although the glycogen accumulation was not reported significant, its functional relevance has been shown to be vital, serving the purpose of an emergency fuel for sustaining different cellular functions [176,256,396]. In our case HUVECs show both a significant amount of glycogen content and an evident futile cycle of glycogen metabolism occurring in these cells.

In Chapter 4.2 the untargeted analysis has revealed other important changes in the metabolites measured, induced by VEGF under normoxia. In this chapter we saw a change in fatty acid

oxidation by VEGF by upregulating acetyl L-carnitine, supporting the results from fluxomics (Chapter 4.1) that showed an upregulation of mitochondrial metabolism by VEGF in HUVECs under normoxia, which is also reported elsewhere [355]. Additional changes by VEGF have also been observed in purine metabolism where metabolites hypoxanthine and guanine were upregulated. The increase in NAD⁺ levels by VEGF induction in this study has predicted the enrichment of this metabolite not only in glycolysis, but also in other metabolic pathways including TCA cycle and ketone body metabolism, recognized by the metabolite enrichment analysis. A similar profile was observed from the ¹³C metabolomics and fluxomics study of Chapter 4.1, where VEGF was found to upregulate alternative pathways in addition to glycolysis, for the production of lactate, in HUVECs under normoxia. Chapter 4.2 also describes the effects of the differentially metastatic prostate cancer cell sub-populations – PC-3/S and PC-3/M on HUVECs *in vitro*, in a condition that closely mimics the heterogeneous cancer-endothelial cell populations in tumours. The results of the global metabolic analysis revealed a completely different metabolic adaptation of HUVECs under the low metastatic PC-3/S cells and high metastatic PC-3/M cells. HUVECs co-cultured with PC-3/S cells showed metabolic reprogramming very similar to that induced by VEGF, in that it showed upregulated acetyl-L-carnitine and NAD⁺ levels. Interestingly a previous study reported a high secretion of VEGF by low metastatic prostate cancer cell lines [346], in addition to an unreported result that showed an increased mRNA expression levels of VEGF-A by PC-3/S cell line, supporting that the metabolic changes induced by PC-3/S in HUVECs could partly be due to its secretion of VEGF. In addition to these changes, additional pathways related to amino acids, glutathione and pantothenic acid, were also up-regulated in HUVECs co-cultured with PC-3/S cells, although the fold change was much lower ($\leq 1.5X$). On the other hand, in contrast to VEGF and PC-3/S, the highly metastatic PC-3/M cells induce a different metabolic alteration in HUVECs. The pathway analysis revealed changes in methionine, tryptophan and tyrosine metabolism by downregulating the respective metabolites. Another important change was the upregulation of oleamide by a factor greater than 2 in HUVECs co-cultured with PC-3/M, while this was not observed in other conditions. Oleamides have been found to interfere with cellular gap junctions during metastasis [358] and are suspected to be protective against cytochrome *c* mediated cellular apoptotic molecules that can pass through the cellular gaps to neighbouring

cells causing their death [359]. During metastasis the tumour cells intravasating or extravasating through the blood vessels can escape from the vessel barrier by inducing disintegration of endothelial cell monolayer by causing its death [361,397], although these observations were made for direct tumour-endothelial cell interactions. In our study though both cell lines were not in contact directly, the production of oleamide infers a protective adaptation of HUVECs against metastatic or cell damaging factors introduced by the PC-3/M cells.

As mentioned above in the fluxomics part, the glycogen accumulation and turnover observed in HUVECs showed an interesting metabolic target in angiogenesis. Our experimental tests of targeting GP, the key enzyme along glycogen degradation, in Chapter 4.3 showed effective against *in vitro* HUVEC viability, migration and wound healing capabilities. Further studies were performed, in Chapter 4.4, to understand the HUVEC glycogen metabolism and its enzymatic characteristics and find some possible explanations for the lower effects of GP inhibition on *in vivo* angiogenesis observed in Chapter 4.3. In Chapter 4.4 we observed the changes in glycogen content and enzyme regulations in HUVECs by depriving glucose and also explored different substrate conditions of HUVECs in the presence of VEGF and in complete medium which induces a higher cell proliferation. In this study HUVECs showed that glycogen is utilized in the absence of glucose and a minimum glycogen level was maintained in these cells, without completely depleting the reservoir, even after 24h of glucose depletion. In addition, under hypoxia without glucose, HUVECs consumed higher glycogen than under normoxia, showing their dependence of glycogen degradation at this low oxygen condition. It has been reported in cancer cells that glycogen utilization serves to protect them from cell death under low oxygen conditions [170,174]. The fact that glycogen might be an important substrate for ATP production under hypoxia, when mitochondrial oxidation normally does not function, makes this an attractive condition to target glycogen degradation pathway to affect cell viability. Also, as discussed before, endothelial cells constantly encounter varying O₂ conditions, in addition to low nutrient conditions in tumours, in the *in vivo* situations and so introducing hypoxia and low substrate conditions while exploring GP enzyme as a target could be an effective strategy against both endothelial and cancer cell viability/function. We additionally noticed that HUVECs

under high proliferating condition showed lower glycogen content and vice versa, agreeing with previously described studies in cancer cells [166,379].

We also explored the enzyme isoforms expressed by HUVECs and found that these cells express muscle GS and interestingly co-express brain and liver GP enzymes. In addition a higher GS activity was found in the glycogen depleted conditions, showing the necessity of the enzyme to receive a substrate to replenish the glycogen stores in HUVECs to their normal levels. On the other hand the GP enzyme activity was lower at glucose and glycogen depleted condition. Absence of glucose reduces ATP levels and increases AMP content in the cellular environment [226]. The brain isoform of the GP enzyme is shown to be activated by the presence of AMP (in conditions of low glucose) in astrocytes [226,386]. Also brain GP is expressed in neurons, which helps in cellular protection during hypoxic stress [256]. These show that brain GP is important for cellular survival or function when glucose is deprived and in low oxygen conditions. While AMP activation of liver GP isoform is low, the covalent phosphorylation activates it to a much higher extent [222], showing that liver isoform responds to hormonal control and hence dependent on the *in vivo* environment. Indeed, the expression of liver GP isoform in endothelial cells observed in this study and the observations of the higher PYGL gene expression by cancer cells under HIF1 α activation, which has shown to be tumour protective [170], can suggest that the liver GP isoform may be important for both cancer and endothelial cell survival or function in a tumour microenvironment.

The characterization of the enzymes of glycogen metabolism from the Chapter 4.4 could provide some possible explanations for the results obtained in the previous Chapter 4.3. In the Chapter 4.3 we found that the GP inhibitor CP-316819 effectively inhibited HUVEC viability and function *in vitro*, while it had a very small effect on *in vivo* tumour angiogenesis. The effect of the GP inhibitors on inhibiting GP enzyme can depend on various factors like the presence of allosteric effectors and on the GP enzyme isoforms. The indole site inhibitors like CP-316819 work by inhibiting the T-state of the GP α form (the active form of the GP enzyme; the enzyme active states are discussed in detail in the Introduction section 1.5.1) and act synergistically with glucose [254,398]. As discussed in the Introduction part-section 1.5.1, the presence of glucose

favours the T-state of the GP_a enzyme form, contrarily AMP does not favour the T-state. We know that the tumour microenvironment is generally nutrient depleted and glucose levels are constantly lower. It was found that the glucose content in tumour tissues were about 10 times lower than in normal tissues [399] which could also increase AMP levels in tumours. Hence in these situations, the low glucose and high AMP might not favour the T-state GP_a form, which might reduce the effectiveness of an indole site GP inhibitor. Additionally CP-316819 was found to be selectively inhibiting liver GP *in vitro*, and contrarily it was found to be selective for skeletal muscle GP *in vivo*, which was attributed to the lower AMP levels in muscle tissues and other T state promoters acting synergistic with the inhibitor in muscles *in vivo* [400]. Hence the lower effect of the indole inhibitor in the *in vivo* anti-angiogenesis and anti-tumour results of Chapter 4.3 could be due to the presence of very low glucose and high AMP levels that could have not favoured the GP_a T-state that is required for the inhibitory action of the indole inhibitor.

Apart from the allosteric effectors like glucose and AMP, GP enzyme isoforms can also influence the GP inhibitors by being selective substrates for them. It was shown that another indole inhibitor CP-91149 reduces the cell growth of tumour and normal cell lines concurrently with the increase in glycogen content and was claimed to be selective for brain GP isoform [401]. If this is true in the case of HUVECs then the *in vitro* effectiveness of CP-316819 in our results could possibly be related to the brain GP isoform as well. Thus from these analyses we observe that the GP enzyme isoforms and allosteric regulators play an important role in regulating the glycogen degradation and anti-angiogenic effects in HUVECs. Hence it is important to consider the levels of the nutrient and energy substrates like glucose, AMP, ATP, etc. in the microenvironment under study and their effects on the GP enzyme isoforms, for designing effective anti-angiogenic therapies targeting glycogen metabolism.

Overall, in this thesis we have provided a global view of the metabolic reprogramming in HUVECs that are affected by different factors that the endothelial cells encounter in the *in vivo* situations. We have shown that hypoxia induces a highly different metabolic reprogramming in HUVECs and factors like VEGF and low and high metastatic cancer cells can induce distinctly

differential metabolic adaptations. In addition we have extensively focussed upon glycogen metabolic regulation and the therapeutic effects of targeting glycogen metabolism in angiogenesis. Our results have reported the importance of glycogen utilization and the expression of enzyme isoforms in HUVECs, in addition to the significance of enzyme effectors in the modulation of glycogen metabolism. Finally, in this thesis we show the intimate relationship between the regulations of endothelial cell metabolism and cellular survival and function, and highlight the importance of endothelial cell metabolism in angiogenesis.

6. CONCLUSIONS

CONCLUSIONS

1. Our ^{13}C -assisted metabolomics and fluxomics approach showed that HUVECs, under hypoxia favours pathways such as glycolysis and the non-oxidative branch of PPP, and induces a higher accumulation of glycogen produced from glucose.

Under normoxia VEGF upregulated alternative pathways in addition to glycolysis for the lactate production in HUVECs, and increased the flux to oxidative branch of PPP. In addition VEGF increased the flux of glucose to fatty acid synthesis and reduced glycogen content irrespective of the oxygen conditions.

2. The untargeted metabolomics analysis revealed that the low metastatic PC-3/S prostate cancer cells and VEGF both induced an increase in the levels of acetyl L-carnitine and NAD⁺. In addition, metabolites related to pathways such as amino acid, glutathione and pantothenate metabolism were upregulated by PC-3/S cells on HUVECs. Whereas, metabolites related to purine metabolism such as hypoxanthine, guanine and AMP were altered by VEGF in HUVECs.

On the other hand, the highly metastatic PC-3/M cells induced a completely different metabolic signature in HUVECs, compared to VEGF and PC-3/S, by upregulating oleamide and downregulating methionine, tyrosine and tryptophan.

3. Glycogen was found to be accumulated at significant levels in HUVECs in the presence of glucose and these cells showed an evident glycogen turnover from the ^{13}C tracer enrichment analysis.

Targeting glycogen metabolism by inhibiting GP enzyme showed a reduction of cell viability and function *in vitro*. *In vivo* the GP inhibition showed a tendency towards reducing microvessel density of tumour tissues.

4. Characterization of glycogen metabolism in HUVECs revealed that in the absence of glucose, glycogen is utilized under both normoxia and hypoxia and showed a tendency of higher utilization under hypoxia. Moreover, HUVECs expressed muscle isoform of GS

enzyme, which increased its activity when glycogen was reduced in the absence of glucose. On the other hand, these cells co-expressed brain and liver isoforms of GP and in contrary to GS, the GP activity reduced with reduction in glycogen, in the absence of glucose. Furthermore, HUVECs incubated in high serum and growth hormone-rich conditions reduced the glycogen content and showed low GS and GP enzyme activities, compared to the cells grown in low serum conditions.

7. REFERENCES

REFERENCES

1. Adair TH, Montani J-P. Overview of angiogenesis. (2010).
2. Carmeliet P. Angiogenesis in life, disease and medicine. *Nature*, 438(7070), 932-936 (2005).
3. Folkman J. Role of angiogenesis in tumor growth and metastasis. In: *Seminars in oncology*. (Ed.^(Eds) (Elsevier, 2002) 15-18.
4. Hanahan D, Weinberg RA. Hallmarks of cancer: the next generation. *cell*, 144(5), 646-674 (2011).
5. Heidenreich R, Röcken M, Ghoreschi K. Angiogenesis drives psoriasis pathogenesis. *International journal of experimental pathology*, 90(3), 232-248 (2009).
6. Nickoloff BJ, Mitra RS, Varani J, Dixit V, Verini PJ. Aberrant production of interleukin-8 and thrombospondin-1 by psoriatic keratinocytes mediates angiogenesis. *The American journal of pathology*, 144(4), 820 (1994).
7. Isozaki T, Rabquer BJ, Ruth JH, Haines GK, Koch AE. ADAM-10 is overexpressed in rheumatoid arthritis synovial tissue and mediates angiogenesis. *Arthritis & Rheumatism*, 65(1), 98-108 (2013).
8. Kim Sj, Chen Z, Chamberlain ND *et al*. Angiogenesis in Rheumatoid Arthritis Is Fostered Directly by Toll-like Receptor 5 Ligation and Indirectly Through Interleukin-17 Induction. *Arthritis & Rheumatism*, 65(8), 2024-2036 (2013).
9. Szekanecz Z, Besenyi T, Szentpetery A, Koch AE. Angiogenesis and vasculogenesis in rheumatoid arthritis. *Current opinion in rheumatology*, 22(3), 299-306 (2010).
10. Willard AL, Herman IM. Vascular complications and diabetes: current therapies and future challenges. *Journal of ophthalmology*, 2012 (2012).
11. Oka T, Akazawa H, Naito AT, Komuro I. Angiogenesis and Cardiac Hypertrophy Maintenance of Cardiac Function and Causative Roles in Heart Failure. *Circulation research*, 114(3), 565-571 (2014).
12. Ergul A, Alhusban A, Fagan SC. Angiogenesis a harmonized target for recovery after stroke. *Stroke; a journal of cerebral circulation*, 43(8), 2270-2274 (2012).
13. Krupinski J, Kaluza J, Kumar P, Kumar S, Wang JM. Role of angiogenesis in patients with cerebral ischemic stroke. *Stroke; a journal of cerebral circulation*, 25(9), 1794-1798 (1994).
14. Ding W-G, Wei Z-X, Liu J-B. Reduced local blood supply to the tibial metaphysis is associated with ovariectomy-induced osteoporosis in mice. *Connective tissue research*, 52(1), 25-29 (2011).
15. Weinstein RS, Wan C, Liu Q *et al*. Endogenous glucocorticoids decrease skeletal angiogenesis, vascularity, hydration, and strength in aged mice. *Aging cell*, 9(2), 147-161 (2010).
16. Cervelli V, Garcovich S, Bielli A *et al*. The effect of autologous activated platelet rich plasma (AA-PRP) injection on pattern hair loss: clinical and histomorphometric evaluation. *BioMed research international*, 2014 (2014).
17. Mecklenburg L, Tobin DJ, Müller-Röver S *et al*. Active hair growth (anagen) is associated with angiogenesis. *Journal of Investigative Dermatology*, 114(5), 909-916 (2000).

18. Carmeliet P. Manipulating angiogenesis in medicine. *Journal of internal medicine*, 255(5), 538-561 (2004).
19. Stapor P, De Bock K, Carmeliet P. Essentials of Angiogenesis. In: *PanVascular Medicine*. Lanzer, P (Ed. (Springer Berlin Heidelberg, 2015) 137-165.
20. Bergers G, Hanahan D. Modes of resistance to anti-angiogenic therapy. *Nature Reviews Cancer*, 8(8), 592-603 (2008).
21. Davis GE. Angiogenesis and proteinases: influence on vascular morphogenesis, stabilization and regression. *Drug Discovery Today: Disease Models*, 8(1), 13-20 (2011).
22. Potente M, Gerhardt H, Carmeliet P. Basic and Therapeutic Aspects of Angiogenesis. *Cell*, 146(6), 873-887 (2011).
23. Carmeliet P. Mechanisms of angiogenesis and arteriogenesis. *Nature medicine*, 6(4), 389-396 (2000).
24. Herbert SP, Stainier DY. Molecular control of endothelial cell behaviour during blood vessel morphogenesis. *Nature reviews Molecular cell biology*, 12(9), 551-564 (2011).
25. Mazzone M, Dettori D, de Oliveira RL *et al*. Heterozygous deficiency of PHD2 restores tumor oxygenation and inhibits metastasis via endothelial normalization. *Cell*, 136(5), 839-851 (2009).
26. Welte J, Loges S, Dimmeler S, Carmeliet P. Recent molecular discoveries in angiogenesis and antiangiogenic therapies in cancer. *The Journal of Clinical Investigation*, 123(8), 3190-3200 (2013).
27. Cattin A-L, Burden JJ, Van Emmenis L *et al*. Macrophage-induced blood vessels guide Schwann cell-mediated regeneration of peripheral nerves. *Cell*, 162(5), 1127-1139 (2015).
28. Fantin A, Vieira JM, Gestri G *et al*. Tissue macrophages act as cellular chaperones for vascular anastomosis downstream of VEGF-mediated endothelial tip cell induction. *Blood*, 116(5), 829-840 (2010).
29. Carmeliet P. VEGF as a key mediator of angiogenesis in cancer. *Oncology*, 69(Suppl. 3), 4-10 (2005).
30. Ferrara N. VEGF-A: a critical regulator of blood vessel growth. *European cytokine network*, 20(4), 158-163 (2009).
31. Nagy JA, Dvorak AM, Dvorak HF. VEGF-A and the induction of pathological angiogenesis. *Annu. Rev. Pathol. Mech. Dis.*, 2, 251-275 (2007).
32. Ferrara N. Role of vascular endothelial growth factor in the regulation of angiogenesis. *Kidney international*, 56(3), 794-814 (1999).
33. Korpelainen EI, Alitalo K. Signaling angiogenesis and lymphangiogenesis. *Current opinion in cell biology*, 10(2), 159-164 (1998).
34. Koch S, Tugues S, Li X, Gualandi L, Claesson-Welsh L. Signal transduction by vascular endothelial growth factor receptors. *Biochemical Journal*, 437(2), 169-183 (2011).
35. Ferrara N, Davis-Smyth T. The biology of vascular endothelial growth factor. *Endocrine reviews*, 18(1), 4-25 (1997).
36. Guerrin M, Moukadir H, Chollet P *et al*. Vasculotropin/Vascular endothelial growth factor is an autocrine growth factor for human retinal pigment epithelial cells cultured in vitro. *Journal of cellular physiology*, 164(2), 385-394 (1995).

37. Öberg-Welsh C, Sandler S, Andersson A, Welsh M. Effects of vascular endothelial growth factor on pancreatic duct cell replication and the insulin production of fetal islet-like cell clusters in vitro. *Molecular and cellular endocrinology*, 126(2), 125-132 (1997).
38. Brushart T, Aspalter M, Griffin J *et al.* Schwann cell phenotype is regulated by axon modality and central–peripheral location, and persists in vitro. *Experimental neurology*, 247, 272-281 (2013).
39. Sondell M, Lundborg G, Kanje M. Vascular endothelial growth factor has neurotrophic activity and stimulates axonal outgrowth, enhancing cell survival and Schwann cell proliferation in the peripheral nervous system. *The Journal of neuroscience*, 19(14), 5731-5740 (1999).
40. Alon T, Hemo I, Itin A, Pe'er J, Stone J, Keshet E. Vascular endothelial growth factor acts as a survival factor for newly formed retinal vessels and has implications for retinopathy of prematurity. *Nature medicine*, 1(10), 1024-1028 (1995).
41. Nishijima K, Ng Y-S, Zhong L *et al.* Vascular endothelial growth factor-A is a survival factor for retinal neurons and a critical neuroprotectant during the adaptive response to ischemic injury. *The American journal of pathology*, 171(1), 53-67 (2007).
42. Byrne AM, Bouchier-Hayes DJ, Harmey JH. Angiogenic and cell survival functions of vascular endothelial growth factor (VEGF). *Journal of cellular and molecular medicine*, 9(4), 777-794 (2005).
43. Harmey JH, Bouchier-Hayes D. Vascular endothelial growth factor (VEGF), a survival factor for tumour cells: Implications for anti-angiogenic therapy. *Bioessays*, 24(3), 280-283 (2002).
44. Gerber H-P, Dixit V, Ferrara N. Vascular endothelial growth factor induces expression of the antiapoptotic proteins Bcl-2 and A1 in vascular endothelial cells. *Journal of Biological Chemistry*, 273(21), 13313-13316 (1998).
45. Le Gouill S, Podar K, Amiot M *et al.* VEGF induces Mcl-1 up-regulation and protects multiple myeloma cells against apoptosis. *Blood*, 104(9), 2886-2892 (2004).
46. Pidgeon GP, Barr MP, Harmey JH, Foley DA, Bouchier-Hayes DJ. Vascular endothelial growth factor (VEGF) upregulates BCL-2 and inhibits apoptosis in human and murine mammary adenocarcinoma cells. *British Journal of Cancer*, 85(2), 273 (2001).
47. Patel KR, Vajaria BN, Begum R *et al.* VEGFA isoforms play a vital role in oral cancer progression. *Tumor Biol.*, 36(8), 6321-6332 (2015).
48. Mao D, Zhang Y, Lu H, Zhang H. Molecular basis underlying inhibition of metastasis of gastric cancer by anti-VEGF α treatment. *Tumor Biol.*, 35(8), 8217-8223 (2014).
49. Chen J, De S, Brainard J, BYZOVA TV. Metastatic properties of prostate cancer cells are controlled by VEGF. *Cell communication & adhesion*, 11(1), 1-11 (2004).
50. Roberts E, Cossigny DA, Quan GM. The role of vascular endothelial growth factor in metastatic prostate cancer to the skeleton. *Prostate cancer*, 2013 (2013).
51. Lanier V, Jeffers M, Walterberger J, Anderson L, Gonzalez R. Leptin Notch VEGFR-2 axis influences cancer stromal cell behavior. *Cancer Research*, 75(15 Supplement), 2911-2911 (2015).
52. Tasaki Y, Nishimura R, Shibaya M, Lee H-Y, Acosta TJ, Okuda K. Expression of VEGF and its receptors in the bovine endometrium throughout the estrous cycle: effects of VEGF on prostaglandin production in endometrial cells. *Journal of Reproduction and Development*, 56(2), 223-229 (2010).

53. Youssoufian H, Hicklin DJ, Rowinsky EK. Review: monoclonal antibodies to the vascular endothelial growth factor receptor-2 in cancer therapy. *Clinical cancer research*, 13(18), 5544s-5548s (2007).
54. Fischer C, Mazzone M, Jonckx B, Carmeliet P. FLT1 and its ligands VEGFB and PlGF: drug targets for anti-angiogenic therapy? *Nature Reviews Cancer*, 8(12), 942-956 (2008).
55. Schwartz JD, Rowinsky EK, Youssoufian H, Pytowski B, Wu Y. Vascular endothelial growth factor receptor-1 in human cancer. *Cancer*, 116(S4), 1027-1032 (2010).
56. Lichtenberger BM, Tan PK, Niederleithner H, Ferrara N, Petzelbauer P, Sibilina M. Autocrine VEGF signaling synergizes with EGFR in tumor cells to promote epithelial cancer development. *Cell*, 140(2), 268-279 (2010).
57. Ahluwalia A, S Tarnawski A. Critical role of hypoxia sensor-HIF-1 α in VEGF gene activation. Implications for angiogenesis and tissue injury healing. *Current medicinal chemistry*, 19(1), 90-97 (2012).
58. Ahn G-O, Kim Y-E, Hong B-J *et al.* Abstract A13: Hypoxia-inducible factor-1 (HIF-1) in myeloid cells promotes angiogenesis by regulating VEGF and S100A8 production. *Cancer Research*, 75(1 Supplement), A13-A13 (2015).
59. Hu K, Babapoor-Farrokhran S, Rodrigues M *et al.* Hypoxia-inducible factor 1 upregulation of both VEGF and ANGPTL4 is required to promote the angiogenic phenotype in uveal melanoma. *Oncotarget*, (2016).
60. Saponaro C, Malfettone A, Ranieri G *et al.* VEGF, HIF-1 α expression and MVD as an angiogenic network in familial breast cancer. *PloS one*, 8(1), e53070 (2013).
61. Albini A, Sporn MB. The tumour microenvironment as a target for chemoprevention. *Nature Reviews Cancer*, 7(2), 139-147 (2007).
62. Helmlinger G, Yuan F, Dellian M, Jain RK. Interstitial pH and pO₂ gradients in solid tumors in vivo: high-resolution measurements reveal a lack of correlation. *Nature medicine*, 3(2), 177-182 (1997).
63. Folkman J. What is the evidence that tumors are angiogenesis dependent? *CancerSpectrum Knowledge Environment*, 82(1), 4-6 (1990).
64. Balkwill F, Mantovani A. Inflammation and cancer: back to Virchow? *The lancet*, 357(9255), 539-545 (2001).
65. Folkman J. Tumor angiogenesis: therapeutic implications. *New England Journal of Medicine*, (285), 1182-1186 (1971).
66. Alitalo A, Detmar M. Interaction of tumor cells and lymphatic vessels in cancer progression. *Oncogene*, 31(42), 4499-4508 (2012).
67. Hanahan D, Coussens LM. Accessories to the crime: functions of cells recruited to the tumor microenvironment. *Cancer cell*, 21(3), 309-322 (2012).
68. Konerding M, Malkusch W, Klapthor B *et al.* Evidence for characteristic vascular patterns in solid tumours: quantitative studies using corrosion casts. *British journal of cancer*, 80(5-6), 724 (1999).
69. Warren B, Shubik P, Wilson R, Garcia H, Feldman R. The microcirculation in two transplantable melanomas of the hamster I. In vivo observations in transparent chambers. *Cancer letters*, 4, 109-116 (1978).
70. Dudley AC. Tumor endothelial cells. *Cold Spring Harbor perspectives in medicine*, 2(3), a006536 (2012).

71. Maniotis AJ, Folberg R, Hess A *et al.* Vascular channel formation by human melanoma cells in vivo and in vitro: vasculogenic mimicry. *The American journal of pathology*, 155(3), 739-752 (1999).
72. Jain RK. Normalization of tumor vasculature: an emerging concept in antiangiogenic therapy. *Science*, 307(5706), 58-62 (2005).
73. Semenza GL. Oxygen sensing, hypoxia-inducible factors, and disease pathophysiology. *Annual Review of Pathology: Mechanisms of Disease*, 9, 47-71 (2014).
74. Taylor C. Mitochondria and cellular oxygen sensing in the HIF pathway. *Biochem. J*, 409, 19-26 (2008).
75. Graven KK, Farber HW. Endothelial cell hypoxic stress proteins. *Journal of Laboratory and Clinical Medicine*, 132(6), 456-463 (1998).
76. Choudhry H, Schödel J, Oikonomopoulos S *et al.* Extensive regulation of the non-coding transcriptome by hypoxia: role of HIF in releasing paused RNAPol2. *EMBO reports*, e201337642 (2013).
77. Ke Q, Costa M. Hypoxia-inducible factor-1 (HIF-1). *Molecular pharmacology*, 70(5), 1469-1480 (2006).
78. Shen C, Kaelin WG. The VHL/HIF axis in clear cell renal carcinoma. In: *Seminars in cancer biology*. (Ed. (Eds) (Elsevier, 2013) 18-25.
79. Agani F, Jiang B-H. Oxygen-independent regulation of HIF-1: novel involvement of PI3K/AKT/mTOR pathway in cancer. *Current cancer drug targets*, 13(3), 245-251 (2013).
80. Favaro E, Lord S, Harris AL, Buffa FM. Gene expression and hypoxia in breast cancer. *Genome Med*, 3(8), 55 (2011).
81. Semenza GL. HIF-1 mediates metabolic responses to intratumoral hypoxia and oncogenic mutations. *The Journal of clinical investigation*, 123(9), 3664 (2013).
82. Singleton D, Rouhi P, Zois C *et al.* Hypoxic regulation of RIOK3 is a major mechanism for cancer cell invasion and metastasis. *Oncogene*, (2014).
83. Gilkes DM, Semenza GL, Wirtz D. Hypoxia and the extracellular matrix: drivers of tumour metastasis. *Nature Reviews Cancer*, 14(6), 430-439 (2014).
84. Tang N, Wang L, Esko J *et al.* Loss of HIF-1 α in endothelial cells disrupts a hypoxia-driven VEGF autocrine loop necessary for tumorigenesis. *Cancer cell*, 6(5), 485-495 (2004).
85. Skuli N, Liu L, Runge A *et al.* Endothelial deletion of hypoxia-inducible factor-2 α (HIF-2 α) alters vascular function and tumor angiogenesis. *Blood*, 114(2), 469-477 (2009).
86. Le Bras A, Lionneton F, Mattot V *et al.* HIF-2 α specifically activates the VE-cadherin promoter independently of hypoxia and in synergy with Ets-1 through two essential ETS-binding sites. *Oncogene*, 26(53), 7480-7489 (2007).
87. Dutta D, Ray S, Vivian JL, Paul S. Activation of the VEGFR1 chromatin domain an angiogenic signal-ETS1/HIF-2 α regulatory axis. *Journal of Biological Chemistry*, 283(37), 25404-25413 (2008).
88. de Oliveira RL, Deschoemaeker S, Henze A-T *et al.* Gene-targeting of Phd2 improves tumor response to chemotherapy and prevents side-toxicity. *Cancer cell*, 22(2), 263-277 (2012).
89. Close A. Antiangiogenesis and vascular disrupting agents in cancer: circumventing resistance and augmenting their therapeutic utility. *Future Medicinal Chemistry*, (0) (2016).

90. Khan K, Cunningham D, Chau I. Targeting angiogenic pathways in colorectal cancer: complexities, challenges and future directions. *Curr Drug Targets*, (2015).
91. Shojaei F. Anti-angiogenesis therapy in cancer: current challenges and future perspectives. *Cancer letters*, 320(2), 130-137 (2012).
92. Wick W, Platten M, Wick A *et al.* Current status and future directions of anti-angiogenic therapy for gliomas. *Neuro-oncology*, 18(3), 315-328 (2015).
93. Gerber H-P, Ferrara N. Pharmacology and pharmacodynamics of bevacizumab as monotherapy or in combination with cytotoxic therapy in preclinical studies. *Cancer research*, 65(3), 671-680 (2005).
94. Kabbinavar F, Hurwitz HI, Fehrenbacher L *et al.* Phase II, randomized trial comparing bevacizumab plus fluorouracil (FU)/leucovorin (LV) with FU/LV alone in patients with metastatic colorectal cancer. *Journal of Clinical Oncology*, 21(1), 60-65 (2003).
95. Ferrara N, Adamis AP. Ten years of anti-vascular endothelial growth factor therapy. *Nature Reviews Drug Discovery*, (2016).
96. Gressett SM, Shah SR. Intricacies of bevacizumab-induced toxicities and their management. *Annals of Pharmacotherapy*, 43(3), 490-500 (2009).
97. Van Cutsem E, Tabernero J, Lakomy R *et al.* Addition of aflibercept to fluorouracil, leucovorin, and irinotecan improves survival in a phase III randomized trial in patients with metastatic colorectal cancer previously treated with an oxaliplatin-based regimen. *Journal of Clinical Oncology*, JCO. 2012.2042. 8201 (2012).
98. Fuchs CS, Tomasek J, Yong CJ *et al.* Ramucirumab monotherapy for previously treated advanced gastric or gastro-oesophageal junction adenocarcinoma (REGARD): an international, randomised, multicentre, placebo-controlled, phase 3 trial. *The Lancet*, 383(9911), 31-39 (2014).
99. Wilke H, Muro K, Van Cutsem E *et al.* Ramucirumab plus paclitaxel versus placebo plus paclitaxel in patients with previously treated advanced gastric or gastro-oesophageal junction adenocarcinoma (RAINBOW): a double-blind, randomised phase 3 trial. *The Lancet Oncology*, 15(11), 1224-1235 (2014).
100. Crinò L, Metro G. Therapeutic options targeting angiogenesis in nonsmall cell lung cancer. *European Respiratory Review*, 23(131), 79-91 (2014).
101. Brufsky AM, Hurvitz S, Perez E *et al.* RIBBON-2: A randomized, double-blind, placebo-controlled, phase III trial evaluating the efficacy and safety of bevacizumab in combination with chemotherapy for second-line treatment of human epidermal growth factor receptor 2–negative metastatic breast cancer. *Journal of Clinical Oncology*, JCO. 2010.2034. 1255 (2011).
102. Ballas MS, Chachoua A. Rationale for targeting VEGF, FGF, and PDGF for the treatment of NSCLC. *Onco Targets Ther*, 4(1), 43-58 (2011).
103. Zhao Y, Adjei AA. Targeting angiogenesis in cancer therapy: moving beyond vascular endothelial growth factor. *Oncologist*, 20(6), 660-673 (2015).
104. Al-Husein B, Abdalla M, Trepte M, DeRemer DL, Somanath PR. Antiangiogenic therapy for cancer: an update. *Pharmacotherapy: The Journal of Human Pharmacology and Drug Therapy*, 32(12), 1095-1111 (2012).
105. Jayson GC, Kerbel R, Ellis LM, Harris AL. Antiangiogenic therapy in oncology: current status and future directions. *The Lancet*, (2016).

106. Nathan P, Zweifel M, Padhani AR *et al.* Phase I trial of combretastatin A4 phosphate (CA4P) in combination with bevacizumab in patients with advanced cancer. *Clinical Cancer Research*, 18(12), 3428-3439 (2012).
107. Liu P, Qin Y, Wu L *et al.* A phase I clinical trial assessing the safety and tolerability of combretastatin A4 phosphate injections. *Anti-cancer drugs*, 25(4), 462-471 (2014).
108. Yopp AC, Schwartz LH, Kemeny N *et al.* Antiangiogenic therapy for primary liver cancer: correlation of changes in dynamic contrast-enhanced magnetic resonance imaging with tissue hypoxia markers and clinical response. *Annals of surgical oncology*, 18(8), 2192-2199 (2011).
109. Hattingen E, Jurcoane A, Bähr O *et al.* Bevacizumab impairs oxidative energy metabolism and shows antitumoral effects in recurrent glioblastomas: a 31P/1H MRSI and quantitative magnetic resonance imaging study. *Neuro-oncology*, nor132 (2011).
110. DeLay M, Jahangiri A, Carbonell WS *et al.* Microarray analysis verifies two distinct phenotypes of glioblastomas resistant to antiangiogenic therapy. *Clinical Cancer Research*, 18(10), 2930-2942 (2012).
111. McIntyre A, Harris AL. Metabolic and hypoxic adaptation to anti-angiogenic therapy: a target for induced essentiality. *EMBO Molecular Medicine*, 7(4), 368-379 (2015).
112. Parks SK, Chiche J, Pouyssegur J. Disrupting proton dynamics and energy metabolism for cancer therapy. *Nature Reviews Cancer*, 13(9), 611-623 (2013).
113. Indraccolo S, Mueller-Klieser W. Potential of Induced Metabolic Bioluminescence Imaging to Uncover Metabolic Effects of Antiangiogenic Therapy in Tumors. *Frontiers in oncology*, 6 (2016).
114. Kumar K, Wigfield S, Gee HE *et al.* Dichloroacetate reverses the hypoxic adaptation to bevacizumab and enhances its antitumor effects in mouse xenografts. *Journal of molecular medicine*, 91(6), 749-758 (2013).
115. Bensaad K, Favaro E, Lewis CA *et al.* Fatty acid uptake and lipid storage induced by HIF-1 α contribute to cell growth and survival after hypoxia-reoxygenation. *Cell reports*, 9(1), 349-365 (2014).
116. Sounni NE, Cimino J, Blacher S *et al.* Blocking lipid synthesis overcomes tumor regrowth and metastasis after antiangiogenic therapy withdrawal. *Cell metabolism*, 20(2), 280-294 (2014).
117. Shen Y, Ou D, Hsu C *et al.* Activating oxidative phosphorylation by a pyruvate dehydrogenase kinase inhibitor overcomes sorafenib resistance of hepatocellular carcinoma. *British journal of cancer*, 108(1), 72-81 (2013).
118. De Bock K, Georgiadou M, Carmeliet P. Role of endothelial cell metabolism in vessel sprouting. *Cell metabolism*, 18(5), 634-647 (2013).
119. De Bock K, Georgiadou M, Schoors S *et al.* Role of PFKFB3-driven glycolysis in vessel sprouting. *Cell*, 154(3), 651-663 (2013).
120. Yeh W-L, Lin C-J, Fu W-M. Enhancement of glucose transporter expression of brain endothelial cells by vascular endothelial growth factor derived from glioma exposed to hypoxia. *Molecular pharmacology*, 73(1), 170-177 (2008).
121. Parra-Bonilla G, Alvarez DF, Al-Mehdi A-B, Alexeyev M, Stevens T. Critical role for lactate dehydrogenase A in aerobic glycolysis that sustains pulmonary microvascular endothelial cell proliferation. *American Journal of Physiology-Lung Cellular and Molecular Physiology*, 299(4), L513-L522 (2010).

122. Blouin A, Bolender RP, Weibel ER. Distribution of organelles and membranes between hepatocytes and nonhepatocytes in the rat liver parenchyma. A stereological study. *The Journal of cell biology*, 72(2), 441-455 (1977).
123. Cucullo L, Hossain M, Puvenna V, Marchi N, Janigro D. The role of shear stress in Blood-Brain Barrier endothelial physiology. *BMC neuroscience*, 12, 40 (2011).
124. Dranka BP, Hill BG, Darley-Usmar VM. Mitochondrial reserve capacity in endothelial cells: The impact of nitric oxide and reactive oxygen species. *Free Radical Biology and Medicine*, 48(7), 905-914 (2010).
125. Cai H. Hydrogen peroxide regulation of endothelial function: origins, mechanisms, and consequences. *Cardiovascular research*, 68(1), 26-36 (2005).
126. Chua CC, Hamdy RC, Chua BH. Upregulation of vascular endothelial growth factor by H₂O₂ in rat heart endothelial cells. *Free Radical Biology and Medicine*, 25(8), 891-897 (1998).
127. Kluge MA, Fetterman JL, Vita JA. Mitochondria and endothelial function. *Circulation Research*, 112(8), 1171-1188 (2013).
128. Mallat Z, Tedgui A. Apoptosis in the vasculature: mechanisms and functional importance. *British journal of pharmacology*, 130(5), 947-962 (2000).
129. Arany Z, Foo S-Y, Ma Y *et al.* HIF-independent regulation of VEGF and angiogenesis by the transcriptional coactivator PGC-1 α . *Nature*, 451(7181), 1008-1012 (2008).
130. Sawada N, Jiang A, Takizawa F *et al.* Endothelial PGC-1 β ; Mediates Vascular Dysfunction in Diabetes. *Cell Metabolism*, 19(2), 246-258).
131. Leopold JA, Zhang Y-Y, Scribner AW, Stanton RC, Loscalzo J. Glucose-6-phosphate dehydrogenase overexpression decreases endothelial cell oxidant stress and increases bioavailable nitric oxide. *Arteriosclerosis, thrombosis, and vascular biology*, 23(3), 411-417 (2003).
132. Zhang Z, Yang Z, Zhu B *et al.* Increasing glucose 6-phosphate dehydrogenase activity restores redox balance in vascular endothelial cells exposed to high glucose. (2012).
133. Zhang Z, Apse K, Pang J, Stanton RC. High glucose inhibits glucose-6-phosphate dehydrogenase via cAMP in aortic endothelial cells. *Journal of Biological Chemistry*, 275(51), 40042-40047 (2000).
134. Pan S, Kovacs CJ, Berk BC. Glucose 6-Phosphate Dehydrogenase Is Regulated Through c-Src-Mediated Tyrosine Phosphorylation in Endothelial Cells. *Arteriosclerosis, thrombosis, and vascular biology*, 29(6), 895-901 (2009).
135. Vizán P, Sánchez-Tena S, Alcarraz-Vizán G *et al.* Characterization of the metabolic changes underlying growth factor angiogenic activation: identification of new potential therapeutic targets. *Carcinogenesis*, 30(6), 946-952 (2009).
136. Jeppesen J, Kiens B. Regulation and limitations to fatty acid oxidation during exercise. *The Journal of physiology*, 590(5), 1059-1068 (2012).
137. Elmasri H, Karaaslan C, Teper Y *et al.* Fatty acid binding protein 4 is a target of VEGF and a regulator of cell proliferation in endothelial cells. *The FASEB Journal*, 23(11), 3865-3873 (2009).
138. Hagberg CE, Falkevall A, Wang X *et al.* Vascular endothelial growth factor B controls endothelial fatty acid uptake. *Nature*, 464(7290), 917-921 (2010).
139. Hagberg CE, Mehlem A, Falkevall A *et al.* Targeting VEGF-B as a novel treatment for insulin resistance and type 2 diabetes. *Nature*, 490(7420), 426-430 (2012).

140. Dagher Z, Ruderman N, Tornheim K, Ido Y. Acute regulation of fatty acid oxidation and amp-activated protein kinase in human umbilical vein endothelial cells. *Circulation research*, 88(12), 1276-1282 (2001).
141. Giacco F, Brownlee M. Oxidative stress and diabetic complications. *Circulation research*, 107(9), 1058-1070 (2010).
142. Schoors S, Bruning U, Missiaen R *et al.* Fatty acid carbon is essential for dNTP synthesis in endothelial cells. *Nature*, 520(7546), 192-197 (2015).
143. Patella F, Schug ZT, Persi E *et al.* Proteomics-Based Metabolic Modeling Reveals That Fatty Acid Oxidation (FAO) Controls Endothelial Cell (EC) Permeability. *Molecular & Cellular Proteomics*, 14(3), 621-634 (2015).
144. Mann GE, Yudilevich DL, Sobrevia L. Regulation of amino acid and glucose transporters in endothelial and smooth muscle cells. *Physiological reviews*, 83(1), 183-252 (2003).
145. Häberle J, Görg B, Rutsch F *et al.* Congenital glutamine deficiency with glutamine synthetase mutations. *New England Journal of Medicine*, 353(18), 1926-1933 (2005).
146. Unterluggauer H, Mazurek S, Lener B *et al.* Premature senescence of human endothelial cells induced by inhibition of glutaminase. *Biogerontology*, 9(4), 247-259 (2008).
147. Croci DO, Cerliani JP, Dalotto-Moreno T *et al.* Glycosylation-dependent lectin-receptor interactions preserve angiogenesis in anti-VEGF refractory tumors. *Cell*, 156(4), 744-758 (2014).
148. Fu ZJ, Li S-Y, Kociok N, Wong D, Chung SK, Lo AC. Aldose Reductase Deficiency Reduced Vascular Changes in Neonatal Mouse Retina in Oxygen-Induced RetinopathyAR Deficiency Protects Retinal Vasculature in OIR. *Investigative ophthalmology & visual science*, 53(9), 5698-5712 (2012).
149. Tammali R, Reddy AB, Srivastava SK, Ramana KV. Inhibition of aldose reductase prevents angiogenesis in vitro and in vivo. *Angiogenesis*, 14(2), 209-221 (2011).
150. Amemiya T. Glycogen metabolism in the capillary endothelium: Electron histochemical study of glycogen synthetase and phosphorylase in the pecten capillary of the chick. *Acta histochemica*, 73(1), 93-96 (1983).
151. Numano F, Takahashi T, Kuroiwa T, Shimamoto T. Glycogen in endothelial cells: Electronmicroscopic studies of polyglucose synthesized by phosphorylase in endothelial cells of aorta and heart muscle of rabbits. *Experimental and molecular pathology*, 20(2), 168-174 (1974).
152. Artwohl M, Brunmair B, Fürnsinn C *et al.* Insulin does not regulate glucose transport and metabolism in human endothelium. *European journal of clinical investigation*, 37(8), 643-650 (2007).
153. Verdegem D, Moens S, Stapor P, Carmeliet P. Endothelial cell metabolism: parallels and divergences with cancer cell metabolism. *Cancer & metabolism*, 2, 19 (2014).
154. Vander Heiden MG, Cantley LC, Thompson CB. Understanding the Warburg effect: the metabolic requirements of cell proliferation. *Science*, 324(5930), 1029-1033 (2009).
155. Juan PB. Adapting glycolysis to cancer cell proliferation: the MAPK pathway focuses on PFKFB3. *Biochemical Journal*, 452(3), e7-e9 (2013).
156. Ros S, Schulze A. Balancing glycolytic flux: the role of 6-phosphofructo-2-kinase/fructose 2, 6-bisphosphatases in cancer metabolism. *Cancer & metabolism*, 1(8) (2013).

157. Peters K, Kamp G, Berz A *et al.* Changes in human endothelial cell energy metabolic capacities during in vitro cultivation. The role of "aerobic glycolysis" and proliferation. *Cell Physiol. Biochem.*, 24(5-6), 483-492 (2009).
158. Schoors S, De Bock K, Cantelmo AR *et al.* Partial and transient reduction of glycolysis by PFKFB3 blockade reduces pathological angiogenesis. *Cell metabolism*, 19(1), 37-48 (2014).
159. Végran F, Boidot R, Michiels C, Sonveaux P, Feron O. Lactate influx through the endothelial cell monocarboxylate transporter MCT1 supports an NF- κ B/IL-8 pathway that drives tumor angiogenesis. *Cancer research*, 71(7), 2550-2560 (2011).
160. van Beijnum JR, Dings RP, van der Linden E *et al.* Gene expression of tumor angiogenesis dissected: specific targeting of colon cancer angiogenic vasculature. *Blood*, 108(7), 2339-2348 (2006).
161. Sonveaux P, Copetti T, De Saedeleer CJ *et al.* Targeting the lactate transporter MCT1 in endothelial cells inhibits lactate-induced HIF-1 activation and tumor angiogenesis. *PloS one*, 7(3), e33418-e33418 (2012).
162. Jose C, Rossignol R. Rationale for mitochondria-targeting strategies in cancer bioenergetic therapies. *The international journal of biochemistry & cell biology*, 45(1), 123-129 (2013).
163. Riganti C, Gazzano E, Polimeni M, Aldieri E, Ghigo D. The pentose phosphate pathway: an antioxidant defense and a crossroad in tumor cell fate. *Free Radical Biology and Medicine*, 53(3), 421-436 (2012).
164. Carracedo A, Cantley LC, Pandolfi PP. Cancer metabolism: fatty acid oxidation in the limelight. *Nature reviews Cancer*, 13(4), 227-232 (2013).
165. Hensley CT, Wasti AT, DeBerardinis RJ. Glutamine and cancer: cell biology, physiology, and clinical opportunities. *The Journal of clinical investigation*, 123(9), 3678 (2013).
166. Rousset M, Zweibaum A, Fogh J. Presence of glycogen and growth-related variations in 58 cultured human tumor cell lines of various tissue origins. *Cancer research*, 41(3), 1165-1170 (1981).
167. Sato A, Kawasaki T, Kashiwaba M *et al.* Glycogen-rich clear cell carcinoma of the breast showing carcinomatous lymphangiosis and extremely aggressive clinical behavior. *Pathology international*, 65(12), 674-676 (2015).
168. Kaelin WG. Treatment of kidney cancer. *Cancer*, 115(S10), 2262-2272 (2009).
169. Pescador N, Villar D, Cifuentes D *et al.* Hypoxia promotes glycogen accumulation through hypoxia inducible factor (HIF)-mediated induction of glycogen synthase 1. *PLoS One*, 5(3), e9644 (2010).
170. Favaro E, Bensaad K, Chong MG *et al.* Glucose utilization via glycogen phosphorylase sustains proliferation and prevents premature senescence in cancer cells. *Cell metabolism*, 16(6), 751-764 (2012).
171. Iida Y, Aoki K, Asakura T *et al.* Hypoxia promotes glycogen synthesis and accumulation in human ovarian clear cell carcinoma. *International journal of oncology*, 40(6), 2122-2130 (2012).
172. Takahashi S, Satomi A, Yano K *et al.* Estimation of glycogen levels in human colorectal cancer tissue: relationship with cell cycle and tumor outgrowth. *Journal of gastroenterology*, 34(4), 474-480 (1999).

173. Mamedova LK, Shneyvays V, Katz A, Shainberg A. Mechanism of glycogen supercompensation in rat skeletal muscle cultures. *Molecular and cellular biochemistry*, 250(1-2), 11-19 (2003).
174. Pelletier J, Bellot G, Gounon P, Lacas-Gervais S, Pouysségur J, Mazure NM. Glycogen synthesis is induced in hypoxia by the hypoxia-inducible factor and promotes cancer cell survival. *Frontiers in oncology*, 2 (2012).
175. Philips KB, Kurtoglu M, Leung HJ *et al.* Increased sensitivity to glucose starvation correlates with downregulation of glycogen phosphorylase isoform PYGB in tumor cell lines resistant to 2-deoxy-d-glucose. *Cancer chemotherapy and pharmacology*, 73(2), 349-361 (2014).
176. Lee WP, Guo P, Lim S *et al.* Metabolic sensitivity of pancreatic tumour cell apoptosis to glycogen phosphorylase inhibitor treatment. *British journal of cancer*, 91(12), 2094-2100 (2004).
177. Terashima M, Fujita Y, Togashi Y *et al.* KIAA1199 interacts with glycogen phosphorylase kinase β -subunit (PHKB) to promote glycogen breakdown and cancer cell survival. *Oncotarget*, 5(16), 7040 (2014).
178. Zois CE, Favaro E, Harris AL. Glycogen metabolism in cancer. *Biochemical pharmacology*, 92(1), 3-11 (2014).
179. Zois CE, Harris AL. Glycogen metabolism has a key role in the cancer microenvironment and provides new targets for cancer therapy. *Journal of Molecular Medicine*, 94(2), 137-154 (2016).
180. Cesca M, Morosi L, Berndt A *et al.* Bevacizumab-induced inhibition of angiogenesis promotes a more homogeneous intratumoral distribution of paclitaxel, improving the antitumor response. *Molecular cancer therapeutics*, 15(1), 125-135 (2016).
181. Rodriguez-Gil JE, Fernandez-Novell JM, Barbera A, Guinovart JJ. Lithium's effects on rat liver glucose metabolism in vivo. *Arch Biochem Biophys*, 375(2), 377-384 (2000).
182. Souza D, Mendes F, Nogueira F, Simões A, Nicolau J. Lithium Induces Glycogen Accumulation in Salivary Glands of the Rat. *Biological trace element research*, 169(2), 271-278 (2016).
183. de Almeida Souza A, da Silva GSS, Velez BS, Santoro ABM, Montero-Lomelí M. Glycogen synthesis in brain and astrocytes is inhibited by chronic lithium treatment. *Neuroscience letters*, 482(2), 128-132 (2010).
184. Hilliard TS, Gaisina IN, Muehlbauer AG, Gaisin AM, Gallier F, Burdette JE. Glycogen synthase kinase 3 beta inhibitors induce apoptosis in ovarian cancer cells and inhibit in vivo tumor growth. *Anti-cancer drugs*, 22(10), 978 (2011).
185. Novetsky AP, Thompson DM, Zigelboim I *et al.* Lithium and inhibition of GSK3 β as a potential therapy for serous ovarian cancer. *International journal of gynecological cancer: official journal of the International Gynecological Cancer Society*, 23(2), 361 (2013).
186. Bilir A, Erguven M, Ermis E, Sencan M, Yazihan N. Combination of imatinib mesylate with lithium chloride and medroxyprogesterone acetate is highly active in Ishikawa endometrial carcinoma in vitro. *Journal of gynecologic oncology*, 22(4), 225-232 (2011).
187. Fu Y, Zheng S, Huang R *et al.* A potential strategy for high-grade gliomas: combination treatment with lithium chloride and Bmk CT. *Biotechnology letters*, 34(1), 9-17 (2012).

188. Greenblatt DY, Ndiaye M, Chen H, Kunnimalaiyaan M. Lithium inhibits carcinoid cell growth in vitro. *Am J Transl Res*, 2(3), 248-253 (2010).
189. Li L, Song H, Zhong L *et al.* Lithium Chloride Promotes Apoptosis in Human Leukemia NB4 Cells by Inhibiting Glycogen Synthase Kinase-3 Beta. *International journal of medical sciences*, 12(10), 805 (2015).
190. Li H, Huang K, Liu X *et al.* Lithium chloride suppresses colorectal cancer cell survival and proliferation through ROS/GSK-3 β /NF- κ B signaling pathway. *Oxidative medicine and cellular longevity*, 2014 (2014).
191. Li B, Thrasher JB, Terranova P. Glycogen synthase kinase-3: A potential preventive target for prostate cancer management. In: *Urologic Oncology: Seminars and Original Investigations*. (Ed. (Eds) (Elsevier, 2015) 456-463.
192. Sun A, Shanmugam I, Song J, Terranova PF, Thrasher JB, Li B. Lithium suppresses cell proliferation by interrupting E2F–DNA interaction and subsequently reducing S–phase gene expression in prostate cancer. *The Prostate*, 67(9), 976-988 (2007).
193. de Luna N, Brull A, Guiu JM *et al.* Sodium valproate increases the brain isoform of glycogen phosphorylase: looking for a compensation mechanism in McArdle disease using a mouse primary skeletal-muscle culture in vitro. *Disease Models and Mechanisms*, 8(5), 467-472 (2015).
194. Bhanot H, Reddy M, Nonami A *et al.* Pathological glycogenesis through glycogen synthase 1 and suppression of excessive AMP kinase activity in myeloid leukemia cells. *Leukemia*, 29(7), 1555-1563 (2015).
195. Matthews Q, Isabelle M, Harder SJ *et al.* Radiation-Induced Glycogen Accumulation Detected by Single Cell Raman Spectroscopy Is Associated with Radioresistance that Can Be Reversed by Metformin. *PloS one*, 10(8), e0135356 (2015).
196. Ball S, Guan H-P, James M *et al.* From glycogen to amylopectin: a model for the biogenesis of the plant starch granule. *Cell*, 86(3), 349-352 (1996).
197. Obel LF, Müller MS, Walls AB *et al.* Brain glycogen-new perspectives on its metabolic function and regulation at the subcellular level. *Front Neuroenergetics*, 4(3), 1-15 (2012).
198. Sickmann HM, Waagepetersen HS, Schousboe A, Benie AJ, Bouman SD. Brain glycogen and its role in supporting glutamate and GABA homeostasis in a type 2 diabetes rat model. *Neurochemistry international*, 60(3), 267-275 (2012).
199. Suzuki A, Stern SA, Bozdagi O *et al.* Astrocyte-neuron lactate transport is required for long-term memory formation. *Cell*, 144(5), 810-823 (2011).
200. Vigoda A, Mamedova LK, Shneyvays V, Katz A, Shainberg A. Glycogen metabolism in rat heart muscle cultures after hypoxia. *Molecular and cellular biochemistry*, 254(1-2), 311-318 (2003).
201. Cammisotto PG, Londono I, Gingras D, Bendayan M. Control of glycogen synthase through ADIPOR1-AMPK pathway in renal distal tubules of normal and diabetic rats. *American Journal of Physiology-Renal Physiology*, 294(4), F881-F889 (2008).
202. Gatica R, Bertinat R, Silva P *et al.* Over-expression of muscle glycogen synthase in human diabetic nephropathy. *Histochemistry and cell biology*, 143(3), 313-324 (2015).
203. Markan KR, Jurczak MJ, Brady MJ. Stranger in a strange land: roles of glycogen turnover in adipose tissue metabolism. *Molecular and cellular endocrinology*, 318(1), 54-60 (2010).

204. Young FG. Claude Bernard and the discovery of glycogen. *Br Med J*, 1(5033), 1431-1437 (1957).
205. DiNuzzo M, Mangia S, Maraviglia B, Giove F. Glycogenolysis in astrocytes supports blood-borne glucose channeling not glycogen-derived lactate shuttling to neurons: evidence from mathematical modeling. *Journal of Cerebral Blood Flow & Metabolism*, 30(12), 1895-1904 (2010).
206. López-Ramos JC, Duran J, Gruart A, Guinovart JJ, Delgado-García JM. Role of brain glycogen in the response to hypoxia and in susceptibility to epilepsy. *Frontiers in cellular neuroscience*, 9 (2015).
207. Melendez-Hevia E, Waddell T, Shelton E. Optimization of molecular design in the evolution of metabolism: the glycogen molecule. *Biochemical Journal*, 295(2), 477-483 (1993).
208. Meléndez R, Meléndez-Hevia E, Cascante M. How did glycogen structure evolve to satisfy the requirement for rapid mobilization of glucose? A problem of physical constraints in structure building. *Journal of molecular evolution*, 45(4), 446-455 (1997).
209. Gunja-Smith Z, Marshall J, Mercier C, Smith E, Whelan W. A revision of the Meyer-Bernfeld model of glycogen and amylopectin. *FEBS letters*, 12(2), 101-104 (1970).
210. Hudson ER, Pan DA, James J *et al.* A novel domain in AMP-activated protein kinase causes glycogen storage bodies similar to those seen in hereditary cardiac arrhythmias. *Current biology*, 13(10), 861-866 (2003).
211. Meyer F, Heilmeyer LM, Haschke RH, Fischer EH. Control of Phosphorylase Activity in a Muscle Glycogen Particle I. ISOLATION AND CHARACTERIZATION OF THE PROTEIN-GLYCOGEN COMPLEX. *Journal of Biological Chemistry*, 245(24), 6642-6648 (1970).
212. Berg JM, Tymoczko JL, Stryer L. Phosphorylase is regulated by allosteric interactions and reversible phosphorylation. (2002).
213. Leloir LF, Goldemberg SH. Synthesis of glycogen from uridine diphosphate glucose in liver. *Journal of Biological Chemistry*, 235(4), 919-923 (1960).
214. Bouskila M, Hunter RW, Ibrahim AF *et al.* Allosteric regulation of glycogen synthase controls glycogen synthesis in muscle. *Cell metabolism*, 12(5), 456-466 (2010).
215. Berg JM, Tymoczko JL, Stryer L. Glycogen Breakdown Requires the Interplay of Several Enzymes. (2002).
216. Berg JM, Tymoczko JL, Stryer L. Glycogen Is Synthesized and Degraded by Different Pathways. (2002).
217. Berg JM, Tymoczko JL, Stryer L. Glycogen Breakdown and Synthesis Are Reciprocally Regulated. (2002).
218. Schmid H, Dolderer B, Thiess U, Verleysdonk S, Hamprecht B. Renal expression of the brain and muscle isoforms of glycogen phosphorylase in different cell types. *Neurochem Res*, 33(12), 2575-2582 (2008).
219. Schmid H, Pfeiffer-Guglielmi B, Dolderer B, Thiess U, Verleysdonk S, Hamprecht B. Expression of the brain and muscle isoforms of glycogen phosphorylase in rat heart. *Neurochem Res*, 34(3), 581-586 (2009).
220. Pfeiffer-Guglielmi B, Francke M, Reichenbach A, Fleckenstein B, Jung G, Hamprecht B. Glycogen phosphorylase isozyme pattern in mammalian retinal Müller (glial) cells and in astrocytes of retina and optic nerve. *Glia*, 49(1), 84-95 (2005).

221. Agius L. Physiological control of liver glycogen metabolism: lessons from novel glycogen phosphorylase inhibitors. *Mini reviews in medicinal chemistry*, 10(12), 1175-1187 (2010).
222. Newgard CB, Hwang PK, Fletterick RJ. The Family of Glycogen Phosphorylases: Structure and Function. *Critical reviews in biochemistry and molecular biology*, 24(1), 69-99 (1989).
223. Kasvinsky PJ, Shechosky S, Fletterick RJ. Synergistic regulation of phosphorylase a by glucose and caffeine. *Journal of Biological Chemistry*, 253(24), 9102-9106 (1978).
224. Kobayashi M, Soman G, Graves DJ. A comparison of the activator sites of liver and muscle glycogen phosphorylase b. *Journal of Biological Chemistry*, 257(23), 14041-14047 (1982).
225. GUÉNARD D, MORANGE M, BUC H. Comparative study of the effect of 5' AMP and its analogs on rabbit glycogen phosphorylase b isoenzymes. *European Journal of Biochemistry*, 76(2), 447-452 (1977).
226. Müller MS, Pedersen SE, Walls AB, Waagepetersen HS, Bak LK. Isoform-selective regulation of glycogen phosphorylase by energy deprivation and phosphorylation in astrocytes. *Glia*, 63(1), 154-162 (2015).
227. Skurat AV, Dietrich AD, Roach PJ. Glycogen synthase sensitivity to insulin and glucose-6-phosphate is mediated by both NH₂- and COOH-terminal phosphorylation sites. *Diabetes*, 49(7), 1096-1100 (2000).
228. Skurat AV, Roach PJ. Phosphorylation of sites 3a and 3b (Ser640 and Ser644) in the control of rabbit muscle glycogen synthase. *Journal of Biological Chemistry*, 270(21), 12491-12497 (1995).
229. Ros S, García-Rocha M, Domínguez J, Ferrer JC, Guinovart JJ. Control of liver glycogen synthase activity and intracellular distribution by phosphorylation. *Journal of Biological Chemistry*, 284(10), 6370-6378 (2009).
230. Roach PJ. Control of glycogen synthase by hierarchical protein phosphorylation. *The FASEB Journal*, 4(12), 2961-2968 (1990).
231. Roach PJ. Control of glycogen synthase by hierarchical protein phosphorylation. *The FASEB Journal*, 4(12), 2961-2968 (1990).
232. Ferrer JC, Favre C, Gomis RR *et al.* Control of glycogen deposition. *FEBS letters*, 546(1), 127-132 (2003).
233. Donnier-Maréchal M, Vidal S. Glycogen phosphorylase inhibitors: a patent review (2013-2015). *Expert opinion on therapeutic patents*, 26(2), 199-212 (2016).
234. Kim KM, Lee K-S, Lee GY *et al.* Anti-diabetic efficacy of KICG1338, a novel glycogen synthase kinase-3 β inhibitor, and its molecular characterization in animal models of type 2 diabetes and insulin resistance. *Molecular and cellular endocrinology*, 409, 1-10 (2015).
235. McCubrey JA, Steelman LS, Bertrand FE *et al.* GSK-3 as potential target for therapeutic intervention in cancer. *Oncotarget*, 5(10), 2881 (2014).
236. Marchand B, Arsenault D, Raymond-Fleury A, Boisvert F-M, Boucher M-J. Glycogen Synthase Kinase-3 (GSK3) inhibition induces prosurvival autophagic signals in human pancreatic cancer cells. *Journal of Biological Chemistry*, 290(9), 5592-5605 (2015).
237. Gao C, Hölscher C, Liu Y, Li L. GSK3: a key target for the development of novel treatments for type 2 diabetes mellitus and Alzheimer disease. *Reviews in the Neurosciences*, 23(1), 1-11 (2012).

238. Chuang D-M, Wang Z, Chiu C-T. GSK-3 as a target for lithium-induced neuroprotection against excitotoxicity in neuronal cultures and animal models of ischemic stroke. *Frontiers in molecular neuroscience*, 4 (2011).
239. Arfeen M, Bharatam PV. Design of glycogen synthase kinase-3 inhibitors: an overview on recent advancements. *Current pharmaceutical design*, 19(26), 4755-4775 (2013).
240. Viollet B, Horman S, Leclerc J *et al.* AMPK inhibition in health and disease. *Critical Reviews in Biochemistry and Molecular Biology*, 45(4), 276-295 (2010).
241. Baldessarini R, Henk H, Sklar A, Chang J, Leahy L. Psychotropic medications for patients with bipolar disorder in the United States: polytherapy and adherence. *Psychiatric Services*, (2015).
242. Martin WH, Hoover DJ, Armento SJ *et al.* Discovery of a human liver glycogen phosphorylase inhibitor that lowers blood glucose in vivo. *Proceedings of the National Academy of Sciences*, 95(4), 1776-1781 (1998).
243. Baker DJ, Timmons JA, Greenhaff PL. Glycogen Phosphorylase Inhibition in Type 2 Diabetes Therapy A Systematic Evaluation of Metabolic and Functional Effects in Rat Skeletal Muscle. *Diabetes*, 54(8), 2453-2459 (2005).
244. Oikonomakos NG, Tsitsanou KE, Zographos SE, Skamnaki VT, Goldmann S, Bischoff H. Allosteric inhibition of glycogen phosphorylase a by the potential antidiabetic drug 3-isopropyl 4-(2-chlorophenyl)-1, 4-dihydro-1-ethyl-2-methyl-pyridine-3, 5, 6-tricarboxylate. *Protein Science*, 8(10), 1930-1945 (1999).
245. Oikonomakos NG, Schnier JB, Zographos SE, Skamnaki VT, Tsitsanou KE, Johnson LN. Flavopiridol inhibits glycogen phosphorylase by binding at the inhibitor site. *Journal of Biological Chemistry*, 275(44), 34566-34573 (2000).
246. Fosgerau K, Westergaard N, Quistorff B, Grunnet N, Kristiansen M, Lundgren K. Kinetic and functional characterization of 1, 4-dideoxy-1, 4-imino-d-arabinitol: a potent inhibitor of glycogen phosphorylase with anti-hyperglycemic effect in ob/ob mice. *Archives of biochemistry and biophysics*, 380(2), 274-284 (2000).
247. Oikonomakos NG, Zographos SE, Skamnaki VT, Archontis G. The 1.76 Å resolution crystal structure of glycogen phosphorylase B complexed with glucose, and CP320626, a potential antidiabetic drug. *Bioorganic & medicinal chemistry*, 10(5), 1313-1319 (2002).
248. Bergans N, Stalmans W, Goldmann S, Vanstapel F. Molecular mode of inhibition of glycogenolysis in rat liver by the dihydropyridine derivative, BAY R3401: inhibition and inactivation of glycogen phosphorylase by an activated metabolite. *Diabetes*, 49(9), 1419-1426 (2000).
249. Andersen B, Westergaard N. The effect of glucose on the potency of two distinct glycogen phosphorylase inhibitors. *Biochem. J*, 367, 443-450 (2002).
250. Latsis T, Andersen B, Agius L. Diverse effects of two allosteric inhibitors on the phosphorylation state of glycogen phosphorylase in hepatocytes. *Biochem. J*, 368, 309-316 (2002).
251. Rath VL, Ammirati M, Danley DE *et al.* Human liver glycogen phosphorylase inhibitors bind at a new allosteric site. *Chemistry & biology*, 7(9), 677-682 (2000).
252. Lerín C, Montell E, Nolasco T, García-Rocha M, Guinovart JJ, Gómez-Foix AM. Regulation of glycogen metabolism in cultured human muscles by the glycogen phosphorylase inhibitor CP-91149. *Biochemical Journal*, 378(3), 1073-1077 (2004).

253. Gaboriaud-Kolar N, Skaltsounis A-L. Glycogen phosphorylase inhibitors: a patent review (2008-2012). *Expert opinion on therapeutic patents*, 23(8), 1017-1032 (2013).
254. Yu LJ, Chen Y, Treadway JL *et al.* Establishment of correlation between in vitro enzyme binding potency and in vivo pharmacological activity: application to liver glycogen phosphorylase a inhibitors. *The Journal of pharmacology and experimental therapeutics*, 317(3), 1230-1237 (2006).
255. Suh SW, Bergher JP, Anderson CM, Treadway JL, Fosgerau K, Swanson RA. Astrocyte Glycogen Sustains Neuronal Activity during Hypoglycemia: Studies with the Glycogen Phosphorylase Inhibitor CP-316,819 ([R-R*,S*]-5-Chloro-N-[2-hydroxy-3-(methoxymethylamino)-3-oxo-1-(phenylmethyl)propyl]-1H-indole-2-carboxamide). *Journal of Pharmacology and Experimental Therapeutics*, 321(1), 45-50 (2007).
256. Saez I, Duran J, Sinadinos C *et al.* Neurons have an active glycogen metabolism that contributes to tolerance to hypoxia. *Journal of Cerebral Blood Flow & Metabolism*, 34(6), 945-955 (2014).
257. Hossain MI, Roulston CL, Stapleton DI. Molecular Basis of Impaired Glycogen Metabolism during Ischemic Stroke and Hypoxia. *PLoS ONE*, 9(5), e97570 (2014).
258. Hibbert B, Lavoie JR, Ma X *et al.* Glycogen Synthase Kinase-3 β Inhibition Augments Diabetic Endothelial Progenitor Cell Abundance and Functionality via Cathepsin B: A Novel Therapeutic Opportunity for Arterial Repair. *Diabetes*, 63(4), 1410-1421 (2014).
259. Yurkovich JT, Palsson BO. Solving Puzzles With Missing Pieces: The Power of Systems Biology [Point of View]. *Proceedings of the IEEE*, 104(1), 2-7 (2016).
260. Ideker T, Galitski T, Hood L. A new approach to decoding life: systems biology. *Annual review of genomics and human genetics*, 2(1), 343-372 (2001).
261. Carrell D, Aston K, Oliva R, Emery B, De Jonge C. The “omics” of human male infertility: integrating big data in a systems biology approach. *Cell and tissue research*, 363(1), 295-312 (2016).
262. Gehlenborg N, O'Donoghue SI, Baliga NS *et al.* Visualization of omics data for systems biology. *Nature methods*, 7, S56-S68 (2010).
263. Patti GJ, Yanes O, Siuzdak G. Innovation: Metabolomics: the apogee of the omics trilogy. *Nat Rev Mol Cell Biol*, 13(4), 263-269 (2012).
264. Sévin DC, Kuehne A, Zamboni N, Sauer U. Biological insights through nontargeted metabolomics. *Current Opinion in Biotechnology*, 34, 1-8 (2015).
265. Sauer U. Metabolic networks in motion: 13C-based flux analysis. *Molecular systems biology*, 2(1) (2006).
266. Lee WP-L. Characterizing phenotype with tracer based metabolomics. *Metabolomics*, 2 (2006).
267. Hasenour CM, Wall ML, Ridley DE *et al.* Mass spectrometry-based microassay of 2H and 13C plasma glucose labeling to quantify liver metabolic fluxes in vivo. *American Journal of Physiology-Endocrinology and Metabolism*, 309(2), E191-E203 (2015).
268. António C, Pöpke C, Rocha M *et al.* Regulation of primary metabolism in response to low oxygen availability as revealed by carbon and nitrogen isotope redistribution. *Plant physiology*, pp. 00266.02015 (2015).
269. Buescher JM, Antoniewicz MR, Boros LG *et al.* A roadmap for interpreting 13 C metabolite labeling patterns from cells. *Current opinion in biotechnology*, 34, 189-201 (2015).

270. Zamboni N, Fendt S-M, Rühl M, Sauer U. ^{13}C -based metabolic flux analysis. *Nature protocols*, 4(6), 878-892 (2009).
271. Selivanov VA, Marin S, Lee PW, Cascante M. Software for dynamic analysis of tracer-based metabolomic data: estimation of metabolic fluxes and their statistical analysis. *Bioinformatics*, 22(22), 2806-2812 (2006).
272. Wiechert W, Nöh K. Isotopically non-stationary metabolic flux analysis: complex yet highly informative. *Current opinion in biotechnology*, 24(6), 979-986 (2013).
273. Buescher JM, Antoniewicz MR, Boros LG *et al.* A roadmap for interpreting C metabolite labeling patterns from cells. *Curr Opin Biotechnol*, 34C, 189-201 (2015).
274. Niedenfuhr S, Wiechert W, Noh K. How to measure metabolic fluxes: a taxonomic guide for C fluxomics. *Curr Opin Biotechnol*, 34C, 82-90 (2015).
275. Cascante M, Marin S. Metabolomics and fluxomics approaches. *Essays Biochem*, 45, 67-82 (2008).
276. Bueschl C, Krska R, Kluger B, Schuhmacher R. Isotopic labeling-assisted metabolomics using LC-MS. *Anal Bioanal Chem*, 405(1), 27-33 (2013).
277. Kowalski GM, De Souza DP, Burch ML *et al.* Application of dynamic metabolomics to examine in vivo skeletal muscle glucose metabolism in the chronically high-fat fed mouse. *Biochemical and biophysical research communications*, 462(1), 27-32 (2015).
278. Jung J-Y, Oh M-K. Isotope labeling pattern study of central carbon metabolites using GC/MS. *Journal of Chromatography B*, 974, 101-108 (2015).
279. Fan TW-M, Lane AN. Applications of NMR spectroscopy to systems biochemistry. *Progress in nuclear magnetic resonance spectroscopy*, 92, 18-53 (2016).
280. Lane AN, Fan TWM, Higashi RM. Isotopomer-Based Metabolomic Analysis by NMR and Mass Spectrometry. *Methods in cell biology*, 84, 541-588 (2008).
281. Antoniewicz MR. Parallel labeling experiments for pathway elucidation and ^{13}C metabolic flux analysis. *Current opinion in biotechnology*, 36, 91-97 (2015).
282. Metallo CM, Walther JL, Stephanopoulos G. Evaluation of ^{13}C isotopic tracers for metabolic flux analysis in mammalian cells. *Journal of biotechnology*, 144(3), 167-174 (2009).
283. Zamboni N. ^{13}C metabolic flux analysis in complex systems. *Current opinion in biotechnology*, 22(1), 103-108 (2011).
284. Antoniewicz MR. ^{13}C metabolic flux analysis: optimal design of isotopic labeling experiments. *Current opinion in biotechnology*, 24(6), 1116-1121 (2013).
285. Dunn WB, Broadhurst DI, Atherton HJ, Goodacre R, Griffin JL. Systems level studies of mammalian metabolomes: the roles of mass spectrometry and nuclear magnetic resonance spectroscopy. *Chemical Society Reviews*, 40(1), 387-426 (2011).
286. Patel S, Ahmed S. Emerging field of metabolomics: big promise for cancer biomarker identification and drug discovery. *Journal of pharmaceutical and biomedical analysis*, 107, 63-74 (2015).
287. Ramautar R, Berger R, van der Greef J, Hankemeier T. Human metabolomics: strategies to understand biology. *Current opinion in chemical biology*, 17(5), 841-846 (2013).
288. Pinu FR. Metabolomics—the new frontier in food safety and quality research. *Food Research International*, 72, 80-81 (2015).

289. Watanabe M, Meyer KA, Jackson TM, Schock TB, Johnson WE, Bearden DW. Application of NMR-based metabolomics for environmental assessment in the Great Lakes using zebra mussel (*Dreissena polymorpha*). *Metabolomics*, 11(5), 1302-1315 (2015).
290. Li L, Wu H, Ji C, van Gestel CA, Allen HE, Peijnenburg WJ. A metabolomic study on the responses of daphnia magna exposed to silver nitrate and coated silver nanoparticles. *Ecotoxicology and environmental safety*, 119, 66-73 (2015).
291. Salek RM, Steinbeck C, Viant MR, Goodacre R, Dunn WB. The role of reporting standards for metabolite annotation and identification in metabolomic studies. *GigaScience*, 2(1), 13 (2013).
292. Griffiths WJ, Koal T, Wang Y, Kohl M, Enot DP, Deigner HP. Targeted metabolomics for biomarker discovery. *Angewandte Chemie International Edition*, 49(32), 5426-5445 (2010).
293. Dudley E, Yousef M, Wang Y, Griffiths W. Targeted metabolomics and mass spectrometry. *Adv Protein Chem Struct Biol*, 80, 45-83 (2010).
294. Zhou B, Xiao JF, Tuli L, Ressom HW. LC-MS-based metabolomics. *Mol Biosyst*, 8(2), 470-481 (2012).
295. Naz S, Vallejo M, García A, Barbas C. Method validation strategies involved in non-targeted metabolomics. *Journal of Chromatography A*, 1353, 99-105 (2014).
296. Cajka T, Fiehn O. Toward Merging Untargeted and Targeted Methods in Mass Spectrometry-Based Metabolomics and Lipidomics. *Analytical chemistry*, 88(1), 524-545 (2015).
297. Snyder NW, Khezam M, Mesaros CA, Worth A, Blair IA. Untargeted metabolomics from biological sources using ultraperformance liquid chromatography-high resolution mass spectrometry (UPLC-HRMS). *JoVE (Journal of Visualized Experiments)*, (75), e50433-e50433 (2013).
298. Gertsman I, Gangoiti JA, Barshop BA. Validation of a dual LC-HRMS platform for clinical metabolic diagnosis in serum, bridging quantitative analysis and untargeted metabolomics. *Metabolomics*, 10(2), 312-323 (2014).
299. Ulaszewska MM, Trost K, Stanstrup J *et al.* Urinary metabolomic profiling to identify biomarkers of a flavonoid-rich and flavonoid-poor fruits and vegetables diet in adults: the FLAVURS trial. *Metabolomics*, 12(2), 1-22 (2016).
300. Dunn WB, Erban A, Weber RJ *et al.* Mass appeal: metabolite identification in mass spectrometry-focused untargeted metabolomics. *Metabolomics*, 9(1), 44-66 (2013).
301. Rochat B. From targeted quantification to untargeted metabolomics: Why LC-high-resolution-MS will become a key instrument in clinical labs. *TrAC Trends in Analytical Chemistry*, (2016).
302. Zamboni N, Saghatelian A, Patti GJ. Defining the metabolome: size, flux, and regulation. *Molecular cell*, 58(4), 699-706 (2015).
303. Milne SB, Mathews TP, Myers DS, Ivanova PT, Brown HA. Sum of the parts: mass spectrometry-based metabolomics. *Biochemistry*, 52(22), 3829-3840 (2013).
304. Cho K, Mahieu NG, Johnson SL, Patti GJ. After the feature presentation: technologies bridging untargeted metabolomics and biology. *Current opinion in biotechnology*, 28, 143-148 (2014).
305. Alonso A, Marsal S, Julià A. Analytical methods in untargeted metabolomics: state of the art in 2015. *Frontiers in bioengineering and biotechnology*, 3 (2015).

306. Gowda H, Ivanisevic J, Johnson CH *et al.* Interactive XCMS Online: simplifying advanced metabolomic data processing and subsequent statistical analyses. *Analytical chemistry*, 86(14), 6931-6939 (2014).
307. Johnson CH, Ivanisevic J, Siuzdak G. Metabolomics: beyond biomarkers and towards mechanisms. *Nature Reviews Molecular Cell Biology*, (2016).
308. Xia J, Sinelnikov IV, Han B, Wishart DS. MetaboAnalyst 3.0—making metabolomics more meaningful. *Nucleic Acids Research*, (2015).
309. Xia J, Wishart DS. Web-based inference of biological patterns, functions and pathways from metabolomic data using MetaboAnalyst. *Nature protocols*, 6(6), 743-760 (2011).
310. Celià-Terrassa T, Meca-Cortés Ó, Mateo F *et al.* Epithelial-mesenchymal transition can suppress major attributes of human epithelial tumor-initiating cells. *J. Clin. Invest.*, 122(5), 1849 (2012).
311. Mosmann T. Rapid colorimetric assay for cellular growth and survival: application to proliferation and cytotoxicity assays. *Journal of immunological methods*, 65(1-2), 55-63 (1983).
312. Rodriguez LG, Wu X, Guan J-L. Wound-healing assay. *Cell Migration: Developmental Methods and Protocols*, 23-29 (2005).
313. Liang C-C, Park AY, Guan J-L. In vitro scratch assay: a convenient and inexpensive method for analysis of cell migration in vitro. *Nature protocols*, 2(2), 329-333 (2007).
314. Gilboe D, Larson K, Nuttall F. Radioactive method for the assay of glycogen phosphorylases. *Analytical biochemistry*, 47(1), 20-27 (1972).
315. Römisch-Margl W, Prehn C, Bogumil R, Röhring C, Suhre K, Adamski J. Procedure for tissue sample preparation and metabolite extraction for high-throughput targeted metabolomics. *Metabolomics*, 8(1), 133-142 (2012).
316. Chevallier O, Graham S, Alonso E *et al.* New insights into the causes of human illness due to consumption of azaspiracid contaminated shellfish. *Scientific reports*, 5 (2015).
317. Graham SF, Chevallier OP, Roberts D, Hölscher C, Elliott CT, Green BD. Investigation of the Human Brain Metabolome to Identify Potential Markers for Early Diagnosis and Therapeutic Targets of Alzheimer's Disease. *Analytical Chemistry*, 85(3), 1803-1811 (2013).
318. Kessner D, Chambers M, Burke R, Agus D, Mallick P. ProteoWizard: open source software for rapid proteomics tools development. *Bioinformatics*, 24(21), 2534-2536 (2008).
319. Xia J, Mandal R, Sinelnikov IV, Broadhurst D, Wishart DS. MetaboAnalyst 2.0—a comprehensive server for metabolomic data analysis. *Nucleic Acids Research*, 40(W1), W127-W133 (2012).
320. Xia J, Wishart DS. MSEA: a web-based tool to identify biologically meaningful patterns in quantitative metabolomic data. *Nucleic acids research*, 38(suppl 2), W71-W77 (2010).
321. De Francesco EM, Lappano R, Santolla MF, Marsico S, Caruso A, Maggiolini M. HIF-1 α /GPER signaling mediates the expression of VEGF induced by hypoxia in breast cancer associated fibroblasts (CAFs). *Breast Cancer Res*, 15(4), R64 (2013).
322. Rodrigues M, Xin X, Jee K *et al.* VEGF secreted by hypoxic Müller cells induces MMP-2 expression and activity in endothelial cells to promote retinal neovascularization in proliferative diabetic retinopathy. *Diabetes*, DB_130014 (2013).

323. Bao B, Ali S, Ahmad A *et al.* Hypoxia-induced aggressiveness of pancreatic cancer cells is due to increased expression of VEGF, IL-6 and miR-21, which can be attenuated by CDF treatment. *PLoS one*, 7(12), e50165 (2012).
324. Lee WNP. Characterizing phenotype with tracer based metabolomics. *Metabolomics*, 2(1), 31-39 (2006).
325. Niedenführ S, Wiechert W, Nöh K. How to measure metabolic fluxes: a taxonomic guide for 13 C fluxomics. *Current opinion in biotechnology*, 34, 82-90 (2015).
326. Lee S-L, Fanburg BL. Glycolytic activity and enhancement of serotonin uptake by endothelial cells exposed to hypoxia/anoxia. *Circulation research*, 60(5), 653-658 (1987).
327. Carmeliet P, Jain RK. Angiogenesis in cancer and other diseases. *nature*, 407(6801), 249-257 (2000).
328. Wittmann C. Fluxome analysis using GC-MS. *Microbial Cell Factories*, 6(1), 1 (2007).
329. Yamaji R, Fujita K, Takahashi S *et al.* Hypoxia up-regulates glyceraldehyde-3-phosphate dehydrogenase in mouse brain capillary endothelial cells: involvement of Na⁺/Ca²⁺ exchanger. *Biochimica et Biophysica Acta (BBA)-Molecular Cell Research*, 1593(2), 269-276 (2003).
330. Wright GL, Maroulakou IG, Eldridge J *et al.* VEGF stimulation of mitochondrial biogenesis: requirement of AKT3 kinase. *The FASEB Journal*, 22(9), 3264-3275 (2008).
331. Kim Y-W, Byzova TV. Oxidative stress in angiogenesis and vascular disease. *Blood*, 123(5), 625-631 (2014).
332. Zhang DX, Gutterman DD. Mitochondrial reactive oxygen species-mediated signaling in endothelial cells. *American Journal of Physiology-Heart and Circulatory Physiology*, 292(5), H2023-H2031 (2007).
333. Leopold JA, Walker J, Scribner AW *et al.* Glucose-6-phosphate dehydrogenase modulates vascular endothelial growth factor-mediated angiogenesis. *Journal of Biological Chemistry*, 278(34), 32100-32106 (2003).
334. Zhao F, Mancuso A, Bui TV *et al.* Imatinib resistance associated with BCR-ABL upregulation is dependent on HIF-1 α -induced metabolic reprogramming. *Oncogene*, 29(20), 2962-2972 (2010).
335. Harjes U, Kalucka J, Carmeliet P. Targeting fatty acid metabolism in cancer and endothelial cells. *Critical Reviews in Oncology/Hematology*.
336. Browne CD, Hindmarsh EJ, Smith JW. Inhibition of endothelial cell proliferation and angiogenesis by orlistat, a fatty acid synthase inhibitor. *The FASEB journal*, 20(12), 2027-2035 (2006).
337. Seguin F, Carvalho M, Bastos D *et al.* The fatty acid synthase inhibitor orlistat reduces experimental metastases and angiogenesis in B16-F10 melanomas. *British journal of cancer*, 107(6), 977-987 (2012).
338. Dringen R, Gebhardt R, Hamprecht B. Glycogen in astrocytes: possible function as lactate supply for neighboring cells. *Brain research*, 623(2), 208-214 (1993).
339. Wender R, Brown AM, Fern R, Swanson RA, Farrell K, Ransom BR. Astrocytic glycogen influences axon function and survival during glucose deprivation in central white matter. *The Journal of Neuroscience*, 20(18), 6804-6810 (2000).
340. Hanahan D, Coussens LM. Accessories to the crime: functions of cells recruited to the tumor microenvironment. *Cancer Cell*, 21(3), 309-322 (2012).

341. Tautenhahn R, Patti GJ, Rinehart D, Siuzdak G. XCMS Online: a web-based platform to process untargeted metabolomic data. *Analytical chemistry*, 84(11), 5035-5039 (2012).
342. Sumner LW, Lei Z, Nikolau BJ, Saito K, Roessner U, Trengove R. Proposed quantitative and alphanumeric metabolite identification metrics. *Metabolomics*, 10(6), 1047-1049 (2014).
343. Creek DJ, Dunn WB, Fiehn O *et al.* Metabolite identification: are you sure? And how do your peers gauge your confidence? *Metabolomics*, 10(3), 350-353 (2014).
344. Sumner L, Amberg A, Barrett D *et al.* Proposed minimum reporting standards for chemical analysis. *Metabolomics*, 3(3), 211 - 221 (2007).
345. Carmeliet P, Jain RK. Molecular mechanisms and clinical applications of angiogenesis. *Nature*, 473(7347), 298-307 (2011).
346. Connolly JM, Rose DP. Angiogenesis in two human prostate cancer cell lines with differing metastatic potential when growing as solid tumors in nude mice. *The Journal of urology*, 160(3), 932-936 (1998).
347. Castellon R, Hamdi HK, Sacerio I, Aoki AM, Kenney MC, Ljubimov AV. Effects of Angiogenic Growth Factor Combinations on Retinal Endothelial Cells☆. *Experimental eye research*, 74(4), 523-535 (2002).
348. Kim SK, Lee J, Song M *et al.* Combination of three angiogenic growth factors has synergistic effects on sprouting of endothelial cell/mesenchymal stem cell-based spheroids in a 3D matrix. *Journal of Biomedical Materials Research Part B: Applied Biomaterials*, (2015).
349. Pettegrew JW, Levine J, McClure RJ. Acetyl-L-carnitine physical-chemical, metabolic, and therapeutic properties: relevance for its mode of action in Alzheimer's disease and geriatric depression. *Molecular psychiatry*, 5(6), 616-632 (2000).
350. Furuichi Y, Goto-Inoue N, L. Fujii N. Role of carnitine acetylation in skeletal muscle. *The Journal of Physical Fitness and Sports Medicine*, 3(2), 163-168 (2014).
351. Sugden MC, Holness MJ. Recent advances in mechanisms regulating glucose oxidation at the level of the pyruvate dehydrogenase complex by PDKs. *American Journal of Physiology-Endocrinology And Metabolism*, 284(5), E855-E862 (2003).
352. McMackin CJ, Widlansky ME, Hamburg NM *et al.* Effect of Combined Treatment With α -Lipoic Acid and Acetyl-L-Carnitine on Vascular Function and Blood Pressure in Patients With Coronary Artery Disease. *The Journal of Clinical Hypertension*, 9(4), 249-255 (2007).
353. Fernandes S, Salta S, Bravo J, Silva AP, Summavielle T. Acetyl-L-Carnitine Prevents Methamphetamine-Induced Structural Damage on Endothelial Cells via ILK-Related MMP-9 Activity. *Mol Neurobiol*, 1-15 (2014).
354. Olsson A-K, Dimberg A, Kreuger J, Claesson-Welsh L. VEGF receptor signalling? In control of vascular function. *Nature reviews Molecular cell biology*, 7(5), 359-371 (2006).
355. Wang Y, Zang QS, Liu Z *et al.* Regulation of VEGF-induced endothelial cell migration by mitochondrial reactive oxygen species. *American Journal of Physiology - Cell Physiology*, 301(3), C695-C704 (2011).
356. Ushio-Fukai M, Alexander RW. Reactive oxygen species as mediators of angiogenesis signaling. Role of NAD (P) H oxidase. *Molecular and cellular biochemistry*, 264(1-2), 85-97 (2004).

357. Mateo F, Meca-Cortés Ó, Celià-Terrassa T *et al.* SPARC mediates metastatic cooperation between CSC and non-CSC prostate cancer cell subpopulations. *Molecular cancer*, 13(1), 1 (2014).
358. Nojima H, Ohba Y, Kita Y. Oleamide Derivatives are Prototypical Anti-Metastasis Drugs that Act by Inhibiting Connexin 26 - See more at: <http://www.eurekaselect.com/59756/article#sthash.H12znOfg.dpuf>. *Current Drug Safety*, 2(3), 8 (2007).
359. Mueller GP, Driscoll WJ. Chapter 3 Biosynthesis of Oleamide. In: *Vitamins & Hormones*. (Academic Press, 2009) 55-78.
360. Lin R-Z, Wang T-P, Hung R-J, Chuang Y-J, Chien C-CM, Chang H-Y. Tumor-induced endothelial cell apoptosis: Roles of NAD(P)H oxidase-derived reactive oxygen species. *Journal of Cellular Physiology*, 226(7), 1750-1762 (2011).
361. Vekemans K, Timmers M, Vermijlen D, Zanger DR, Wisse E, Braet F. Cytotoxic reactions of CC531s towards liver sinusoidal endothelial cells: a microscopical study. *Comparative hepatology*, 3(1), 1 (2004).
362. Bisogno T, Katayama K, Melck D *et al.* Biosynthesis and degradation of bioactive fatty acid amides in human breast cancer and rat pheochromocytoma cells. *European Journal of Biochemistry*, 254(3), 634-642 (1998).
363. Bisogno T, Sepe N, De Petrocellis L, Mechoulam R, Di Marzo V. The sleep inducing factor oleamide is produced by mouse neuroblastoma cells. *Biochemical and biophysical research communications*, 239(2), 473-479 (1997).
364. Arafat ES, Trimble JW, Andersen RN, Dass C, Desiderio DM. Identification of fatty acid amides in human plasma. *Life sciences*, 45(18), 1679-1687 (1989).
365. Cravatt BF, Prospero-Garcia O, Siuzdak G *et al.* Chemical characterization of a family of brain lipids that induce sleep. *SCIENCE-NEW YORK THEN WASHINGTON-*, 1506-1506 (1995).
366. Baker DJ, Greenhaff PL, Timmons JA. Glycogen phosphorylase inhibition as a therapeutic target: a review of the recent patent literature. *Expert Opinion on Therapeutic Patents*, 16(4), 459-466 (2006).
367. Agius L. New hepatic targets for glycaemic control in diabetes. *Best Practice & Research Clinical Endocrinology & Metabolism*, 21(4), 587-605 (2007).
368. Akhtar N, Dickerson EB, Auerbach R. The sponge/Matrigel angiogenesis assay. *Angiogenesis*, 5(1-2), 75-80 (2002).
369. Gylling H, Vanhanen H, Miettinen T. Effects of ketoconazole on cholesterol precursors and low density lipoprotein kinetics in hypercholesterolemia. *Journal of lipid research*, 34(1), 59-67 (1993).
370. Gylling H, Vanhanen H, Miettinen TA. Hypolipidemic effect and mechanism of ketoconazole without and with cholestyramine in familial hypercholesterolemia. *Metabolism*, 40(1), 35-41 (1991).
371. Auerbach R, Lewis R, Shinnars B, Kubai L, Akhtar N. Angiogenesis assays: a critical overview. *Clinical chemistry*, 49(1), 32-40 (2003).
372. Carmeliet P, Jain RK. Principles and mechanisms of vessel normalization for cancer and other angiogenic diseases. *Nature reviews Drug discovery*, 10(6), 417-427 (2011).
373. Dickson PV, Hamner JB, Sims TL *et al.* Bevacizumab-induced transient remodeling of the vasculature in neuroblastoma xenografts results in improved delivery and efficacy of

- systemically administered chemotherapy. *Clinical cancer research*, 13(13), 3942-3950 (2007).
374. Inai T, Mancuso M, Hashizume H *et al.* Inhibition of vascular endothelial growth factor (VEGF) signaling in cancer causes loss of endothelial fenestrations, regression of tumor vessels, and appearance of basement membrane ghosts. *The American journal of pathology*, 165(1), 35-52 (2004).
375. Kim KJ, Li B, Winer J *et al.* Inhibition of vascular endothelial growth factor-induced angiogenesis suppresses tumour growth in vivo. (1993).
376. Eklund L, Bry M, Alitalo K. Mouse models for studying angiogenesis and lymphangiogenesis in cancer. *Molecular oncology*, 7(2), 259-282 (2013).
377. Berg JM, Tymoczko JL, Stryer L. Glycogen metabolism. (2002).
378. Rousset M, Dussaulx E, Chevalier G, Zweibaum A. Growth-related glycogen levels of human intestine carcinoma cell lines grown in vitro and in vivo in nude mice. *Journal of the National Cancer Institute*, 65(5), 885-889 (1980).
379. Witney TH, Carroll L, Alam IS *et al.* A novel radiotracer to image glycogen metabolism in tumors by positron emission tomography. *Cancer research*, 74(5), 1319-1328 (2014).
380. Gérard C, Goldbeter A. The balance between cell cycle arrest and cell proliferation: control by the extracellular matrix and by contact inhibition. *Interface focus*, 4(3), 20130075 (2014).
381. Browner MF, Nakano K, Bang AG, Fletterick RJ. Human muscle glycogen synthase cDNA sequence: a negatively charged protein with an asymmetric charge distribution. *Proceedings of the National Academy of Sciences*, 86(5), 1443-1447 (1989).
382. Nuttall FQ, Gannon MC, Bai G, Lee EY. Primary structure of human liver glycogen synthase deduced by cDNA cloning. *Archives of biochemistry and biophysics*, 311(2), 443-449 (1994).
383. Danforth WH. Glycogen synthetase activity in skeletal muscle interconversion of two forms and control of glycogen synthesis. *Journal of Biological Chemistry*, 240(2), 588-593 (1965).
384. Richter F, Böhme H, Hofmann E. Developmental changes of glycogen phosphorylase b isozymes in rat tissues. *Biomedica biochimica acta*, 42(10), 1229-1235 (1982).
385. Sato K, Satoh K, Sato T, Imai F, Morris HP. Isozyme patterns of glycogen phosphorylase in rat tissues and transplantable hepatomas. *Cancer research*, 36(2 Part 1), 487-495 (1976).
386. Crerar MM, Karlsson O, Fletterick RJ, Hwang PK. Chimeric muscle and brain glycogen phosphorylases define protein domains governing isozyme-specific responses to allosteric activation. *Journal of Biological Chemistry*, 270(23), 13748-13756 (1995).
387. Hahn T, Hartmann M, Blaschitz A *et al.* Localisation of the high affinity facilitative glucose transporter protein GLUT 1 in the placenta of human, marmoset monkey (*Callithrix jacchus*) and rat at different developmental stages. *Cell and tissue research*, 280(1), 49-57 (1995).
388. Winter SC, Buffa FM, Silva P *et al.* Relation of a hypoxia metagene derived from head and neck cancer to prognosis of multiple cancers. *Cancer research*, 67(7), 3441-3449 (2007).
389. Abaci HE, Truitt R, Luong E, Drazer G, Gerecht S. Adaptation to oxygen deprivation in cultures of human pluripotent stem cells, endothelial progenitor cells, and umbilical vein

- endothelial cells. *American Journal of Physiology-Cell Physiology*, 298(6), C1527-C1537 (2010).
390. Paternotte E, Gaucher C, Labrude P, Stoltz JF, Menu P. Review: Behaviour of endothelial cells faced with hypoxia. *Bio-Medical Materials and Engineering*, 18(4), 295-299 (2008).
391. Liao D, Johnson RS. Hypoxia: a key regulator of angiogenesis in cancer. *Cancer and Metastasis Reviews*, 26(2), 281-290 (2007).
392. Semenza GL. Cancer–stromal cell interactions mediated by hypoxia-inducible factors promote angiogenesis, lymphangiogenesis, and metastasis. *Oncogene*, 32(35), 4057-4063 (2013).
393. Haseloff RF, Krause E, Bigl M, Mikoteit K, Stanimirovic D, Blasig IE. Differential protein expression in brain capillary endothelial cells induced by hypoxia and posthypoxic reoxygenation. *Proteomics*, 6(6), 1803-1809 (2006).
394. Yamaji R, Fujita K, Nakanishi I *et al.* Hypoxic up-regulation of triosephosphate isomerase expression in mouse brain capillary endothelial cells. *Archives of biochemistry and biophysics*, 423(2), 332-342 (2004).
395. Vizan P, Sanchez-Tena S, Alcarraz-Vizan G *et al.* Characterization of the metabolic changes underlying growth factor angiogenic activation: identification of new potential therapeutic targets. *Carcinogenesis*, 30(6), 946-952 (2009).
396. Sinadinos C, Valles-Ortega J, Boulan L *et al.* Neuronal glycogen synthesis contributes to physiological aging. *Aging cell*, 13(5), 935-945 (2014).
397. Lin RZ, Wang TP, Hung RJ, Chuang YJ, Chien CCM, Chang HY. Tumor-induced endothelial cell apoptosis: Roles of NAD (P) H oxidase-derived reactive oxygen species. *Journal of cellular physiology*, 226(7), 1750-1762 (2011).
398. Oikonomakos NG, Skamnaki VT, Tsitsanou KE, Gavalas NG, Johnson LN. A new allosteric site in glycogen phosphorylase b as a target for drug interactions. *Structure*, 8(6), 575-584 (2000).
399. Hirayama A, Kami K, Sugimoto M *et al.* Quantitative metabolome profiling of colon and stomach cancer microenvironment by capillary electrophoresis time-of-flight mass spectrometry. *Cancer Res*, 69(11), 4918-4925 (2009).
400. Freeman S, Bartlett JB, Convey G *et al.* Sensitivity of glycogen phosphorylase isoforms to indole site inhibitors is markedly dependent on the activation state of the enzyme. *British journal of pharmacology*, 149(6), 775-785 (2006).
401. Schnier JB, Nishi K, Monks A, Gorin FA, Bradbury EM. Inhibition of glycogen phosphorylase (GP) by CP-91,149 induces growth inhibition correlating with brain GP expression. *Biochemical and biophysical research communications*, 309(1), 126-134 (2003).

8. APPENDIX 1

COMPUTATIONAL ¹³C METABOLIC FLUX ANALYSIS

1.1. Description of the procedure

The reliability of hypotheses regarding intracellular reaction fluxes suggested by our previous direct ¹³C tracer analyses can be evaluated by comparing measured and predicted ¹³C isotopologue distributions. A variety of different methods have been developed, assuming stationary or dynamic conditions [1-6]. In many cases, a system of balance equations around isotopomers, which depend on specific fluxes, is solved to predict label enrichments. Fluxes are iteratively changed until the difference among measured and predicted label enrichments is reduced.

In our analysis, two computer programs were developed with Mathematica [7] and applied iteratively until a flux distribution is found that is compatible with the measured labelling patterns. In summary, taking the known reaction network (reactions included are detailed in Table A1.1) and the measured uptake and secretion rates and assuming steady state, the first program estimates by linear programming the range of possible values for each reaction flux, where each flux is maximised or minimised while leaving all other fluxes free [4-6]. The second program solves a non-linear problem to predict isotopologue abundances by solving a system of balance equations around isotopomers, which take into account label transitions and the refined solution for fluxes obtained by applying the first program. The two programs are repeatedly applied to estimate flux distributions and to predict the associated label distribution in experiments using 50% [1,2-¹³C₂]-glucose as the labelled substrate. For each flux distribution, the enrichment in ¹³C-labelled products can be predicted and then compared with the measured enrichments, where comparisons are made at the isotopologue level. Selected ratios among fluxes are set to specific values, which additionally constraints the space of possible solutions for fluxes. These selected ratios among fluxes are iteratively changed until the difference among predicted and measured label enrichments is reduced.

Our analysis compared HUVECs cultured in restricted media (RM) at 40 hours and those cells cultured in restricted media with 30 ng/mL of VEGF (RMV) at 40 hours.

Table A1.1: Biochemical reaction network: The metabolic network included reactions (R_i) covering central carbon metabolism (R_N refers to normoxia, R_H refers to hypoxia), given in the table below (units: $\mu\text{mol}\cdot\text{h}^{-1}\cdot\text{million_cell}^{-1}$):

ID	Reaction stoichiometry and carbon transitions for label propagation		Resulting flux distributions	
	substrates	products	RM	RMV
R_{Glc}	c1,c2,c3,c4,c5,c6.extGlc	c1,c2,c3,c4,c5,c6.Glc	$0.282 < R_N < 0.282$ $0.463 < R_H < 0.463$	$0.201 < R_N < 0.201$ $0.49 < R_H < 0.49$
R_{Gln}	c1,c2,c3,c4,c5.extGln	c1,c2,c3,c4,c5.Gln	$0.235 < R_N < 0.235$ $0.099 < R_H < 0.099$	$0.243 < R_N < 0.243$ $0.051 < R_H < 0.051$
R_{Glu}	Glu		$0.061 < R_N < 0.061$ $0.05 < R_H < 0.05$	$0.055 < R_N < 0.055$ $0.046 < R_H < 0.046$
R_{Lac}	Lac		$1.558 < R_N < 1.558$ $1.169 < R_H < 1.17$	$1.948 < R_N < 1.948$ $1.466 < R_H < 1.466$
R_{OXPHOS}	$R_{\text{Cl}} + R_{\text{ClI}} + 7 R_{\text{FA}}$	$R_{\text{Cl}} + R_{\text{ClI}} + 7 R_{\text{FA}}$	$3.571 < R_N < 6.4674$ $1.3052 < R_H < 2.0971$	$4.3943 < R_N < 7.9885$ $1.6886 < R_H < 2.5797$
R_{Glc1}	c1,c2,c3,c4,c5,c6.Glc + ATP	c1,c2,c3,c4,c5,c6.G6P + ADP	$0.282 < R_N < 0.282$ $0.463 < R_H < 0.463$	$0.201 < R_N < 0.201$ $0.49 < R_H < 0.49$
R_{Glc2d}	c1,c2,c3,c4,c5,c6.G6P	c1,c2,c3,c4,c5,c6.H6P	$0.354 < R_N < 0.354$ $0.579 < R_H < 0.579$	$0.2531 < R_N < 0.2531$ $0.6129 < R_H < 0.6129$
R_{Glc2r}	c1,c2,c3,c4,c5,c6.H6P	c1,c2,c3,c4,c5,c6.G6P	$0.0708 < R_N < 0.0708$ $0.1158 < R_H < 0.1158$	$0.0506 < R_N < 0.0506$ $0.1226 < R_H < 0.1226$
R_{Glc2}	$R_{\text{Glc2d}} - R_{\text{Glc2r}}$	$R_{\text{Glc2d}} - R_{\text{Glc2r}}$	$0.282 < R_N < 0.282$ $0.463 < R_H < 0.463$	$0.2025 < R_N < 0.2025$ $0.4904 < R_H < 0.4904$
			$R_{\text{Glc2r}}/R_{\text{Glc2}} = 25/100$	$R_{\text{Glc2r}}/R_{\text{Glc2}} = 25/100$
R_{Glc3}	c1,c2,c3,c4,c5,c6.H6P + ATP	c1,c2,c3.DHAP + c4,c5,c6.G3P + ADP	$0.2794 < R_N < 0.2794$ $0.4609 < R_H < 0.4609$	$0.1985 < R_N < 0.1985$ $0.4879 < R_H < 0.4879$
R_{Glc4}	c1,c2,c3.DHAP	c3,c2,c1.G3P	$0.2794 < R_N < 0.2794$ $0.4609 < R_H < 0.4609$	$0.1985 < R_N < 0.1985$ $0.4879 < R_H < 0.4879$
R_{Glc5}	c1,c2,c3.G3P + cNAD + ADP	c1,c2,c3.C3PG + cNADH + ATP	$0.5626 < R_N < 0.5626$ $0.924 < R_H < 0.924$	$0.401 < R_N < 0.401$ $0.9783 < R_H < 0.9783$
R_{Glc6}	c1,c2,c3.C3PG + ADP	c1,c2,c3.Pyr1 + ATP	$0.5626 < R_N < 0.5626$ $0.924 < R_H < 0.924$	$0.401 < R_N < 0.401$ $0.9783 < R_H < 0.9783$
R_{LDH}	c1,c2,c3.Pyr1 + cNADH	c1,c2,c3.Lac + cNAD	$1.558 < R_N < 1.558$ $1.169 < R_H < 1.17$	$1.948 < R_N < 1.948$ $1.466 < R_H < 1.466$
R_{PyrEd}	c1,c2,c3.Pyr1	c1,c2,c3.Pyr2	$199.078 < R_N < 199.078$ $48.993 < R_H < 49.193$	$309.409 < R_N < 309.409$ $97.546 < R_H < 97.546$

R_{PyrEr}	c1,c2,c3-Pyr2	c1,c2,c3-Pyr1	200.073 < R_N < 200.073 49.238 < R_H < 49.439	310.956 < R_N < 310.956 98.0337 < R_H < 98.0337
R_{PyrE}	$R_{PyrEd} - R_{PyrEr}$	$R_{PyrEd} - R_{PyrEr}$	-0.9954 < R_N < -0.9954 -0.246 < R_H < -0.245	-1.547 < R_N < -1.547 -0.4877 < R_H < -0.4877
			$R_{PyrEd}/R_{PyrE} = 20000/-100$	$R_{PyrEd}/R_{PyrE} = 20000/-100$
R_{Glyc}		G6P	0.0012 < R_N < 0.0012 0.0002 < R_H < 0.0002	0.0015 < R_N < 0.0015 0.0004 < R_H < 0.0004
R_{G6PD}	c1,c2,c3,c4,c5,c6-H6P	c2,c3,c4,c5,c6-PenP	0.0113 < R_N < 0.0113 0.0069 < R_H < 0.0069	0.0121 < R_N < 0.0121 0.0074 < R_H < 0.0074
			$R_N: R_{G6PD}/R_{Glc} = 4/100$ $R_H: R_{G6PD}/R_{Glc} = 1.5/100$	$R_N: R_{G6PD}/R_{Glc} = 6/100$ $R_H: R_{G6PD}/R_{Glc} = 1.5/100$
R_{TKTad}	c1,c2,c3,c4,c5-PenP + c6,c7,c8,c9-E4P	c3,c4,c5-G3P + c1,c2,c6,c7,c8,c9-H6P	0.0066 < R_N < 0.0066 0.0069 < R_H < 0.0069	0.006 < R_N < 0.006 0.0074 < R_H < 0.0074
R_{TKTar}	c3,c4,c5-G3P + c1,c2,c6,c7,c8,c9-H6P	c1,c2,c3,c4,c5-PenP + c6,c7,c8,c9-E4P	0.0028 < R_N < 0.0028 0.0046 < R_H < 0.0046	0.002 < R_N < 0.002 0.0049 < R_H < 0.0049
			$R_{TKTar}/R_{Glc} = 1/100$	$R_{TKTar}/R_{Glc} = 1/100$
R_{TKTa}	$R_{TKTad} - R_{TKTar}$	$R_{TKTad} - R_{TKTar}$	0.0038 < R_N < 0.0038 0.0023 < R_H < 0.0023	0.004 < R_N < 0.004 0.0025 < R_H < 0.0025
R_{TKTbd}	c1,c2,c3,c4,c5-PenP + c6,c7,c8,c9,c10-PenP	c1,c2,c6,c7,c8,c9,c10-S7P + c3,c4,c5-G3P	0.0066 < R_N < 0.0066 0.0069 < R_H < 0.0069	0.006 < R_N < 0.006 0.0074 < R_H < 0.0074
R_{TKTbr}	c1,c2,c6,c7,c8,c9,c10-S7P + c3,c4,c5-G3P	c1,c2,c3,c4,c5-PenP + c6,c7,c8,c9,c10-PenP	0.0028 < R_N < 0.0028 0.0046 < R_H < 0.0046	0.002 < R_N < 0.002 0.0049 < R_H < 0.0049
			$R_{TKTbr}/R_{Glc} = 1/100$	$R_{TKTbr}/R_{Glc} = 1/100$
R_{TKTb}	$R_{TKTbd} - R_{TKTbr}$	$R_{TKTbd} - R_{TKTbr}$	0.0038 < R_N < 0.0038 0.0023 < R_H < 0.0023	0.004 < R_N < 0.004 0.0025 < R_H < 0.0025
R_{TAd}	c1,c2,c3,c4,c5,c6,c7-S7P + c8,c9,c10-G3P	c4,c5,c6,c7-E4P + c1,c2,c3,c8,c9,c10-H6P	0.4268 < R_N < 0.4268 0.6968 < R_H < 0.6968	0.3055 < R_N < 0.3055 0.7375 < R_H < 0.7375
R_{TAr}	c4,c5,c6,c7-E4P + c1,c2,c3,c8,c9,c10-H6P	c1,c2,c3,c4,c5,c6,c7-S7P + c8,c9,c10-G3P	0.423 < R_N < 0.423 0.6945 < R_H < 0.6945	0.3015 < R_N < 0.3015 0.735 < R_H < 0.735
			$R_{TAr}/R_{Glc} = 150/100$	$R_{TAr}/R_{Glc} = 150/100$
R_{TA}	$R_{TAd} - R_{TAr}$	$R_{TAd} - R_{TAr}$	0.0038 < R_N < 0.0038 0.0023 < R_H < 0.0023	0.004 < R_N < 0.004 0.0025 < R_H < 0.0025
R_{PDH}	c1,c2,c3-Pyr2 + mCoA + mNAD	c2,c3-mAcCoA + mNADH	0.0779 < R_N < 0.0779 0.0468 < R_H < 0.0468	0.0974 < R_N < 0.0974 0.0293 < R_H < 0.0293
			$R_N: R_{PDH}/R_{Lac} = 5/100$ $R_H: R_{PDH}/R_{Lac} = 4/100$	$R_N: R_{PDH}/R_{Lac} = 5/100$ $R_H: R_{PDH}/R_{Lac} = 2/100$
R_{PC}	c1,c2,c3-Pyr2 + c4.extCO2 + ATP	c1,c2,c3,c4-mOAA + ADP	0.008 < R_N < 0.008 0.0056 < R_H < 0.0064	0.0096 < R_N < 0.0096 0.0028 < R_H < 0.0028

R_{CS}	$c1,c2,c3,c4.mOAA + c5,c6.mAcCoA$	$c4,c3,c2,c1,c6,c5.Cit + mCoA$	$0.4674 < R_N < 0.4674$ $0.1754 < R_H < 0.1755$	$0.5844 < R_N < 0.5844$ $0.2199 < R_H < 0.2199$
			$R_N: R_{CS}/R_{Lac} = 30/100$ $R_H: R_{CS}/R_{Lac} = 15/100$	$R_N: R_{CS}/R_{Lac} = 30/100$ $R_H: R_{CS}/R_{Lac} = 15/100$
R_{IDH}	$c1,c2,c3,c4,c5,c6.Cit + mNAD$	$c1,c2,c3,c5,c6.\alpha KG + mNADH$	$0.4674 < R_N < 0.4674$ $0.1754 < R_H < 0.1755$	$0.5844 < R_N < 0.5844$ $0.2199 < R_H < 0.2199$
R_{SUC}	$c1,c2,c3,c4,c5.\alpha KG + mNAD + ADP$	$0.5 c2,c3,c4,c5.Suc + 0.5 c5,c4,c3,c2.Suc + mNADH + ATP$	$0.6414 < R_N < 1.2409$ $0.2243 < R_H < 0.3656$	$0.7724 < R_N < 1.3719$ $0.2249 < R_H < 0.366$
R_{CII}	$c1,c2,c3,c4.Suc + 1.5 ADP$	$c1,c2,c3,c4.Fum + 1.5 ATP$	$1.1721 < R_N < 1.4721$ $0.3906 < R_H < 0.4624$	$1.541 < R_N < 1.841$ $0.513 < R_H < 0.5836$
R_{CI}	$mNADH + 2.5 ADP$	$mNAD + 2.5 ATP$	$2.3988 < R_N < 4.9953$ $0.9145 < R_H < 1.6347$	$2.8533 < R_N < 6.1475$ $1.1756 < R_H < 1.9961$
R_{FH}	$c1,c2,c3,c4.Fum$	$c1,c2,c3,c4.Mal$	$1.4721 < R_N < 1.4721$ $0.4612 < R_H < 0.4624$	$1.841 < R_N < 1.841$ $0.5836 < R_H < 0.5836$
R_{CMDH}	$c1,c2,c3,c4.Mal + cNAD$	$c1,c2,c3,c4.COAA + cNADH$	$0.9954 < R_N < 0.9954$ $0.245 < R_H < 0.246$	$1.547 < R_N < 1.547$ $0.4877 < R_H < 0.4877$
R_{mMDHd}	$c1,c2,c3,c4.Mal + mNAD$	$c1,c2,c3,c4.mOAA + mNADH$	$107.19 < R_N < 107.19$ $15.197 < R_H < 15.21$	$194.449 < R_N < 194.449$ $54.1247 < R_H < 54.1247$
R_{mMDHr}	$c1,c2,c3,c4.mOAA + mNADH$	$c1,c2,c3,c4.Mal + mNAD$	$107.726 < R_N < 107.726$ $15.273 < R_H < 15.286$	$195.422 < R_N < 195.422$ $54.3953 < R_H < 54.3953$
R_{mMDH}	$R_{mMDHd} - R_{mMDHr}$	$R_{mMDHd} - R_{mMDHr}$	$-0.536 < R_N < -0.536$ $-0.0761 < R_H < -0.076$	$-0.9722 < R_N < -0.9722$ $-0.2706 < R_H < -0.2706$
			$R_{mMDHr}/R_{MDH} = 20000/-$ 100	$R_{mMDHr}/R_{MDH} = 20000/-$ 100
R_{GLS}	$c1,c2,c3,c4,c5.Gln$	$c1,c2,c3,c4,c5.Glu$	$0.235 < R_N < 0.235$ $0.099 < R_H < 0.099$	$0.243 < R_N < 0.243$ $0.051 < R_H < 0.051$
R_{GDH}	$c1,c2,c3,c4,c5.Glu + mNAD$	$c1,c2,c3,c4,c5.\alpha KG + mNADH$	$0.9039 < R_N < 1.7623$ $0.2622 < R_H < 0.4919$	$1.1558 < R_N < 2.2723$ $0.3907 < R_H < 0.6787$
R_{mAST}	$c1,c2,c3,c4.Asp + c5,c6,c7,c8,c9.\alpha KG$	$c1,c2,c3,c4.mOAA + c5,c6,c7,c8,c9.Glu$	$0.9954 < R_N < 0.9954$ $0.245 < R_H < 0.246$	$1.547 < R_N < 1.547$ $0.4877 < R_H < 0.4877$
R_{cAST}	$c1,c2,c3,c4.COAA + c5,c6,c7,c8,c9.Glu$	$c1,c2,c3,c4.Asp + c5,c6,c7,c8,c9.\alpha KG$	$0.9954 < R_N < 0.9954$ $0.245 < R_H < 0.246$	$1.547 < R_N < 1.547$ $0.4877 < R_H < 0.4877$
R_{ME}	$c1,c2,c3,c4.Mal$	$c1,c2,c3.Pyr2$	$1.0127 < R_N < 1.0127$ $0.2922 < R_H < 0.2925$	$1.2662 < R_N < 1.2662$ $0.3665 < R_H < 0.3665$
			$R_N: R_{ME}/R_{Lac} = 65/100$ $R_H: R_{ME}/R_{Lac} = 25/100$	$R_N: R_{ME}/R_{Lac} = 65/100$ $R_H: R_{ME}/R_{Lac} = 25/100$
R_{Ala}	$c1,c2,c3.Ala + c4,c5,c6,c7,c8.\alpha KG$	$c1,c2,c3.Pyr2 + c4,c5,c6,c7,c8.Glu$	$0. < R_N < 0.0303$ $0. < R_H < 0.0058$	$0. < R_N < 0.0303$ $0.0039 < R_H < 0.0071$

R_{Arg}	c1,c2,c3,c4,c5-Arg + c6,c7,c8,c9,c10- α KG + mNAD	c1,c2,c3,c4,c5-Glu + c6,c7,c8,c9,c10-Glu + mNADH	0. < R_N < 0.2995 0. < R_H < 0.0705	0. < R_N < 0.2995 0. < R_H < 0.0705
R_{His}	c1,c2,c3,c4,c5-His	c1,c2,c3,c4,c5-Glu	0. < R_N < 0.2 0. < R_H < 0.0471	0. < R_N < 0.2 0. < R_H < 0.0471
R_{Pro}	c1,c2,c3,c4,c5-Pro + mNAD	c1,c2,c3,c4,c5-Glu + mNADH	0. < R_N < 0.1 0. < R_H < 0.0235	0. < R_N < 0.1 0. < R_H < 0.0235
R_{Ile}	c1,c2,c3,c4,c5,c6-Ile + mCoA + c8,c9,c10,c11,c12- α KG + 2 mNAD	c5,c6-mAcCoA + 0.5 c7,c4,c3,c2-Suc + 0.5 c2,c3,c4,c7-Suc + c8,c9,c10,c11,c12- Glu + 2 mNADH	0. < R_N < 0.3895 0. < R_H < 0.1185	0. < R_N < 0.487 0. < R_H < 0.1185
R_{Met}	c1,c2,c3,c4,c5-Met + c6,c7,c8-Ser + mNAD + c10,c11,c12,c13,c14- α KG	0.5 c9,c4,c3,c2-Suc + 0.5 c2,c3,c4,c9-Suc + mNADH + c6,c7,c8-Pyr2 + c10,c11,c12,c13,c14-Glu	0. < R_N < 0.0686 0. < R_H < 0.0058	0. < R_N < 0.1007 0.0205 < R_H < 0.0237
R_{Val}	c1,c2,c3,c4-Val + 3 mNAD + c6,c7,c8,c9,c10- α KG	0.5 c5,c4,c3,c2-Suc + 0.5 c2,c3,c4,c5-Suc + 3 mNADH + c6,c7,c8,c9,c10-Glu	0. < R_N < 0.8307 0. < R_H < 0.2353	0. < R_N < 1. 0. < R_H < 0.2353
R_{Tyr}	c1,c2,c3,c4,c5,c6,c7,c8,c9-Tyr + c10,c11,c12,c13,c14- α KG	0.5 c4,c5,c6,c7-Fum + 0.5 c7,c6,c5,c4-Fum + c10,c11,c12,c13,c14-Glu	0. < R_N < 0.1 0. < R_H < 0.0235	0. < R_N < 0.1 0. < R_H < 0.0235
R_{Phe}	c1,c2,c3,c4,c5,c6,c7,c8,c9-extPhe + c10,c11,c12,c13,c14- α KG	0.5 c4,c5,c6,c7-Fum + 0.5 c7,c6,c5,c4-Fum + c10,c11,c12,c13,c14-Glu	0. < R_N < 0.2 0. < R_H < 0.0471	0. < R_N < 0.2 0. < R_H < 0.0471
R_{Cys}	c1,c2,c3-Cys + c4,c5,c6,c7,c8- α KG	c1,c2,c3-Pyr2 + c4,c5,c6,c7,c8-Glu	0. < R_N < 0.0686 0. < R_H < 0.0058	0. < R_N < 0.1989 0.0436 < R_H < 0.0468
R_{SerGly}	c1,c2,c3-Ser	c1,c2,c3-Pyr2	0. < R_N < 0.0686 0. < R_H < 0.0058	0.058 < R_N < 0.3354 0.0757 < R_H < 0.0789
R_{Thr}	c1,c2,c3,c4-Thr + c5-extCO ₂ + mNAD	0.5 c5,c4,c3,c2-Suc + 0.5 c2,c3,c4,c5-Suc + mNADH	0. < R_N < 0.1008 0. < R_H < 0.0237	0. < R_N < 0.1008 0. < R_H < 0.0237
R_{Leu}	c1,c2,c3,c4,c5,c6-Leu + 3 mCoA + c7-extCO ₂ + c8,c9,c10,c11,c12- α KG + mNAD + ATP	c2,c3-mAcCoA + c7,c4-mAcCoA + c5,c6- mAcCoA + c8,c9,c10,c11,c12-Glu + mNADH + ADP	0. < R_N < 0.1298 0. < R_H < 0.0429	0. < R_N < 0.1623 0. < R_H < 0.0635
R_{Lys}	c1,c2,c3,c4,c5,c6-Lys + 2 mCoA + 2 mNAD + c7,c8,c9,c10,c11- α KG + c12,c13,c14,c15,c16- α KG	c2,c3-mAcCoA + c4,c5-mAcCoA + 2 mNADH + c7,c8,c9,c10,c11-Glu + c12,c13,c14,c15,c16-Glu	0. < R_N < 0.1948 0. < R_H < 0.0643	0. < R_N < 0.2435 0. < R_H < 0.0953
R_{Trp}	c1,c2,c3,c4,c5,c6,c7,c8,c9,c10,c11- Trp + 2 mCoA + 2 mNAD	c10,c9-mAcCoA + c8,c7-mAcCoA + 2 mNADH	0. < R_N < 0.0201 0. < R_H < 0.0047	0. < R_N < 0.0201 0. < R_H < 0.0047

R_{FA}	7 mNAD + 8 mCoA + 10.5 ADP	8 $c_{1,c2}$.mAcCoA + 7 mNADH + 10.5 ATP	0. < R_N < 0.0487 0. < R_H < 0.0161	0. < R_N < 0.0609 0. < R_H < 0.0238
R_{OT1}	$R_{Ala} + R_{Met} + R_{Cys} + R_{SerGly} +$ R_{Thr}	$R_{Ala} + R_{Met} + R_{Cys} + R_{SerGly} +$ R_{Thr}	0.0686 < R_N < 0.0686 0.0058 < R_H < 0.0058	0.3878 < R_N < 0.3878 0.1533 < R_H < 0.1533
			$R_N: R_{OT1}/R_{Lac} = 4.4/100$ $R_H: R_{OT1}/R_{Lac} = 0.5/100$	$R_N: R_{OT1}/R_{Lac} = 19.91/100$ $R_H: R_{OT1}/R_{Lac} = 10.46/100$
R_{OT2}	$R_{Ile} + R_{Thr} + 3 R_{Leu} + 2 R_{Lys} +$ $2 R_{Trp} + 8 R_{FA}$	$R_{Ile} + R_{Thr} + 3 R_{Leu} + 2 R_{Lys} + 2$ $R_{Trp} + 8 R_{FA}$	0.3895 < R_N < 0.3895 0.1286 < R_H < 0.1287	0.487 < R_N < 0.487 0.1906 < R_H < 0.1906
R_{OT3}	$R_{Arg} + R_{His} + R_{Pro} + R_{Ile} + R_{Met}$ $+ R_{Val} + R_{Tyr} + R_{Phe}$	$R_{Arg} + R_{His} + R_{Pro} + R_{Ile} + R_{Met}$ $+ R_{Val} + R_{Tyr} + R_{Phe}$	0.8307 < R_N < 0.8307 0.2369 < R_H < 0.2379	1.0686 < R_N < 1.0686 0.3587 < R_H < 0.3587
R_{conATP}	ATP	ADP	9.0765 < R_N < 16.1931 4.0486 < R_H < 5.9939	10.7701 < R_N < 19.5951 4.9558 < R_H < 7.1692

where abbreviations are 3PG (3-Phosphoglycerate); AcCoA (Acetyl-CoA); Ala (Alanine); Arg (Arginine); Asp (Aspartate); Cit (Citrate); CoA (Coenzyme A); Cys (Cysteine); DHAP (Dihydroxyacetone phosphate); E4P (Erythrose 4-phosphate); F6P (Fructose 6-phosphate); Fum (Fumarate); G3P (Glyceraldehyde 3-phosphate); G1P (Glucose 1-phosphate); G6P (Glucose 6-phosphate); Glc (Glucose); Gln (Glutamine); Glu (Glutamate); Gly (Glycine); H6P (Hexose phosphate (G6P+F6P)); His (Histidine); Ile (Isoleucine); Lac (Lactate); Leu (Leucine); Lys (Lysine); Mal (Malate); Met (Methionine); OAA (Oxaloacetate); PenP (Ribulose 1-phosphate, Ribose 1-phosphate, Xylulose 1-phosphate); Phe (Phenylalanine); Pro (Proline); Pyr1 and Pyr 2 (two pools of Pyruvate); Ser (Serine); S7P (Sedoheptulose 7-phosphate); Suc (Succinate); Thr (Threonine); Trp (Tryptophan); Tyr (Tyrosine); Val (Valine); α KG (α -Ketoglutarate), and were ext means external, c cytoplasmic and m means mitochondrial. The model covers glycolysis, pentose phosphate pathways and TCA cycle. Glucose and glutamine are included as the main sources of carbons, although the alternative uptake of other amino acids and fatty acids is also included. Reactions include the energy and redox balances for ATP/ADP and NADH/NAD⁺, including mitochondrial respiration and oxidative phosphorylation and the malate-aspartate shuttle for NADH transfer. The process of model refinement takes advantage of the redox balanced nature of the model – *i.e.*, the high energy electron (NADH or FADH₂) production rate matches the consumption rate by oxidative phosphorylation [8] – which constrains additionally the space of solutions for fluxes.

1.2. Measured cellular uptake and secretion rates

Units for reaction fluxes are micromole per hour per millions of cells ($\mu\text{mol}\cdot\text{h}^{-1}\cdot\text{million-cells}^{-1}$). Reaction fluxes for glucose uptake (R_{Glc}), glutamine uptake (R_{Gln}), glutamate secretion (R_{Glu}), and lactate secretion (R_{Lac}) (estimated from the experimental data reported in Chapter 4.1) were assumed to be 0.282, 0.235, 0.061 and 1.558 (RM, normoxia), 0.463, 0.099, 0.05 and 1.17 (RMV, normoxia), 0.201, 0.243, 0.055 and 1.948 (RM, hypoxia), and 0.49, 0.051, 0.046 and 1.466 (RMV, hypoxia), respectively, according to experimental data. A net uptake of glycogen (R_{Glyc}) is included, according to experimental measurements, to be 0.0012 (RM, normoxia),

0.0015 (RMV, normoxia), 0.0002 (RM, hypoxia) and 0.0004 (RMV, hypoxia). Finally, the maximum utilization of most of the amino acids is fixed according to the media composition, which depended on the number of cells. For example, under normoxia this maximum value was fixed to be 0.030 for Alanine (R_{Ala}), 0.300 for Arginine (R_{Arg}), 0.200 for Histidine (R_{His}), 0.100 for Proline (R_{Pro}), 0.504 for Isoleucine (R_{Ile}), 0.101 for Methionine (R_{Met}), 1.000 for Valine (R_{Val}), 0.100 for Tyrosine (R_{Tyr}), 0.200 for Phenylalanine (R_{Phe}), 0.199 for Cysteine (R_{Cys}), 0.305 + 0.031 for Serine + Glycine (R_{SerGly}), 0.101 for Threonine (R_{Thr}), 1.000 for Leucine (R_{Leu}), 0.995 for Lysine (R_{Lys}), and 0.020 for Tryptophan (R_{Trp}).

1.3. Set ratios among fluxes

The initial space of solutions for fluxes was constrained to the reduced solution space showed above (Table A1.1) by setting some ratios among fluxes. In order to fit the measured label enrichments appropriately, some of these ratios needed to be different between the four conditions.

On the one hand, the ratio of oxidative PPP versus glycolysis (R_{G6PD}/R_{Glc}) reflects an important change in the activity of oxidative PPP, which is in correspondence with the observed (Figure 4.1.3 in Chapter 4.1) changes in the ratio of oxidative versus non-oxidative PPP when comparing normoxia and hypoxia.

On the other hand, several ratios associated with mitochondrial activity (R_{ME}/R_{Lac} , R_{CS}/R_{Lac} , R_{PDH}/R_{Lac}) were required to be different, reflecting the expected lower mitochondrial activity compared with glycolysis in hypoxia. To avoid unrealistic cycles, the ratio “non-mitochondrial-other sources” versus lactate secretion (R_{OT1}/R_{Lac}) was adjusted differently in each condition to have a ratio pyruvate carboxylase versus pyruvate dehydrogenase (R_{PC}/R_{PDH}) around 10/100. This last change was not required to fit label enrichments.

1.4. Estimated intracellular metabolic fluxes

The iterative process described above constrained the reaction fluxes associated with glucose uptake, glycolysis, PPP and parts of the TCA cycle, although maintained a high level of uncertainty for fluxes associated with the use of alternative sources of carbons. These alternative sources of carbons were required to satisfy the high level of lactate secreted to the media according to the experiments, which also required an additional source of NADH. A scheme of the metabolic network with the more relevant values for fluxes is provided as a separate figure, included in Chapter 4.1 as Figure 4.1.8. A detailed list of the resulting values for all fluxes is provided in the Table A1.1 together with the description of the reactions. In this figure and the table the alternative sources of carbons are grouped in three super-reactions (R_{OT1} , R_{OT2} and R_{OT3}).

The predicted and measured label enrichments from the labelled glucose to the metabolites ribose, glycogen, lactate and glutamate under normoxia and hypoxia, in the presence and absence of VEGF are shown in Figures A1.1 and A1.2. It is observed from these measurements that the predicted label enrichments perfectly fit the measured experimental data, increasing the confidence of the fluxes predicted from the computational model (shown in Figure 4.1.8 in Chapter 4.1).

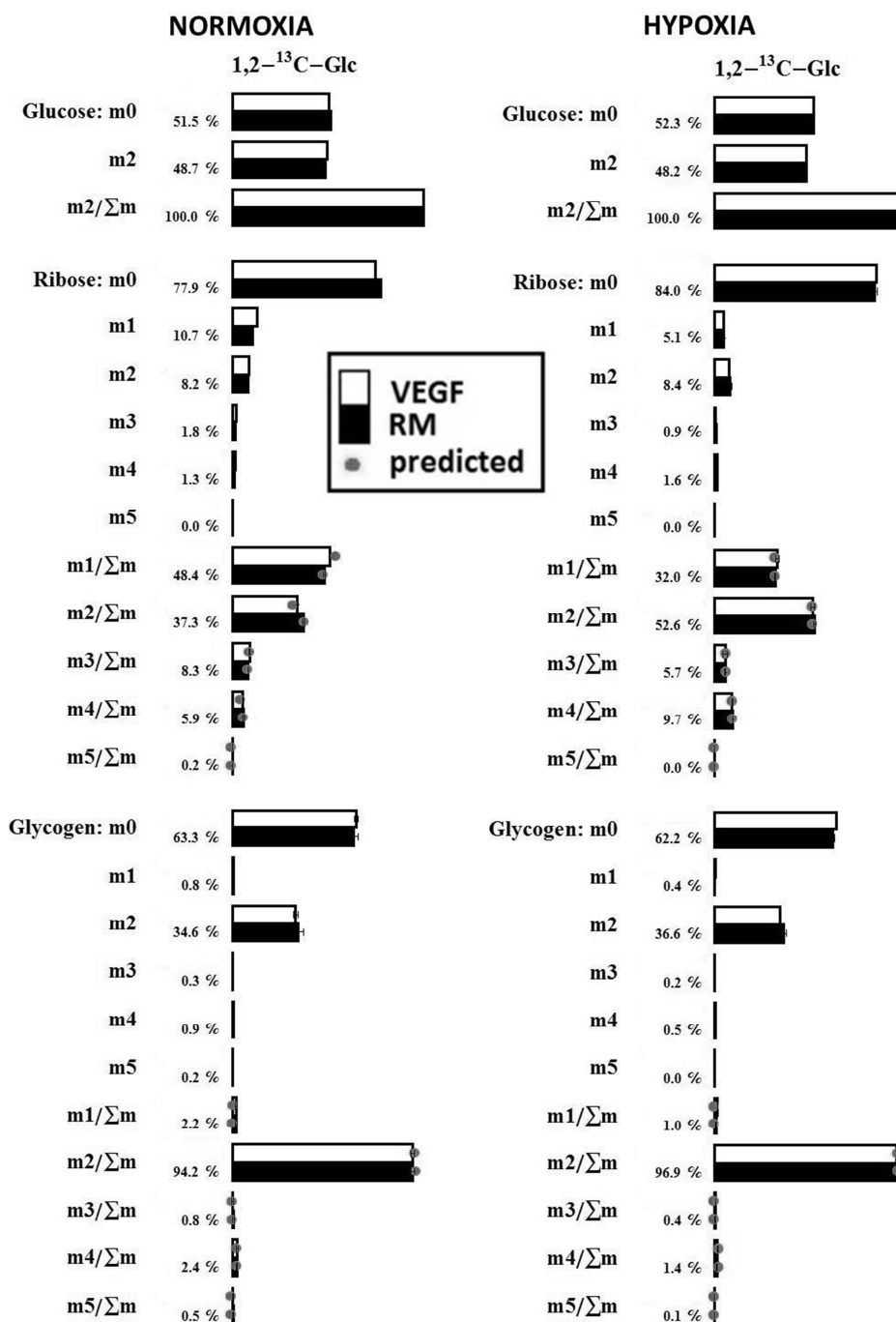


Figure A1.1: Predicted and measured label enrichments I. Label enrichment of ^{13}C label from labelled glucose to ribose and glycogen, under normoxia and hypoxia, with VEGF (RMV). The fraction m0 is an isotopologue with zero ^{13}C , m1 with one ^{13}C , m2 with two ^{13}C and so on. Σm refers to the summation of all isotopologues with one or more ^{13}C ($\Sigma m = m1 + m2 + \dots$). The measured enrichments for glucose, lactate, alanine and glutamate were obtained from the media. The measured enrichments for ribose and glycogen were obtained from cells. Notice that predicted enrichments in ribose, glycogen, lactate, alanine and glutamate are based on the model counterparts pentose phosphate (PenP), glucose 6-phosphate (G6P), first pool of pyruvate (Pyr1), second pool of pyruvate (Pyr2), and glutamate (Glu), respectively.

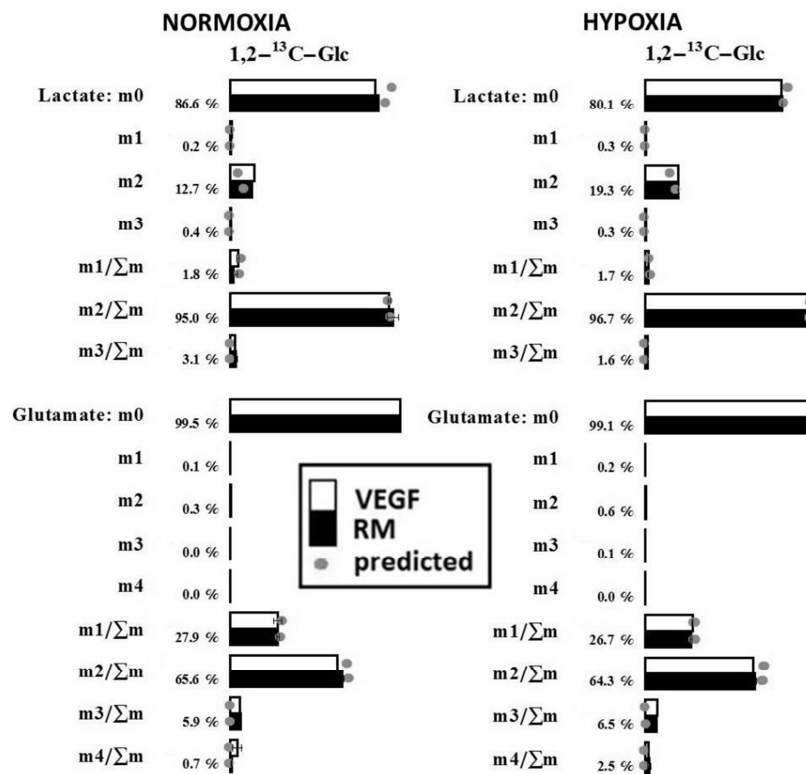


Figure A1.2: Predicted and measured label enrichments II. Label enrichment of ^{13}C label from labelled glucose to lactate and glutamate, under normoxia and hypoxia, with VEGF (RMV). See Figure A1.1 legend for details.

1.5. References

1. Sauer U. Metabolic networks in motion: ^{13}C -based flux analysis. *Molecular systems biology*, 2(1) (2006).
2. Kruger NJ, Ratcliffe RG. Insights into plant metabolic networks from steady-state metabolic flux analysis. *Biochimie*, 91(6), 697-702 (2009).
3. Wiechert W, Nöh K. Isotopically non-stationary metabolic flux analysis: complex yet highly informative. *Current opinion in biotechnology*, 24(6), 979-986 (2013).
4. Zamboni N. ^{13}C metabolic flux analysis in complex systems. *Current opinion in biotechnology*, 22(1), 103-108 (2011).
5. Crown SB, Antoniewicz MR. Parallel labeling experiments and metabolic flux analysis: Past, present and future methodologies. *Metabolic engineering*, 16, 21-32 (2013).
6. Niedenführ S, Wiechert W, Nöh K. How to measure metabolic fluxes: a taxonomic guide for ^{13}C fluxomics. *Current opinion in biotechnology*, 34, 82-90 (2015).
7. Wolfram S. *The Mathematica Book* (Wolfram Media, 2003).
8. Fan J, Kamphorst JJ, Mathew R *et al.* Glutamine-driven oxidative phosphorylation is a major ATP source in transformed mammalian cells in both normoxia and hypoxia. *Molecular systems biology*, 9, 712 (2013).

9. APPENDIX 2

MEASURED ¹³C LABEL ENRICHMENTS

Table A2.1. Measured ¹³C isotopomer enrichments using [1,2-¹³C₂]-glucose, under normoxia and hypoxia in extracellular metabolites: glucose, lactate, glutamate, aspartate and proline, and the intracellular metabolites: ribose, glycogen, palmitate and stearate.

		Normoxia				Hypoxia			
		RM		RMV		RM		RMV	
		mean	SD	mean	SD	mean	SD	mean	SD
Glc-328	m0	0.527	0.001	0.519	0.001	0.523	0.001	0.523	0.001
	m1	0.000	0.000	0.000	0.000	0.000	0.000	0.000	0.000
	m2	0.475	0.000	0.484	0.000	0.482	0.001	0.482	0.001
	m3	0.000	0.000	0.000	0.000	0.000	0.000	0.000	0.000
	m4	0.000	0.000	0.000	0.000	0.000	0.000	0.000	0.000
	m5	0.000	0.000	0.000	0.000	0.000	0.000	0.000	0.000
	m6	0.000	0.000	0.000	0.000	0.000	0.000	0.000	0.000
Lac-328	m0	0.866	0.004	0.847	0.003	0.801	0.001	0.797	0.002
	m1	0.002	0.003	0.007	0.001	0.003	0.000	0.004	0.000
	m2	0.127	0.003	0.142	0.002	0.193	0.001	0.195	0.002
	m3	0.004	0.001	0.004	0.000	0.003	0.000	0.003	0.000
Glu-198	m0	0.995	0.000	0.995	0.000	0.991	0.000	0.991	0.000
	m1	0.001	0.000	0.001	0.000	0.002	0.000	0.002	0.000
	m2	0.003	0.000	0.003	0.000	0.006	0.000	0.006	0.000
	m3	0.000	0.000	0.000	0.000	0.001	0.000	0.001	0.000
	m4	0.000	0.000	0.000	0.000	0.000	0.000	0.000	0.000
Asp/Asn-342	m0	0.996	0.001	0.997	0.004	0.995	0.002	0.995	0.001
	m1	0.002	0.000	0.002	0.000	0.003	0.001	0.003	0.001
	m2	0.002	0.000	0.001	0.000	0.002	0.000	0.002	0.000
	m3	0.000	0.000	0.000	0.000	0.000	0.000	0.000	0.000
	m4	0.000	0.001	0.000	0.004	0.000	0.000	0.000	0.000
Glu/Gln-384	m0	0.994	0.003	0.995	0.002	0.991	0.000	0.991	0.000
	m1	0.003	0.001	0.001	0.000	0.002	0.001	0.002	0.000
	m2	0.003	0.000	0.003	0.000	0.007	0.000	0.007	0.000
	m3	0.000	0.000	0.000	0.001	0.000	0.000	0.000	0.000
	m4	0.000	0.000	0.000	0.000	0.000	0.000	0.000	0.000
	m5	0.000	0.001	0.000	0.001	0.000	0.000	0.000	0.000

Pro-296	m0	0.989	0.002	0.992	0.001	0.994	0.002	0.994	0.001
	m1	0.002	0.000	0.002	0.000	0.003	0.001	0.003	0.000
	m2	0.009	0.003	0.006	0.001	0.003	0.000	0.003	0.001
	m3	0.000	0.000	0.000	0.000	0.000	0.000	0.000	0.001
	m4	0.000	0.000	0.000	0.000	0.000	0.001	0.000	0.000
	m5	0.000	0.001	0.000	0.001	0.000	0.000	0.000	0.000
Rib-256	m0	0.779	0.004	0.747	0.004	0.840	0.017	0.849	0.003
	m1	0.107	0.002	0.129	0.003	0.051	0.005	0.050	0.001
	m2	0.082	0.001	0.087	0.000	0.084	0.008	0.078	0.002
	m3	0.018	0.001	0.023	0.001	0.009	0.001	0.009	0.002
	m4	0.013	0.001	0.014	0.000	0.016	0.002	0.014	0.001
	m5	0.000	0.000	0.000	0.000	0.000	0.000	0.000	0.000
Glyc-328	m0	0.633	0.024	0.649	0.009	0.622	0.010	0.640	0.001
	m1	0.008	0.001	0.008	0.001	0.004	0.001	0.006	0.000
	m2	0.346	0.026	0.332	0.012	0.366	0.011	0.345	0.001
	m3	0.003	0.001	0.001	0.001	0.002	0.000	0.002	0.000
	m4	0.009	0.000	0.009	0.001	0.005	0.001	0.007	0.000
	m5	0.002	0.001	0.002	0.000	0.000	0.000	0.000	0.000
	m6	0.000	0.000	0.000	0.000	0.001	0.000	0.001	0.000
Palm-270	m0	0.961	0.009	0.950	0.008	0.955	0.002	0.921	0.011
	m1	0.004	0.005	0.003	0.004	0.000	0.000	0.001	0.000
	m2	0.022	0.009	0.025	0.004	0.028	0.001	0.047	0.006
	m3	0.001	0.000	0.004	0.004	0.000	0.000	0.001	0.000
	m4	0.009	0.003	0.012	0.002	0.013	0.001	0.022	0.003
	m5	0.001	0.000	0.001	0.000	0.000	0.000	0.000	0.000
	m6	0.002	0.001	0.003	0.000	0.003	0.000	0.006	0.001
	m7	0.000	0.000	0.001	0.002	0.000	0.000	0.000	0.000
	m8	0.000	0.000	0.000	0.001	0.001	0.000	0.001	0.000
	m9	0.000	0.000	0.000	0.001	0.000	0.000	0.000	0.000
	m10	0.000	0.000	0.000	0.000	0.000	0.000	0.000	0.000
Stear-298	m0	0.994	0.006	0.970	0.038	0.994	0.001	0.987	0.005
	m1	0.000	0.001	0.001	0.003	0.000	0.001	0.000	0.001
	m2	0.004	0.001	0.005	0.001	0.006	0.000	0.010	0.002
	m3	0.000	0.001	0.004	0.006	0.000	0.000	0.000	0.000
	m4	0.002	0.001	0.004	0.001	0.001	0.000	0.003	0.001
	m5	0.000	0.000	0.003	0.005	0.000	0.000	0.000	0.000
	m6	0.000	0.000	0.000	0.001	0.000	0.000	0.000	0.000

m7	0.000	0.002	0.010	0.019	0.000	0.001	0.000	0.002
m8	0.000	0.000	0.002	0.003	0.000	0.000	0.000	0.000
m9	0.000	0.000	0.001	0.002	0.000	0.000	0.000	0.000
m10	0.000	0.000	0.000	0.000	0.000	0.000	0.000	0.000

Abbreviations, according to Materials and Methods: Glc-328, C1-C6 glucose in the range 327-334 m/z; Lac-328, C1-C3 lactate in the range 327-332 m/z; Glu-198, C2-C5 glutamate in the range 197-203 m/z; Asp/Asn-342, C1-C4 aspartate and asparagine in the range 341-348 m/z; Glu/Gln-384, C1-C5 glutamate and glutamine in the range 383-390 m/z; Pro-296, C1-C5 proline in the range 295-302 m/z; Rib-256, C1-C5 ribose in the range 256-262 m/z; Glyc-328, C1-C6 glucose in the range 327-334 m/z; Palm-270, C1-C10 palmitate in the range 269-279 m/z, Stear-298, C1-C10 stearate in the range 297-307 m/z.

10. APPENDIX 3

UNTARGETED METABOLOMICS OF ENDOTHELIAL CELLS INDUCED BY VEGF AND METASTATICALLY DIFFERENT PROSTATE CANCER CELL LINES

Table A3.1. Metabolite identification scoring system. The summation of each of these points for the respective data parameters gives the confidence level for the metabolite identification of the features.

IR absorbance spectrum	0.5
UV absorbance spectrum	0.5
Retention time ($\pm 2.5\%$)	1.0
High resolution retention time $W_{1/2} < 10s$	1.5
High resolution retention index ($\pm 0.5\%$, $RI \pm 25$, $W_{1/2} < 10s$)	2.0
Nominal mass of parent ion	0.5
Accurate mass of parent ion (< 5 ppm)	1.0
Molecular formula based upon accurate m/z and isotope pattern	1.0
Confident EI Spectral match to commercial library	1.0
Tandem mass spectrum	1.5
Accurate mass tandem mass spectrum	2.0
1H 1D NMR	2.0
1H 2D NMR	3.0
$^1H \times ^{13}C$ 2D NMR	4.0

IR infrared spectroscopy, *UV* ultraviolet, *RI* retention index, $W_{1/2}$ peak width at half-height, m/z mass-to-charge ratio, *EI* electron ionization, *1D* one-dimensional, *2D* two-dimensional, *NMR* nuclear magnetic resonance spectroscopy

*Table obtained with permission from Springer (Sumner, 2014).

Table A3.2. Quantitative peak area values for metabolites analysed using ESI+ and ESI-ionisation modes. The peak area values extracted from the raw chromatographic data using XCMS Online software, for the identified metabolites, were normalized with cell number values.

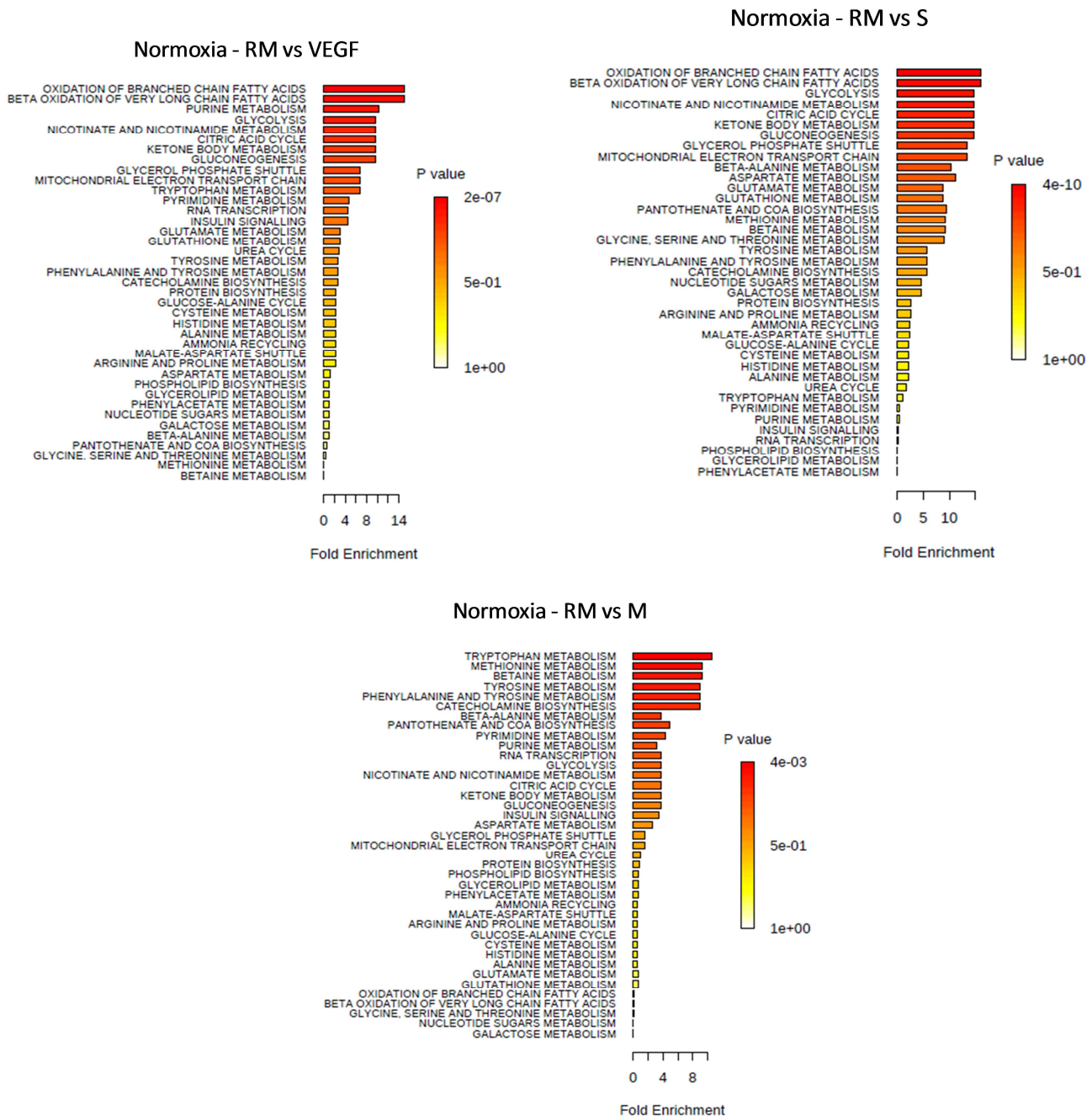
ESI+

Identified metabolites	Peak area (arbitrary units per 10 ⁶ cells)			
	RM	VEGF	PC-3/S	PC-3/M
L-Glutamate	66951254 ± 10674565	60992435 ± 3955201	72793180 ± 3482523	62494526 ± 13847139
L-Arginine	2850696 ± 369503	2517868 ± 214860	2331266 ± 204334	3011323 ± 575637
L-Glutathione reduced	147457447 ± 13614146	138056413 ± 3400935	175365361 ± 11071488	154091478 ± 19812579
L-Tryptophan	6426731 ± 230788	7203514 ± 673466	6657208 ± 669328	5561158 ± 447360
L-Tyrosine	15231094 ± 772657	15901039 ± 873714	16843892 ± 1494436	13488768 ± 954533
L-Methionine	11781372 ± 843742	11785904 ± 444868	13535238 ± 879145	9864736 ± 1002319
Nicotinamide dinucleotide (NAD ⁺)	349585 ± 80340	579638 ± 126952	777683 ± 95892	425925 ± 72943
Pantothenic acid (CID match)	10573990 ± 705837	10812162 ± 522376	12247706 ± 865008	9241784 ± 1403771
Oleamide	210787 ± 24989	242042 ± 116576	295589 ± 144044	874802 ± 482152
γ-L-Glutamyl-L-Glutamic acid	325453 ± 57026	359204 ± 53875	373348 ± 51076	347485 ± 51410
Inosine	4477199 ± 1528783	5556422 ± 775440	4514688 ± 2478730	5939550 ± 1121325
Spermine	1582 ± 1614	385951 ± 416964	1236 ± 789	598696 ± 757055
<i>trans</i> 3-Indole acrylic acid/Indole 3-acrylic acid	7834998 ± 306567	8760753 ± 786143	8112445 ± 815039	6740205 ± 546530
Cysteinylglycine	2625137 ± 201836	2463979 ± 72958	3114935 ± 200785	2709193 ± 351143
Guanine	731455 ± 217760	2866933 ± 1288558	642033 ± 438881	1350835 ± 1074163
Creatine	9604021 ± 1560719	9974211 ± 699518	11891689 ± 483560	9381733 ± 2024394
Hypoxanthine (RT - 1.19 min)	8228745 ± 2318231	25984608 ± 8815781	6797809 ± 4899521	13325046 ± 8236728
Acetyl L-Carnitine	125615 ± 15138	192802 ± 9752	221326 ± 6966	129106 ± 24962

ESI-

Identified metabolites	Peak area (arbitrary units per 10 ⁶ cells)			
	RM	VEGF	PC-3/S	PC-3/M
L-Aspartate	4026645 ± 951907	4435094 ± 677350	5885484 ± 328430	4970474 ± 1385427
L-Glutamate	17083370 ± 3074331	13386798 ± 1453575	18918489 ± 667475	16034316 ± 3746532
Glycerol 3-phosphate	188690 ± 87424	251507 ± 112517	193762 ± 64197	268337 ± 144276
Pantothenic acid	4313972 ± 224135	4238894 ± 275881	4969068 ± 354539	3999473 ± 544548
Uridine	678202 ± 325545	1357260 ± 466045	706975 ± 664597	1461404 ± 881076
L-Glutathione reduced	50317037 ± 2771427	48217214 ± 3361789	60203491 ± 5163431	56410579 ± 5028755
Uridine monophosphate	4343895 ± 3007429	1729642 ± 1314237	3633971 ± 2666633	1775034 ± 1427553
Adenosine monophosphate	6265769 ± 6184181	1259364 ± 915144	7451180 ± 5603151	1911056 ± 1437925
Galactonic acid	135979 ± 50315	91977 ± 9055	127242 ± 10561	120871 ± 32839
Guanosine	1707467 ± 658309	2383234 ± 652545	1463307 ± 1032962	2946629 ± 1780239

Figure A3.1: Pathways generated with identified metabolites in HUVEC in the presence of VEGF, PC-3/S and PC-3/M cells, by metabolite set enrichment analysis using MetaboAnalyst 3.0.

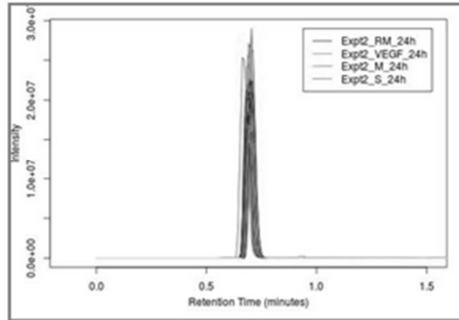


11. APPENDIX 4

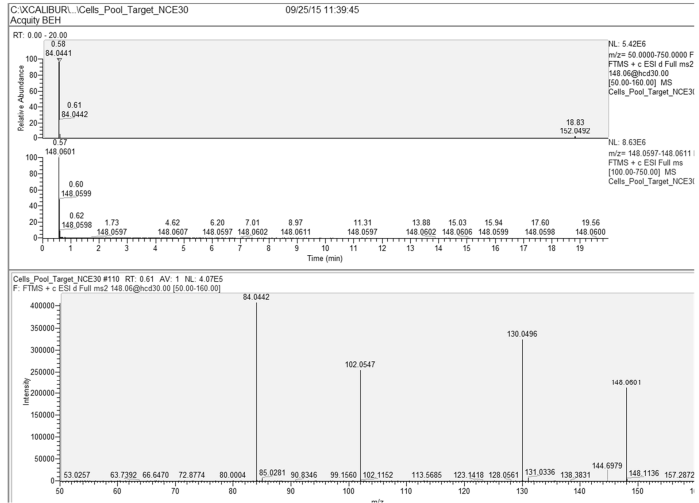
CHROMATOGRAPHIC PEAK AND MASS SPECTRAL DATA FROM THE UNTARGETED ANALYSIS.

Figure A4.1: (a) Chromatographic peaks from XCMS Online [1,2], (b) accurate mass of the precursor ion, (c) fragmentation spectral match of the identified metabolites from mzcloud (<https://www.mzcloud.org>) and (d) the isotopic pattern match. Some metabolites do not show peaks in XCMS Online as $p > 0.05$. RM – control HUVECs grown in restricted medium, VEGF – HUVECs grown in restricted medium supplemented with VEGF, M – HUVECs co-cultured with PC-3/M cells, S – HUVECs co-cultured with PC-3/S cells.

L-Glutamate



a



b

Recalibrated Spectrum

FTMS + ESI ms2 148.0604@hcd30.00 [50.00-160.00]

Precursor Structure $C_5H_{10}NO_4^{1-}$

m/z 148.06043

Blue Structure: Heuristic Prediction
Brown Structure: Quantum Chemical Prediction

NC(C(O)C(=O)O)C(=O)O

Metadata Hide empty fields

Cite current compound: www.mzcloud.org/dataviewer.aspx#Reference470 **Copy**

Cite current tree: www.mzcloud.org/dataviewer.aspx#Reference470#T853#c **Copy**

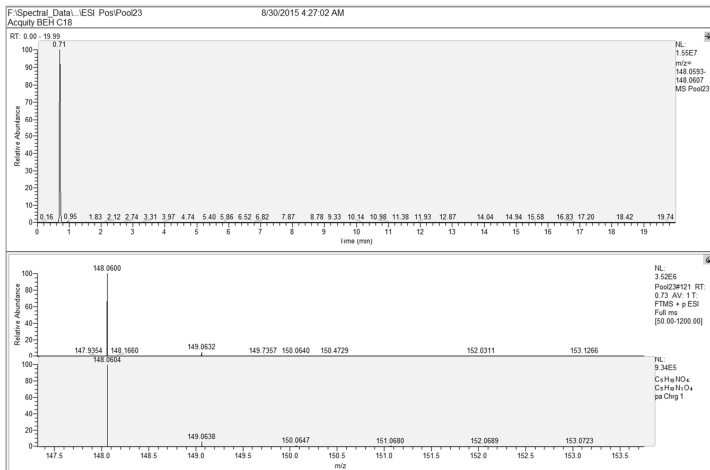
Cite current spectrum: www.mzcloud.org/dataviewer.aspx#Reference470#T853#e#112961 **Copy**

Compound

Names

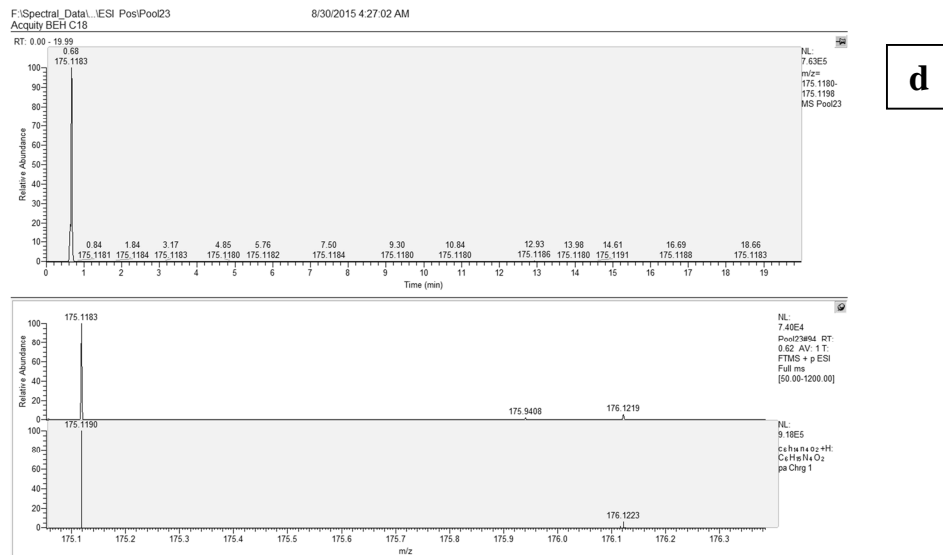
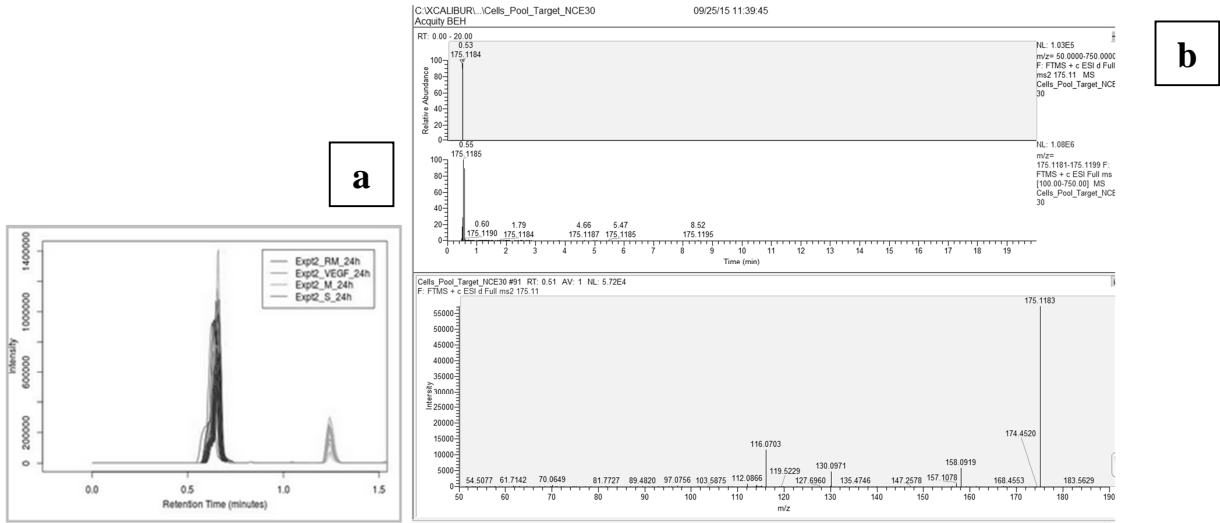
Compound Name: L-Glutamic acid

c

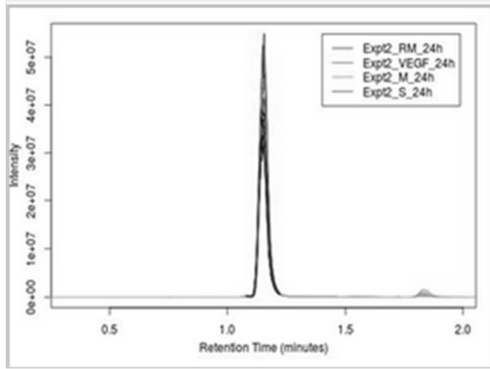


d

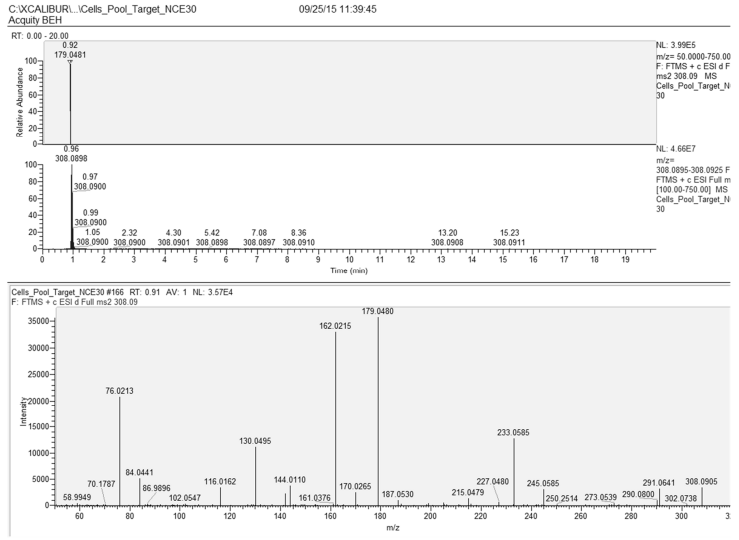
L- Arginine



L- Glutathione reduced



a



b

Recalibrated Spectrum
FTMS + ESI ms2 308.0911@hcd30.00 [50.00-320.00]

Precursor Structure C₁₀H₁₈N₂O₆S₃⁺
m/z 308.09108

Blue Structure: Heuristic Prediction
Brown Structure: Quantum Chemical Prediction

Metadata Hide empty fields

Cite current compound: www.mzcloud.org/dataviewer.aspx#Reference472 **Copy**

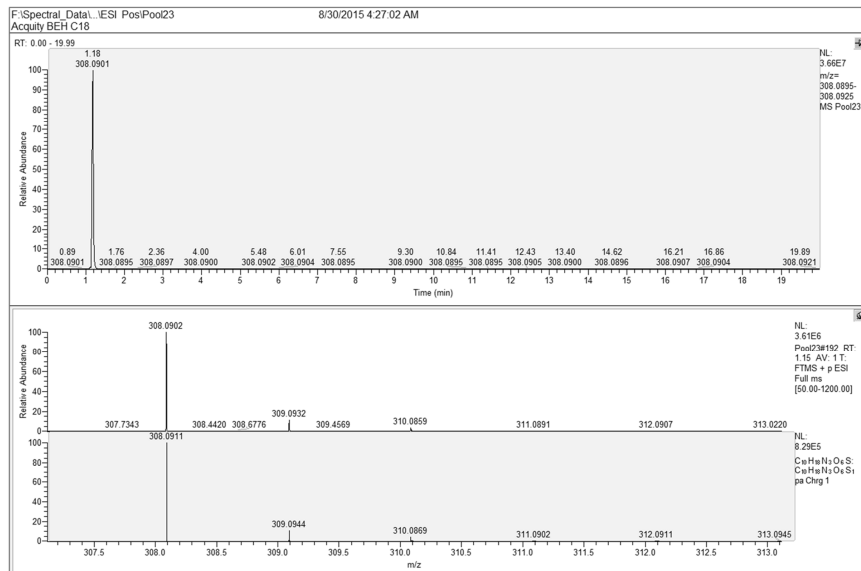
Cite current tree: www.mzcloud.org/dataviewer.aspx#Reference472#T858#c **Copy**

Cite current spectrum: www.mzcloud.org/dataviewer.aspx#Reference472#T858#c#113711 **Copy**

Compound

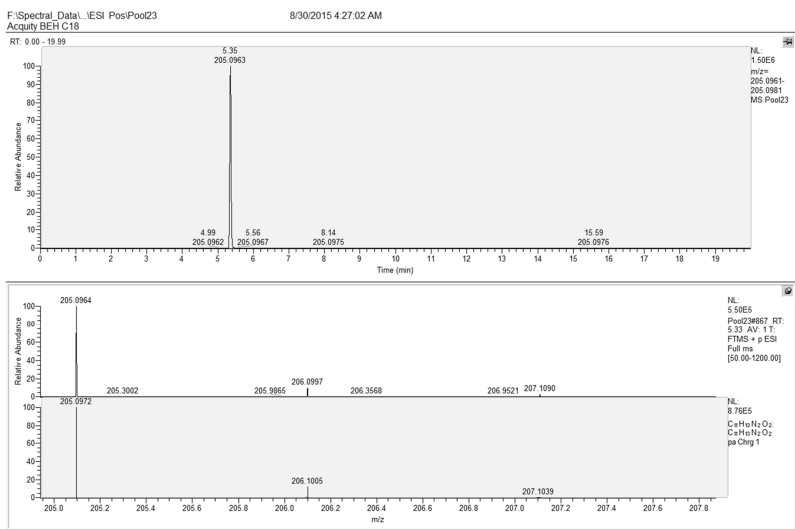
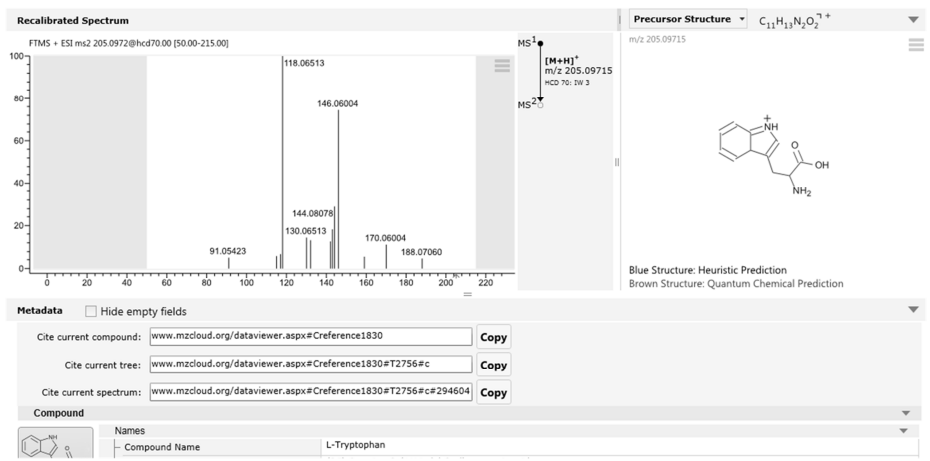
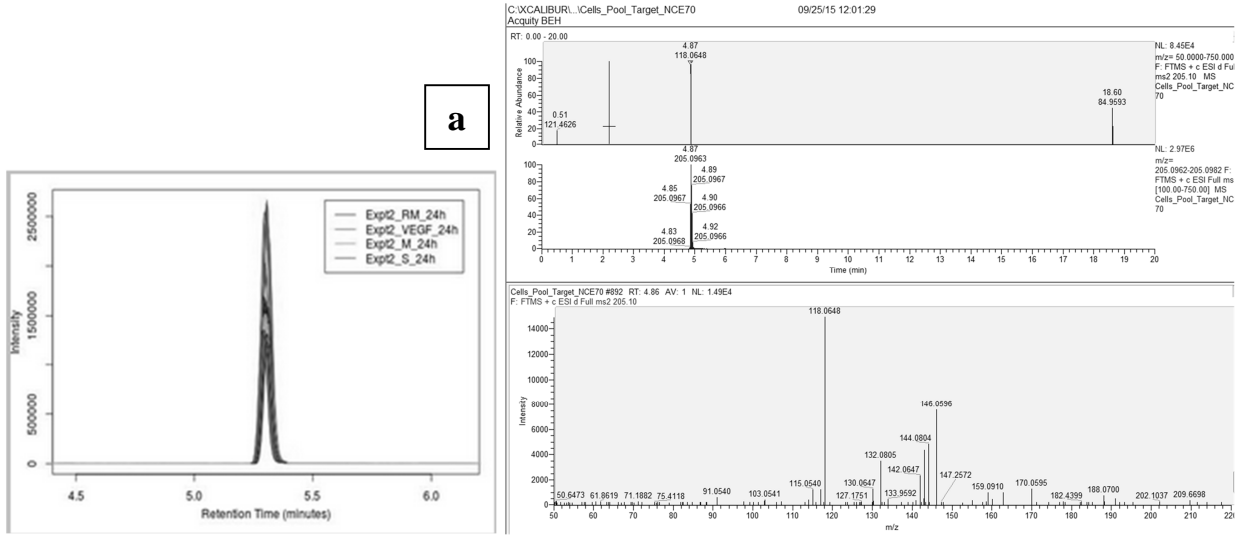
Names
Compound Name: L-Glutathione (reduced)

c

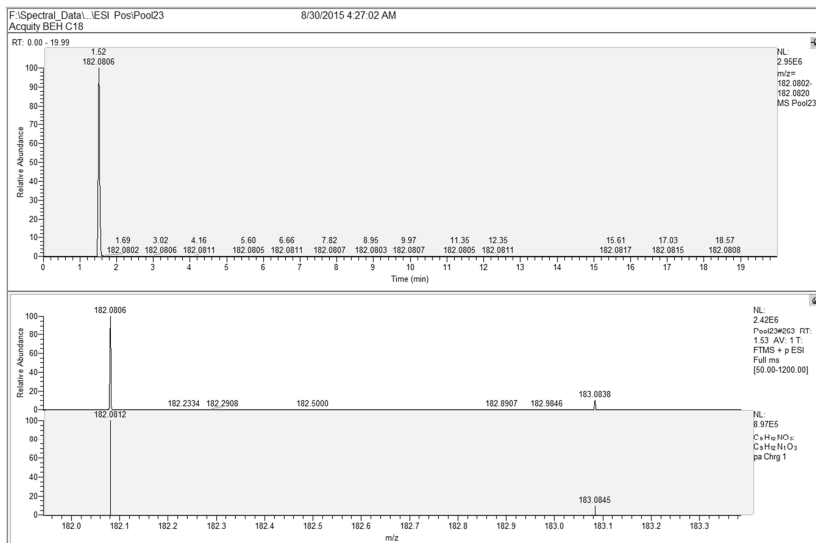
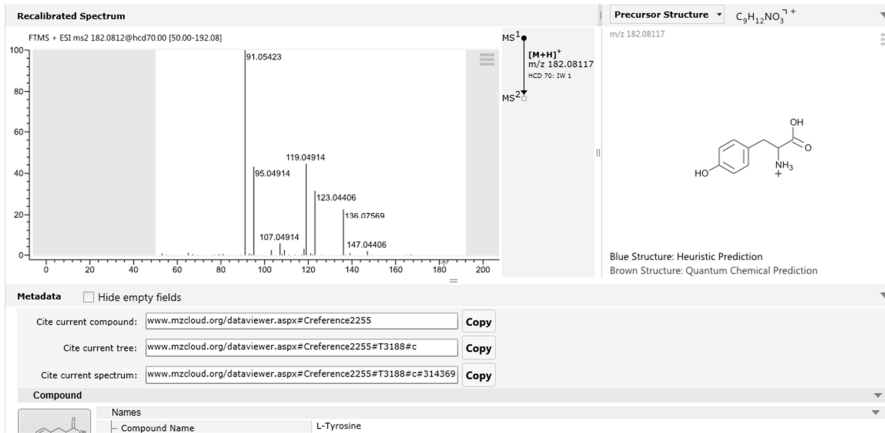
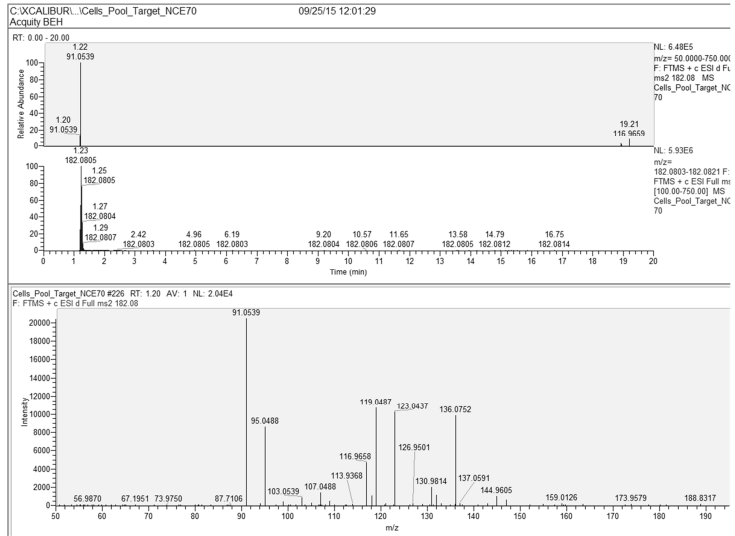
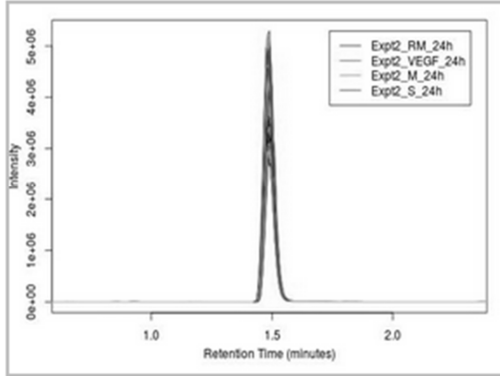


d

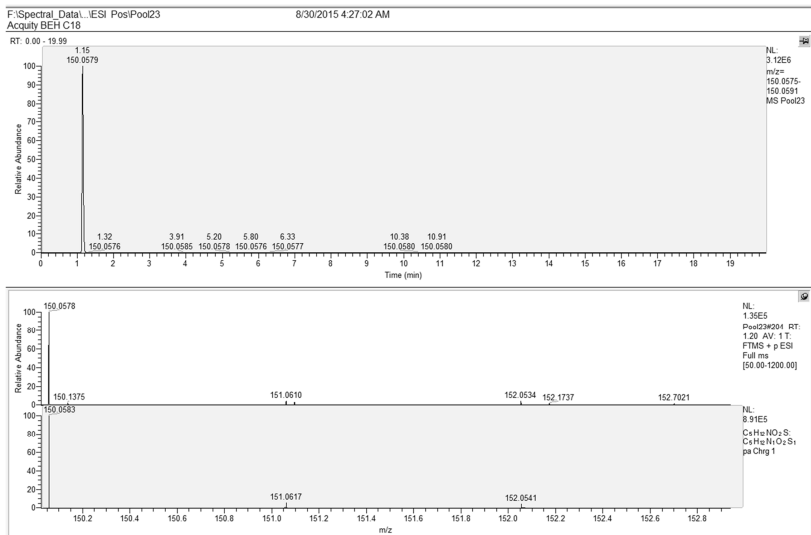
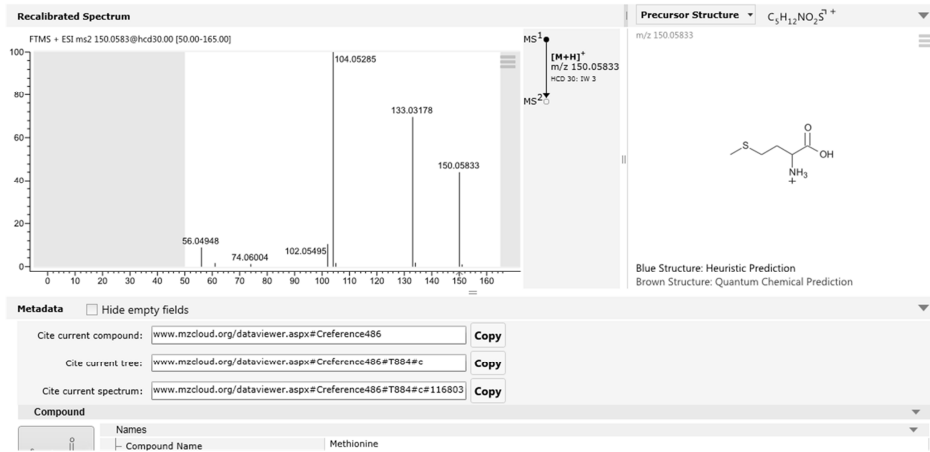
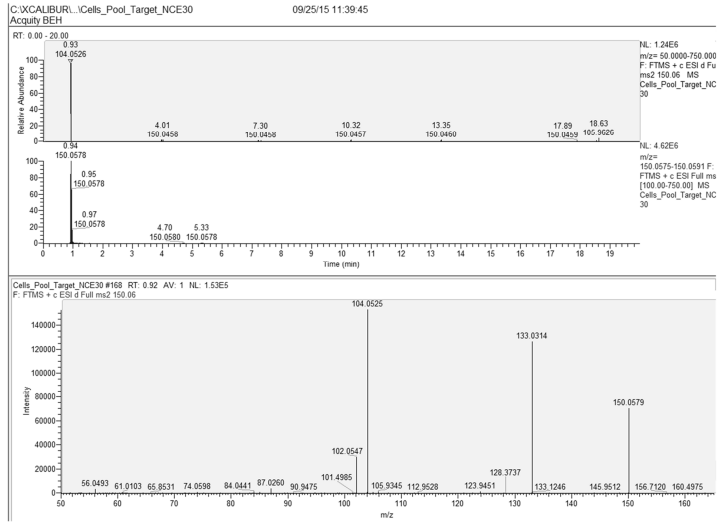
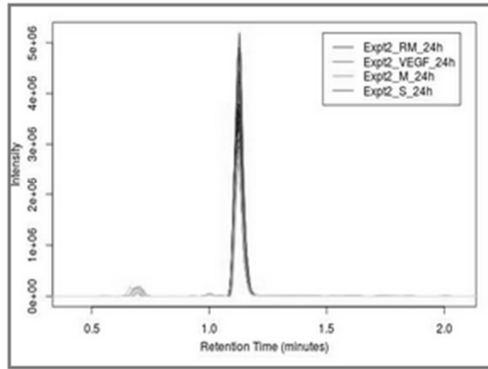
L-Tryptophan



L-Tyrosine

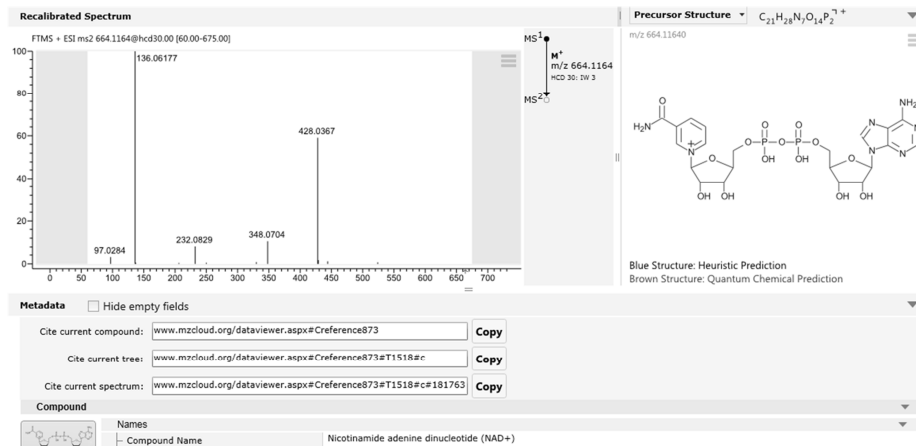
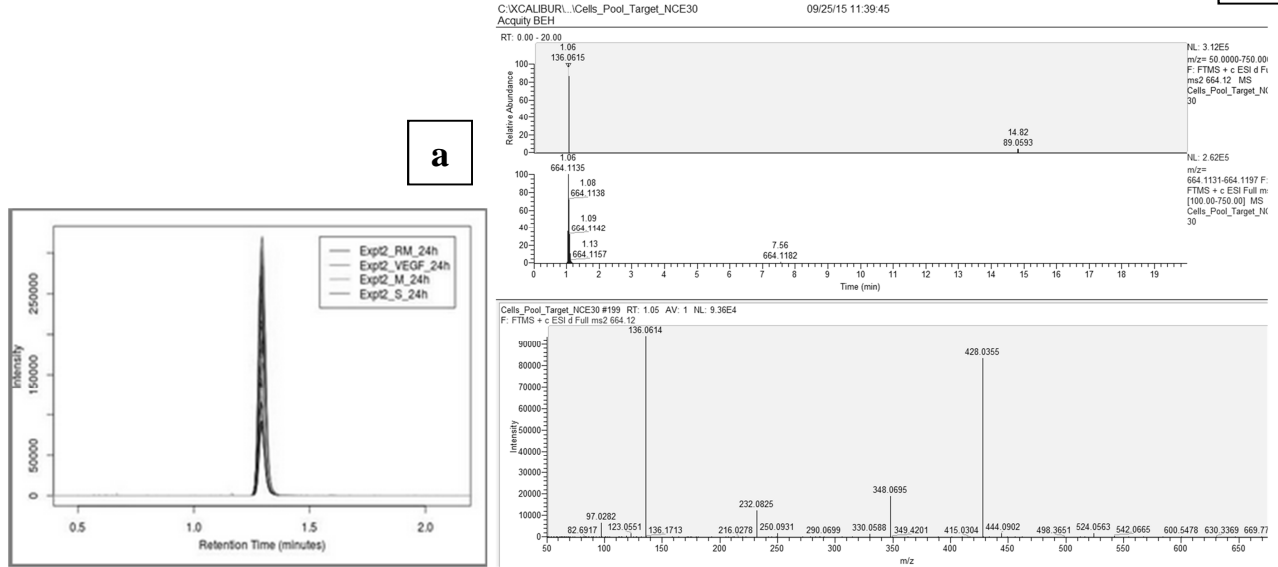


L-Methionine

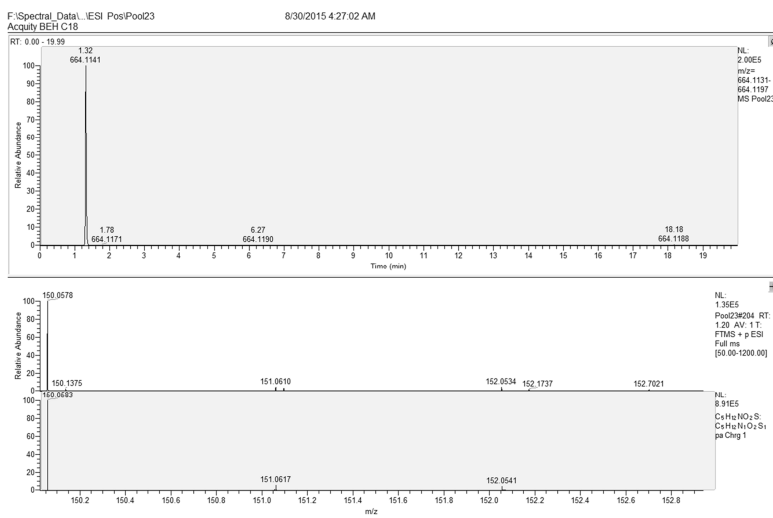


Nicotinamide dinucleotide (NAD⁺)

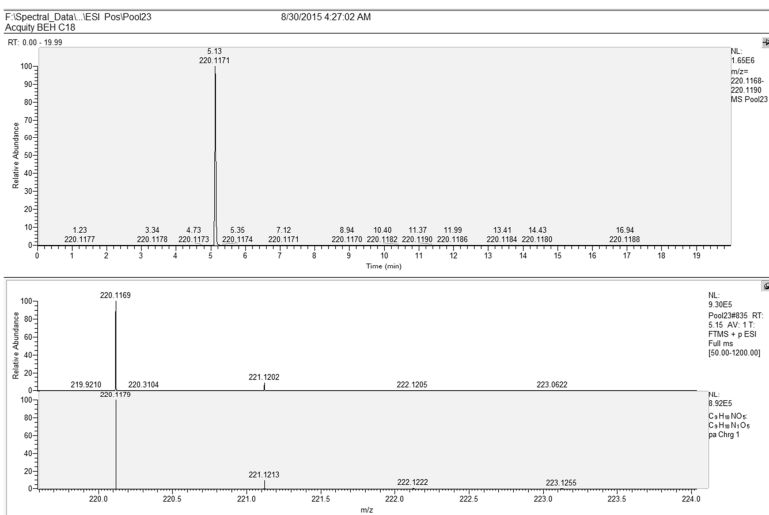
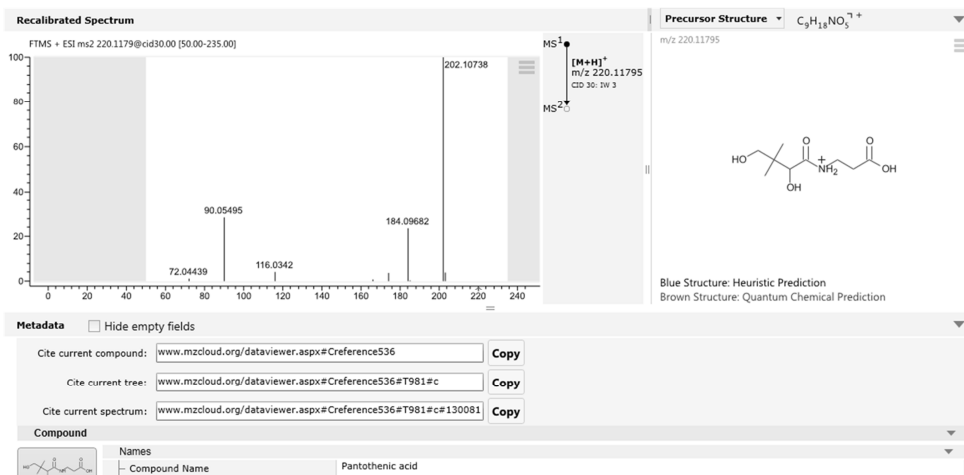
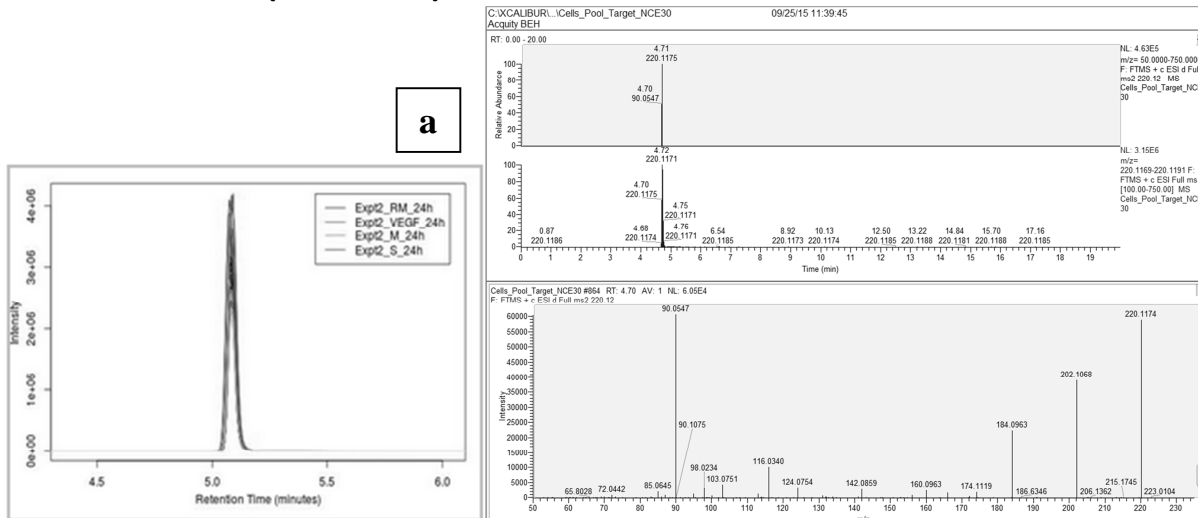
b



c



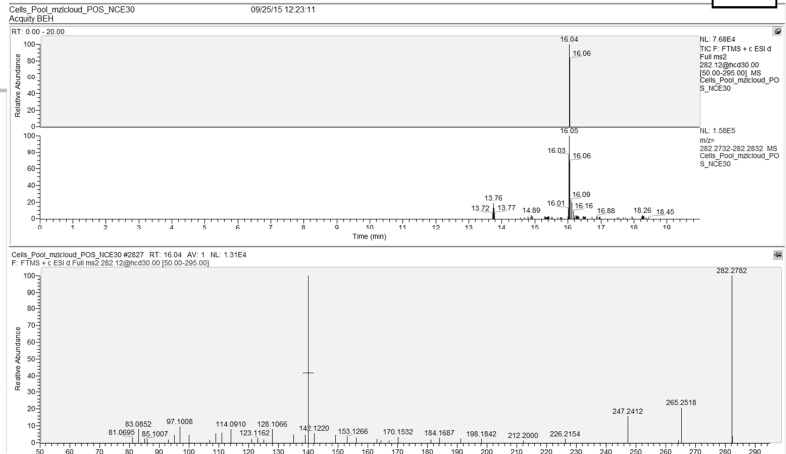
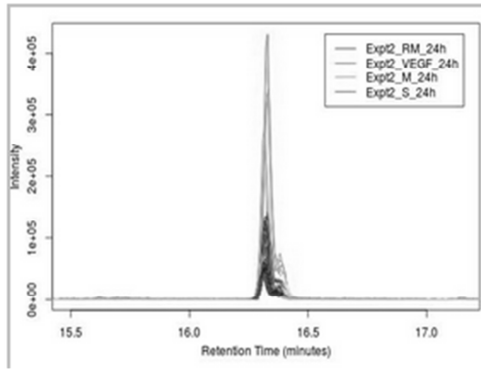
Pantothenic acid (CID match)



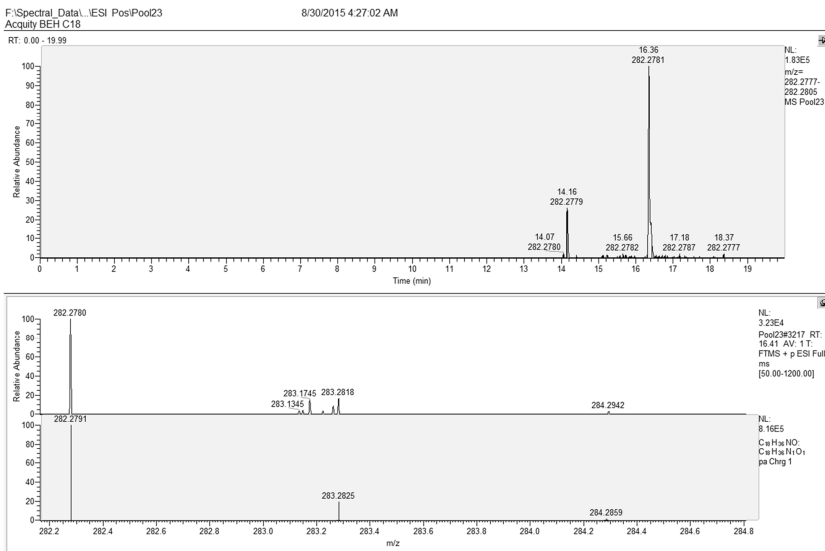
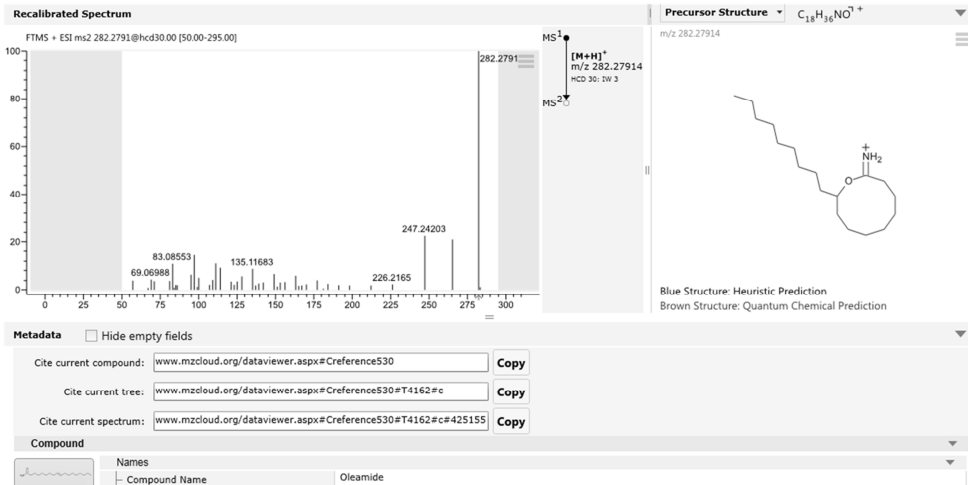
Oleamide

b

a

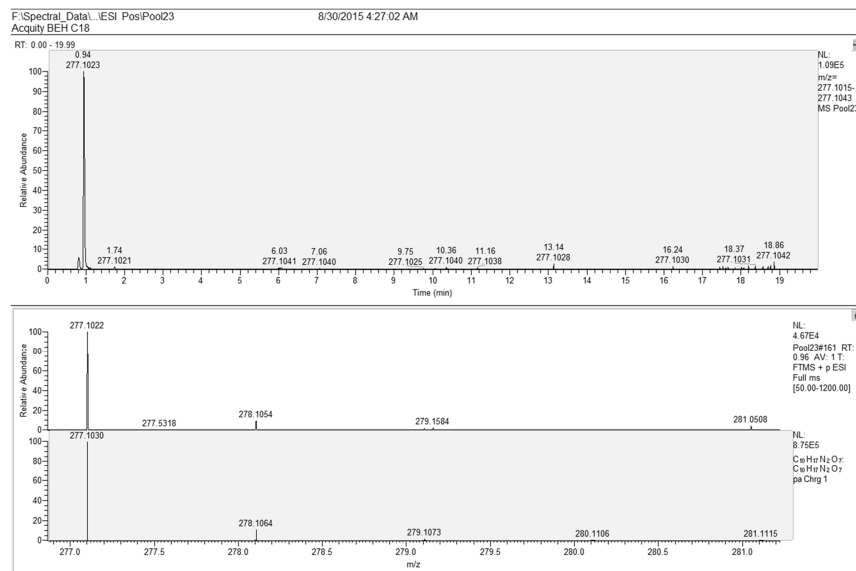
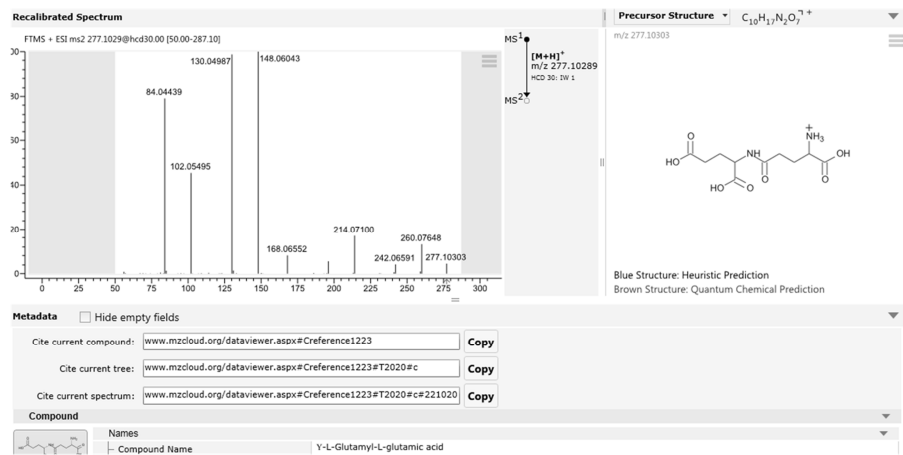
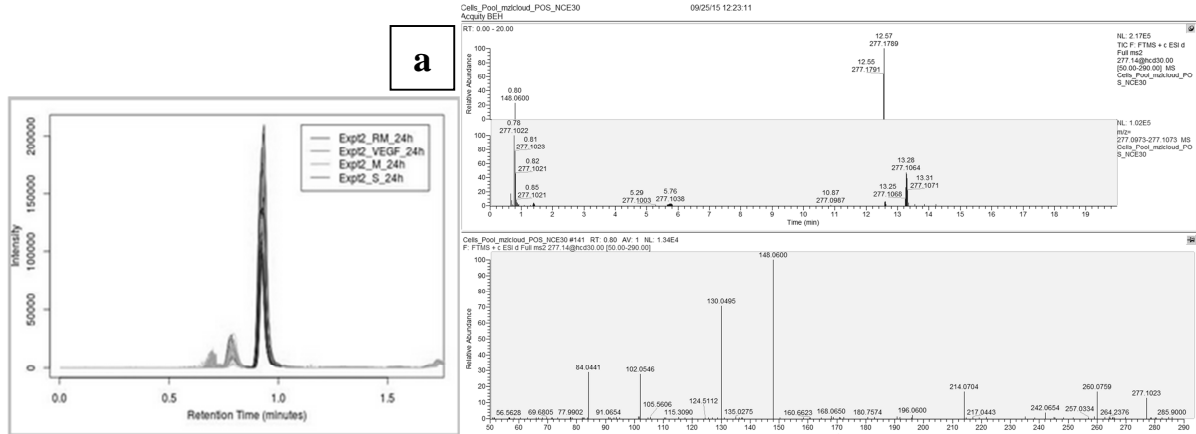


c

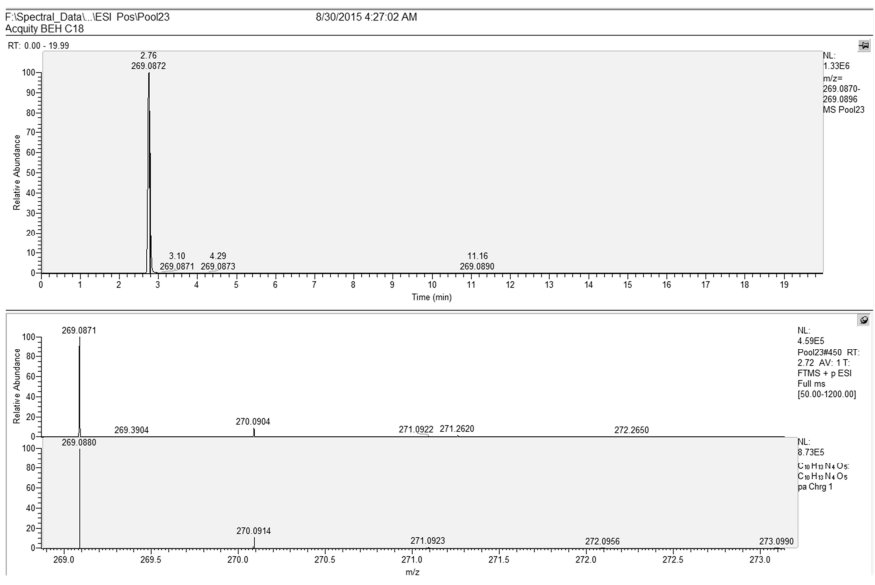
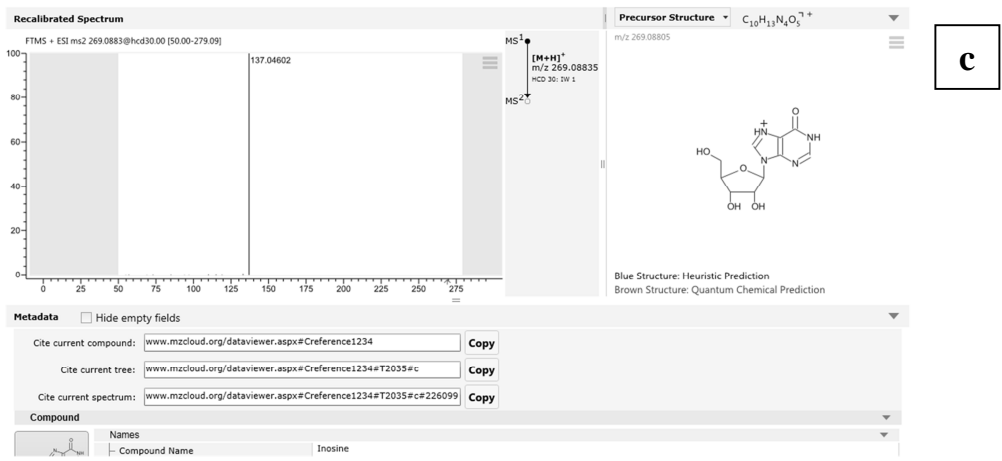
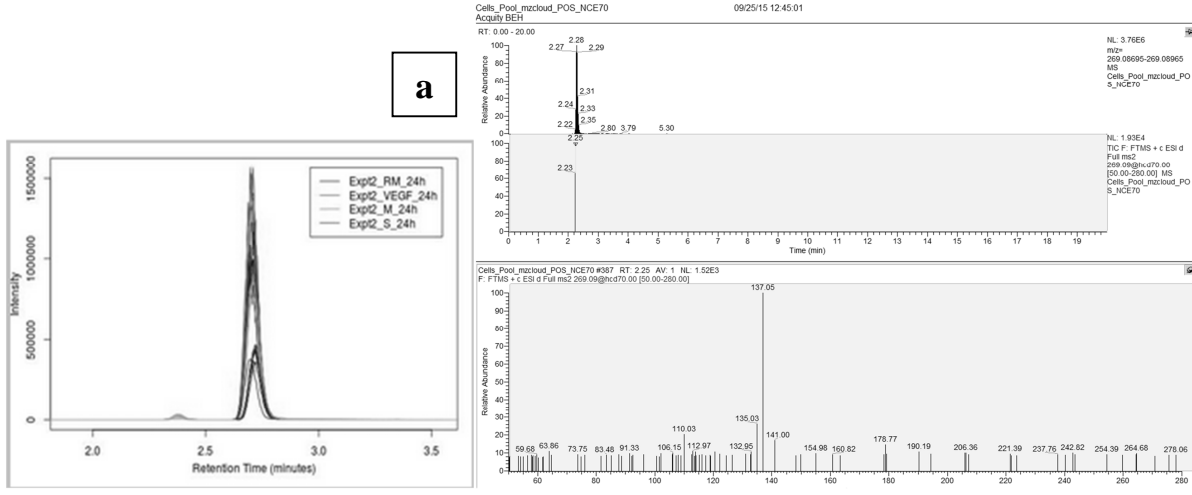


d

Y-L-Glutamyl-L-Glutamic acid

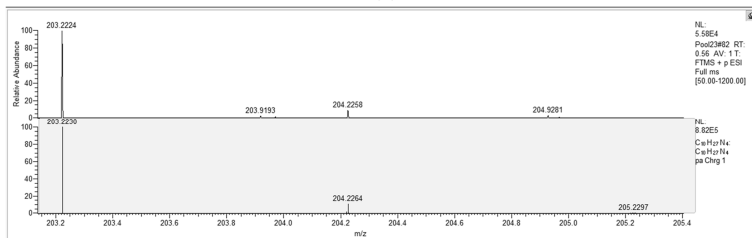
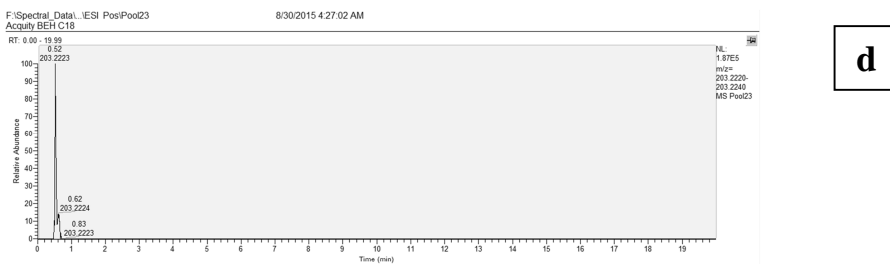
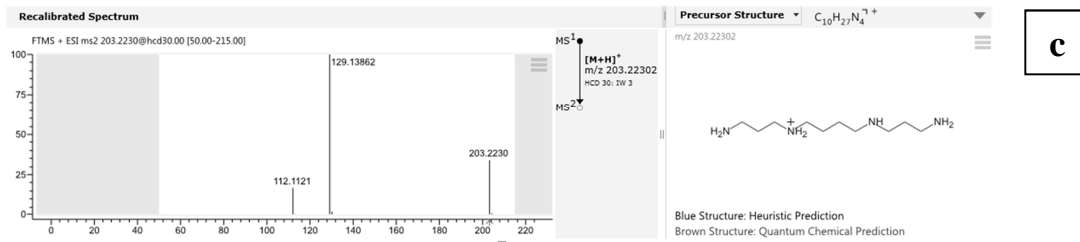
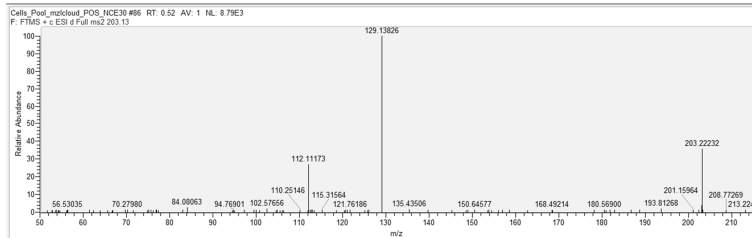
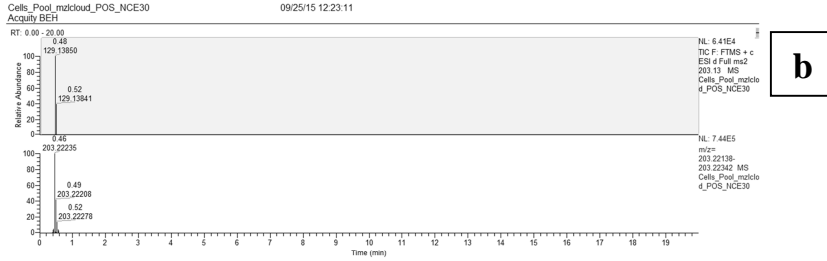


Inosine

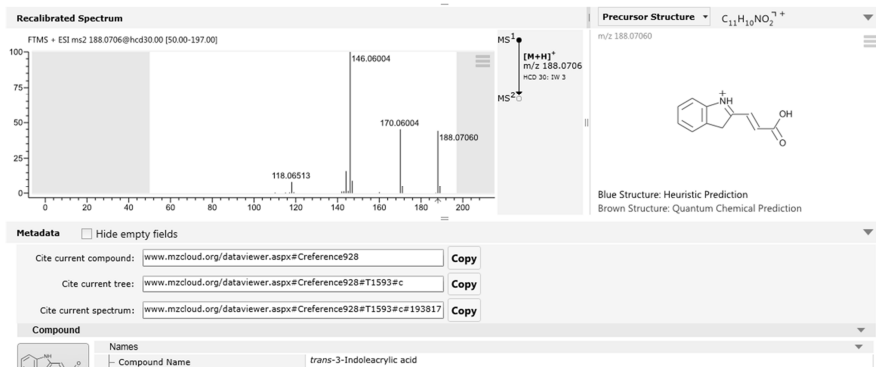
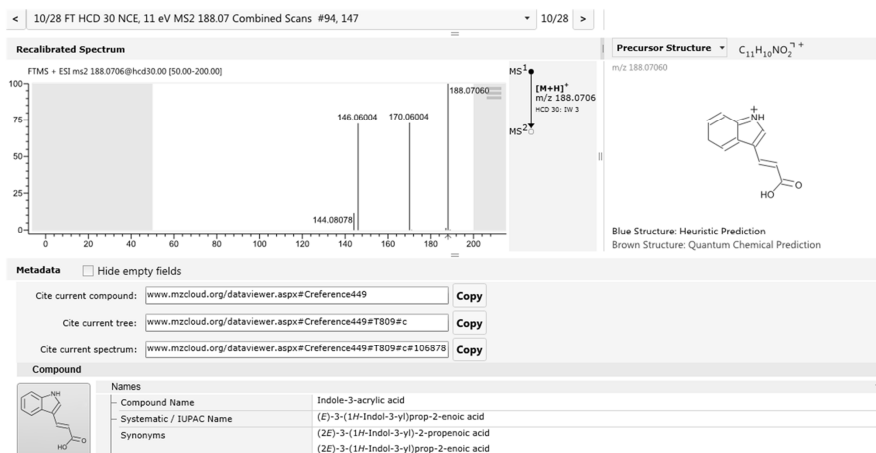
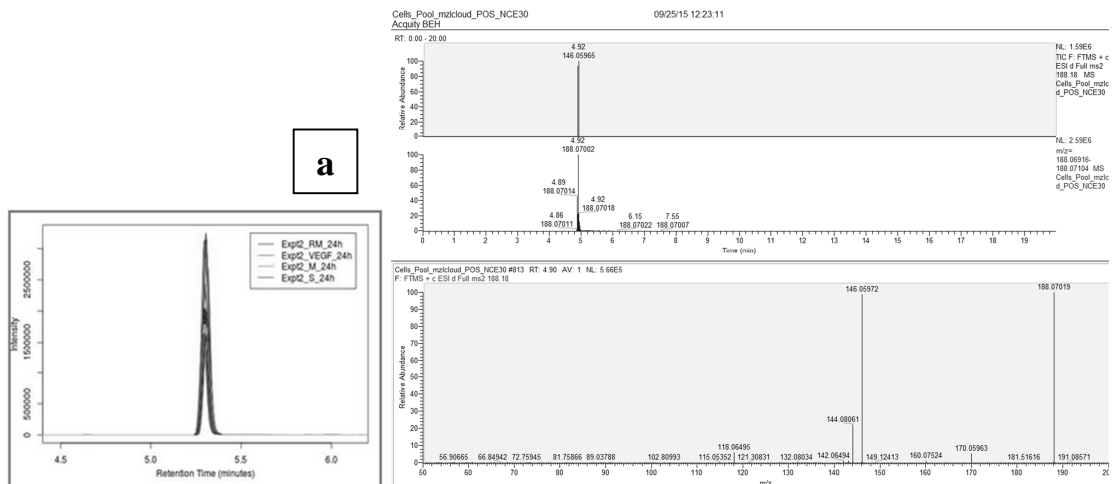


Spermine

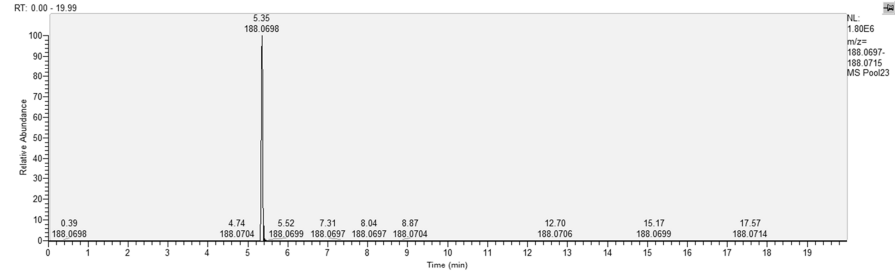
a. Peak not shown in XCMS Online as $p > 0.05$.



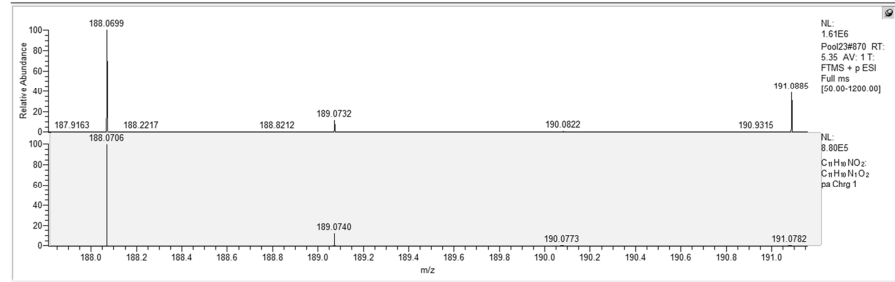
Indole 3-acrylic acid / *trans* 3-Indole acrylic acid



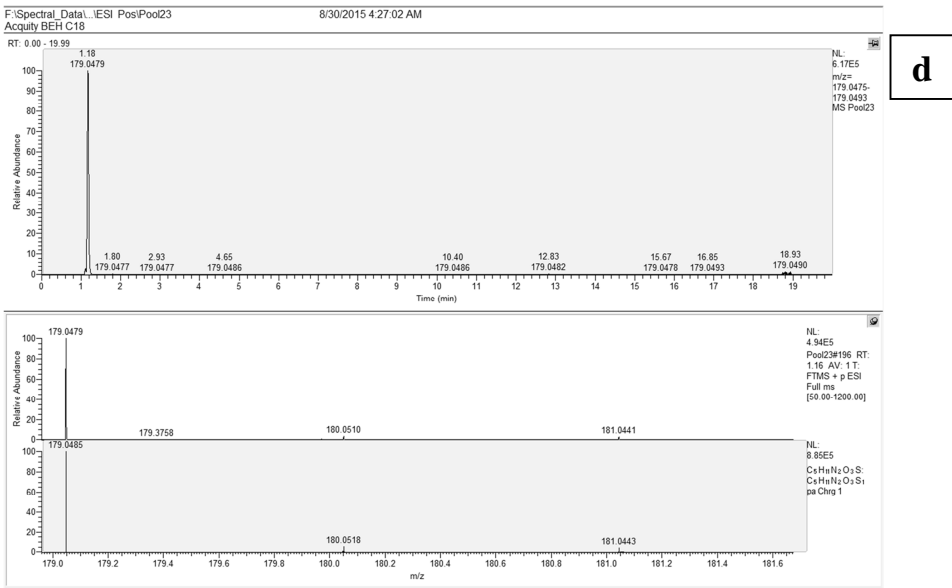
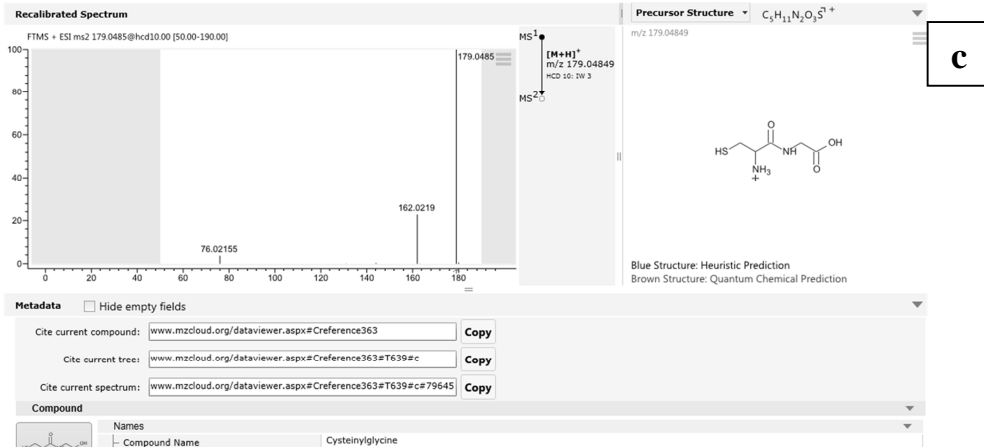
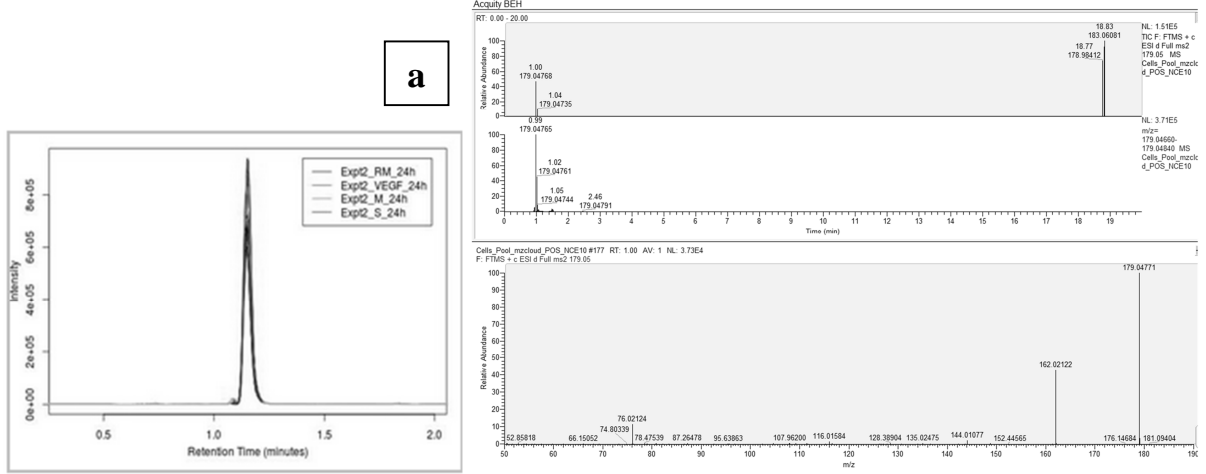
F:\Spectral_Data\1.E51 PosiPool23 8/30/2015 4:27:02 AM
Acquity BEH C18



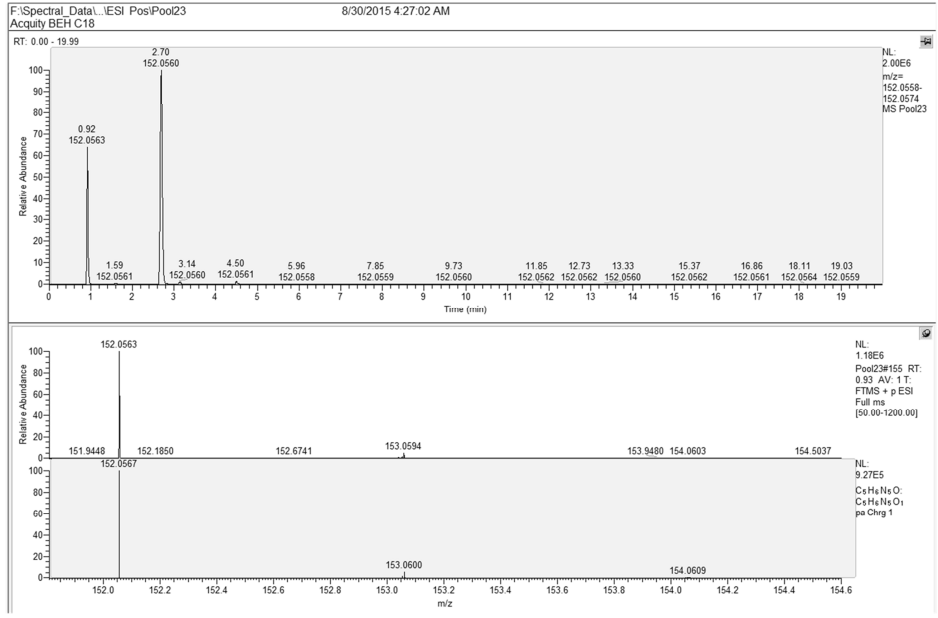
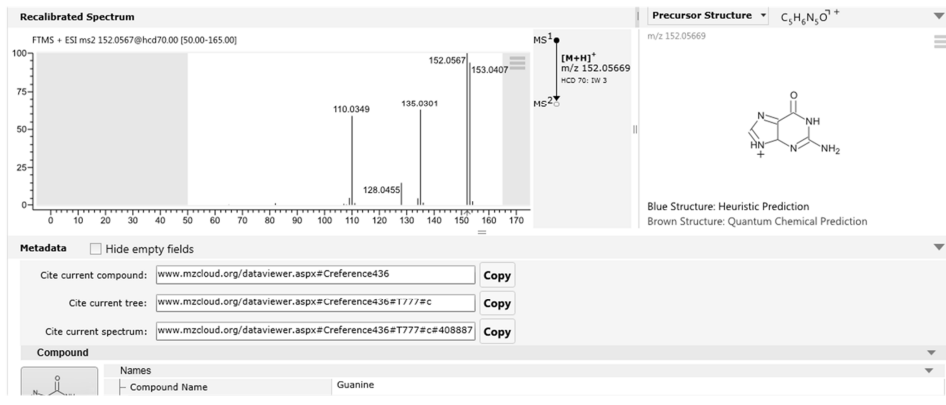
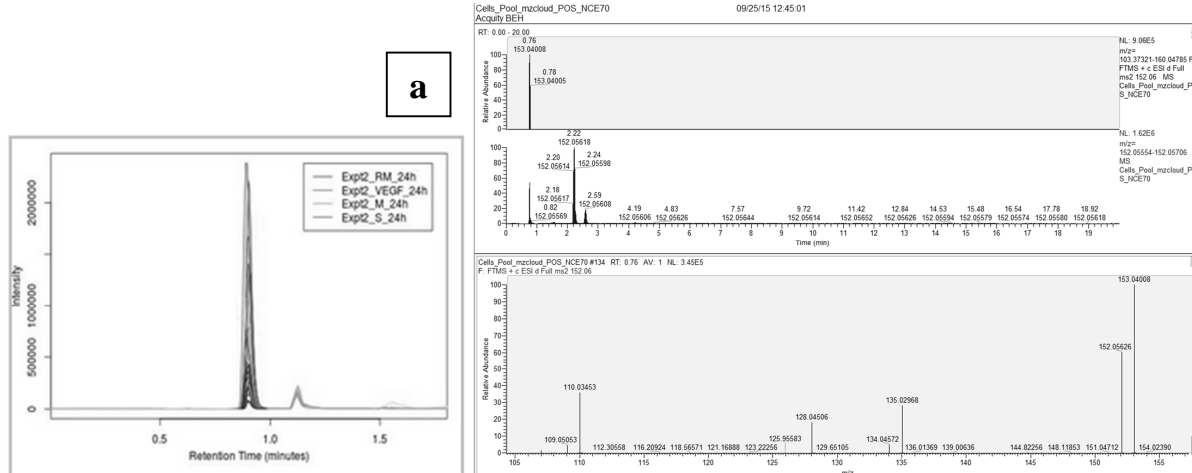
d



Cysteinylglycine

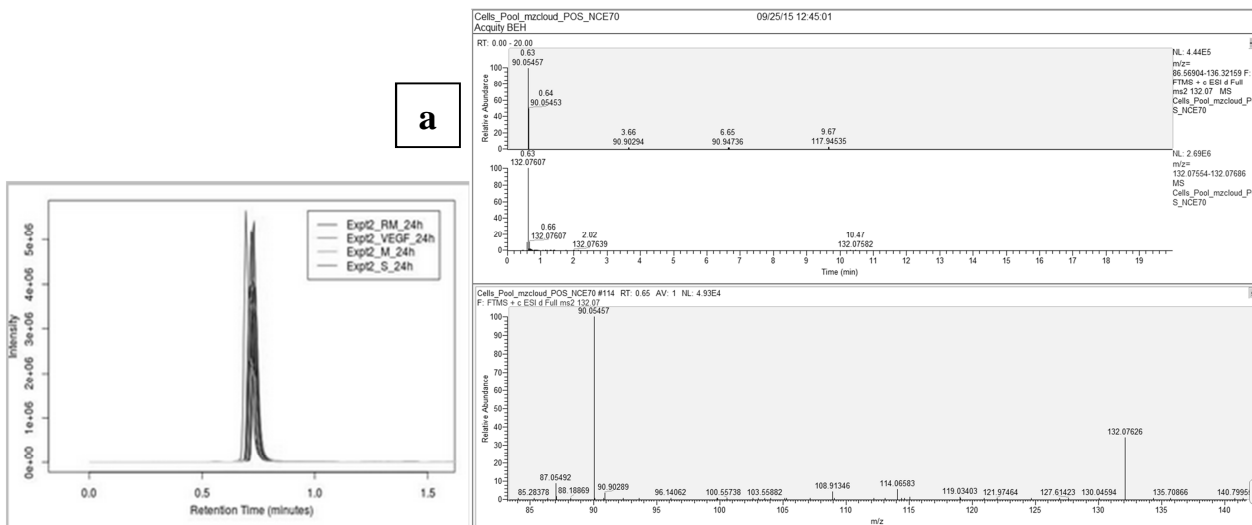


Guanine

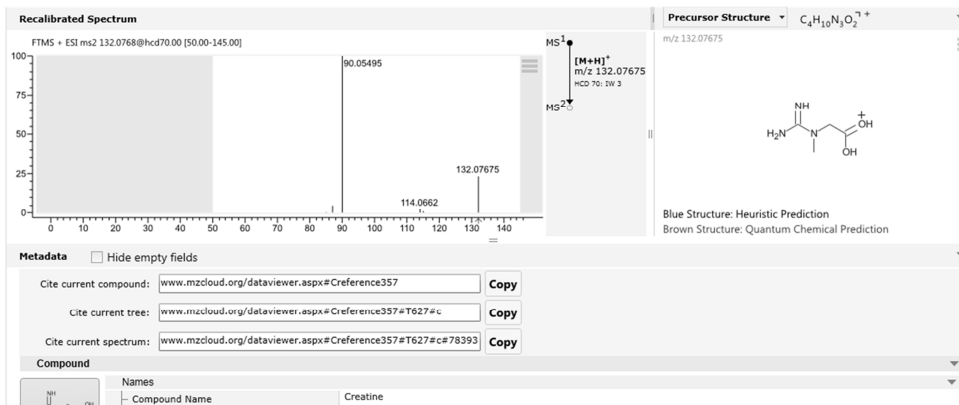


Creatine

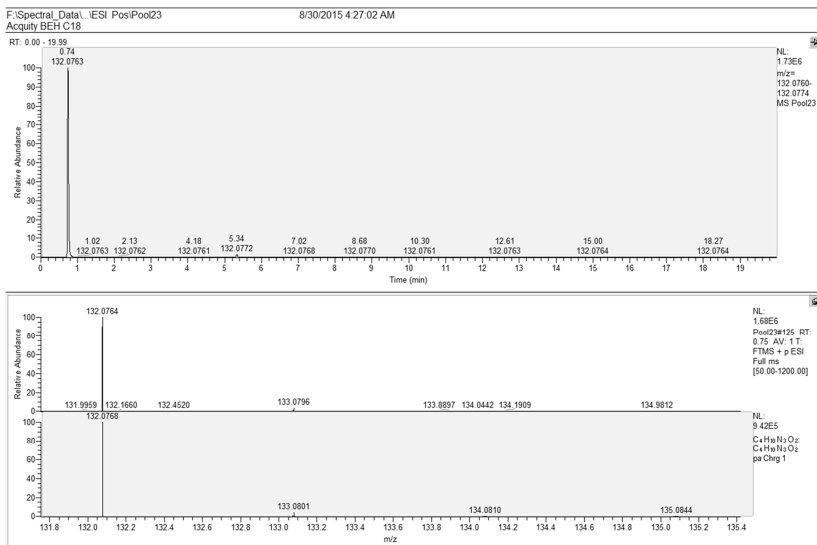
b



c



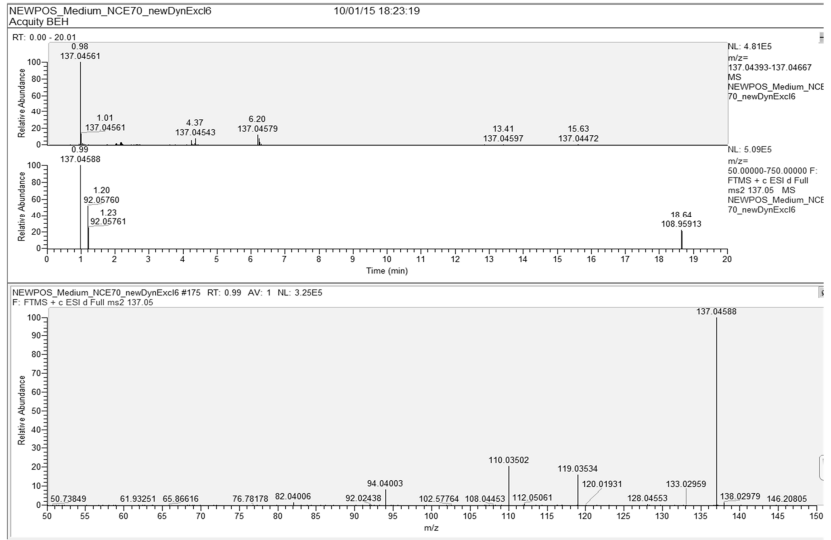
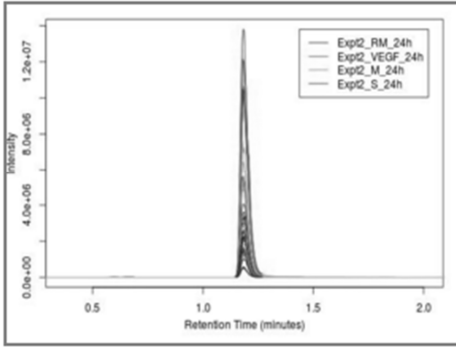
d



Hypoxanthine (RT 1.19 min)

b

a



c

Recalibrated Spectrum
FTMS + ESI ms2 137.0458@hcd70.00 [50.00-150.00]

Precursor Structure $C_5H_7N_2O^+$
m/z 137.04579

Blue Structure: Heuristic Prediction
Brown Structure: Quantum Chemical Prediction

Metadata Hide empty fields

Cite current compound: www.mzcloud.org/dataviewer.aspx#Reference441 **Copy**

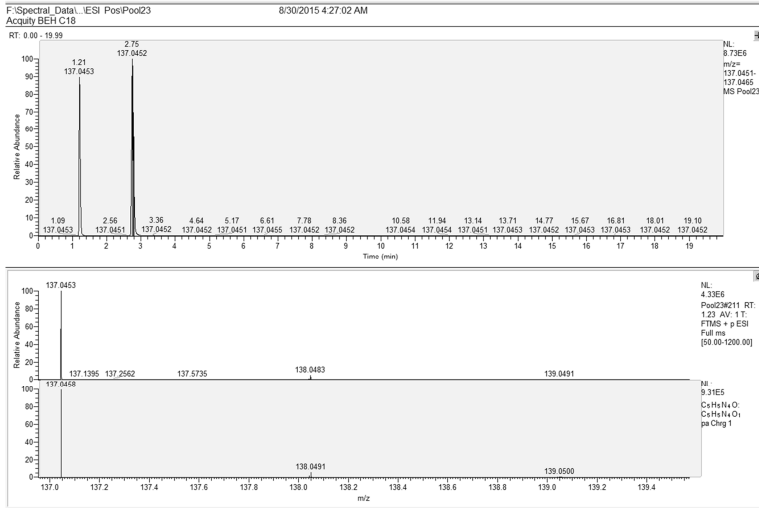
Cite current tree: www.mzcloud.org/dataviewer.aspx#Reference441#T789#c **Copy**

Cite current spectrum: www.mzcloud.org/dataviewer.aspx#Reference441#T789#c#104144 **Copy**

Compound

Names	Compound Name
	Hypoxanthine

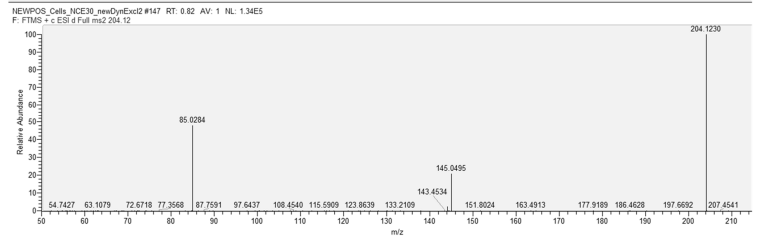
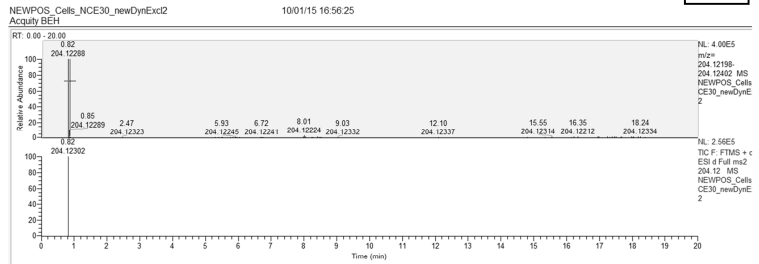
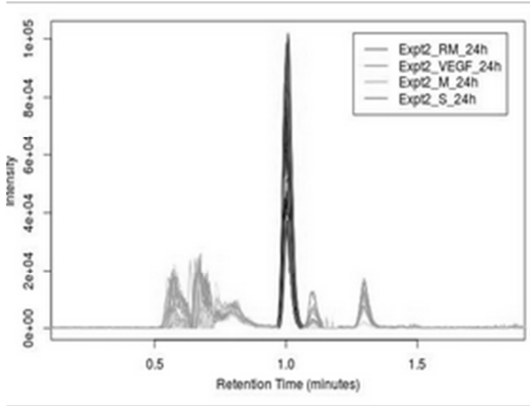
d



Acetyl L-Carnitine

b

a



c

Recalibrated Spectrum

FTMS + ESI+ ms2 204.1230@hcd30,00 [50,00-215,00]

Precursor Structure $C_9H_{18}NO_4^{-1}$

m/z 204.12303

Blue Structure: Heuristic Prediction
Brown Structure: Quantum Chemical Predictor

Metadata Hide empty fields

Cite current compound: <https://www.mzcloud.org/DataViewer.aspx#Reference879> **Copy**

Cite current tree: <https://www.mzcloud.org/DataViewer.aspx#Reference879#T1526#c> **Copy**

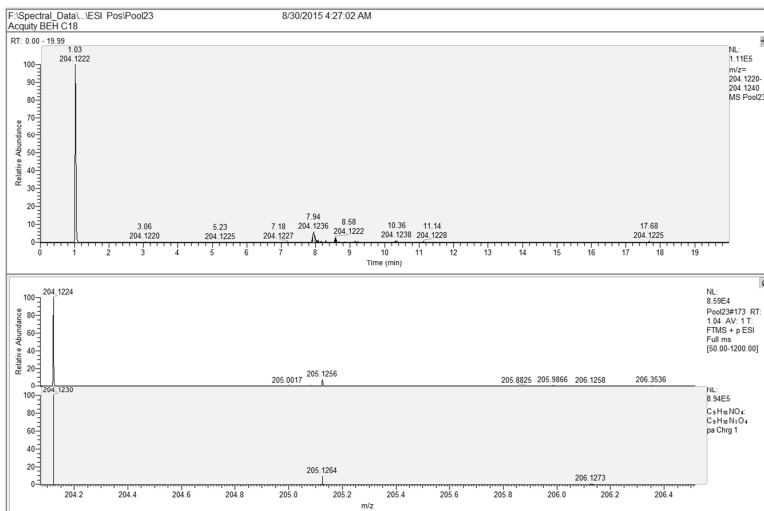
Cite current spectrum: <https://www.mzcloud.org/DataViewer.aspx#Reference879#T1526#c#186907> **Copy**

Compound

Names

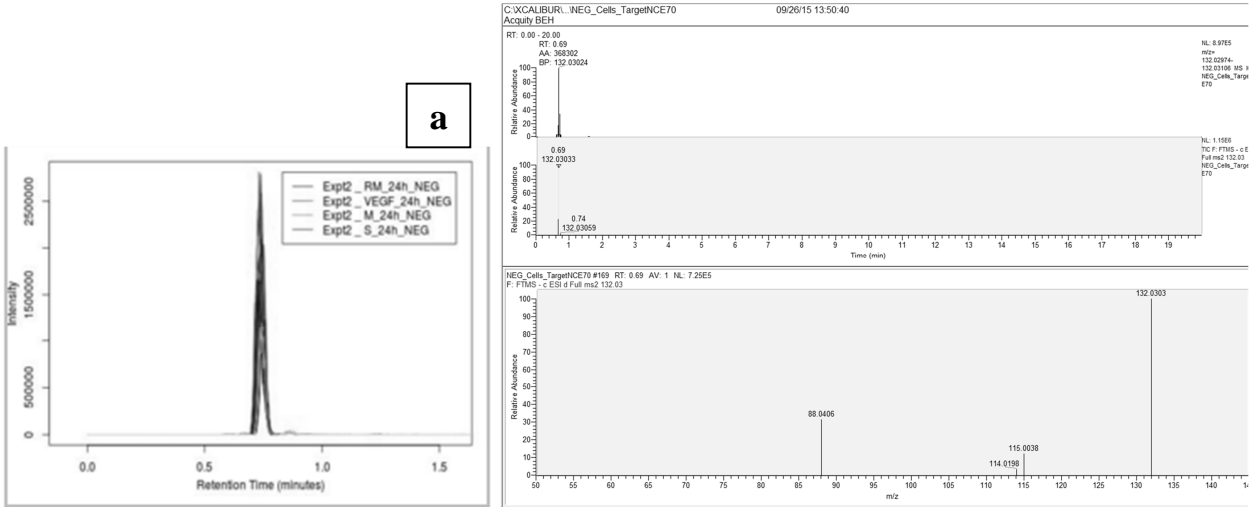
Compound Name: Acetyl-L-carnitine

d

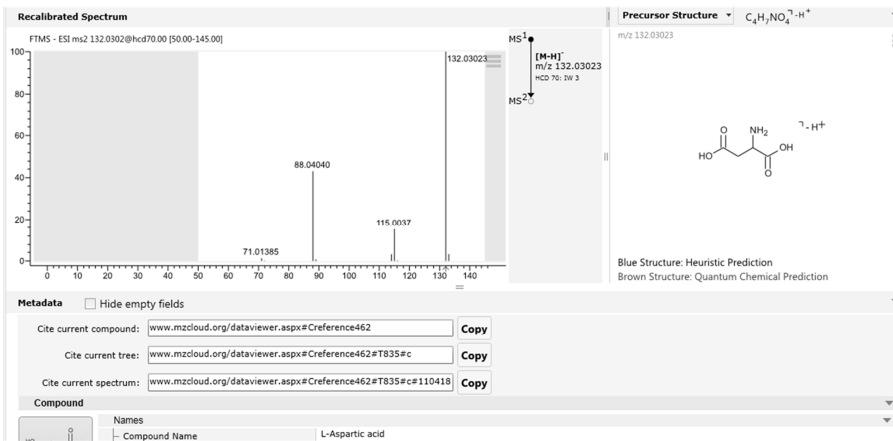


L-Aspartate

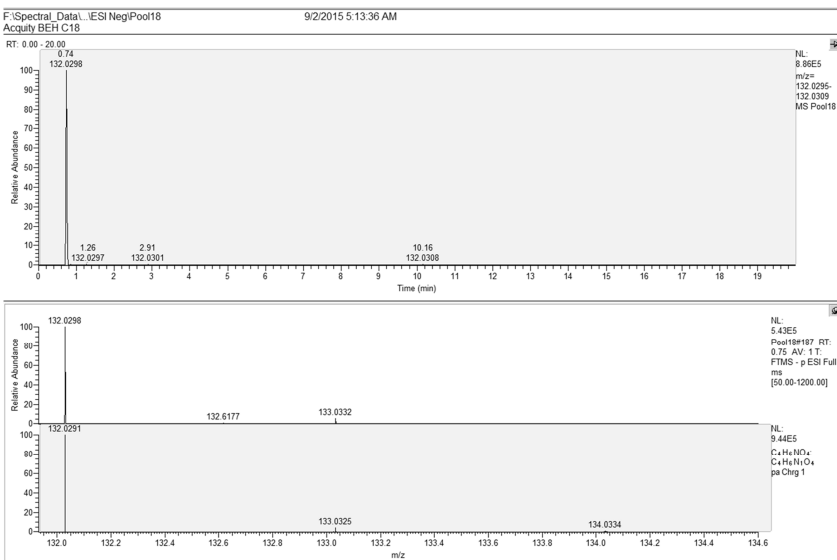
b



c

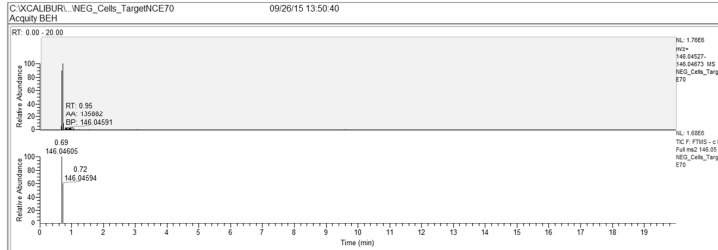


d

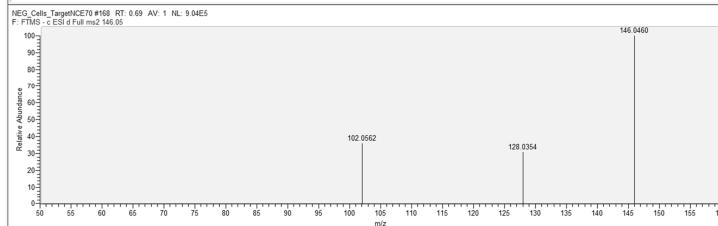


L- Glutamate (ESI-)

a. Peak not displayed in XCMS Online as $p > 0.05$.



b



Recalibrated Spectrum
FTMS - ESI ms2 146.0459@hd470.00 [50.00-160.00]

Metadata Hide empty fields

Cite current compound: www.mzcloud.org/dataviewer.aspx#Reference470 **Copy**

Cite current tree: www.mzcloud.org/dataviewer.aspx#Reference470#T852#c **Copy**

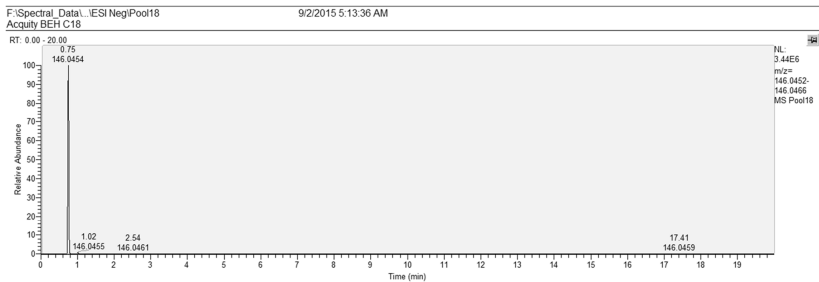
Cite current spectrum: www.mzcloud.org/dataviewer.aspx#Reference470#T852#c#112839 **Copy**

Compound

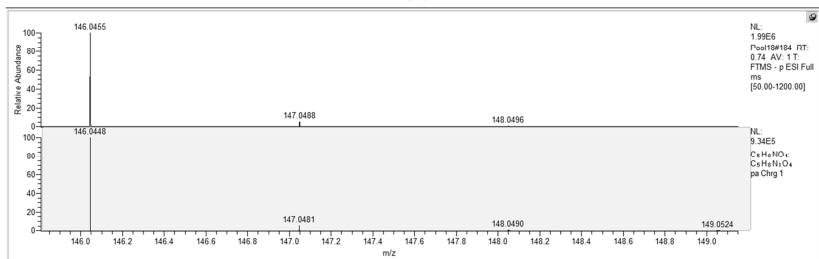
Names

Compound Name: L-Glutamic acid

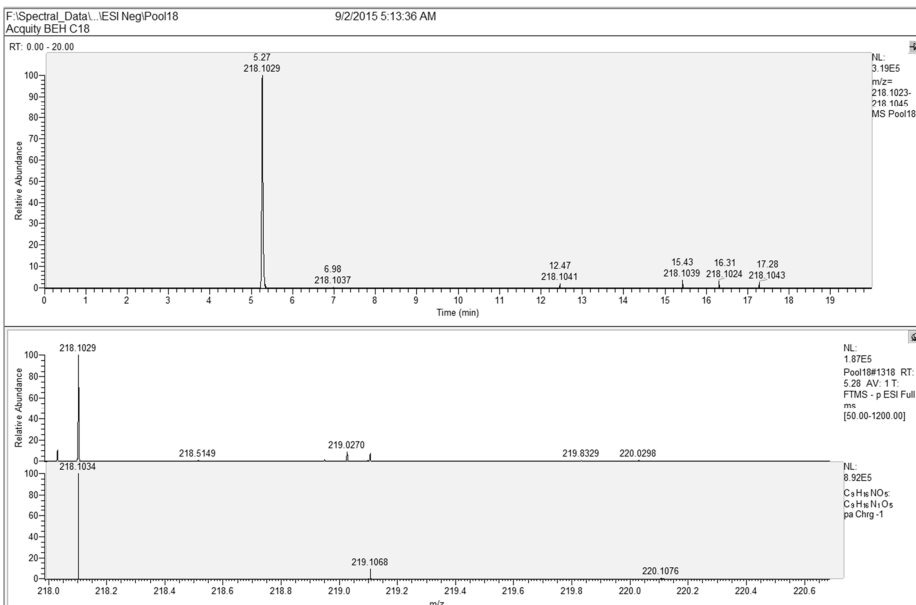
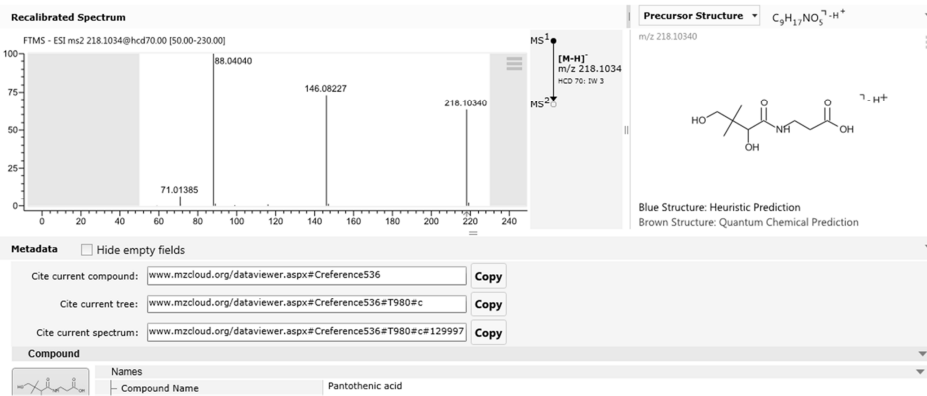
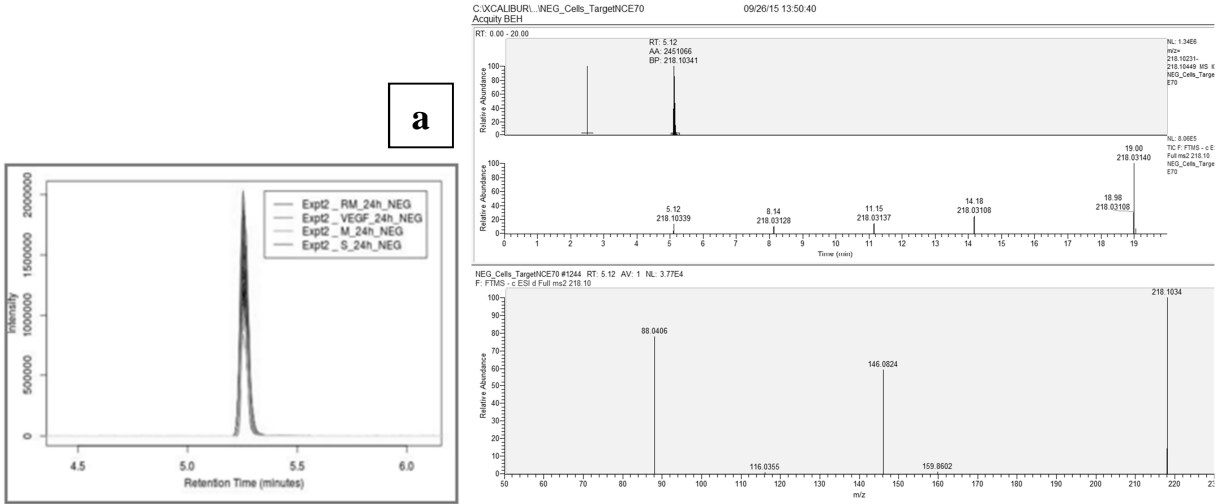
c



d



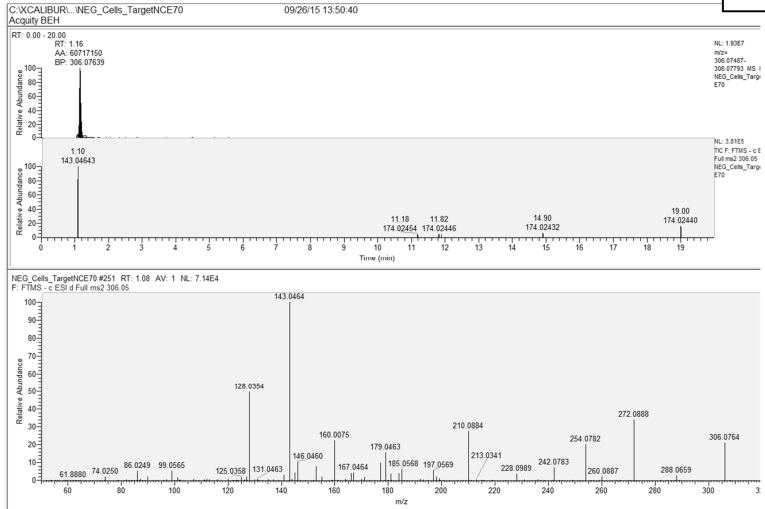
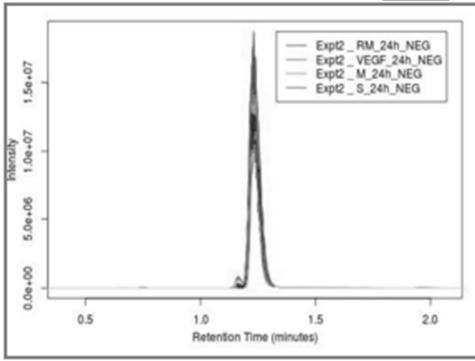
Pantothenic acid (ESI-)



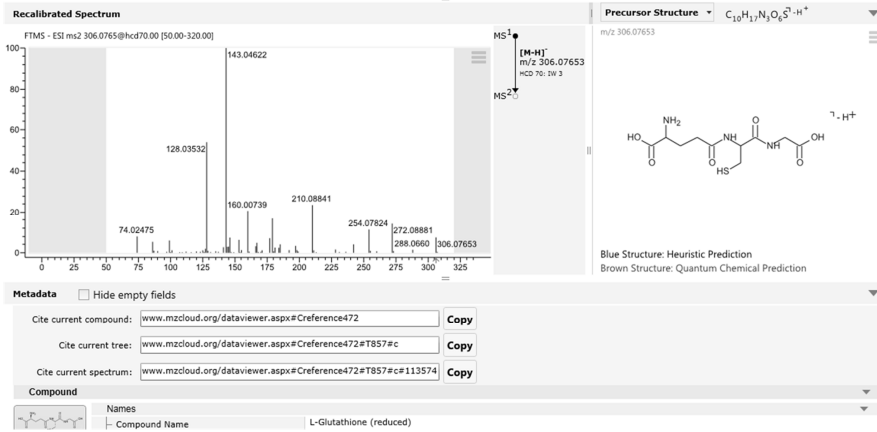
L-Glutathione reduced (ESI-)

b

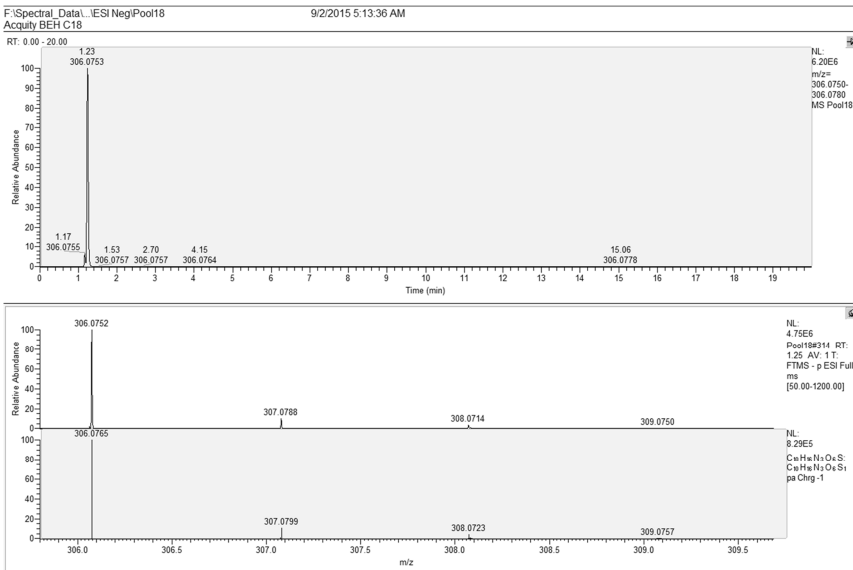
a



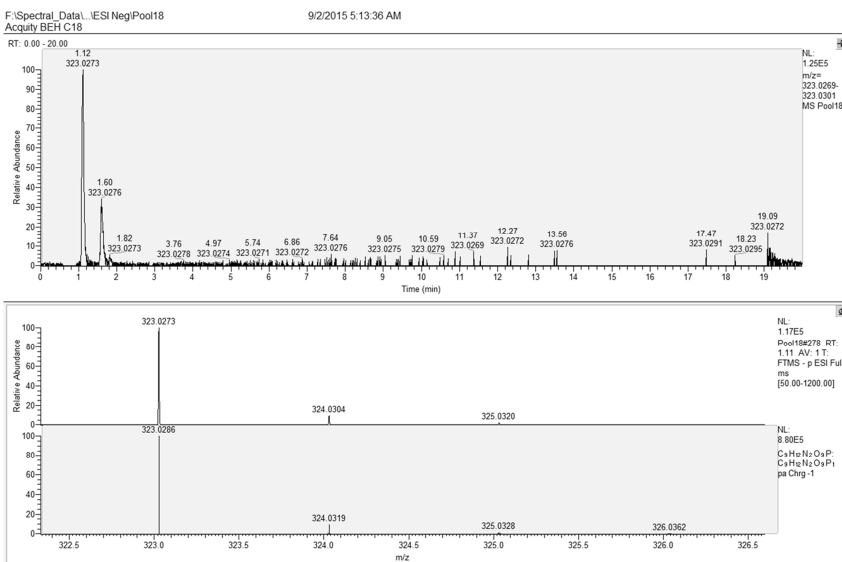
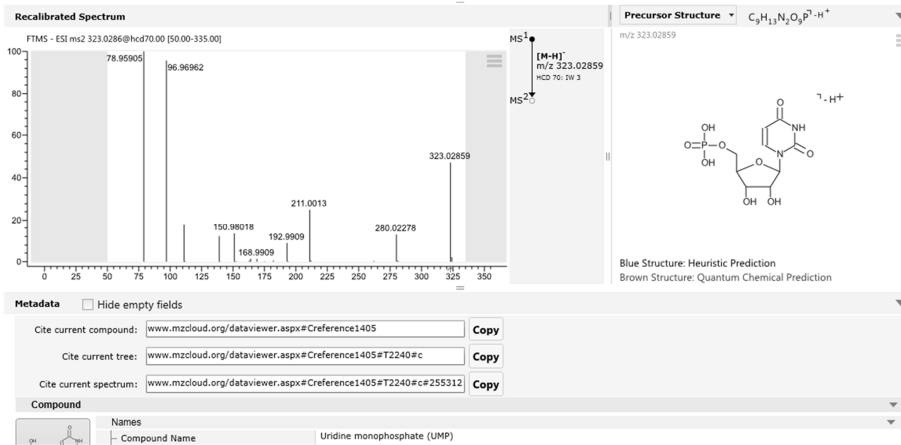
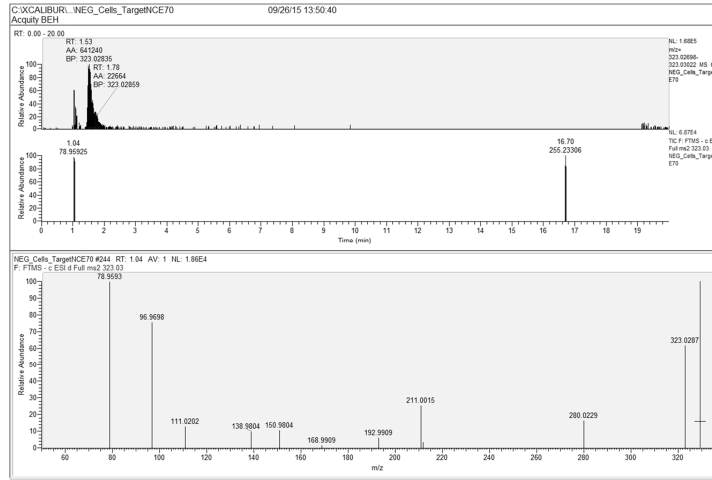
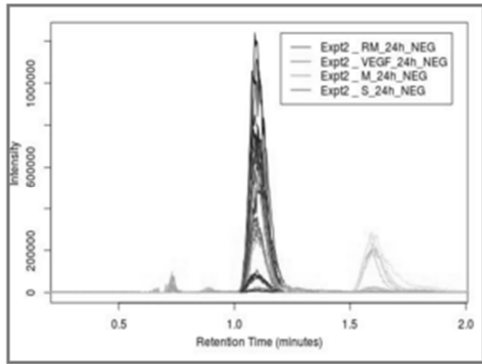
c



d

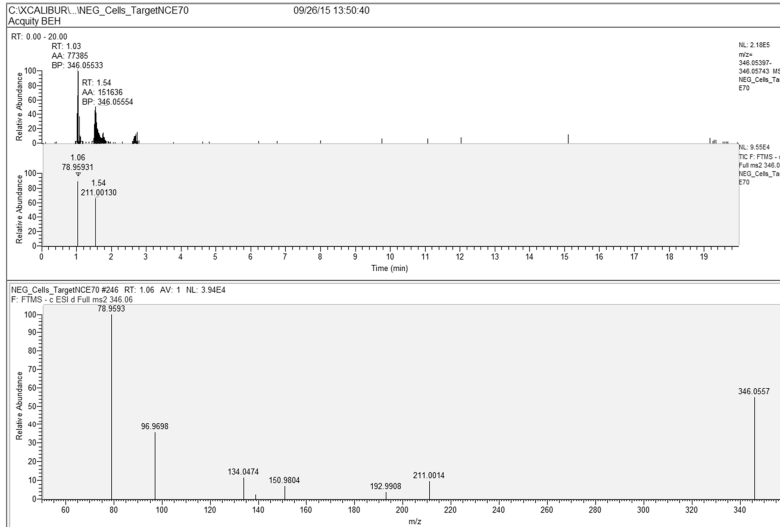


Uridine monophosphate (UMP)

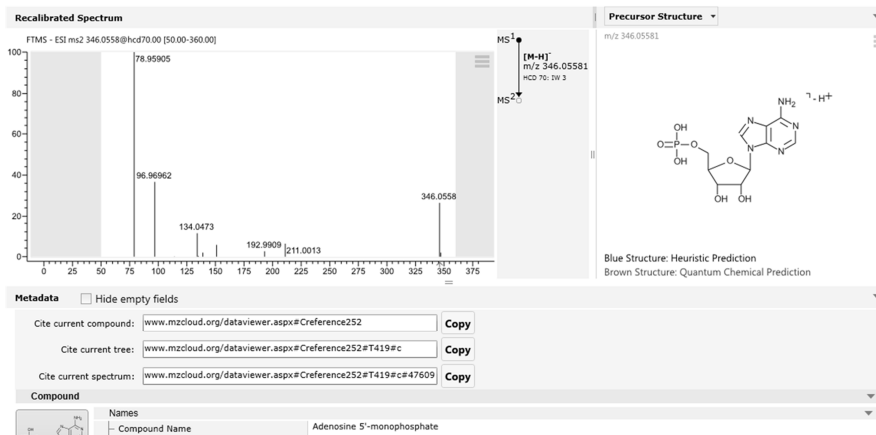


Adenosine monophosphate (AMP)

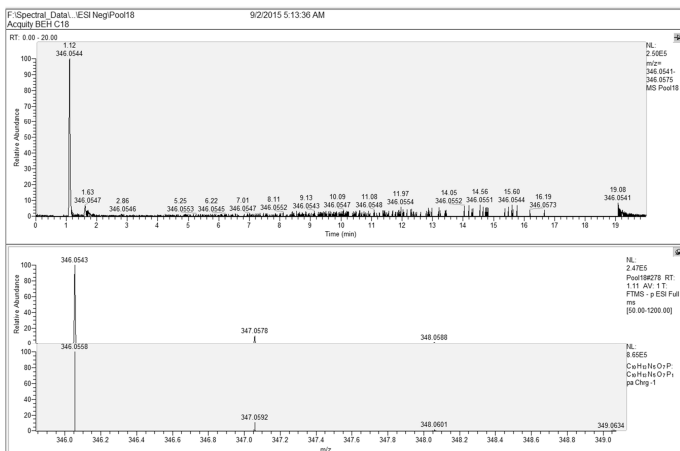
a. Peak not displayed in XCMS Online as $p > 0.05$.



b



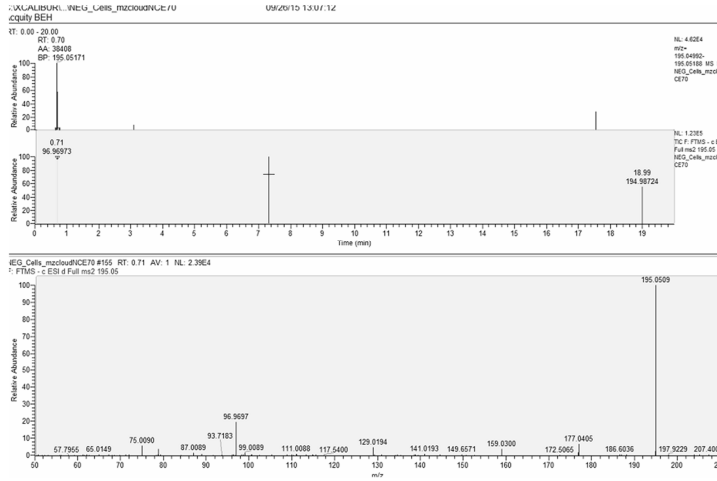
c



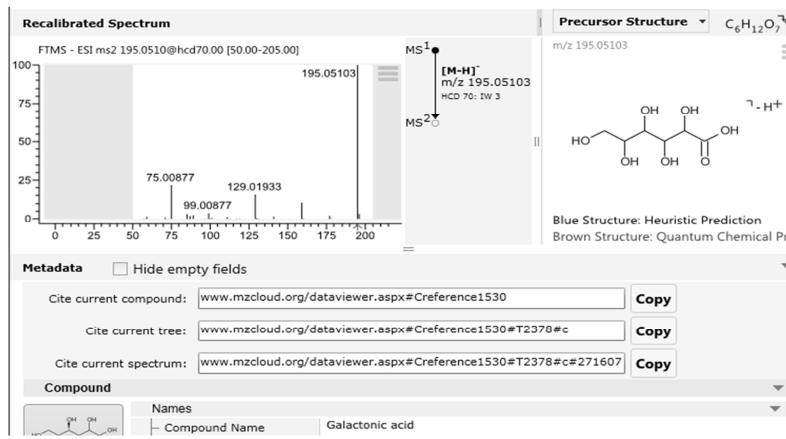
d

Galactonic acid

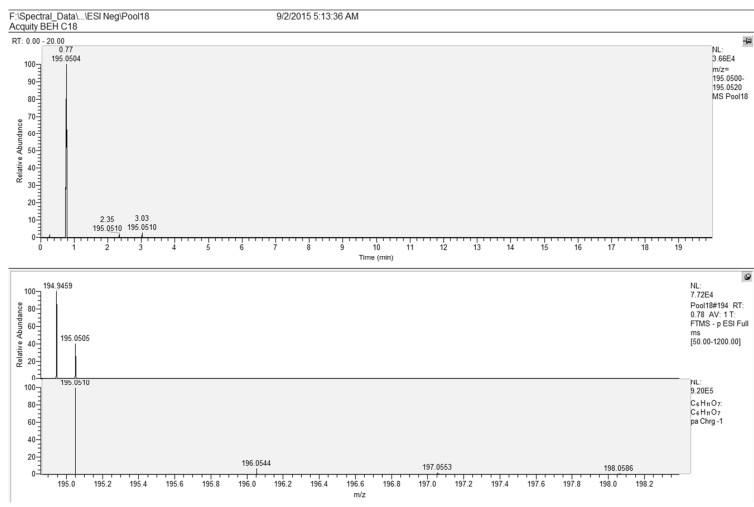
a. Peak not displayed in XCMS Online as $p > 0.05$.



b

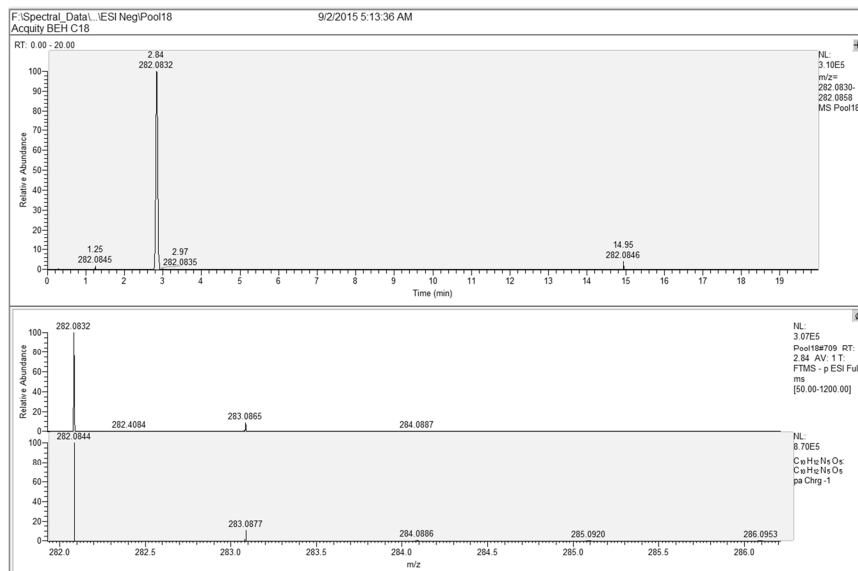
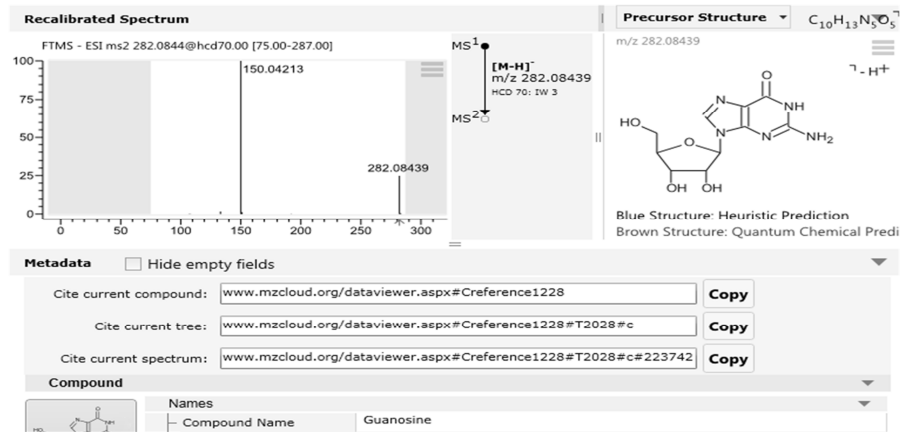
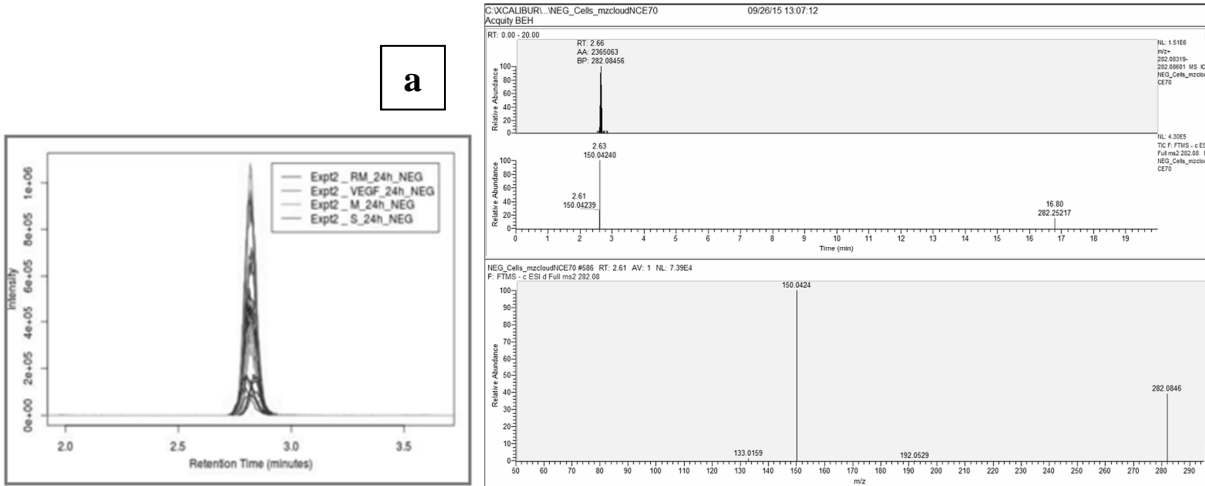


c



d

Guanosine



References

1. Gowda H, Ivanisevic J, Johnson CH *et al.*: Interactive XCMS Online: simplifying advanced metabolomic data processing and subsequent statistical analyses. *Analytical chemistry* 86(14), 6931-6939 (2014).
2. Tautenhahn R, Patti GJ, Rinehart D, Siuzdak G: XCMS Online: a web-based platform to process untargeted metabolomic data. *Analytical chemistry* 84(11), 5035-5039 (2012).

12. APPENDIX 5

For reprint orders, please contact reprints@future-science.com

Cancer cell metabolism as new targets for novel designed therapies

Metabolic processes are altered in cancer cells, which obtain advantages from this metabolic reprogramming in terms of energy production and synthesis of biomolecules that sustain their uncontrolled proliferation. Due to the conceptual progresses in the last decade, metabolic reprogramming was recently included as one of the new hallmarks of cancer. The advent of high-throughput technologies to amass an abundance of omic data, together with the development of new computational methods that allow the integration and analysis of omic data by using genome-scale reconstructions of human metabolism, have increased and accelerated the discovery and development of anticancer drugs and tumor-specific metabolic biomarkers. Here we review and discuss the latest advances in the context of metabolic reprogramming and the future in cancer research.

Cancer is still one of the major causes of death worldwide and the statistics are devastating. According to the WHO the global burden of cancer has risen to 14.1 million new cases and 8.2 million cancer deaths in 2012 and the estimates predict that it could increase in its global incidence [1].

It was proposed 15 years ago by Hanahan and Weinberg that cancer development relies on the following basic biological capabilities, known as the 'hallmarks of cancer' that are acquired during the multistep process of tumor development: the capability to sustain proliferative signaling, resistance to cell death, evasion of growth suppression, ability of replicative immortality, tumor-promoting inflammation, genome instability and mutation, induction of angiogenesis and activation of invasion and metastasis. Owing to conceptual progress in the last decade, two new hallmarks, **metabolic reprogramming** and evasion of immune destruction, have been identified (Figure 1) [2].

Nowadays, it is widely recognized that metabolic reprogramming is essential to sustain tumor progression. Several metabolic adaptations described in cancer cells, such as the metabolization of glucose to lactate in

the presence of oxygen (Warburg effect), are quite common among different cancer types. These changes are promoted by genetic and epigenetic alterations producing mutations or alterations in the expression of key metabolic enzymes that modify flux distributions in metabolic networks, providing advantages to cancer cells in terms of energy production and synthesis of biomolecules [3,4].

Understanding the mechanisms that trigger metabolic reprogramming in cancer cells and its role in tumoral progression is crucial, not only from a biological but also from a clinical stance, since this can be the basis towards improving existing cancer therapies or developing new ones.

In this review, we discuss the role of: the crosstalk between oncogenic signaling pathways and metabolism; the influence of non-genetic factors, such as tumor microenvironment, on metabolic reprogramming of cancer and stromal cells; the changes in isoenzymes patterns as potential therapeutic targets; and the new computational tools used by a systems biology approach in drug-target and biomarker discovery based on **genome-scale metabolic models** (GSMMs). Finally, we also discuss the future challenges in

Igor Marín de Mas^{1,2},
Esther Aguilar¹, Anusha
Jayaraman¹, Ibrahim H
Polat¹, Alfonso Martín-
Bernabé¹, Rohit Bharat¹,
Carles Foguet¹, Enric
Milà¹, Balázs Papp²,
Josep J Centelles¹
& Marta Cascante^{*1}

¹Department of Biochemistry
& Molecular Biology, Faculty of Biology,
IBUB, Universitat de Barcelona & Institut
d'Investigacions Biomèdiques August Pi i
Sunyer (IDIBAPS), Unit Associated with
CSIC, Diagonal 643, E-08028-Barcelona,
Spain

²Institute of Biochemistry, Biological
Research Center of the Hungarian
Academy of Sciences, Temesvári krt.
62, H-6726 Szeged, Hungary

*Author for correspondence:

Tel.: +34 934021593

Fax: +34 934021559

martacascante@ub.edu

[†]Authors contributed equally

**FUTURE
SCIENCE** part of

fsg

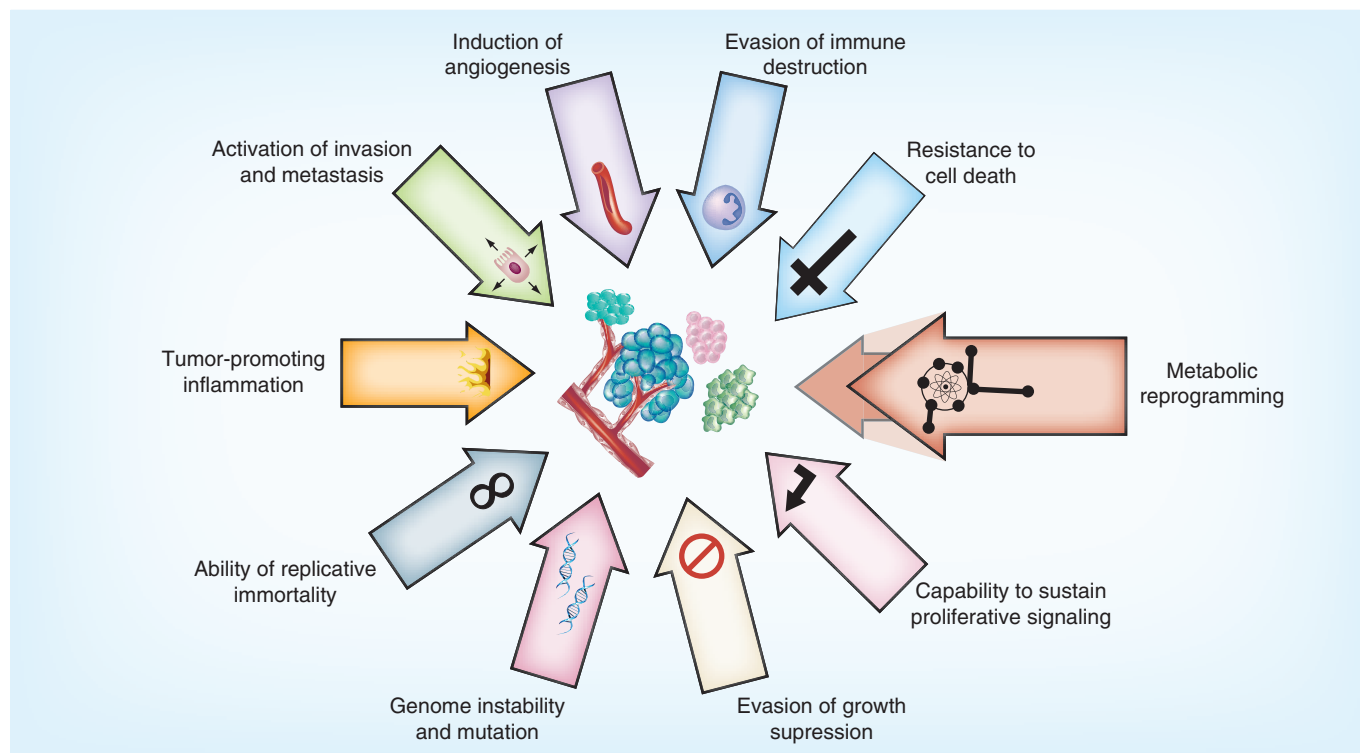


Figure 1. Hallmarks of cancer. The hallmarks of cancer comprise ten capabilities required during a multistep tumor pathogenesis to enable cancer cells to become tumorigenic and ultimately malignant. Metabolic reprogramming has been identified as an emerging hallmark and as a promising target for the treatment of cancer as there is a deregulation of bioenergetic controls and an abnormal use of metabolic pathways to sustain their biosynthetic and energetic needs. Reproduced with permission from [2] © Elsevier.

developing new strategies and methods to drug and biomarker discovery, exploiting the reprogramming of metabolism that sustains cancer progression.

Crosstalk between oncogenic signaling events & cancer cell metabolism

Through a better understanding of the complex networks of oncogenic signaling pathways, altered cellular metabolism emerges as one of the major routes through which oncogenes promote tumor formation and progression. Many key oncogenic signaling pathways converge to adapt tumor cell metabolism in order to support their growth and survival. The identification of new

metabolic coordination mechanisms between altered metabolism and regulators of cell signaling networks, controlling both proliferation and survival, triggers the interest for new metabolism-based anticancer therapies. Several oncogenes, tumor suppressor genes and cell cycle regulators controlling cell proliferation and survival are intimately involved in modulating glycolysis, mitochondrial oxidative phosphorylation (OXPHOS), lipid metabolism, glutaminolysis and many other metabolic pathways (Figure 2). The accumulation of genetic abnormalities required for oncogenesis leads to changes in energetic and biosynthetic requirements that in turn affects the metabolic signature of cancer cells through interactions between enzymes, metabolites, transporters and regulators. High-throughput sequencing data reveals that the mutational events causing tumorigenesis are much more complex than previously thought and that the mutational range can vary even among tumors with identical histopathological features [5]. Some of the metabolic adaptations driven by oncogenic signaling events have been described as common to different tumors, but metabolic profiles can be significantly tissue/cell specific [6]. Here, we will highlight some of the most prevalent examples of crosstalks between oncogenic signaling events and pivotal metabolic pathways. *HIF-1* is a key regulator that initiates

Key terms

Metabolic reprogramming: Process in which the cellular metabolism evolves in order to adapt to new environmental conditions and perturbations. In the case of tumor, the energy metabolism is reprogrammed in order to sustain the high proliferative rate of cancer cells.

Genome-scale metabolic models: Those models that summarize and codify the information known about the metabolism of an organism based on the literature and databases. These models represent the metabolic reaction encoded by an organism's genome and can be transformed into a mathematical formulation in order to study the metabolic cell behavior.

a coordinated transcriptional program activated by hypoxic stress (in response to low-oxygen conditions), to promote the metabolic shift from mitochondrial OXPHOS to glycolysis (Figure 2) through the induction of several genes, including glucose transporters and gly-

colytic enzymes, leading to an increased flux of glucose to lactate [7]. Additionally, *HIF-1* actively downregulates the OXPHOS flux by activation of PDK1, which inhibits the conversion of pyruvate to acetyl-CoA catalyzed by the tricarboxylic acid (TCA) cycle enzyme PDH.

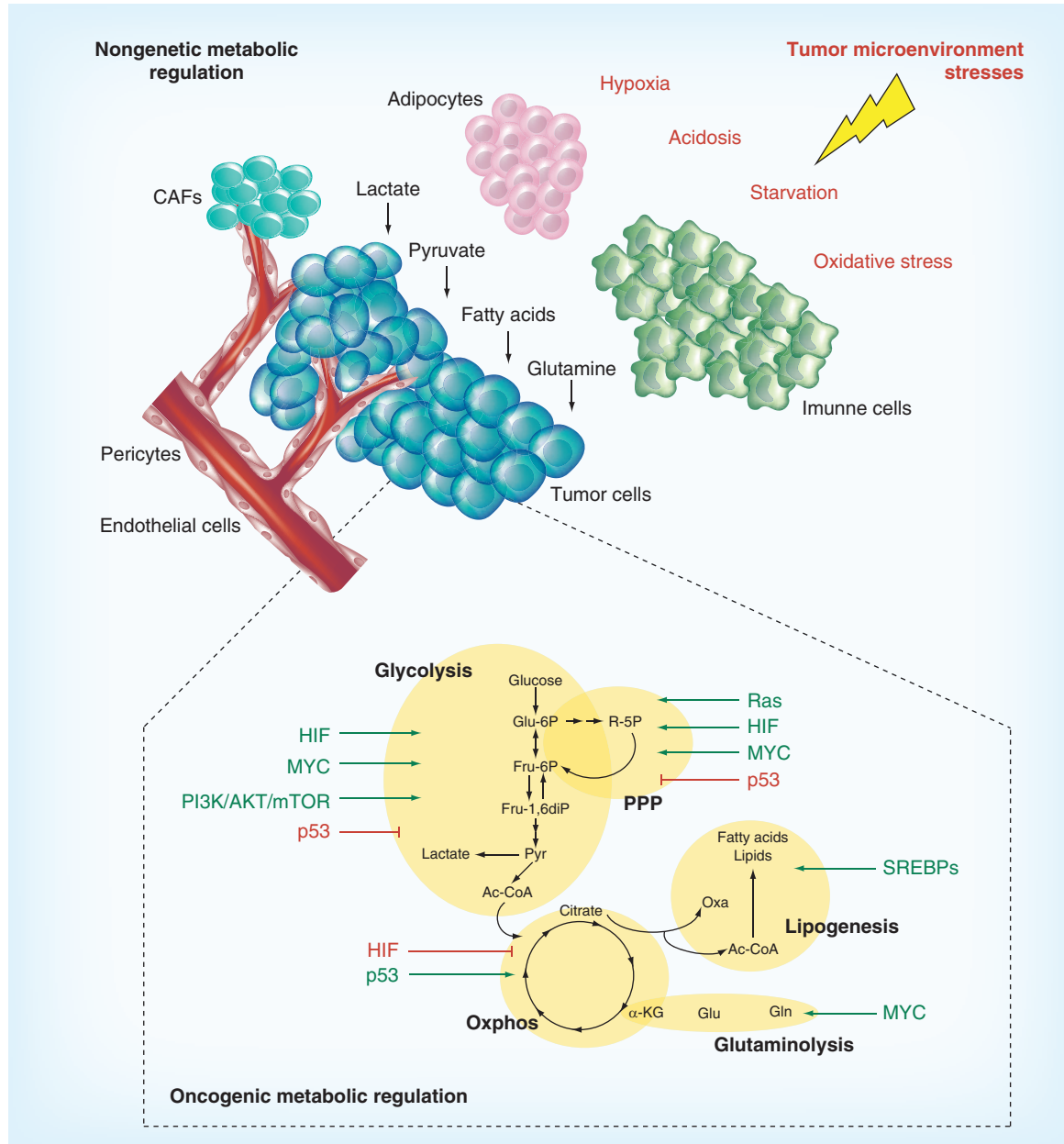


Figure 2. Nongenetic and oncogenic influences on tumor metabolic reprogramming. The nongenetic component (the tumor microenvironment) influences metabolic changes in tumor cells as a result of gradients of oxygenation and pH, nutrient availability, oxidative stress and the intercellular communication with stromal cells by means of metabolites such as lactate, pyruvate, fatty acids and glutamine. Combined with tumor microenvironment, the genetic component (oncogenes and tumor suppressors) plays a key role in metabolic reprogramming to ensure metabolites are shunted into pathways that support the energetic requirements and the biosynthesis of structural components, achieved by maintaining high rates of glycolysis and/or glutaminolysis, promoting the pentose phosphate pathway, slowing mitochondrial metabolism (oxidative phosphorylation) and utilizing tricarboxylic acid intermediates for biosynthetic precursors (e.g., fatty acids and lipids).

CAF: Cancer-associated fibroblastic cell; PPP: Pentose phosphate pathway; SREBP: Sterol regulatory element binding protein.

Similar to *HIF-1*, oncogenic activation of *Myc* also triggers a transcriptional program that enhances glycolysis by directly inducing glucose transporters and glycolytic enzymes. Indeed, there is a crosstalk between *HIF-1* and *Myc*, whereby they cooperate to confer metabolic advantages to tumor cells by oxygen-dependent mechanisms, with a difference that, contrary to *HIF-1*, *Myc* upregulation has more significant consequences for many cells as it alters not only glycolysis but also glutaminolysis (Figure 2) and many other biosynthetic pathways [8]. The *Myc* oncogene stimulates glutamine uptake and glutaminolysis by inducing glutamine transporters directly and GLS, the enzyme that converts glutamine to glutamate, indirectly [9]. Besides glycolysis, glutaminolysis is another important metabolic pathway in cancer cells, which contributes not only as a source to replenish the TCA cycle, but also to control the redox potentials through generation of reductive equivalents, such as NADPH. In addition to glucose, a vast amount of glutamine is consumed by cancer cells. Glutamine is converted to glutamate and then to α -ketoglutarate (α -KG), which feeds the TCA cycle. Some tumors that show an upregulation of glutamine metabolism have been reported to exhibit 'glutamine addiction', that is, glutamine becomes essential during rapid growth. However, glutamine consumption and addiction are dependent on the metabolic profile of the cancer cells and in particular on the oncogene/tumor suppressor involved in tumor progression [10].

Activated PI3K/AKT/mTOR pathway is one of the most common signaling cascades altered in tumor cells and this pathway is one of the most heavily targeted to develop anticancer therapies. Many cancers are driven by aberrations in the PI3K/AKT/mTOR pathway promoting metabolic transformation through multiple metabolic pathways, including an increase in glucose and amino acid uptake (Figure 2), upregulation of glycolysis and lipogenesis and enhanced protein translation through Akt-dependent mTOR activation [11].

In cancer cells, the increased rate of *de novo* lipid biosynthesis is an important aspect of the metabolic reprogramming during oncogenesis. Lipid metabolism is regulated via activation of the sterol regulatory element binding proteins (SREBPs) (Figure 2), which are important regulators of the Akt/mTOR signaling pathway [12]. Indeed, various genes coding for enzymes involved in fatty acid and cholesterol biogenesis are

targets of SREBPs, including ATP-citrate lyase, acetyl-CoA carboxylase and fatty acid synthase [13]. Lipogenesis is also controlled by the *RAS* oncogene through the action of *HIF-1*, which has been reported to induce the expression of fatty acid synthase in human breast cancer cell lines [14]. However, the *RAS* oncogene also modulates mitochondrial metabolism roughly increasing the activity of *Myc* and *HIF-1* [4], glycolysis and the pentose phosphate pathway (PPP) [15]. Proliferating cells, such as tumors, require high amounts of pentose phosphates for biosynthesis of macromolecules and NADPH for redox homeostasis maintenance [16]. Therefore, PPP plays a fundamental role in defining the metabolic phenotype of tumor cells. Hence, there are also examples of coordinated crosstalk between the main enzymes that control the PPP during oncogenesis and oncogenic signaling pathways. K-RAS and PI3K signaling have been shown to positively regulate G6PD, whereas p53, which is a transcription factor and regulator of the cell cycle and apoptosis, physically interacts with G6PD to negatively modulate its activity [17], and thereby downregulates PPP. On the other hand, active *HIF-1* signaling has been linked to both TKT and TKTL1, the enzymes catalyzing the rate-limiting step of the non-oxidative branch of the PPP [18].

In addition, alterations in *p53* are frequent events in tumorigenesis. The loss or inactivation of *p53* downregulates OXPHOS by inducing aerobic glycolysis through inhibiting glucose transporters and the glycolytic enzyme PGM and inducing TP53-induced glycolysis and apoptosis regulator, a negative regulator of glycolysis [19]. On the other hand PHF20 stabilizes and upregulates p53 resulting in a gain of functionality that drives the reprogramming of the metabolism of certain cancers cell lines, such as U87 (glioblastoma) or MCF7 (breast cancer) [20].

Other examples of oncogene-mediated metabolic reprogramming include mutations in genes encoding FH and succinate dehydrogenase, which are loss-of-function mutations and behave as tumor suppressor genes [21]. On the other hand, mutations in IDH-1 and IDH-2, do not result in inactivation of normal IDH enzymatic function but generation of novel gain-of-function mutation that enables the conversion of α -KG to D2-HG, which may act as an 'oncometabolite' by inhibiting multiple α -KG-dependent dioxygenases involved in epigenetic regulation [22].

Tumorigenesis occurs as a consequence, not only of the dysregulation of numerous oncogenic pathways, but also due to many nongenetic factors, including tumor microenvironment stresses, such as hypoxia, lactic acidosis and nutrient deprivation. The integration of these nongenetic factors within the genetic framework of cancer is the next logical step in understanding

Key term

Tumor heterogeneity: Variability among different tumors in the same organ (intertumoral heterogeneity) or the variability among cells in a tumor (intratumoral heterogeneity).

tumor heterogeneity. Research over the years has elucidated the cellular and molecular interactions (including metabolic reprogramming) occurring in the tumor microenvironment and are closely linked to the processes of angiogenesis and metastasis.

Tumor microenvironment

Since the discovery of immune cells in tumor samples by Rudolf Virchow in 1863, various studies have shown the linkage of cancer to inflammation, vascularization and other conditions, which suggest that tumors do not act alone. Without its ‘neighborhood’ the survival of tumor cells could be a big question mark. The cellular heterogeneity in this microenvironment is complex and comprises of extracellular matrix, tumor cells and non-transformed normal cell types that co-evolve with the tumor cells (e.g., cancer-associated fibroblastic cells [CAFs], infiltrating immune cells and endothelial cells that constitute the tumor-associated vasculature) that are embedded within this matrix and nourished by the vascular network. In addition, there are many signaling molecules and chemicals, such as oxygen and protons, all of which can influence tumor cell proliferation, survival, invasion, metastasis and energy metabolism reprogramming. CAFs, one of the most abundant stromal cell types in different carcinomas, are activated fibroblasts that share similarities with fibroblasts, stimulated by inflammatory conditions or activated during wound healing. But, instead of suppressing tumor formation, CAFs can significantly promote tumorigenesis, invasion and *de novo* cancer initiation by some unique growth factors and cytokines secretion (e.g., EGF, FGF, IL6, IL8, VEGF etc), extensive tissue remodeling mediated by augmented expression of proteolytic enzymes (e.g., matrix metalloproteinases), deposition of extracellular matrix and pathogenic angiogenesis by liberating pro-angiogenic factors within the matrix [23]. Significant cell plasticity exists within this cell population, as both mesenchymal-to-epithelial and epithelial-to-mesenchymal transitions are known to occur, further enhancing stromal heterogeneity. Moreover, CAFs can enhance proliferation and invasion by inducing the epithelial-to-mesenchymal transitions on tumor cells [24,25]. Immune cell recruitment and localization in the tumor milieu vary widely in the lesions. Heterogeneity of tumor immune contexture is influenced by various factors, including those secreted by CAFs, the extension and permeability of the vasculature, and the tumor cells themselves. Importantly, macrophages comprise the most abundant immune population in the tumor microenvironment and are responsible for the production of cytokines, chemokines, growth factors, proteases and toxic intermediates, such as nitric oxide and reactive oxygen species [26]. Their contribution to

tumor initiation, progression and metastasis can be attenuated by antioxidant treatments, such as butylated hydroxyanisole, as reactive oxygen species levels have been reported to regulate the differentiation and polarization state of macrophages. Endothelial cells that are ‘hijacked’ by the tumors play an important part in forming a transport system, although ineffective, but essential for its survival and growth. In addition, blood vessel formation needs a protein matrix for the endothelial cells to be attached to and also it needs pericytic cells to strengthen these vessels. But, since the pericytes are not known to function very well in tumor vessel formation, the vessels are always malformed and leaky [27].

In the last few years the concept of cancer stem cells (CSC), a small minority of cells in the tumor, has evolved to be a possible cause and source of tumor heterogeneity. Currently there are two models that describe tumor cell heterogeneity: the hierarchical CSC model, where self-renewing CSCs sustain the stem cell population while giving rise to progenitor cells that are not capable of self-renewal and can give rise to differentiating clones that contribute to overall tumor heterogeneity, and the stochastic (tumor microenvironment-driven) model in which cancer cells are clonally evolved, and virtually every single cell can self-renew and propagate tumors. In this model, the self-renewal capability of each cell is determined by distinct signals from the tumor microenvironment. Recent studies have suggested that tumor heterogeneity may exist in a model coordinating with both the CSC and the stochastic concepts [28].

Metabolic reprogramming associated with cancer & stromal cell interaction

Recently, the relationship between tumor microenvironment and metabolic reprogramming has been highlighted and there has been extensive research about metabolic symbiosis between cancer and stromal cells. Among these interactions, it was shown that epithelial tumor cells induce oxidative stress in the normal stroma, inducing aerobic glycolysis in CAFs, as well as changes in inflammation, autophagy and mitophagy (Figure 2). As a consequence of this rewiring in CAFs metabolism, energy-rich metabolites (such as lactate, pyruvate and ketones) are secreted, feeding adjacent cancer cells. This tumor–stroma metabolic relationship is referred to as the ‘reverse Warburg effect’. CSCs that are present within the tumor also rely more heavily on glycolysis, even in the presence of oxygen (Warburg effect), and decrease their mitochondrial activity in order to limit reactive oxygen species production. As these glycolytic and mitochondrial signatures help to maintain the CSC phenotype, recent studies have

focused their attention to these metabolic weaknesses to be combined with traditional chemotherapy that, alone, usually fails to target CSCs [29,30]. In addition, other stromal cells, such as adipocytes, are able to act as energy sources, transferring fatty acids that come from lipolysis to ovarian tumor cells for β -oxidation [31]. Deregulated lipogenesis has been shown to play an important role in the interactions between cancer cells and the surrounding stromal cells. Studies suggest that it affects the epithelial cell polarity during the early stages of cancer development [32], inducing cancer cell migration [33] and activation of angiogenesis involving signaling lipids (e.g., diacyl glycerides, lysophosphatidic acid and prostaglandins), fatty acid synthesis enzymes and overof the monoglyceride-lipase [34–36].

Loss of stromal caveolin-1 in CAFs has been associated with tumor progression and metastasis [37] and causes oxidative stress and induction of autophagy, which results in increased levels of glutamine and ammonia in the stromal microenvironment. This glutamine could be consumed by cancer cells for energy and anaplerotic reactions and ammonia acts as a potent inducer of autophagy, creating a vicious cycle [37]. The migration stimulating factor, a truncated isoform of fibronectin identified to be overexpressed by CAFs and other 'activated' fibroblasts, has been shown to increase lactate production in the stromal environment and decrease mitochondrial activity, suggesting a shift towards glycolysis during hypoxia in addition to promoting tumor growth without affecting tumor angiogenesis [38].

Angiogenesis has been long known to play a major role in supporting cancer cell growth in the tumor microenvironment. But since the newly formed blood vessels are mostly defective there is always a nutrition deficiency and acidosis in these areas (Figure 2). A biomarker study in the gastric cancer environment where a quantitative analysis of the organic acids that are the end products of metabolism, using GC–MS, showed an increase in glycolytic end-products, such as pyruvic and lactic acids, with respect to normal tissues [39]. The pattern of high acidification in the tumor microenvironment due to the accumulation of glycolytic end-products results in a nutrient-deficient environment. In addition, metabolic reprogramming of tumor-associated endothelial cells has been showing up wide interests. Upon tumor angiogenic activation, endothelial cells are pushed to a state of metabolic stress for increasing their proliferation rate to form new blood vessels, although the resulting network is abnormal and inefficient. These normal cells show higher glycolytic enzyme activities and lactate production, even in the presence of oxygen [40], and they continue proliferating even in the presence of hostile conditions and high

nutrient deficiency [41]. Also it has been shown that endothelial cells, similar to tumor cells, have a high expression of monocarboxylate transporter 1 required for the lactate influx, revealing that these cells seek alternative metabolites in a nutrition-deficient environment [42]. Moreover, the inhibition of glycogenolysis in human umbilical vein endothelial cells has been shown to decrease cell viability and migration, elucidating the importance of glycogen for the survival of these cells [43]. The role of the PPP in cell viability has also been demonstrated, in that, the direct inhibition of G6PDH has been shown to decrease endothelial cell survival [43]. When tumor cells choose the less energy-efficient metabolic pathways, such as glycolysis and glutaminolysis, both leading to the production of lactic acid, the pH of the tumor microenvironment decreases. It has been shown that endothelial cells behave in a similar fashion while forming new tumor blood vessels. While this phenomenon is known, it has also been found that the decrease in pH in the surrounding microenvironment actually increases cancer survival by immune suppression. Loss of T-cell function has been reported under low pH environment, while restoring the pH to normal conditions has been found to restore T-cell function [44]. Similarly, the lactic acid generated has been shown to increase the proliferation of endothelial cells by increased interleukin8/CXCL8 production [41,45]. From a therapeutic point of view, targeting the altered metabolic pathways leading to lactic acid accumulation in tumor microenvironment could inhibit tumor growth as this mechanism would restore the impaired immune response and also a combinatorial therapy with antiangiogenesis drugs could reduce the proliferation of endothelial cells and formation of new blood vessels [46].

An important event that occurs during the changes in tumor microenvironment, as the cancer progresses, is the metastasis of some selected cancer cells to distant sites. A receptive microenvironment is required for tumor cells to engraft distant tissues and metastasize. Although several studies have indicated the formation of a premetastatic niche in the secondary sites before the primary tumor metastasizes [47], we have to consider how metastatic cells are able to adapt to their new metabolic environment, which can differ to a greater or lesser extent with respect to its nutrient and oxygen availability. Metastatic cells should exhibit a remarkable and dynamic flexibility that enables them to rapidly switch between metabolic states [48]. In addition, the homeostasis of the sites for metastasis can be disrupted as consequence of the metabolic activity of metastatic cells. This has been observed in bone, where metastatic prostate cancer cells secrete glutamate into their extracellular environment as a side effect of cel-

lular oxidative stress protection, promoting the development of pathological changes in bone turnover [49]. Further studies are required to analyze these metabolic interplays between metastatic cells and tumor microenvironment in order to obtain more specific treatments and therapies.

Isoenzymes: therapeutic targets in cancer

The technological advances that have occurred over the past decade and the increasing number of evidences that have emerged from previous studies show a wide array of metabolic rewiring in cancer cells. Many metabolic enzymes that are specific to important metabolic pathways and those altered in cancer cells have been identified. These enzymes have a key role in mediating the aberrant metabolism of cancer cells and could serve as a promising source of novel drug targets. Isoforms of many of these metabolic enzymes are found to be specifically expressed in tumor cells affecting important pathways of the energetic metabolism. The current research is being refocused on specifically targeting these isoforms that has shown to be a promising strategy to develop new anticancer treatments. In this part, we will highlight some of the most important, altered pathways and the specific isoenzymes, that could be used for drug targeting, in cancer disease.

Glycolytic isoenzymes

Glycolytic pathway serves as the principal energetic source for a cell. The higher dependency of cancer cells upon glycolytic metabolism for the production of ATP provides a greater motive to target glycolytic enzymes (Figure 2). Many isoforms of these enzymes have been found to be specifically expressed in tumor cells and are being exploited as potential candidates to be used as drug targets. The transport of glucose across the plasma membrane is regulated by various isoforms of glucose transporters (GLUT1–14 or SLC2A1–14). GLUT1, -3 and -4 are found to be expressed at higher levels in cancer [50]. GLUT3 and other transporters could be targeted by the use of specific antibodies or drugs, such as phloretin or ritonavir, causing the cells to starve by blocking their nutrient uptake through these transporters.

Another important metabolic enzyme of the glycolytic pathway is HK, which regulates the first rate-limiting step of glucose metabolism. Cancer cells are heavily dependent on HK isoforms, such as HK2 [51]. The specific expression of HK2 in adipose tissue and skeletal muscles provides an opportunity to target this enzyme without having the risk of affecting other tissues. Compounds such as methyl jasmonate isolated from plants have been shown to disrupt the association between mitochondria and HKs (HK1 and -2).

involved in regulating apoptosis [52] and have shown to be lethal to cancer cells *in vitro* [53].

Recent publications suggest a key role of PK isoenzyme – PKM2 – in mediating the Warburg effect in cancer cells [54], proving its prospective as an enzymatic anticancer drug target. The enzyme activity of PKM2 is inhibited downstream of cellular growth signals [55]. Cell proliferation and aerobic glycolysis in tumors are greatly dependent on this ability to inhibit the activity of the PKM2 enzyme. Many approaches using small-molecule inhibitors and small-hairpin RNA-based inhibition of *PKM2* have been shown to cause cell death and slow down cell proliferation *in vitro* [54,56]. The PFKFB3 isoform is shown to be important in RAS-mediated tumors and inhibition of PFKFB3 by small-molecule inhibitors has been shown to have cytostatic effect on the growth of cancer [57]. Inhibition of LDHA using FX11 or oxamate has been shown to induce oxidative stress and cause cell death in cancer cells [58,59]. Targeting LDHA combined with NAMPT inhibitors has been shown to slow down tumor regression and thus making it a potential candidate for drug targets [59].

TCA isoenzymes/mitochondrial complex

PDK phosphorylates PDH and inhibits the conversion of pyruvate to acetyl-CoA, a key metabolite in the TCA cycle (Figure 2). Isoenzyme PDK3 is induced by upregulation of HIF-1 α under hypoxic conditions and results in cells undergoing glycolysis instead of TCA for energy production. Inhibition of PDK3 increases the susceptibility of tumor cells towards anticancer drugs and causes inhibition of hypoxia-induced glycolysis [60]. Thus PDK3 could be used as a drug target to overcome drug resistance and improve chemotherapy.

Isoforms of IDH1 and -2 are found to be mutated in glioma and acute myeloid leukemia [61,62]. Mutations in IDH1 and -2 result in the overexpression of both of these enzymes and the production of 2-HG, which inhibits α -KG-dependent dioxygenase enzymes. Association between high levels of 2-HG and tumorigenicity is yet to be established, but interestingly the levels of several TCA metabolites remain unaltered, suggesting an alternate pathway that could be acting in normalizing the metabolite levels in cells with IDH1 mutations.

Isoenzymes of the PPP

Cancer cells are in a constant demand for greater amounts of purines and pyrimidines to maintain their high proliferative nature (Figure 2). The key enzyme for the oxidative PPP, the G6PDH enzyme, is overexpressed in certain types of cancers and it has been shown to transform fibroblasts and help in tumor cell

proliferation [63]. On the other hand, the overexpression of TKTL1 in many forms of cancer could increase the concentration of glyceraldehyde-3-phosphate and help in mediating the Warburg effect in cancer cells [64]. Combinatorial approach of targeting G6PDH and TKTL1 can help overcome drug resistance and may cause cell death [65].

Targeting isoenzymes of glutamine metabolism

Recent findings that point to the use of glutamine as a carbon source for the TCA cycle [66] in cancer cells encouraged researchers to consider enzymes of glutamine metabolism as potential therapeutic targets. 6-diazo-5-oxo-L-norleucine- or bis-2-(5-phenylacetamido-1,2,4-thiadiazol-2-yl)ethyl sulphide-mediated inhibition of GLS or siRNA-induced silencing of GLS and GDH have been shown to inhibit the activation of mTORC1 [67]. Thus, combinatorial targeting of GLS and GDH along with chemotherapy may prove to be more effective in cancer treatment. The differential expression of these cancer-associated isoenzymes can be used as potential biomarkers for early cancer prognosis or as **enzymatic drug targets**. However, the role and importance of these mutations in the reprogramming of the energetic metabolism observed in cancer cells is not always obvious. This makes it extremely difficult to evaluate the effects of these mutations in the cancer metabolism qualitatively or quantitatively. Additionally, the effects of these isoenzymes on metabolism can be attenuated or enhanced by compensatory and regulatory mechanisms. Taking into account these rationales, the need for a tool that permits a holistic analysis of the metabolic system is essential, in order to qualitatively evaluate the effects of a single or combination of different mutations within the whole metabolic network system. In the last few years, genome-scale metabolic network models have demonstrated their suitability for the integrated analysis of large and complex metabolic networks providing new clues for identifying drug targets.

GSMMs as new tools emerging from systems biology approach to drug discovery

In the previous sections, we have presented evidences that support cancer onset and that the progression relies on metabolic abnormalities to balance energy demand and biomolecular synthesis (metabolic reprogramming) [68]. GSMMs are emerging as a potential solution to decipher the molecular mechanisms underlying

Key term

Enzymatic drug target: A component in a metabolic pathway to which some other entity, such as a drug, is directed and/or binds.

cancer in the context of systems biology [69]. GSMMs represent the metabolic reaction complement encoded by an organism's genome. These models are built based on the literature and databases and enable one to summarize and codify information known about the metabolism of an organism.

Over 100 GSMMs have been built for different species, ranging from archaea to mammals [70–84]. Reconstructions of human metabolism, such as Recon1 [81], Edinburgh Human Metabolic Network [82] or the most recent reconstructions of human metabolism, Recon2 [83], are widely used to study the mechanism of diseases with a strong metabolic component, such as cancer or diabetes [85–88].

This systems biology tool enables the mathematical representation of biotransformations and metabolic processes occurring within the organism and offers an appropriate framework to integrate the increasing amount of 'omic' data generated by the different high-throughput technologies.

The transformation into a mathematical formulation is mostly driven by constraint-based modeling (CBM) [89] and allows the systematic simulation of different phenotypes, environmental conditions, gene deletion and so on. This approach allows for modeling the complexity of cancer metabolism and tackling more problematic biological questions, such as the role of metabolism in cancer disease [90].

Genome-scale constraint-based metabolic models have been used for a variety of applications, involving studies on evolution [91], metabolic engineering [92–94], genome annotation [95] or drug discovery [96], with a high relevance in cancer research.

Indeed, GSMMs can efficiently capture the complexity of cancer metabolism in a holistic manner and permit to improve existing therapies or develop new ones [97].

In this chapter we discuss methods for building GSMMs and computational approaches to analyze and integrate 'omic' data into these large-scale metabolic network models. Finally, we introduce some of the most relevant softwares and algorithms developed for drug-target discovery that can be used in cancer research.

GSMM reconstruction

Genome-scale metabolic reconstructions are created in a bottom-up manner based on genomic and bibliomic data and, thus, represent a biochemical, genetic and genomic knowledge base for the target organism [81–83]. However, to date we are still not able to completely and automatically reconstruct high-quality metabolic networks (**Figure 3A**) [98]. Genome-scale reconstruction starts with the generation of a draft,

automated reconstruction based on the genome annotation and biochemical databases of the target organism. This task can be achieved by using software tools, such as Pathways tool [99]. The genomic sequence of the targeted organism is coupled with the most recent annotations available from databases [100], such as GOLD or NCBI Entrez Gene databases [101,102].

Metabolic reactions can be associated with the annotated metabolic genes by using enzyme commission (E.C.), ID and biochemical reaction databases (e.g., KEGG [103] and BRENDA [104]). This process permits both linking metabolic genes with their corresponding encoded enzymes and determining the stoichiometric relationship of metabolic reactions with the metabolites and cofactors that they consume and/or produce.

The gene–protein–reaction association (GPR), is represented as Boolean relationships in which isoenzymes that catalyze the same reaction have an “OR” relation (only one of the genes that encode the different isoenzymes is required to have the reaction active) and the complexes that catalyze a reaction have an “AND” relation (all the genes that encode the different complex subunits are necessary to have the reaction active) [81]. GPR associations enable the mapping of transcriptomics or proteomics to the level of reactions.

Reactions can be located into different subcellular compartments based on protein location [81]. Reaction directionality can be determined from thermodynamic data. Additionally, artificial reactions, such as biomass reaction that define the ratio at which biomass constituents are produced (nucleic acids, lipid, proteins, etc) or exchange reactions that define the overall rate of nutrients consumption or production, are also defined in the reconstruction. These artificial reactions are necessary to predict or impose certain phenotypic conditions on the mathematical model.

Next, it is necessary to manually curate and refine the draft, automated reconstruction. The main objective of curation is to identify and correct incomplete or erroneous annotation, add reactions that occur spontaneously and remove gaps and metabolites that cannot be produced or consumed [81] through search on the literature and other databases.

Once the model is curated, it is evaluated and validated in an iterative fashion by using mathematical tools [105]. The aim of the validation process is to evaluate if the model is stoichiometrically balanced, find gaps in the network and search for candidate reactions for gap filling, quantitative evaluation of biomass precursor production and growth rate, compare predicted physiological properties with known properties and determine the metabolic capabilities of the model.

It is worth noting that once a GSMM has been constructed, it can be used in future reconstructions in order to expand and refine the model [81,83].

Constraint-based methods as tools for tumor metabolism characterization

As was previously mentioned, GSMMs include stoichiometric details for the set of known reactions in a given organism. These large scale metabolic models require computational methods to be qualitatively analyzed. Traditionally, approaches based on ordinary differential equation have been used for characterization of dynamic cell states. However, this full-scale dynamic modeling is frequently infeasible for large-scale networks because of a paucity of necessary parameter values.

Constraint-based methods (CBMs) permit the analysis of large-scale biochemical systems under conditions where kinetic parameters need not be defined (steady state). Genome-scale constraint-based metabolic models can be used to predict or describe cellular behaviors, such as growth rates, uptake/secretion rate or intracellular fluxes [89]. Flux balance analysis (FBA) is one of the most widely used CBMs for the study of biochemical networks. The variables used in FBA include the fluxes through transport and metabolic reactions and model parameters include reaction stoichiometry, biomass composition, ATP requirements and the upper and lower bounds for individual fluxes, which define the maximum and minimum allowable fluxes of the reactions.

The first step in FBA is the mathematical representation of the metabolic reactions in the form of a numerical matrix, with stoichiometric coefficients of each reaction (stoichiometric matrix), where the metabolites are represented in rows and reactions in columns. FBA employs mass actions formalism for the mathematical representation of the metabolic networks: $dC/Dt = S \cdot v$, where v and C are vectors of reaction fluxes and metabolite concentration respectively, t is time and S is the stoichiometric matrix (Figure 3A).

The next step is to impose constraints to the metabolic network. Constraints are fundamentally represented in two ways:

- Steady-state mass-balance imposes constraints on stoichiometry and network topology on the metabolic fluxes through the network. Additionally, steady state assumption also imposes constraints that narrow the space of solutions. By definition, the change in the concentration of a certain metabolite over time at steady state is 0: $dC/Dt = 0$, thus: $S \cdot v = 0$. These constraints ensure that for each metabolite in the network the net production rate equals the net consumption rate;

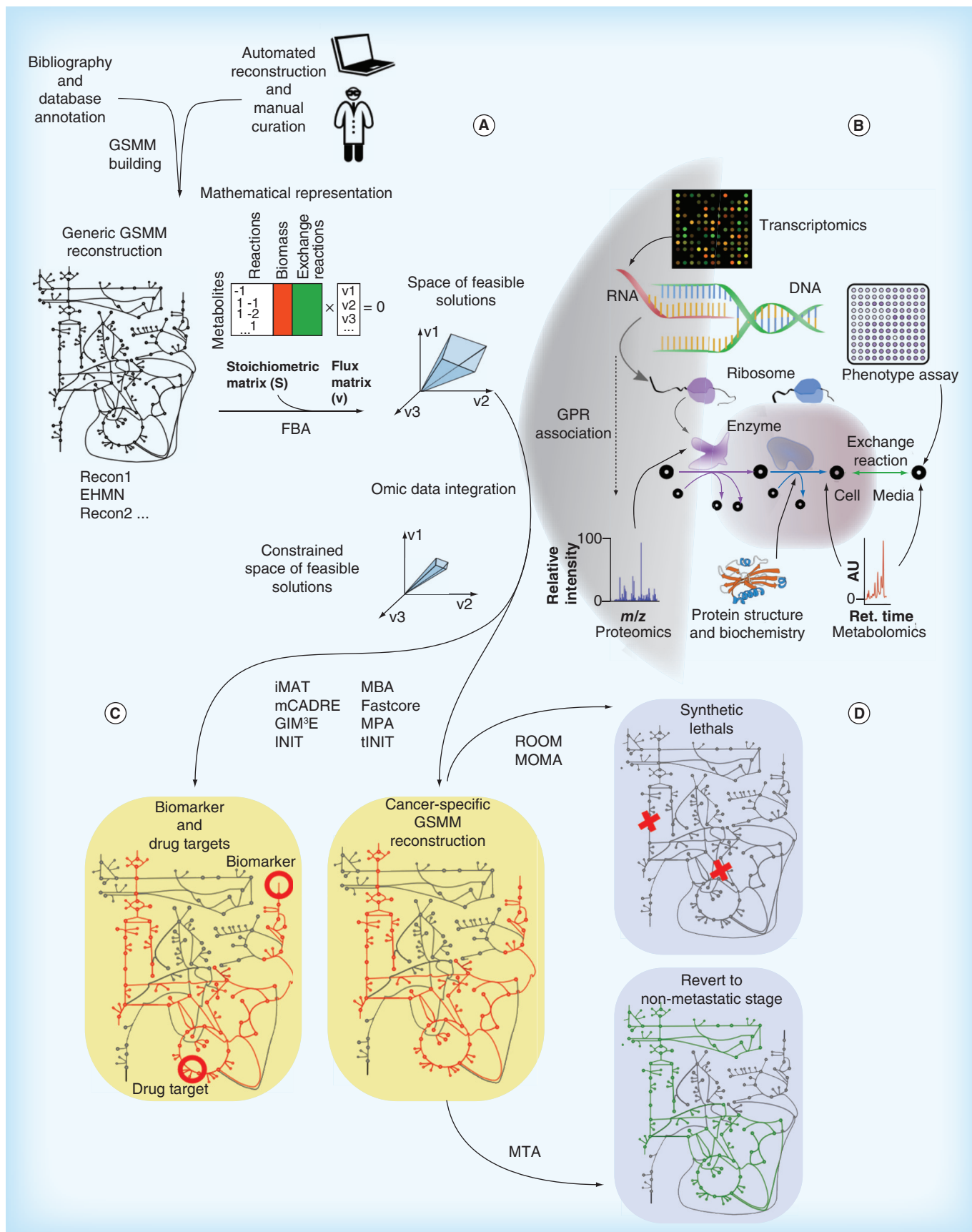


Figure 3. Genome-scale metabolic model building and analysis (facing page). (A) GSMM reconstruction starts with a draft automated version based on literature and databases, finally this version is manually curated in order to refine the model. Typically, these models are analyzed by using flux balance analysis, assuming steady state. (B) GSMMs can be used as a platform to integrate and combine omic data from multiple layers. In these models, metabolomics data can be associated with metabolites, while genomics, transcriptomics and proteomics can be associated with metabolic reactions, these associations are established through gene–protein–reaction associations. The phenotypic assays can constrain properties of the network, such as growth rate under certain experimental conditions. (C) By integrating omic data into a GSMM we can determine either tumor-specific biomarkers or anticancer drug-targets and reconstruct cancer-specific GSMM. (D) Cancer-specific reconstructions can be used to determine synthetic lethals specific for each cancer type for which the non-tumor cells are insensitive (ROOM and MOMA methods), Additionally if we reconstruct an initial GSMM describing metastatic phenotype and a target GSMM describing non-metastatic phenotype we can determine the actors that would permit to revert the metastatic phenotype into a non-metastatic one (MTA method).
FBA: Flux balance analysis; GSMM: Genome-scale metabolic model; Ret.: Retention.

- Inequalities that impose bounds on the system: every reaction can also be given upper and lower bounds. These restrictions are based on measured rates (e.g., metabolite uptake/secretion rates) or reaction reversibility (e.g., irreversible fluxes have a zero lower bound) and are used to define the environmental conditions in a given simulation, such as nutrient or O₂ availability, which can be related with a specific tumor microenvironment or stages in tumor progression.

Finally it is necessary to define a phenotype in the form of a biological objective that is relevant to the problem being studied (objective function). Typically, objective functions are related to growth rate prediction. GSMMs define this phenotype by an artificial biomass production reaction, that is, the rate at which metabolic compounds are converted into biomass constituents (nucleic acids, lipid, proteins, etc). The biomass reaction is based on experimental measurements of biomass composition and is unique for each organism or cell type. Thus, an objective function could be the maximization of growth rate that can be accomplished by calculating the set of metabolic fluxes that result in the maximum flux through biomass production reaction. Since uncontrolled cell growth is the basis of tumor progression, this approach is widely used in the simulation of cancer cell metabolism. The objective function can be adapted to the specific cell type or organism; however, the objective that better defines our case of study is not always obvious, especially in multicellular organisms [106].

Taken together, the mathematical representation of the metabolic reactions and of the objective function, is defined as a system of linear equations that are solved by a number of algorithms and software developed for this purpose [105]. Predictions of values for these fluxes are obtained by optimizing for an objective function, while simultaneously satisfying constraint specifications.

Omic data integration

The advent of high-throughput technologies have transformed molecular biology into a data-rich discipline by providing quantitative data for thousands of cellular

components across a wide variety of scales. However, extraction of ‘knowledge’ from this ocean of omic data has been challenging [107]. GSMMs have emerged as an advantageous platform for the integration of omic data (e.g., [108]; **Figure 3B**). In this framework cellular and molecular phenotypes are simulated allowing the development of biological hypotheses and discoveries [109]. Metabolic reconstruction of the human metabolism has been successfully used for a variety of analyses of omic data, including applications in data visualization [110], deducing regulatory rules [111], network medicine [112], constructing tissue-specific models [113] or multicellular modeling [114]. Thus, omic data can be used to further constrain the non-uniqueness of constraint-based solutions space and thereby enhance the precision and accuracy of model prediction (**Figure 3A–C**) [109]. To achieve this aim a number of FBA-driven algorithms that integrate omic data into GSMMs have been developed. **Table 1** highlights some of the most relevant approaches recently developed to incorporate experimental omic data into GSMMs [86,87,113,115–117]

Drug-target & biomarker discovery

Cancer cells maintain their high proliferation rate by adapting their metabolism based on the environmental conditions, such as pH, O₂ availability, vascularization or nutrient availability [118]. The elucidation of diverse metabolic alterations for the identification of biomarkers and novel drug targets has, therefore, been increased in recent years. An increasing number of methods and algorithms have been recently developed to integrate tumor-specific omic data into GSMMs. It has enabled the gain of further biological and mechanistic understanding of how cancer benefits from metabolic modifications [90]. This model-driven approach allows the discovery

Key term

Omic data integration: Computational process in which multi-omic data obtained from different high-throughput technologies, considering different aspects of the molecular biology, are integrated into genome-scale metabolic models in order to unveil emergent properties of the biological systems.

Table 1. Computation method for integrating omic data into global-scale metabolic models.

Name	Input	Description	Ref.
iMAT	Gene expression data	Seeks to maximize the similarity between the gene expression and the metabolic profiles	[115]
mCADRE	Gene expression and metabolomic data	Uses tissue-specific data to identify a set of core reactions. Seeks to build a consistent network using all the core reactions and the minimum number of non-core reactions	[86]
GIM ³ E	Gene expression and metabolomic data	Builds a network that satisfies an objective function while penalizing the inclusion of reactions catalyzed by genes with expression below a certain threshold. It can be further constrained to produce certain metabolites based on experimental evidences	[116]
INIT	Gene expression and metabolomic data	Seeks to build a model prioritizing the addition of reactions with strong evidence of their presence based on gene expression data. Can be forced to produce metabolites that have been detected experimentally	[87]
MBA	Transcriptomic, proteomic, metabolomic, bibliomic data	Uses tissue-specific data to identify high and moderate probability core reactions. Seeks to build a network with all the high-probability core reactions, the maximum moderate probability core reactions and the non-core reaction required to prevent gaps	[113]
Fastcore	Transcriptomic, proteomic, metabolomic, bibliomic data	Identify a set of core reactions based on tissue-specific data. Seeks to build a network that contains all reactions from the core set with the minimum set of additional reactions necessary	[117]

of potential biomarkers and drug targets [87,97,119]. The identification of new biomarkers is of major importance to biomedical research for early diagnosis and monitoring treatments efficiently. The identification of cancer biomarkers is possible due to aberrant metabolism of tumors that alters the profile of absorption and nutrients secretion.

Omic data of clinical samples (mainly transcriptomics data) can be used to infer the exchange rates of different metabolites for each individual sample via GSMM analysis (alterations in exchange reactions in the model). Thus, those metabolites that significantly differ between two clinical groups in their exchange rates are then considered as potential biomarkers. However, this task is especially challenging in the case of cancer owing to metabolic abnormalities resulting from complex and elaborate genetic and epigenetic alterations that modify the expression of a variety of cancer-associated isoenzymes. In order to determine potential biomarkers in cancer, several computational approaches has been developed. For example, the metabolic phenotypic analysis (MPA) method uses GPR association to integrate transcriptomic and proteomic data within a GSMM to infer metabolic phenotypes [88]. MPA was used to study breast cancer metabolism and predict potential biomarkers. These predictions, which include amino acid and cho-

line-containing metabolites, are supported by a number of experimental evidences [120]. Another recently developed algorithm is mCADRE, which has been used to systematically simulate the metabolic function of 26 cancer cell types (among other cell types) [86]. This algorithm has been able to identify several pathways, such as folate metabolism, eicosanoid metabolism, fatty acid activation and nucleotide metabolism, that are enriched in tumor tissue compared with their corresponding normal tissue. Many enzymes involved in these pathways are already used as chemotherapy targets. Other approaches, such as flux variability analysis [121] or sampling analysis [122], are also suitable to predict metabolic biomarker candidates by integrating omic data into a GSMM. The novel drug discovery is based on the abnormalities existing in various reactions/pathways of cancer metabolism. These differences can be used as drug targets to attack specific weaknesses of the tumor and hence compromising its viability, but not that of non-cancerous cells [123]. For example, the INIT method [87] was used to identify characteristic metabolic features of cancer cells by inferring the active metabolic network of 16 different cancer types and compare them with the healthy cell types where they come from. These metabolic differences may play an important role in proliferation of cancer cells and could be potential drug targets. This method found

significant differences in polyamine metabolism, the isoprenoid biosynthesis and the prostaglandins and leukotrienes pathways in cancer cells compared with healthy cells. Some of the reactions that were found that have different activity in cancer cells, are already used in the clinical practice as therapeutic targets [124,125]. Based on the rationale that the differences between normal and tumoral cells can be potential therapeutic targets, several approaches have been developed that consider different aspects of cancer metabolism for the discovery of new drug targets:

Antimetabolite

One of the most common anticancer drugs are antimetabolites. An antimetabolite is structurally similar to a certain metabolite but it cannot be used to produce any physiologically important molecule. Antimetabolite-based drugs act on key enzymes preventing the use of endogenous metabolites, resulting in the disruption of the robustness of cancer cells and reduction or suppression of cell growth. For example, antimetabolites, such as antifolates or antipurines, mimic folic acid and purines [126]. The GSMM approach can be used to systematically simulate the effect of potential antimetabolites in cancer research. To achieve this, methods such as the tINIT (Task-driven Integrative Network Inference for Tissues) algorithm have been developed [97]. This method has been used to reconstruct personalized GSMMs for six hepatocellular carcinoma patients based on proteomics data and the Human Metabolic Reaction database [87] and identify anticancer drugs that are structural analogs to targeted metabolites (antimetabolites). The tINIT algorithm was able to identify 101 antimetabolites, 22 of which are already used in cancer therapies and the remaining can be considered as new potential anticancer drugs.

Synthetic lethal

The genetic lesions occurring in cancer not only promote the oncogenic state but are also associated with dependencies that are specific to these lesions and absent in non-cancer cells. Two genes are considered 'synthetic lethal' if the isolated mutation on either of them is compatible with cell viability but the simultaneous mutation is lethal [127]. Analogously, two genes are considered to interact in a 'synthetic sick' fashion, if simultaneous mutation reduces cell fitness below a certain threshold without being lethal [127].

Enzymes encoded by genes that are in synthetic lethal or sick interactions with known, non-druggable cancer-driving mutations can be potential anticancer drug targets. This approach has two main advantages: first, we can indirectly target non-druggable cancer-promoting lesions by inhibiting druggable synthetic

lethal interactors and secondly we can achieve a high selectivity by exploiting true synthetic lethal interactions for anticancer therapy. This is especially remarkable in the case of cancer-specific isoenzymes, which are emerging as one of the most promising anticancer drug targets. GSMMs provide an excellent tool for the systematic simulation of specific pairs of gene knock-out (KO) to unveil those combinations that compromise the viability of cancer cells (synthetic lethal). By definition, gene KO is simulated by giving value zero to gene expression and the effect of gene deletion is transferred to the metabolic reaction level by GPR association. Thus, for instance, the flux through a reaction that is associated only to one knocked-out gene would be zero. If the reaction is catalyzed by isoenzymes or complexes, the effect of a gene deletion is more complex.

However, predicting the metabolic state of a cell after a gene KO is a challenging task, because after the gene KO the system evolves into a new steady-state that tends to be as close as possible to the original steady-state [128]. To overcome these difficulties several algorithms have been developed. For example, the MOMA algorithm minimizes the euclidean norm of flux differences between metabolic states of the KO compared with the wild type [129]. The ROOM method minimizes the total number of significant flux changes from the wild type flux distribution [129].

In other words, MOMA minimizes the changes in the overall flux distribution while ROOM minimizes the number of fluxes to be modified after the gene KO (Figure 3D). As an example of employing the concept of synthetic lethality in cancer, a GSMM approach has been used to develop a genome scale network model of cancer metabolism [119]. The model predicted 52 cytostatic drug targets (40% of which were known) and further predicted combinations of synthetic lethal drug targets, which were validated using NCI-60 cancer cell collection. In a remarkable example, synthetic lethality between heme oxygenase and fumarate hydratase was predicted by the GSMM approach and was also experimentally validated [130]. The number and the quality of these predictions prove the capabilities of this approach to identify synthetic lethal pairs of genes as potential novel drug target in cancer.

Future perspective

Metabolism represents the essence of how cells interact with their environment to provide themselves with energy and the essential building blocks for life. In this review, we highlighted the role of a wide range of factors that trigger the malignant transformation of cancer metabolism as well as experimental and computational approaches to develop new therapies. Despite the encouraging achievements and improvements in cancer

research, there still exist limitations that need to be overcome in order to enhance the effectiveness of drug therapies in cancer disease.

One of the major challenges in targeting key metabolic pathways is the lack of clear understanding of how the cancer cell metabolic profile varies from a non-tumor proliferating cell and the potential toxicity risk associated with targeting metabolism. A better understanding of how the metabolism differs in a specific type of cancer or within the same type may help us predict and identify targets without affecting non-tumor cells. In this context, combination of metabolic and signaling pathway inhibitors has been proposed as one of the rational approaches [131]. Using computational approaches permits the systematic simulation of gene perturbations, either metabolic and/or non-metabolic, that could contribute to unveil novel key signaling nodes resulting in potential anticancer drug targets. Recently developed algorithms, such as PROM [111], allow the integration of transcriptomic data into GSMMs while considering the gene regulatory network structure of a given organism. This approach has been developed for predicting metabolic changes that result from genetic or environmental perturbation in *Escherichia coli*. However, it is obvious that algorithms accounting for both gene regulatory and metabolic networks could be used to analyze more precisely the effect of perturbations on oncogenes in cancer metabolism.

Tumor heterogeneity represents a hurdle that must be overcome in order to develop new and more efficient anticancer therapies. One of the factors triggering intratumoral heterogeneity is the tumor microenvironment, which interferes with the ability of drugs to penetrate tumor tissue and reach the entire tumor cells in a potentially lethal concentration. In addition, heterogeneity within the tumor microenvironment leads to marked gradients in the rate of cell proliferation and to regions of hypoxia and acidity, all of which can influence the sensitivity of the tumor cells to drug treatment. Better understanding of how tumor microenvironment protects cancer cells, during and immediately after chemoradiotherapy is imperative to design new therapies aimed at targeting this tumor-protective niche [132,133]. The use of drug delivery systems can improve the pharmacological properties of traditional chemotherapeutics by altering pharmacokinetics and biodistribution to overcome the harsh conditions of the tumor microenvironment. Moreover, the co-administration of chemotherapeutics and tumor-associated stromal-depleting drugs helps to target the fibrous structure of the modified extracellular matrix, which can result in a less penetrable tumor microenvironment [134].

Another interesting approach considers therapies that interfere in the metabolic co-operation between

cancer cells and stromal cells in their microenvironment [135] or between intratumoral subpopulations. The study of the metabolic coupling between different cellular populations as potential drug targets can be achieved by reconstructing an artificial tumor microenvironment by using GSMMs approach. To date several algorithms have been developed that integrate omic data into a GSMM reconstruction that permit to compute the secretion and uptake rates of nutrients (Table 1) and hence study the complementary secretomes within a heterogeneous cellular community. However, test and validation of a metabolic model becomes more complex if it considers a heterogeneous cellular population. Nevertheless, recent studies on artificial microbial ecosystems have demonstrated the potential of this type of approach to study synergies in heterogeneous cellular communities [136] that could be extrapolated to the study of cancer to unveil the mechanisms underlying the cooperation between tumoral and stromal cells, as well as between intratumoral subpopulations.

The intratumoral microenvironment also confers an extreme flexibility and adaptation capability to cancer cells that enhances tumor progression and represents a challenge for target-directed therapies [137]. The intratumoral heterogeneity is driven by two main processes: epithelial-to-mesenchymal transitions, by which epithelial cells gain invasive properties and lose at least part of their epithelial phenotypes [138]; and mesenchymal-to-epithelial transitions, by which mesenchymal cells can revert to an epithelial gene program displaying strong self-renewal and survival properties [138–140]. Drug targets that repress these processes have been proposed to significantly reduce tumoral progression.

Anti-angiogenic therapy has been proposed for a long time as an interesting approach to reduce tumor growth. Tumor blood vessels are surrounded by a very hostile environment, with a high amount of acidosis, low oxygen regions, weak pericyte–endothelial cell interaction, leading to its tortuous and leaky vessels with gaps that allow easy escape of invading tumor cells [141,142]. Additionally, restoring the blood vessels to a ‘normal’ state would get the tumor vessels back on track to its proper functional form, reducing hypoxia-induced metastasis and improving the effects of chemotherapy [143,144]. Also it is expected to reduce the spreading of cancer cells, because pericytes that are required to strengthen blood vessels would be acting more efficiently and hence prevent the intravasation of the cancer cells through the gaps found in the normally leaky tumor vessels.

Therapies based on both metastatic targets arresting cancer cells in a non-metastatic stage and angiogenic targets normalizing tumor vessels are promising strategies to design new anticancer therapies. Coupling

this strategy with associated key metabolic pathways is a good approach in cancer treatment and requires computational tools to identify the putative targets. Recently developed methods, such as the ‘metabolic transformation algorithm’ allows the identification of the actors involved in metabolic transformations [145]. This methodology identifies targets that alter the metabolism retrieving the cells back from a given metabolic state to another metabolic state (Figure 3D). This method has been successfully used to find drug targets that revert disrupted metabolism focused on aging. However, this approach could be suitable to determine drug targets arresting tumor in a non-metastatic stage, normalize tumor vessels or prevent tumor intravasation, resulting in a reduction of tumor progression. Additionally, GSMM predictions could be refined by integrating information from dynamic ¹³C FBA [146].

Moreover, **combinatorial therapies**, targeting angiogenesis and metastatic targets, have been proposed as a way to enhance anticancer therapies [27]. Traditionally, these approaches has been focused on

Key term

Combinatorial therapies: Strategy that takes profit of the synergistic effects of two therapeutic treatments targeting different processes of the cellular biology.

targeting signaling pathways, such as the VEGF inhibition or VEGF receptors (R1/R2) blockade [147,148] and CXCR4 protein, which is involved in tumor colonization, or the cytokine PIGF, which prepares the metastatic niche in bone marrow for the cells invading from breast cancer [149]. However, studies on the metabolic reprogramming in endothelial cells have opened new avenues to explore the combinatorial therapies of targeting both tumors and their angiogenesis, in the context of metabolism.

The approaches reviewed here provide a guideline to improve the anticancer drug-target therapies focused on metabolic reprogramming. However, the lack of a proper model depicting the complete map of metabolic reactions, regulatory processes as well as tumor heterogeneity and synergistic cooperation between cellular

Executive summary

Background

- Nowadays, it is widely recognized that metabolic reprogramming is essential to sustain tumor progression. These changes are promoted by genetic and epigenetic alterations producing mutations in key metabolic enzymes that modify flux distributions in metabolic networks, providing advantages to cancer cells in terms of energy production and synthesis of biomolecules.

Crosstalk between oncogenic signaling events & cancer cell metabolism

- Many key oncogenic signaling pathways, such as *HIF*, *Myc*, PI3K/AKT/mTOR or SREBPs, converge to adapt tumor cell metabolism in order to support their growth and survival. They are intimately involved in modulating glycolysis, mitochondrial oxidative phosphorylation, lipid metabolism and glutaminolysis.

Tumor microenvironment

- The tumor microenvironment is complex and comprises the extracellular matrix, tumor and stromal cells (e.g., epithelial cells, fibroblasts and inflammatory cells) that are embedded within this matrix and nourished by vascular network. The tumor heterogeneity, signaling molecules and chemicals, such as oxygen and protons, can influence tumor cell proliferation, survival, invasion, metastasis and energy metabolism reprogramming.

Isoenzymes: therapeutic targets in cancer

- Isoforms of many of the enzymes specific to important metabolic pathways are found to be overexpressed in tumor cells affecting important pathways of the energetic metabolism. These isoforms have a key role in mediating the aberrant metabolism of cancer cells and could serve as a promising source of novel drug targets.
- These tumor-specific isoforms can be involved in important pathways, such as glycolysis, tricarboxylic acid cycle, pentose phosphate pathway and glutamine metabolism, among other important energetic pathways

Genome-scale metabolic models as new tools emerging from systems biology approach to drug discovery

- Genome-scale metabolic models are emerging as a potential solution to decipher the molecular mechanisms underlying cancer in the context of systems biology. These models represent the metabolic reactions encoded by an organism’s genome and summarize and codify information known about the metabolism of that organism.
- These models use constraint-based methods for the mathematical representation of biotransformations and metabolic processes occurring within the organism and offer an appropriate framework to integrate the increasing amount of ‘omic’ data generated by the different high-throughput technologies.
- Genome-scale metabolic models approaches have allowed to identify a number of tumor-specific biomarkers, anticancer drug-target and synthetic lethal genes opening a promising avenue in the development of new anticancer therapies.

communities, makes selecting the best possible target combinations difficult. Thus, in order to develop more efficient anticancer therapies, more efforts need to be made in developing new methods to study tumor metabolism and obtain a better understanding of the molecular processes underlying tumor progression and invasion.

Financial & competing interests disclosure

This work was supported by funds of European Commission METAFUX (Marie Curie FP7-PEOPLE-2010 ITN-264780);

Spanish Government and European Union FEDER Funds (SAF2011–25726); and Generalitat de Catalunya (2014SGR-1017 and Icrea Academia award 2010 granted to M Cascante). The authors have no other relevant affiliations or financial involvement with any organization or entity with a financial interest in or financial conflict with the subject matter or materials discussed in the manuscript. This includes employment, consultancies, honoraria, stock ownership or options, expert testimony, grants or patents received or pending, or royalties.

No writing assistance was utilized in the production of this manuscript.

References

- Siegel R, Naishadham D, Jemal A. Cancer statistics, 2012. *CA Cancer J. Clin.* 62(1), 10–29 (2012).
- Hanahan D, Weinberg RA. Hallmarks of cancer: the next generation. *Cell* 144(5), 646–674 (2011).
- Ward PS, Thompson CB. Metabolic reprogramming: a cancer hallmark even warburg did not anticipate. *Cancer Cell* 21(3), 297–308 (2012).
- Vander Heiden MG, Cantley LC, Thompson CB. Understanding the Warburg effect: the metabolic requirements of cell proliferation. *Science* 324(5930), 1029–1033 (2009).
- Stratton MR. Exploring the genomes of cancer cells: progress and promise. *Science* 331(6024), 1553–1558 (2011).
- Yuneva MO, Fan TW, Allen TD *et al.* The metabolic profile of tumors depends on both the responsible genetic lesion and tissue type. *Cell Metab.* 15(2), 157–170 (2012).
- Obacz J, Pastorekova S, Vojtesek B, Hrstka R. Cross-talk between HIF and p53 as mediators of molecular responses to physiological and genotoxic stresses. *Mol. Cancer* 12(1), 93 (2013).
- Dang CV. Links between metabolism and cancer. *Genes Dev.* 26(9), 877–890 (2012).
- Wise DR, Deberardinis RJ, Mancuso A *et al.* Myc regulates a transcriptional program that stimulates mitochondrial glutaminolysis and leads to glutamine addiction. *Proc. Natl Acad. Sci. USA* 105(48), 18782–18787 (2008).
- Pecqueur C, Oliver L, Oizel K, Laliere L, Vallette FM. Targeting metabolism to induce cell death in cancer cells and cancer stem cells. *Int. J. Cell Biol.* 2013, 805975 (2013).
- Dan HC, Ebbs A, Pasparakis M, Van Dyke T, Basseres DS, Baldwin AS. Akt-dependent activation of mTORC1 Involves phosphorylation of mTOR by IKK α . *J. Biol. Chem.* 289(36), 25227–25240 (2014).
- Porstmann T, Santos CR, Griffiths B *et al.* SREBP activity is regulated by mTORC1 and contributes to Akt-dependent cell growth. *Cell Metab.* 8(3), 224–236 (2008).
- Alvarez MS, Fernandez-Alvarez A, Cucarella C, Casado M. Stable SREBP-1a knockdown decreases the cell proliferation rate in human preadipocyte cells without inducing senescence. *Biochem. Biophys. Res. Commun.* 447(1), 51–56 (2014).
- Furuta E, Pai SK, Zhan R *et al.* Fatty acid synthase gene is up-regulated by hypoxia via activation of Akt and sterol regulatory element binding protein-1. *Cancer Res.* 68(4), 1003–1011 (2008).
- Cascante M, Benito A, Zanuy M, Vizán P, Marín S, De Atauri P. Metabolic network adaptations in cancer as targets for novel therapies. *Biochem. Soc. Trans.* 38(5), 1302–1306 (2010).
- Doherty JR, Yang C, Scott KEN *et al.* Blocking lactate export by inhibiting the MYC target MCT1 disables glycolysis and glutathione synthesis. *Cancer Res.* 74(3), 908–920 (2014).
- Jiang P, Du W, Wang X *et al.* p53 regulates biosynthesis through direct inactivation of glucose-6-phosphate dehydrogenase. *Nat. Cell Biol.* 13(3), 310–316 (2011).
- Bentz S, Cee A, Endlicher E *et al.* Hypoxia induces the expression of transketolase-like 1 in human colorectal cancer. *Digestion* 88(3), 182–192 (2013).
- Sinthupibulyakit C, Ittarat W, St Clair WH, St Clair DK. p53 protects lung cancer cells against metabolic stress. *Int. J. Oncol.* 37(6), 1575–1581 (2010).
- Cui G, Park S, Badeaux AI *et al.* PHF20 is an effector protein of p53 double lysine methylation that stabilizes and activates p53. *Nat. Struct. Mol. Biol.* 19(9), 916–924 (2012).
- Xiao M, Yang H, Xu W *et al.* Inhibition of α -KG-dependent histone and DNA demethylases by fumarate and succinate that are accumulated in mutations of FH and SDH tumor suppressors. *Genes Dev.* 26(12), 1326–1338 (2012).
- Xu W, Yang H, Liu Y *et al.* Oncometabolite 2-hydroxyglutarate is a competitive inhibitor of α -ketoglutarate-dependent dioxygenases. *Cancer Cell* 19(1), 17–30 (2011).
- Commandeur S, Ho SH, De Gruijl FR, Willemze R, Tensen CP, El Ghalbzouri A. Functional characterization of cancer-associated fibroblasts of human cutaneous squamous cell carcinoma. *Exp. Dermatol.* 20(9), 737–742 (2011).
- Zhou B, Chen WL, Wang YY *et al.* A role for cancer-associated fibroblasts in inducing the epithelial-to-mesenchymal transition in human tongue squamous cell carcinoma. *J. Oral Pathol. Med.* 43(8), 585–592 (2014).
- Yu Y, Xiao CH, Tan LD, Wang QS, Li XQ, Feng YM. Cancer-associated fibroblasts induce epithelial-mesenchymal transition of breast cancer cells through paracrine TGF- β signalling. *Br. J. Cancer* 110(3), 724–732 (2014).

- 26 Zhang Y, Choksi S, Chen K, Pobezinskaya Y, Linnoila I, Liu ZG. ROS play a critical role in the differentiation of alternatively activated macrophages and the occurrence of tumor-associated macrophages. *Cell Res.* 23(7), 898–914 (2013).
- 27 De Bock K, Mazzone M, Carmeliet P. Antiangiogenic therapy, hypoxia, and metastasis: risky liaisons, or not? *Nat. Rev. Clin. Oncol.* 8(7), 393–404 (2011).
- 28 Wang W, Quan Y, Fu Q *et al.* Dynamics between cancer cell subpopulations reveals a model coordinating with both hierarchical and stochastic concepts. *PLoS ONE* 9(1), e84654 (2014).
- 29 Feng W, Gentles A, Nair RV *et al.* Targeting unique metabolic properties of breast tumor initiating cells. *Stem Cells* 32(7), 1734–1745 (2014).
- 30 Ciavardelli D, Rossi C, Barcaroli D *et al.* Breast cancer stem cells rely on fermentative glycolysis and are sensitive to 2-deoxyglucose treatment. *Cell Death Dis.* 5, e1336 (2014).
- 31 Nieman KM, Kenny HA, Penicka CV *et al.* Adipocytes promote ovarian cancer metastasis and provide energy for rapid tumor growth. *Nat. Med.* 17(11), 1498–1503 (2011).
- 32 Willemarck N, Rysman E, Brusselmans K *et al.* Aberrant activation of fatty acid synthesis suppresses primary cilium formation and distorts tissue development. *Cancer Res.* 70(22), 9453–9462 (2010).
- 33 Park JB, Lee CS, Jang JH *et al.* Phospholipase signalling networks in cancer. *Nat. Rev. Cancer* 12(11), 782–792 (2012).
- 34 Nomura DK, Long JZ, Niessen S, Hoover HS, Ng SW, Cravatt BF. Monoacylglycerol lipase regulates a fatty acid network that promotes cancer pathogenesis. *Cell* 140(1), 49–61 (2010).
- 35 Karnezis T, Shayan R, Caesar C *et al.* VEGF-D promotes tumor metastasis by regulating prostaglandins produced by the collecting lymphatic endothelium. *Cancer Cell* 21(2), 181–195 (2012).
- 36 Seguin F, Carvalho MA, Bastos DC *et al.* The fatty acid synthase inhibitor orlistat reduces experimental metastases and angiogenesis in B16-F10 melanomas. *Br. J. Cancer* 107(6), 977–987 (2012).
- 37 Pavlides S, Tsirigos A, Migneco G *et al.* The autophagic tumor stroma model of cancer. Role of oxidative stress and ketone production in fueling tumor cell metabolism. *Cell Cycle* 9(17), 3485–3505 (2010).
- 38 Carito V, Bonuccelli G, Martinez-Outschoorn UE *et al.* Metabolic remodeling of the tumor microenvironment: migration stimulating factor (MSF) reprograms myofibroblasts toward lactate production, fueling anabolic tumor growth. *Cell Cycle* 11(18), 3403–3414 (2012).
- 39 Hur H, Paik MJ, Xuan Y *et al.* Quantitative measurement of organic acids in tissues from gastric cancer patients indicates increased glucose metabolism in gastric cancer. *PLoS ONE* 9(6), e98581 (2014).
- 40 Peters K, Kamp G, Berz A *et al.* Changes in human endothelial cell energy metabolic capacities during *in vitro* cultivation. The role of “aerobic glycolysis” and proliferation. *Cell Physiol. Biochem.* 24(5–6), 483–492 (2009).
- 41 Harjes U, Bensaad K, Harris AL. Endothelial cell metabolism and implications for cancer therapy. *Br. J. Cancer* 107(8), 1207–1212 (2012).
- 42 Vegran F, Boidot R, Michiels C, Sonveaux P, Feron O. Lactate influx through the endothelial cell monocarboxylate transporter MCT1 supports an NF-kappaB/IL-8 pathway that drives tumor angiogenesis. *Cancer Res.* 71(7), 2550–2560 (2011).
- 43 Vizan P, Sanchez-Tena S, Alcarraz-Vizan G *et al.* Characterization of the metabolic changes underlying growth factor angiogenic activation: identification of new potential therapeutic targets. *Carcinogenesis* 30(6), 946–952 (2009).
- 44 Calcinotto A, Filipazzi P, Grioni M *et al.* Modulation of microenvironment acidity reverses anergy in human and murine tumor-infiltrating T lymphocytes. *Cancer Res.* 72(11), 2746–2756 (2012).
- 45 Polet F, Feron O. Endothelial cell metabolism and tumour angiogenesis: glucose and glutamine as essential fuels and lactate as the driving force. *J. Intern. Med.* 273(2), 156–165 (2013).
- 46 Choi SY, Collins CC, Gout PW, Wang Y. Cancer-generated lactic acid: a regulatory, immunosuppressive metabolite? *J. Pathol.* 230(4), 350–355 (2013).
- 47 Wels J, Kaplan RN, Rafii S, Lyden D. Migratory neighbors and distant invaders: tumor-associated niche cells. *Genes Dev.* 22(5), 559–574 (2008).
- 48 Cardenas-Navia LI, Mace D, Richardson RA, Wilson DF, Shan S, Dewhirst MW. The pervasive presence of fluctuating oxygenation in tumors. *Cancer Res.* 68(14), 5812–5819 (2008).
- 49 Sharma MK, Seidlitz EP, Singh G. Cancer cells release glutamate via the cystine/glutamate antiporter. *Biochem. Biophys. Res. Commun.* 391(1), 91–95 (2010).
- 50 Meneses AM, Medina RA, Kato S *et al.* Regulation of GLUT3 and glucose uptake by the cAMP signalling pathway in the breast cancer cell line ZR-75. *J. Cell. Physiol.* 214(1), 110–116 (2008).
- 51 Chen J, Zhang S, Li Y, Tang Z, Kong W. Hexokinase 2 overexpression promotes the proliferation and survival of laryngeal squamous cell carcinoma. *Tumor Biol.* 35(4), 3743–3753 (2014).
- 52 Robey RB, Hay N. Mitochondrial hexokinases, novel mediators of the antiapoptotic effects of growth factors and Akt. *Oncogene* 25(34), 4683–4696 (2006).
- 53 Galluzzi L, Kepp O, Tajeddine N, Kroemer G. Disruption of the hexokinase-VDAC complex for tumor therapy. *Oncogene* 27(34), 4633–4635 (2008).
- 54 Christofk HR, Vander Heiden MG, Harris MH *et al.* The M2 splice isoform of pyruvate kinase is important for cancer metabolism and tumour growth. *Nature* 452(7184), 230–233 (2008).
- 55 Christofk HR, Vander Heiden MG, Wu N, Asara JM, Cantley LC. Pyruvate kinase M2 is a phosphotyrosine-binding protein. *Nature* 452(7184), 181–186 (2008).
- 56 Vander Heiden MG, Christofk HR, Schuman E *et al.* Identification of small molecule inhibitors of pyruvate kinase M2. *Biochem. Pharmacol.* 79(8), 1118–1124 (2010).

- 57 Clem B, Telang S, Clem A *et al.* Small-molecule inhibition of 6-phosphofructo-2-kinase activity suppresses glycolytic flux and tumor growth. *Mol. Cancer Ther.* 7(1), 110–120 (2008).
- 58 Zhou M, Zhao Y, Ding Y *et al.* Warburg effect in chemosensitivity: targeting lactate dehydrogenase-A re-sensitizes Taxol-resistant cancer cells to Taxol. *Mol. Cancer* 9(1), 33 (2010).
- 59 Le A, Cooper CR, Gouw AM *et al.* Inhibition of lactate dehydrogenase A induces oxidative stress and inhibits tumor progression. *Proc. Nat. Acad. Sci. USA* 107(5), 2037–2042 (2010).
- 60 Lu CW, Lin SC, Chen KF, Lai YY, Tsai SJ. Induction of pyruvate dehydrogenase kinase-3 by hypoxia-inducible factor-1 promotes metabolic switch and drug resistance. *J. Biol. Chem.* 283(42), 28106–28114 (2008).
- 61 Yan H, Parsons DW, Jin G *et al.* IDH1 and IDH2 mutations in gliomas. *N. Engl. J. Med.* 360(8), 765–773 (2009).
- 62 Dang L, Jin S, Su SM. IDH mutations in glioma and acute myeloid leukemia. *Trends Mol. Med.* 16(9), 387–397 (2010).
- 63 El-Ashmawy N, El-Bahrawy H, Shamloula M, El-Feky O. Biochemical/metabolic changes associated with hepatocellular carcinoma development in mice. *Tumor Biol.* 35(6), 5459–5466 (2014).
- 64 Xu X, Zur Hausen A, Coy JF, Löchelt M. Transketolase-like protein 1 (TKTL1) is required for rapid cell growth and full viability of human tumor cells. *Int. J. Cancer* 124(6), 1330–1337 (2009).
- 65 Vizán P, Alcarraz-Vizán G, Díaz-Moralli S, Solovjeva ON, Frederiks WM, Cascante M. Modulation of pentose phosphate pathway during cell cycle progression in human colon adenocarcinoma cell line HT29. *Int. J. Cancer* 124(12), 2789–2796 (2009).
- 66 Dang CV. Glutaminolysis: supplying carbon or nitrogen or both for cancer cells? *Cell Cycle* 9(19), 3914–3916 (2010).
- 67 Durán RV, Opliger W, Robitaille AM *et al.* Glutaminolysis activates Rag-mTORC1 signaling. *Mol. Cell* 47(3), 349–358 (2012).
- 68 Deberardinis RJ, Thompson CB. Cellular metabolism and disease: what do metabolic outliers teach us? *Cell* 148(6), 1132–1144 (2012).
- 69 Mardinoglu A, Nielsen J. Systems medicine and metabolic modelling. *J. Intern. Med.* 271(2), 142–154 (2012).
- 70 Gonnerman MC, Benedict MN, Feist AM, Metcalf WW, Price ND. Genomically and biochemically accurate metabolic reconstruction of *Methanosarcina barkeri fusaro*, iMG746. *Biotechnol. J.* 8(9), 1070–1079 (2013).
- 71 Benedict MN, Gonnerman MC, Metcalf WW, Price ND. Genome-scale metabolic reconstruction and hypothesis testing in the methanogenic archaeon *Methanosarcina acetivorans* C2A. *J. Bacteriol.* 194(4), 855–865 (2012).
- 72 Lee NR, Lakshmanan M, Aggarwal S *et al.* Genome-scale metabolic network reconstruction and *in silico* flux analysis of the thermophilic bacterium *Thermus thermophilus* HB27. *Microb. Cell Fact.* 13(1), 61 (2014).
- 73 Orth JD, Conrad TM, Na J *et al.* A comprehensive genome-scale reconstruction of *Escherichia coli* metabolism – 2011. *Mol. Syst. Biol.* 7(1), 535 (2011).
- 74 Nagarajan H, Sahin M, Nogales J *et al.* Characterizing acetogenic metabolism using a genome-scale metabolic reconstruction of *Clostridium ljungdablii*. *Microb. Cell Fact.* 12(1), 118 (2013).
- 75 Song C, Chiasson MA, Nursimulu N *et al.* Metabolic reconstruction identifies strain-specific regulation of virulence in *Toxoplasma gondii*. *Mol. Syst. Biol.* 9(1), 708 (2013).
- 76 Heavner B, Smallbone K, Barker B, Mendes P, Walker L. Yeast 5 – an expanded reconstruction of the *Saccharomyces cerevisiae* metabolic network. *BMC Syst. Biol.* 6(1), 55 (2012).
- 77 Caspeta L, Shoaie S, Agren R, Nookaew I, Nielsen J. Genome-scale metabolic reconstructions of *Pichia stipitis* and *Pichia pastoris* and *in silico* evaluation of their potentials. *BMC Syst. Biol.* 6(1), 24 (2012).
- 78 Liu J, Gao Q, Xu N, Liu L. Genome-scale reconstruction and *in silico* analysis of *Aspergillus terreus* metabolism. *Mol. Biosyst.* 9(7), 1939–1948 (2013).
- 79 Arnold A, Nikoloski Z. Bottom-up metabolic reconstruction of arabidopsis and its application to determining the metabolic costs of enzyme production. *Plant Physiol.* 165(3), 1380–1391 (2014).
- 80 Dal'molin CG, Quek LE, Palfreyman RW, Brumbley SM, Nielsen LK. C4GEM, a genome-scale metabolic model to study C4 plant metabolism. *Plant Physiol.* 154(4), 1871–1885 (2010).
- 81 Duarte NC, Becker SA, Jamshidi N *et al.* Global reconstruction of the human metabolic network based on genomic and bibliomic data. *Proc. Natl Acad. Sci. USA* 104(6), 1777–1782 (2007).
- 82 Hao T, Ma HW, Zhao XM, Goryanin I. The reconstruction and analysis of tissue specific human metabolic networks. *Mol. Biosyst.* 8(2), 663–670 (2012).
- 83 Thiele I, Swainston N, Fleming RM *et al.* A community-driven global reconstruction of human metabolism. *Nat. Biotech.* 31(5), 419–425 (2013).
- 84 Sigurdsson MI, Jamshidi N, Steingrimsdottir E, Thiele I, Palsson BØ. A detailed genome-wide reconstruction of mouse metabolism based on human Recon 1. *BMC Syst. Biol.* 4(1), 140 (2010).
- 85 Bordbar A, Feist AM, Usaite-Black R, Woodcock J, Palsson BØ, Famili I. A multi-tissue type genome-scale metabolic network for analysis of whole-body systems physiology. *BMC Syst. Biol.* 5(1), 180 (2011).
- 86 Wang Y, Eddy JA, Price ND. Reconstruction of genome-scale metabolic models for 126 human tissues using mCADRE. *BMC Syst. Biol.* 6(1), 153 (2012).
- 87 Agren R, Bordel S, Mardinoglu A, Pornputtapong N, Nookaew I, Nielsen J. Reconstruction of genome-scale active metabolic networks for 69 human cell types and 16 cancer types using INIT. *PLoS Comput. Biol.* 8(5), e1002518 (2012).
- 88 Jerby L, Wolf L, Denkert C *et al.* Metabolic associations of reduced proliferation and oxidative stress in advanced breast cancer. *Cancer Res.* 72(22), 5712–5720 (2012).
- 89 Orth JD, Thiele I, Palsson BØ. What is flux balance analysis? *Nat. Biotech.* 28(3), 245–248 (2010).

- 90 Rajcevic U, Knol J, Piersma S *et al.* Colorectal cancer derived organotypic spheroids maintain essential tissue characteristics but adapt their metabolism in culture. *Proteome Sci.* 12(1), 39 (2014).
- 91 Papp B, Notebaart RA, Pál C. Systems-biology approaches for predicting genomic evolution. *Nat. Rev. Genet.* 12(9), 591–602 (2011).
- 92 Matsuda F, Furusawa C, Kondo T, Ishii J, Shimizu H, Kondo A. Engineering strategy of yeast metabolism for higher alcohol production. *Microb. Cell Fact.* 10(1), 70 (2011).
- 93 Park JM, Song H, Lee HJ, Seung D. Genome-scale reconstruction and *in silico* analysis of *Klebsiella oxytoca* for 2,3-butanediol production. *Microb. Cell Fact.* 12(1), 20 (2013).
- 94 Lütke-Eversloh T, Bahl H. Metabolic engineering of *Clostridium acetobutylicum*: recent advances to improve butanol production. *Curr. Opin. Biotechnol.* 22(5), 634–647 (2011).
- 95 Kumar VS, Maranas CD. GrowMatch: an automated method for reconciling *in silico* *in vivo* growth predictions. *PLoS Comput. Biol.* 5(3), e1000308 (2009).
- 96 Kim HU, Kim SY, Jeong H *et al.* Integrative genome-scale metabolic analysis of *Vibrio vulnificus* for drug targeting and discovery. *Mol. Syst. Biol.* 7(1), 460 (2011).
- 97 Agren R, Mardinoglu A, Asplund A, Kampf C, Uhlen M, Nielsen J. Identification of anticancer drugs for hepatocellular carcinoma through personalized genome-scale metabolic modeling. *Mol. Syst. Biol.* 10(3), 721 (2014).
- 98 Feist AM, Herrgård MJ, Thiele I, Reed JL, Palsson BØ. Reconstruction of biochemical networks in microorganisms. *Nat. Rev. Microbiol.* 7(2), 129–143 (2009).
- 99 Caspi R, Altman T, Dale JM *et al.* The MetaCyc database of metabolic pathways and enzymes and the BioCyc collection of pathway/genome databases. *Nucleic Acids Res.* 38(Suppl. 1), D473–D479 (2010).
- 100 Henry CS, Dejongh M, Best AA, Frybarger PM, Linsay B, Stevens RL. High-throughput generation, optimization and analysis of genome-scale metabolic models. *Nat. Biotech.* 28(9), 977–982 (2010).
- 101 Coordinators NR. Database resources of the National Center for Biotechnology Information. *Nucleic Acids Res.* 41(D1), D8–D20 (2013).
- 102 Pagani I, Liolios K, Jansson J *et al.* The Genomes OnLine Database (GOLD) v.4: status of genomic and metagenomic projects and their associated metadata. *Nucleic Acids Res.* 40(D1), D571–D579 (2012).
- 103 Kanehisa M, Goto S, Sato Y, Furumichi M, Tanabe M. KEGG for integration and interpretation of large-scale molecular data sets. *Nucleic Acids Res.* 40(D1), D109–D114 (2012).
- 104 Chang A, Scheer M, Grote A, Schomburg I, Schomburg D. BRENDA, AMENDA and FRENDA the enzyme information system: new content and tools in 2009. *Nucleic Acids Res.* 37(Suppl. 1), D588–D592 (2009).
- 105 Schellenberger J, Que R, Fleming RM *et al.* Quantitative prediction of cellular metabolism with constraint-based models: the COBRA Toolbox v2.0. *Nat. Protoc.* 6(9), 1290–1307 (2011).
- 106 Wintermute E, Lieberman T, Silver P. An objective function exploiting suboptimal solutions in metabolic networks. *BMC Syst. Biol.* 7(1), 98 (2013).
- 107 Palsson B, Zengler K. The challenges of integrating multi-omic data sets. *Nat. Chem. Biol.* 6(11), 787–789 (2010).
- 108 Bordbar A, Mo ML, Nakayasu ES *et al.* Model-driven multi-omic data analysis elucidates metabolic immunomodulators of macrophage activation. *Mol. Syst. Biol.* 8(1), 558 (2012).
- 109 Lewis NE, Nagarajan H, Palsson BØ. Constraining the metabolic genotype–phenotype relationship using a phylogeny of *in silico* methods. *Nat. Rev. Microbiol.* 10(4), 291–305 (2012).
- 110 Jensen PA, Papin JA. MetDraw: automated visualization of genome-scale metabolic network reconstructions and high-throughput data. *Bioinformatics* 30(9), 1327–1328 (2014).
- 111 Chandrasekaran S, Price ND. Probabilistic integrative modeling of genome-scale metabolic and regulatory networks in *Escherichia coli* and *Mycobacterium tuberculosis*. *Proc. Natl Acad. Sci. USA* 107(41), 17845–17850 (2010).
- 112 Barabási AL, Gulbahce N, Loscalzo J. Network medicine: a network-based approach to human disease. *Nat. Rev. Genet.* 12(1), 56–68 (2011).
- 113 Jerby L, Shlomi T, Ruppin E. Computational reconstruction of tissue-specific metabolic models: application to human liver metabolism. *Mol. Syst. Biol.* 6(1), 401 (2010).
- 114 Lewis NE, Schramm G, Bordbar A *et al.* Large-scale *in silico* modeling of metabolic interactions between cell types in the human brain. *Nat. Biotech.* 28(12), 1279–1285 (2010).
- 115 Zur H, Ruppin E, Shlomi T. iMAT: an integrative metabolic analysis tool. *Bioinformatics* 26(24), 3140–3142 (2010).
- 116 Schmidt BJ, Ebrahim A, Metz TO, Adkins JN, Palsson BØ, Hyduke DR. GIM3E: condition-specific models of cellular metabolism developed from metabolomics and expression data. *Bioinformatics* 29(22), 2900–2908 (2013).
- 117 Galhardo M, Sinkkonen L, Berninger P, Lin J, Sauter T, Heinäniemi M. Integrated analysis of transcript-level regulation of metabolism reveals disease-relevant nodes of the human metabolic network. *Nucleic Acids Res.* 42(3), 1474–1496 (2013).
- 118 Lazar MA, Birnbaum MJ. De-meaning of metabolism. *Science* 336(6089), 1651–1652 (2012).
- 119 Folger O, Jerby L, Frezza C, Gottlieb E, Ruppin E, Shlomi T. Predicting selective drug targets in cancer through metabolic networks. *Mol. Syst. Biol.* 7(1), 501 (2011).
- 120 Davis VW, Bathe OF, Schiller DE, Slupsky CM, Sawyer MB. Metabolomics and surgical oncology: potential role for small molecule biomarkers. *J. Surg. Oncol.* 103(5), 451–459 (2011).
- 121 Murabito E, Simeonidis E, Smallbone K, Swinton J. Capturing the essence of a metabolic network: a flux balance analysis approach. *J. Theor. Biol.* 260(3), 445–452 (2009).
- 122 Schellenberger J, Palsson BØ. Use of randomized sampling for analysis of metabolic networks. *J. Biol. Chem.* 284(9), 5457–5461 (2009).

- 123 Duggal R, Minev B, Geissinger U *et al.* Biotherapeutic approaches to target cancer stem cells. *J. Stem Cells* 8(3–4), 135–149 (2013).
- 124 Philips MR, Cox AD. Geranylgeranyltransferase I as a target for anti-cancer drugs. *J. Clin. Invest.* 117(5), 1223–1225 (2007).
- 125 Dudakovic A, Tong H, Hohl R. Geranylgeranyl diphosphate depletion inhibits breast cancer cell migration. *Invest. New Drugs* 29(5), 912–920 (2011).
- 126 Hebar A, Valent P, Selzer E. The impact of molecular targets in cancer drug development: major hurdles and future strategies. *Expert Rev. Clin. Pharmacol.* 6(1), 23–34 (2013).
- 127 Conde-Pueyo N, Munteanu A, Solé RV, Rodríguez-Caso C. Human synthetic lethal inference as potential anti-cancer target gene detection. *BMC Syst. Biol.* 3(1), 116 (2009).
- 128 Barbash DA, Lorigan JG. Lethality in *Drosophilamelanogaster/Drosophila simulans* species hybrids is not associated with substantial transcriptional misregulation. *J. Exp. Zool. Part B Mol. Dev. Evol.* 308(1), 74–84 (2007).
- 129 Ren S, Zeng B, Qian X. Adaptive bi-level programming for optimal gene knockouts for targeted overproduction under phenotypic constraints. *BMC Bioinformatics* 14(Suppl. 2), S17 (2013).
- 130 Frezza C, Zheng L, Folger O *et al.* Haem oxygenase is synthetically lethal with the tumour suppressor fumarate hydratase. *Nature* 477(7363), 225–228 (2011).
- 131 Zhao Y, Butler EB, Tan M. Targeting cellular metabolism to improve cancer therapeutics. *Cell Death Dis.* 4, e532 (2013).
- 132 Vaupel P. Tumor microenvironmental physiology and its implications for radiation oncology. *Sem. Radiat. Oncol.* 14(3), 198–206 (2004).
- 133 Tannock IF, Lee CM, Tunggal JK, Cowan DS, Egorin MJ. Limited penetration of anticancer drugs through tumor tissue a potential cause of resistance of solid tumors to chemotherapy. *Clin. Cancer Res.* 8(3), 878–884 (2002).
- 134 Olive KP, Jacobetz MA, Davidson CJ *et al.* Inhibition of Hedgehog signaling enhances delivery of chemotherapy in a mouse model of pancreatic cancer. *Science* 324(5933), 1457–1461 (2009).
- 135 Hulit J, Howell A, Gandara R, Sartini M, Arafat H, Bevilacqua G. Creating a tumor-resistant microenvironment. *Cell Cycle* 12(3), 480–490 (2013).
- 136 Ye C, Zou W, Xu N, Liu L. Metabolic model reconstruction and analysis of an artificial microbial ecosystem for vitamin C production. *J. Biotech.* 182, 61–67 (2014).
- 137 Peinado H, Olmeda D, Cano A. Snail, Zeb and bHLH factors in tumour progression: an alliance against the epithelial phenotype? *Nat. Rev. Cancer* 7(6), 415–428 (2007).
- 138 Celià-Terrassa T, Meca-Cortés Ó, Mateo F *et al.* Epithelial-mesenchymal transition can suppress major attributes of human epithelial tumor-initiating cells. *J. Clin. Invest.* 122(5), 1849 (2012).
- 139 Korpál M, Ell BJ, Buffa FM *et al.* Direct targeting of Sec23a by miR-200s influences cancer cell secretome and promotes metastatic colonization. *Nat. Med.* 17(9), 1101–1108 (2011).
- 140 Ocaña OH, Córcoles R, Fabra Á *et al.* Metastatic colonization requires the repression of the epithelial-mesenchymal transition inducer Prrx1. *Cancer Cell* 22(6), 709–724 (2012).
- 141 Rundqvist H, Johnson RS. Hypoxia and metastasis in breast cancer. In: *Diverse Effects of Hypoxia on Tumor Progression*. Simon MC (Ed.) Springer, Berlin/Heidelberg, Germany, 121–139 (2010).
- 142 Nagy JA, Chang S-H, Shih S-C, Dvorak AM, Dvorak HF. Heterogeneity of the tumor vasculature. *Semin. Thromb. Hemost.* 36(3), 321–331 (2010).
- 143 Mazzone M, Dettori D, Leite De Oliveira R *et al.* Heterozygous deficiency of PHD2 restores tumor oxygenation and inhibits metastasis via endothelial normalization. *Cell* 136(5), 839–851 (2009).
- 144 Rolny C, Mazzone M, Tugues S *et al.* HRG inhibits tumor growth and metastasis by inducing macrophage polarization and vessel normalization through downregulation of PlGF. *Cancer Cell* 19(1), 31–44 (2011).
- 145 Yizhak K, Gabay O, Cohen H, Ruppin E. Model-based identification of drug targets that revert disrupted metabolism and its application to ageing. *Nat. Commun.* 4, 2632 (2013).
- 146 De Mas IM, Selivanov VA, Marín S *et al.* Compartmentation of glycogen metabolism revealed from ¹³C isotopologue distributions. *BMC Syst. Biol.* 5(1), 175 (2011).
- 147 Hassan S, Buchanan M, Jahan K *et al.* CXCR4 peptide antagonist inhibits primary breast tumor growth, metastasis and enhances the efficacy of anti-VEGF treatment or docetaxel in a transgenic mouse model. *Int. J. Cancer* 129(1), 225–232 (2011).
- 148 Coenegrachts L, Maes C, Torrekens S *et al.* Anti-placental growth factor reduces bone metastasis by blocking tumor cell engraftment and osteoclast differentiation. *Cancer Res.* 70(16), 6537–6547 (2010).
- 149 Hiratsuka S, Duda DG, Huang Y *et al.* CXC receptor type 4 promotes metastasis by activating p38 mitogen-activated protein kinase in myeloid differentiation antigen (Gr-1)-positive cells. *Proc. Natl Acad. Sci. USA* 108(1), 302–307 (2011).